CONSEQUENCE EVALUATION OF IN-VESSEL FUEL COOLANT INTERACTIONS IN THE EUROPEAN PRESSURIZED WATER REACTOR

D. Struwe, H. Jacobs, U. Imke, R. Krieg, W. Hering, M. Böttcher, M. Lummer, T. Malmberg, G. Messemer, Ph. Schmuck , B. Göller, G. Vorberg

Institut für Reaktorsicherheit

Institut für Neutronenphysik und Reaktortechnik

Zusammenfassung

Die vorliegende Untersuchung betrachtet mögliche Konsequenzen einer Verlagerung von Kernschmelze in das untere Plenum des European Pressurized Water Reactor (EPR). Im Gegensatz zu früheren Studien ist die gewählte Vorgehensweise nicht Risiko orientiert, sondern orientiert sich an den Konsequenzen des Vorganges, d.h. in jedem Schritt werden die extremsten Konsequenzen, die nicht mit hoher Zuverlässigkeit ausgeschlossen werden konnten, als Grundlage für den nächsten Schritt angenommen.

Für drei unterschiedliche, zu Kernschmelze führende Szenarien, wurde mit den drei Kernschmelzecodesystemen SCDAP/RELAP5, MELCOR, und MAAP der Zustand der Schmelze im Reaktorkern vor dem Absturz in das untere Plenum berechnet. Aus dem Ergebnisspektrum wurden maximale Werte für die Konfiguration des Schmelzepools als Startbedingungen für die Vorvermischungsrechnungen mit MATTINA und MC3D extrahiert. Für jeden Code wurde ein genereller Parametersatz erstellt, der eine bestmögliche Analyse von sowohl FARO als auch PREMIX und QUEOS Versuchen ermöglichte.

Es wurden axiale und laterale Ausfluss-Szenarien aus verschiedenen Höhen untersucht. Generell wird die berechnete Vorvermischung durch große Schmelze-Verlagerungsraten, große anfängliche Tropfen, und durch Druckverlustkoeffizienten in der „flow distribution plate" im unteren Plenum erhöht.

Die thermische Energie für eine mögliche Dampfexplosion wurde konservativ für verschiedene Szenarien abgeschätzt. Unter Berücksichtigung der verfügbaren experimentellen und analytischen Ergebnisse wurde ein angemessener, konservativer Konversionsfaktor festgelegt.

Ferner wurde angenommen, dass 40% der mechanischen Energie zur Beschleunigung des Schüttbettes und des restlichen Schmelzepools auf der unteren Gitterplatte zur Verfügung steht, was zu einer beträchtlichen Belastung des Reaktordeckels führen kann. Die Belastungsenergien, denen der Reaktordeckel widerstehen kann, wurden aus Modell-Experimenten im BERDA Programm abgeleitet, die ein weites Spektrum von möglichen Bedingungen umfassen. Unter Berücksichtigung spezieller Ähnlichkeits-Bedingungen wurden die Ergebnisse auf Reaktormaßstab übertragen.

Allgemein kann man aus den Ergebnissen der Untersuchung schließen, daß die kinetische Energie des abrupt nach oben beschleunigten Slugs in Wechselwirkung mit dem Reaktordeckel die Grenzen der Belastbarkeit des Deckels erreichen würde. Jedoch basieren diese Resultate auf Anwendung von sehr konservativen Annahmen in jedem Zwischenschritt. In der Mehrheit der betrachteten pessimistischen Fälle bleibt jedoch die kinetische Energie unter der Lastabtragungsfähigkeit des Deckels. In diesem Sinne ist keine Notwendigkeit für zusätzliche Design-Maßnahmen gegen In-vessel Dampfexplosion erkennbar, und zum α-mode Versagen des Containments führende Pfade müssen nicht betrachtet werden.

Abstract

In this study consequences of in-vessel melt relocation scenarios into the lower plenum of the European Pressurized Water Reactor (EPR) are considered. In contrast to former work the approach is not risk oriented but consequence oriented. In every step, the most adverse consequences that cannot be excluded with high reliability are taken as basis for the next step. From three different core melt initiators the state of the molten pool prior to crust failure was calculated by SCDAP/RELAP5, MAAP, and MELCOR. From these data upper values for molten pool mass and pool temperature were chosen for premixing analyses with MC3D and MATTINA. For each code a parameter set was selected derived from code validation using selected FARO, PREMIX, and QUEOS experiments. Various outflow scenarios at bottom and lateral positions at different elevations of the molten pool were calculated. All calculations were performed in axial symmetry (2D) except one 3D MC3D calculation. Generally, the calculated premixing process is enhanced by large melt release rates, large initial droplet size and pressure loss of the flow distribution plate in the lower plenum.

The thermal energy available for an in-vessel steam explosion was estimated conservatively from selected premixing configurations. Based on available theoretical and experimental information a reasonably conservative energy conversion factor was selected. Then 40 % of the mechanical energy may accelerate the remnants of debris and the molten pool on top of the lower core support plate in upward direction. This may lead to a considerable mechanical load to the upper vessel head. The load energies which the reactor vessel head can withstand are determined on basis of experimental results from the BERDA facility that cover a broad spectrum of conditions and applying similarity theory to convert experimental results to the reactor scale.

In general one can conclude from results of these investigations, that the kinetic energy of a core melt moving potentially rapidly upward as consequence of an in-vessel fuel coolant interaction might reach the load carrying capabilities of the vessel head. However, this result is only obtained when the most pessimistic assumptions are applied in every step of the analyses. In the majority of the considered pessimistic cases the kinetic energy remains below the load carrying capabilities of the reactor vessel head. In so far there is no need for additional design measures against steam explosions and alpha-mode containment failure sequences need not to be considered.

Table of Contents

List of Tables:

List of Figures:

Executive summary

In the case of a hypothetical core melt-down accident in a pressurised light water reactor (PWR), relocation of large amounts of molten core material into a water filled lower coolant plenum would lead to more or less violent thermal interactions of that melt with the water that, in the extreme case, might have explosive nature. As indicated by the word 'hypothetical' such accident sequences have a small probability of occurrence only and respective investigations belong to residual risk evaluations. However, consequences must be assessed in order to positively exclude that they might lead to non-tolerable plant conditions. Above all that means that early containment failure (alpha-mode failure) must be excluded. To this end it is advantageous to show that the head of the reactor pressure vessel will not fail in a catastrophic manner when it is hit by core material that is accelerated upward as consequence of a steam explosion in the lower coolant plenum. But also the failure of the lower vessel head and other potentially dangerous consequences of steam explosions within the primary circuit must be assessed. In these analyses a conservative approach is often indicated because currently available tools are not yet sufficiently well qualified to perform 'best estimate' analyses. On the other side, unrealistically pessimistic assumptions should be avoided as far as possible.

In this study related to the EPR plant design [1] we partly follow the procedure developed by Theophanous et. al. [2] in that we split the whole problem up into topics that can be evaluated using specific methods. However, in contrast with the former work cited above, our study is not risk oriented but consequence oriented. So individual results are not combined in a probabilistic framework but in every step the most adverse consequences that we cannot exclude with high reliability are taken as the basis of the next step. In this way we arrive at a definite conclusion concerning alpha-mode failure without relying on the fact that some of the processes that have been taken into account certainly have a small conditional probability of occurrence.

To evaluate the above outlined task the following items have been treated:

Selection of accident scenarios (initiators) that have to be considered.

Three initiating events leading to core disruption have been considered in detail. These were the loss of off-site power (LOOP), the surge line rupture with a leak size of 962 cm² (LBLOCA) and the small break LOCA with a leak size of 50 cm² in the cold leg (SBLOCA).

Determination of initial and boundary conditions for the thermal interaction of molten core material with water in the lower plenum, such as the state of the primary system (pressure, distribution of water etc.), temperatures of relevant structures, the water and the melt, mass, composition and location of the molten pool, and possible relocation paths for the melt.

Judging on the basis of a broad spectrum of calculations performed for the EPR with the codes SCDAP/RELAP, MAAP and MELCOR it appears that calculated melt relocation scenarios approach initial conditions for core melt outflow which are similar to each other and

do not depend decisively on the considered initiator. Keeping in mind the uncertainties of the analyses to follow only a single initial state was chosen for evaluation of core melt outflow scenarios which covers in a conservative way all possible conditions. This state is characterised as follows:

The amount of core melt for core material outflow evaluations has been chosen to an upper limit value of 110 t. The core melt consists mainly of UO2 with about 25 to 30 % of ZrO2. In addition non oxidised Zr might amount to values of 1 to 17 t and the amount of steel is calculated to reach values of 3 to 16 t. These steel components will most probably accumulate on top of the corium melt and result in a contact mode with the heavy reflector which favours a more pronounced radial melt progression at the upper boundary of the corium melt. The average core melt temperature was chosen to amount to 3000 K. Because the material property differences would not be too important during the premixing analyses that we performed, we considered only corium and no steel in our core material outflow studies.

The ambient system pressure at the expected time of core material outflow onset is calculated to reach values of 0.2 up to 0.42 MPa, the higher values being representative for the LOOP-scenarios. Therefore most of the premixing calculations were performed choosing a value of 0.25 MPa as ambient system pressure. Impact of a higher system pressure of 0.45 MPa on the results was investigated as well. The remnant water level amounts to 2.0 up to 2.2 m which implies that the lower plenum is filled with saturated water up to the upper edge of the lower core support plate (LCSP) but there is no water left within the LCSP.

For consequence evaluation of fuel coolant interactions calculated results at the chosen time of core material outflow onset have been evaluated characterising the thermodynamic state of reactor vessel volumes and the reactor coolant system volumes as well as temperature levels reached in the enclosing structures as heavy reflector, core support plate, core barrel, lower and upper reactor vessel head structures etc. However, for the purpose of this study it is of main importance to state that most of the upper internal structures with the exception of the upper support structure are largely molten away or at least very much weakened. In so far they are not further available to mitigate mechanical loads to the upper reactor vessel head.

Conditions of core material outflow are difficult to predict. Integral codes do not provide sufficiently detailed information. Therefore, conditions have been defined coherently with the physical picture evolving from integral calculations and based on specific analyses of the melt through characteristics of the molten pool enclosures as heavy reflector/core barrel and lower core support plate. Nevertheless, a broad spectrum of possibilities have been investigated which can not be ruled out with certainty.

Three basic scenarios have been investigated:

- a compact jet like axial relocation through a circular breach in the LCSP with a 25 cm radius,

- an axial relocation through holes in the LCSP within a circular area of 45 cm radius which results in a dispersed core material outflow with the 33 % porosity of the LCSP,

- a radial relocation at the bottom or close to the top of the core melt pool. Most cases were performed in axial symmetry smearing out the ruptures of the core barrel along it's whole circumference. However, one 3D-case was analysed as well smearing out the rupture along a $1/8^{th}$ sector of the circumference of the core barrel only. The total opening was chosen similarly large as in the axial outflow scenarios.

<u>Determination of core melt and water configurations and of the pressures developing during premixing</u> as consequence of the different core material outflow scenarios.

Premixing has been studied with the help of the codes MC3D and MATTINA. All calculations except one with MC3D have been performed in axial symmetry. Model parameters have been chosen as deduced from theoretical interpretation of experiments performed in the framework of the FARO-, PREMIX-, and QUEOS- programmes.

Parameter studies were done to cover a band of uncertainties. A very strong influence on the results is recognised for the variation of the initial size and the transient increase of the melt release area. The initial droplet size is a key value for the strength of the thermal melt water interaction. Pressure losses at the distribution flow plate in the lower plenum influence the mixing of corium with water considerably. The spatial discretization has a strong impact on the overall results due to the nonlinear behaviour of most of the simulated processes and the utilisation of a first order scheme for the convective terms in the basic equations. Feedback of pressure losses at coolant inlet and outlet pipes and at the junction between downcomer and lower inlet plenum is of minor importance. Moderate variations of the system pressure give similar results.

As observed in the respective experiments at low pressures, calculations indicate that the water of the lower plenum is displaced rapidly by vapour into the downcomer for axial and radial outflow scenarios. Radial outflow scenarios should be investigated by 3D-simulations, to avoid an artificial enclosure of water in the lower plenum.

The two applied codes show a similar results spectrum. MATTINA gives lower thermal premixing energies due to stronger water displacement, which is caused by strong evaporation events after intensive fragmentation of melt droplets. The presently used MC3D code version simulates a more moderate fragmentation behaviour leading to less evaporation and water depletion. Both codes predict removal of non negligible amounts of fragmented core material into the primary circuit if radial outflow scenarios are considered.

<u>Selection of premixing configurations in which a trigger could initiate a steam explosion and determination of the thermal energy available within the melt that could participate in a steam explosion.</u>

The premixing state can be described qualitatively by the volume fraction distribution of melt and water in the lower plenum. The upper level of the lower plenum is defined at the lower edge of the core support grid. The development of pressures with time give information about the strength of the interaction between melt and water during premixing. To compare different

calculations and to estimate the probability and the efficiency of a steam explosion we define integral key values, which characterise the premixing state and which are evaluated as functions of time. With the objective of a definitely conservative evaluation these values were chosen as follows:

- Sum of mass and thermal energy of melt in all cells with water volume fractions greater than 0.1 (These values are called premixed melt mass and premixed thermal energy)

- Average volume fraction of water considering all cells with water volume fractions greater than 0.1 and melt volume fractions greater than 0.01.

- Total amount of melt in the lower plenum

- Total amount of water in the lower plenum.

The definition of the values for the premixed melt mass and the premixed thermal energy is based on a very low value of the water volume fraction. The reason for that conservative evaluation is that calculations of low pressure premixing experiments result in a strong overestimation of voiding around the penetrating melt. If the codes would be better validated for these low ambient pressure situations a water volume fraction limit of about 0.4 would be a more reasonable choice for the evaluation. It is difficult to evaluate quantitatively whether it is too conservative to compensate the effect of excessive water displacement by using the limit value of only 0.1. The integral values of water and melt available in the lower plenum give no information about the premixing state, but they are representative for the general risk of a steam explosion.

The conservatively oriented evaluation of all investigated cases leads to a maximum of the premixed thermal energy of 3 GJ and a respective average water volume fraction of about 0.5 to 0.6 in the premixing zone. However in the majority of the calculated cases the maximum of the premixed thermal energies vary between 0.5 up to 2 GJ and the respective values of the average water volume fraction in the premixing zone amounts to values between 0.2 to 0.5. The total amount of melt in the lower plenum can be much larger than the premixed melt mass with a considerable water inventory still available. At the end of the calculations water is largely separated from a rather compact molten corium pool mostly located at the bottom of the lower plenum.

<u>Assessment of the mechanical energy that might result from steam explosions triggered in the different premixing configurations</u>

Evaluation of consequences of steam explosions is ideally done by applying a verified model of steam explosions to possible premixing configurations. Such model would deliver the pressure time histories produced and the mechanical energy that is released. At the time being, however, such model is not yet available and one way to solve the problem is to apply an energy conversion factor to the thermal energy available to the steam explosion. This approach is rather conservative and will have to be refined in the future. Only then it will be

possible to asses lower head integrity and other mechanical consequences within the primary system.

Judging on basis of the available theoretical and experimental information, we concluded that a conservative energy conversion factor amounts to a value of 15 %. But in view of the uncertainties involved, we also considered a value of 30 %. As triggering of steam explosions is so little understood we could neither rely on a trigger to occur in a certain situation nor exclude it to happen in other situations. Therefore we looked for the maximum of the premixed thermal energy during the whole mixing process and applied the conservatively estimated conversion factors to that thermal energy to get an estimate on the related mechanical explosion energies if a steam explosion might occur. This gives maximum values of the mechanical explosion energies which amount to 0.45 and 0.9 GJ, respectively. In our opinion the higher values are extremely pessimistic. In the majority of the analysed cases the respective maximum values amount to 0.075 GJ up to 0.6 GJ.

<u>Assessment of the kinetic energy accumulated in the core material that is accelerated upward (energy partitioning) assuming that the lower head remains intact.</u>

Mechanical explosion energies do not convert directly to the kinetic energy of the core melt which is accelerated upward as consequence of the steam explosion. Part of the explosion energy is consumed to accelerate the lower core support plate along with the core material. Part of it is as well consumed deforming the lower reactor vessel head and part is consumed accelerating the water inventory in the downcomer. This energy partitioning is difficult to evaluate and we have to accept uncertainties. We consider a 40 % fraction of the explosion energy that is transferred to the core material on top of the core support plate as a reasonable estimate. On this basis a loading energy to the upper vessel head is estimated to amount to maximum values of 0.18 GJ and 0.36 GJ, respectively. In the majority of the analysed cases theses maximum values amount to 0.03 GJ up to 0.24 GJ, respectively.

<u>Judgement whether the impact of the loading energy on the upper internal structures and the vessel head might cause a catastrophic vessel head failure.</u>

Loading energies which the reactor vessel head can withstand are determined on basis of experimental results from the BERDA programme. These experiments cover a broad spectrum of conditions and similarity theory can be applied to convert the experimental results to the reactor scale. Results show a quite complicated dependency of admissible loading energies from the actual state of in-vessel reactor structures and temperature levels of these structures. For a configuration representative for the state of in-vessel structures established as consequence of the event sequence calculations discussed above, BERDA experiments have shown that for loading energies up to 0.4 GJ the vessel head and the head bolts will essentially remain in the elastic range. This value is larger than the conservatively evaluated maximum values of the loading energies which might result from postulated steam explosions in the lower plenum of the EPR so that there is by far no danger of a catastrophic head failure.

We can thus conclude that there is no danger of an early containment failure caused by a steam explosion in the EPR reactor vessel.

Concluding remarks

This study has been performed with not all of the required theoretical tools being available and others not being verified to the necessary extent. So, some remaining uncertainties had to be covered in a definitely conservative way and this report is not a final statement on the topic. Rather the report describes what can be concluded on the basis of the presently assured knowledge and available tools. Further improved analyses become necessary, especially concerning the following items:

- Evaluation of possible relocation paths for the core melt after failure of either molten pool enveloping crusts, the core barrel and/or the lower core support plate.

- Realistic assessment of pressure time histories and explosion energy releases that might result from steam explosions following different premixing conditions.

- Realistic assessment of the kinetic energy in the upward accelerated core material

- Assessment of the lower vessel head integrity.

Future research and development activities concentrate on these items and will lead to better qualified tools and criteria for a more realistic evaluation of consequences of an in-vessel steam explosion in the EPR.

References

[1] Topical Issue, Nucl. Eng. Design, vol 187, (1999) No. 1

[2] T.G.Theophanous et.al., "An Assessment of Steam-Explosion-Induced Containment Failure", Parts I-IV, Nucl. Science Eng. **97** (1987) p 256-326

1 Introduction

In the case of a hypothetical core melt-down accident in a pressurised light water reactor (PWR), relocation of large amounts of molten core materials into a water filled lower coolant plenum would lead to more or less violent thermal interactions of that melt with the water that, in the extreme case, might have explosive nature. As indicated by the word 'hypothetical' such accident sequences have a small probability of occurrence only and respective investigation belong to residual risk evaluations. However, consequences must be assessed in order to positively exclude that they might lead to non-tolerable plant conditions. Above all that means that early containment failure (α-mode failure) must be excluded. To this end it is advantageous to show that the head of the reactor pressure vessel will not fail in a catastrophic manner when it is hit by core material that is accelerated upward as consequence of a steam explosion in the lower coolant plenum. But also the failure of the lower vessel head and other potentially dangerous consequences of steam explosions within the primary circuit must be assessed. In these analyses a conservative approach is often indicated because tools are not yet sufficiently well qualified to perform 'best estimate' analyses. On the other side unrealistically pessimistic assumptions should be avoided as far as possible.

In this study related to the EPR plant design [1] we partly follow the procedure developed by Theophanous et. al. [2] in that we split the whole problem up into topics that can be evaluated using specific methods. However, in contrast with the former work cited above, our study is not risk oriented but consequence oriented. So individual results are not combined in a probabilistic framework but in every step the most adverse consequences that we cannot exclude with high reliability are taken as the basis of the next step. In this way we arrive at a definite conclusion concerning alpha-mode failure without relying on the fact that some of the processes that have been taken into account certainly have a small conditional probability of occurrence.

The task as outlined above requires to treat the following items:

(A) Selection of accident scenarios (initiators) that have to be considered.

(B) Determination of initial and boundary conditions for the thermal interaction of molten core material with water in the lower plenum, such as

- the state (pressure, distribution of water) of the primary system,
- temperatures of relevant structures, water and melt,
- mass, composition and location of the molten pool, and
- possible relocation paths for the melt.

(C) Determination of core melt and water configurations and of the pressures developing during premixing as consequence of the different core material outflow scenarios.

(D) Selection of premixing configurations in which a trigger could initiate a steam explosion and determination of the thermal energy available within the melt that could participate in a steam explosion.

(E) Assessment of the mechanical energy that might result from steam explosions triggered in the different premixing conditions.

(F) Assessment of the kinetic energy accumulated in the core material that is accelerated upward (energy partitioning) assuming that the lower head remains intact.

(G) Judgement whether the impact of the loading energy on the upper internal structures and the vessel head might cause a catastrophic vessel head failure.

The work done related to the above described items is documented in the following chapters. Chapter 2 covers discussion of evaluation results for items (A) and (B) on basis of calculations performed with different code systems as SCDAP/RELAP, MAAP and MELCOR. One main topic of this report is the discussion of core melt and water configurations developing during premixing as consequence of different core melt outflow scenarios (item (C)). Code systems used for these analyses are shortly characterised in chapter 3 where some information on the actual status of their experimental qualification is given as well. Initial and boundary conditions established in the different calculations are defined in chapter 4 and integral quantities used for characterisation of the premixing state are defined and shortly discussed in chapter 5. Results of calculations performed with the codes MC3D and MATTINA are documented and discussed in chapters 6 and 7 covering axial and radial core melt outflow scenarios separately. In chapter 8 main findings of the evaluation of melt water configurations developing during premixing are summarised which then form the basis of evaluations related to the other above mentioned items of interest. Considerations about items (D), (E),and (F) are presented and discussed in chapter 9. In chapter 10 the current state of knowledge regarding mitigation capabilities of upper internal structures and the reactor vessel head in case of large loads are described on basis of experimental results obtained during performance of the BERDA-I programme. How these results then are used to determine admissible energies which the reactor vessel head can withstand is discussed in some detail. Finally conclusions are derived from the different stages of the analyses. They are presented in chapter 11.

2 Initial and Boundary Conditions for Core Material

For determination of boundary conditions of the evaluation from event sequence calculations with codes like SCDAP/RELAP, MELCOR and/or MAAP three different core melt initiators were considered as representative for the whole spectrum of core melt initiators:

  (i)   consequences of a loss of off-site power accident (LOOP)
  (ii)   consequences of a surge line rupture with a leak size of 962 cm ^{2}
  (iii)   consequences of a SBLOCA with a leak size of 50 cm ^{2}

Information about the state of the core, the reactor vessel and the reactor coolant system at the time when the relocating molten pool reaches either the lower core support structure or the inner boundary of the heavy reflector are shown in Tables 2.1–2.4. These data include information of calculations with the ICARE-mod V2 code for the late phase behaviour, i.e. the in-vessel molten pool relocation. In Table 2.1 and 2.2 information on the time difference between molten pool formation onset and the time of the molten pool arrival at the lower core support structure and /or the heavy reflector are given as well as information on the composition of the molten pool, its enthalpy level and the state and shape of neighbouring crusts. These data are given together with information on the temperature level of structures in the immediate vicinity of the crusts, i.e. temperatures of the lower core support structure, temperatures at one third, two thirds and full height of the heavy reflector and the respective information about temperature levels of the core barrel. Given as well are values of the vapour pressure established above the molten pool and estimates about the state of the upper core plate and the support columns.

For characterisation of the molten pool state two categories are defined: the first one is identified by HM which means homogeneously mixed and the second one is identified by LS which means layered structure of the molten pool inventory. This later configuration assumes that the metallic components of the melt lay either on top or sidewise or below of the fuel component of the mixture. In this case it is assumed that the metallic layer on top of the molten fuel pool consists of two layers: one sublayer close to the oxydic melt where the composition varies linearly from a pure oxyd to a pure metal and a second layer which consists only of the metallic phase. It is assumed that the temperature profile along the pure metallic layer thickness is linearly decreasing from the molten fuel/steel temperature to the solidus temperature of the steel component of the metallic melt. This assumption of a sublayer structure of the metallic phase is based on the fact that the existence of the turbulent natural convection in the molten pool hardly will allow a clear separation of the two main material components of the molten pool at the outer interface of the molten fuel pool limit. The thickness of the transition layer needs to be specified. Its location most probably determines the most likely axial location of failure if a radial melt through type failure of the molten pool enclosure is assumed.

For characterisation of the state of crusts enclosing the molten pool two states are defined : the first one is identified by SS – solid state - which means that these crusts can withstand differential pressure loads without immediate failure and the second one is identified by PS – porous state - which means that the crusts have a dominantly porous structure and thus cannot withstand differential pressure loads. The later ones are characterised by an average porosity which is assumed to amount to a value of 30 %. Thickness variations along the boundary of the molten pool would need to be defined coherently with results of the integral code systems.

To evaluate estimates on the conditional probability of a downward directed failure mode of the molten pool versus the conditional probability of a failure mode in radial direction erosion

rates of the lower core support structure and the heavy reflector upon contact with the molten pool have been evaluated.

As characteristic values of the state of the reactor vessel and the reactor coolant system at the time of the expected onset of molten pool drainage into the lower plenum information on the saturation pressure and temperature in the different compressible volumes of the reactor coolant system are given in Table 3.3 together with information on the residual volume fraction of still liquid water. This information is given in only a quite crude spatial resolution covering average values for the reactor vessel downcomer including loop nozzles, reactor pressure vessel lower plenum with the filling height of the lower plenum with water and its temperature, reactor pressure vessel upper plenum and upper dome , hot and cold leg, U-leg, steam generator headers and tubes, reactor coolant pumps and pressurizer. Accordingly ranges of structure temperatures enclosing the reactor coolant system are given in Table 3.4.

2.1   In-Vessel core degradation scenarios

LOOP

In this scenario the loss of off-site power (LOOP) supply as well as the unavailability of all diesel engines is assumed. Only battery power is available for a certain time allowing to maintain operation of the reactor safety system as well as the actuation of valves. No pump is available for core reflooding to terminate the accident early before onset of core degradation. For reflood scenarios a recovery of electrical power is assumed after 4 h so that the low head and medium head systems can operate. However, core heat–up may have started so that the core may be damaged partially.

The EPR has a built-in system to depressurize the primary system to avoid high pressure vessel failure. This system is activated by signals of the reactor safety system derived from core instrumentation (gas temperature at core outlet) and opens the dedicated depressurization valves on top of the pressurizer dome. The two phase fluid is then condensed in the in-containment refueling water storage tank (IRWST).

At app. 160 min at a system pressure of 4.5 MPa accumulators feed in flooding the reactor pressure vessel. Due to the long discharge path (hot leg, surge line, pressurizer, dedicated valves) the primary pressure drops slowly so that decay heat is effectively transported to the containment. During boil-down phase the core heats up until oxidation of the zircaloy cladding which starts at app. 227 min in the upper third of the active core.

First relocation of metallic melts is calculated to occur at app. 230 min (absorber melt) and at 235 min (U-Zr-O melt) respectively. The upper core plate starts melting at 241 min and 2 min later a pool of molten material is formed. At app. 270 min the pool reached a mass of app. 35 t in the inner four rings of the core. The S/R5 calculations were stopped at this time due to numerical problems.

SURGE-line rupture

The surge line is the largest pipe welded to the hot leg of the primary circuit piping and connects it with the pressurizer. If at all necessary to be considered this rupture is the conditionally most probable large break LOCA leading to a leak of 962 cm² size. This is rather conservative since normally creep rupture processes lead to a leak of app. 40-50% of the pipe cross section only. Nevertheless, the generic sequence is not influenced, only time scales are reduced for the assumed large break.

After rupture the water inventory of the pressurizer and of the primary system is sprayed out due to pressure drop and evaporation until accumulators feed in. After refill the dry-out phase starts at app. 14 min leading to an onset of oxidation at app. 21 min, due to the relatively high decay heat (just after scram) and the low primary system pressure of app. 0.3 MPa. Onset of absorber melting occurs 5 min later and the liquefied pellet-clad material starts relocating at 2 min later. Due to rapid heat-up the onset of pool formation is reached at 32 min leading to a molten pool of 122 t at 65 min.

If the heavy reflector is simulated, the pool is restricted to the inner four rings of the simulated core region whereas in case of a quasi adiabatic boundary condition in radial direction the pool is spread over the whole area of the core in the calculation.

SBLOCA

The SBLOCA scenario assumes the rupture of a 3" tube (cross section area app. 45 cm²) connected at the vertical elevation of the axis line of the primary system cold leg piping. The original small break scenario assumes the availability of both X-diesels allowing to maintain all four emergency feed water systems (EFWS) operational to feed all the steam generators. Due to this effective heat sink the time scale till core heat up extends to more than 10 h. This long duration causes data storage and computation time problems of the SCDAP/RELAP calculation so that it was assumed that only one steam generator is filled by one EFWS, whereas the other three are allowed to dry out. As a consequence, the primary system becomes unbalanced. As part of a code benchmark problem for the EPR with increased power the radial core nodalization as well as boundary conditions were adapted to a MAAP configuration. With this assumption the whole transient until pool spreading was calculated with S/R5 mod 3.1. Rel.F since S/R5 mod3.2 fails when nitrogen enters the primary system.

In the first 32 min the primary system pressure is aligned to the secondary system pressure until the accumulators feed in after manual primary depressurization. The three steam generators dried out 33 min later and at app. 4 h hydrogen production starts. This long time period is due to the reflux-condenser flow in the hot leg to the full steam generator. At 262 min the absorber rod fail and 3 min later the fuel rods. At app. 277 min the upper core plate and at 304 min the inner surface of the heavy reflector reach melting temperature. At 307 min the total mass in the molten pool is about 49 t located between 1.6 and 2.7 m in the inner four rings of the core. At that time the melting zone of the inner surface of the heavy reflector extends axially along the same length as the molten pool.

2.2   Severe Core Degradation Codes

For better understanding of some of the results discussed in the next chapter code systems are shortly characterised here which have been used to provide results for the different core melt initiators considered. However, this characterisation is by far not sufficient to enter into a

detailed discussion of the differences of results, but it should be sufficient to understand better how this information is used to fulfil the main purpose of this investigation, which is to define reasonable boundary conditions for core melt relocation scenarios.

MAAP

The MAAP code is an industrial code used at EDF and Framatome to quantify safety margins for the EPR concept in design basis accidents (DBA) and severe fuel damage accidents. The code has been validated at CEA/DRN using several severe fuel damage tests e.g. CORA-13 and Phebus FPT0. The fuel rod failure criteria used in the calculations was set to a value of 2500 K.

MELCOR

The MELCOR code (vers. 1.8.3 and 1.8.4) /7/. has been used for EPR calculations at Siemens-KWU and at Forschungszentrum (INR). The MELCOR code is an integral code with some special model for reactor components, i.e. the core model. The basic solution technique is first order upwind (as used in S/R5 and MAAP). The primary circuit is rather simplified using single volumes for each component of the piping. The thermal-hydraulic models have to be adjusted by several user parameters and validated against adequate tests. Results of the code are only reliable if validation is performed for all possible states which may arise during the course of a severe accident. Therefore, reliability of code results is mainly restricted to global parameters such as system pressure. In MELCOR 1.8.3 the fuel rod failure criteria is set to 2500 K, the zircaloy melting temperature is set to 2100K, whereas in MELCOR 1.8.4 the failure criteria is 2400 K and the melting point of zircaloy is set to 2250 K.

SCDAP/RELAP5 mod 3.1

SCDAP/RELAP5 (S/R5) is a best estimate code with detailed mechanistic models in the early core melt phase and in the transition phase to the late phase. However, some shortcomings in the coupling of molten pool models with core structures prevents to calculate reliably the interaction with the heavy reactor. Crust failure occurs only when the pool reaches the SCDAP boundaries. Therefore calculations are stopped earlier.

The new code version (mod3.2) should overcome these deficiencies, however, the area of model improvement is focussed on the TMI-2 accident. S/R5 mod3.1 underestimates the hydrogen production by about 5-10 % when compared to experimental data.

All calculations were performed with S/R5 mod3.1 Rel.F an improved code version which includes significant error corrections introduced at the Forschungszentrum (IRS)as well as model improvements. To broaden the data base some calculations with an early release (Rel.D) were performed too, however, these results have to be handled with care since hydrogen production is underestimated due to code errors, i. e. the oxidation of absorber rod guide tubes as well as the debris oxidation are not included.

For the severe fuel damage parameters same values as in the Phebus and CORA tests were used to assure consistency of results. Fuel rod failure criteria is set to 2350 K, slightly higher as the melting point of α-Zr(O). Pool formation temperature is set to the solidus temperature of ZrO_2-UO_2 .

S/R5 mod 3.2

A new feature of the S/R5mod3.2 code is that upper plenum structures (UPS) can melt and the melt can relocate to the position of the lowest UPS element, which is the upper core plate. Here it is kept until relocation into the pool or lower plenum is initiated by user command. No radiation heat transfer is possible between UPS elements or RELAP5 heat structures or SCDAP core components, so that the heat-up is only due to convective heat transfer.

The S/R5 mod 3.2 code has been validated and tested against CORA, Phebus FP, and QUENCH experiments, the UPS/IRS code improvements were implemented and sent for further testing to INEEL in August 1998. For reactor applications this code version could not be used because of convergence problems in the thermohydraulic phase when the driving gas of the accumulators enters the primary circuit through the stand pipes. The problem is solved in the stand alone version R5 mod 3.2.2 but the coupled code version still relies on R5 mod 3.2fg which shows the same problems. Presently the coupling of the R5 mod 3.2.2β version is not yet foreseen at INEEL.

S/R5 nodalization

Based on RELAP5 input decks provided by Siemens-KWU a detailed S/R5 input deck was established which was used as a guideline for the MELCOR input deck. Therefore, core nodalization of the S/R5 and MELCOR calculations are similar. For the SBLOCA benchmark problem (EPR-2) the radial core nodalization was adapted to MAAP configuration to allow comparison. The axial core discretization, however, was kept at 14 axial levels.

The core is divided into five axial rings each with 16 thermal hydraulic levels (0.3m high), 14 for the active core plus 2 for the top and bottom structures. In each component a representative fuel rod and one absorber rod simulate the fuel elements. The water rods are considered as part of the absorber rods too. The heavy reflector as well as the reactor pressure vessel wall are simulated by SCDAP shroud components, allowing radiative heat transfer between core barrel and reactor pressure vessel wall.

The five rings are coupled by cross-flow simulation as well as by radiative heat transfer. Also radiation is calculated between the components in the outermost ring and the shroud inner surface. The upper plenum internals are modeled by RELAP5 heat structures which are coupled by radiative heat transfer in each of the three rings. In the upper plenum internal structures and the lower core support structure are RELAP heat structures. Also the piping walls as well as the steam generators and the pressurizer walls are simulated as heat structures with adiabatic boundary conditions at the outer side.

2.3   Evaluation of the Results Spectrum

In this section it is not intended to enter into a detailed discussion of differences in the results of the different calculations as documented in Tables 2.1 up to 2.12. The main purpose is to evaluate whether current code capabilities predict generic differences what concerns initial and boundary conditions for core melt outflow scenarios. This concerns differences in between the different code systems as well as differences as consequence of different core melt initiators. Data provided by SCDAP/RELAP5 partly represent results obtained up to some time into the considered transients where core melt outflow is not yet to be expected. This occurs either due to the fact that the calculated results become wrong afterwards due to

model deficiencies or that the code stops due to instability problems. In so far these results should be valued cautiously.

First of all it is of importance to evaluate whether calculated molten pool data differ considerably from each other in the different calculations. It can be observed, that the total molten pool inventory is considerably smaller in all MELCOR-type calculations when compared with the different MAAP- and S/R5- calculations. This is related to the fact, that temperatures calculated in the lower core support plate and in heavy reflector structures increase much more rapidly in the MELCOR-calculations leading to postulated failure conditions earlier than in the respective MAAP and S/R5- calculations. The total pool inventory as calculated by MELCOR varies between values of 32 t up to 80 t and in the different MAAP and S/R5-calculations between values of 83 t to 122 t. Differences between results of the different code systems are larger than differences between calculations for different core melt initiators. Therefore, it seems reasonable to choose the amount of core melt for the core outflow evaluations independent on the considered scenario and to consider a value of 110 t as an upper limit value.

Evaluation of results concerning calculated core melt compositions lead to similar conclusions as above. Differences in between different code applications are larger than differences in between results for different core melt initiators. The core melt consists mainly of UO_2 with about 25 to 30% of ZrO_2.

In addition other contributions to the core melt are calculated: Non oxidised Zr might amount to values of 1 to 17 t and the amount of steel is calculated to reach values of 3 to 16 t. These steel components will most probably accumulate at top of the corium melt and lead to a contact mode with the heavy reflector which results in a more pronounced radial melt progression. Failure of the heavy reflector in radial direction is most probably to be expected at these axial locations. However, real conditions determining melt-through of surrounding structures are more complicated and need analyses with special purpose codes and appropriate consideration of the respective experimental investigations. System codes provide only little information on this topic (see discussion in the next section 2.4).

Average temperatures of the core melt amount to values of 2600 K up to 2840 K. Peak temperatures reached values of 3100 K. There are no dramatic differences observed between the various calculations. It is therefore reasonable to define the average core melt temperature at the time of core melt outflow onset to a value of 3000 K.

The ambient system pressure at the expected time of core melt outflow onset is calculated to be 0.2 to 0.28 MPa in case of the LOCA-scenarios and about 0.3 to 0.42 MPa in case of the LOOP-scenarios. It is therefore decided to perform most of the premixing calculations with a value of 0.25 MPa for the ambient system pressure. In one representative case influence of a different ambient system pressure of 0.45 MPa on results of the premixing calculations will be evaluated.

Comparison of the status of RPV-internal structures in the immediate vicinity of crusts enclosing the core melt leads to some interesting aspects to be considered during consequence evaluation of fuel coolant interactions in the lower reactor plenum.

Up to the time of core melt outflow onset upper core support plate and most parts of the respective support columns are molten. Upper support plate structures are heated up to some extent, most pronouncedly in case of the LOOP-core melt initiator and to a lesser degree in

case of the two LOCA-initiators considered here. Reactor vessel temperatures in upper dome remain low in all considered cases.

Heavy reflector structures are heated up considerably in all cases but differences between different codes are again larger than differences as consequence of different core melt initiators. Peak thermal loads are calculated at the middle third of total height. Calculations by MAAP and partially by S/R5 predict radial melt through at this axial location. Core barrel temperatures are increased considerably as well. However differences between the different calculations are large dependent on the assumptions used for simulation of thermal coupling between heavy reflector and core barrel as well as core barrel and reactor vessel wall. In any case one has to consider a considerably reduced mechanical strength of these structures when compared to nominal operation conditions.

Basic differences in results appear when comparing temperature levels reached in lower core support structures up to the considered time in the transient. In case of MAAP and S/R5 calculations these structures are hardly heated up except for the immediate vicinity of the contact area with crusts of or directly with the molten pool. In so far axial core melt outflow scenarios appear improbable when identifying the calculated conditions as reliable. However, calculated results on basis of MELCOR indicate a considerable heat-up of lower core support structures and predict an early failure of this structure. In so far these results define boundary conditions which do not allow to disqualify the option of an axial core melt outflow scenario without more detailed analyses and evaluation of respective experimental information.

Common to all calculations is the fact that temperatures in the lower plenum remain small and that the remnant water level amounts to a value of 2.0 to 2.2 m at most. MELCOR calculations indicate the possibility that the water inventory is smaller, but there is hardly a chance to prove that these simulations are more reliable than the ones performed with MAAP or S/R5. The remnant water level for evaluation of premixing characteristics therefore has been chosen for all calculations to stay at the upper level of the lower core support plate independent on the considered core melt initiator. This value represents a conservative estimate in view of the expected real conditions once late core melt outflow scenarios are considered.

Interesting aspects for consequence evaluations of fuel coolant interactions in the lower plenum can be derived from calculated results characterising the thermodynamic state of reactor vessel volumes and the reactor coolant system as well as temperature levels reached in their enclosures. If one considers late core melt outflow scenarios the reactor coolant system is nearly empty from water other than in the pump U-leg which is still filled with nearly pure water in most of the calculated cases. Structure and piping temperatures are highest in the hot leg and in the surge line to the pressurizer and heated up slightly in steam generator tubes. This information about the state of the reactor system becomes of importance only if consequences of fuel coolant interactions are analysed under the condition that the upper head remains intact as well as the lower plenum enclosure. Then it needs to be analysed whether integrity of the primary system can be demonstrated and thus limit consequences of fuel coolant interactions solely to the primary system. Once these aspects become of importance some more precision on the respective states of the primary system could become necessary, including creep-rupture analysis of all primary enclosures circuits. This then needs to be provided on basis of other tools than system codes as well. However, that kind of an analysis was not the objective of the current evaluation.

2.4   Conditions of Core Material Outflow

One important boundary condition for the calculations is the postulated failure mode of the enclosure of the molten pool and the direction of core material outflow, i.e. axially downward through the lower core support structure or radial outward through the heavy reflector and the core barrel. The second important boundary condition is the assumption on the density of the molten material draining into the water pool and the cross section along which the molten material drains into the water pool coherently. Thirdly it is necessary to define the driving mechanism for the melt flow. Integral codes like SCDAP/RELAP, MELCOR or MAAP do not provide sufficiently detailed information on theses aspects. Therefore respective conditions have to be defined independently from results of integral code calculations. However, boundary conditions should be defined coherently with the physical picture evolving from these integral calculations on the one side but coherently as well with observations from respective experiments on the other side.

From integral code calculation one does not get any other information on the driving mechanism for molten material drainage into the water in the lower inlet plenum than to assume gravity as the dominant driving mechanism. It is therefore decided to use this mechanism as the only driving mechanism initially.

Experiments simulating drainage of a superheated melt into a water pool show in a rather generic manner that the superheated melt and the water inventory normally gets separated from each other rather quickly, i.e. in a time period of a several seconds. This implies that calculations should consider an initial cross section for coherent drainage out of the molten pool area which could be established coherently in a similarly short time period .This limits the spectrum of assumptions on openings becoming available initially for molten material drainage if a thermally dominated failure mode is to be considered.. All experimental information on the qualitative behaviour of thermally progressing erosion fronts indicate that these mechanisms are leading to local incoherencies of the melt front progression. Consequently it seems reasonable to assume that coherent openings as consequence of thermal melt-through phenomena can not become much larger than the cross section of a few subassemblies in a time period of several seconds. The open question is mainly related to the behaviour of crusts in neighbouring subassembly positions if differential pressure loads are build-up subsequently. This topic has been dealt with parametrically because there is no chance to evaluate the involved physics deterministically.

The only exception of the assumption that the initial cross section for material drainage remains limited to the cross section of a few subassemblies could be deduced from a coherent structural failure of the core barrel as consequence of a creep fatigue failure mode at elevated temperatures under the weight load of the core melt. However even then it seems reasonable to postulate a cross section for a coherent material drainage which is considerably less than the free cross section of a timely increasing multiple of the circumference of the core barrel. This argument goes along a similar line as the one developed previously. The circumferencial temperature variation will prevent a coherent failure along the whole circumference in a time period less than a few seconds.

On basis of the arguments presented consequences of three base cases were evaluated what concerns coherent opening of cross sections for melt relocation. The first two cases postulate a downward directed drainage in the center of the core cross section and the third one a release of the molten core material in radial direction in most of the investigated cases homogeneously distributed along the circumference of the core barrel. The cases are defined as follows:

- cross section opening according to the equivalence of one plus eight half cross sections of neighbouring subassemblies where it is postulated that the cumulated cross sections become available coherently for material drainage of a compact jet of molten material

- the equivalence of about 14 cross sections of a subassembly where it is postulated that the density of the evolving jet corresponds to the porosity of the lower core support structure, i. e. corresponding to the as fabricated holes in the lower core support structure (33%).

- for definition of a failure mode in radial direction it is postulated that the core barrel fails along 20 cm height coherently at eight azimuthal positions providing openings of 10 cm width each. This would result in a free cross section equivalent to a porosity of the circumference of the core barrel which amounts to about 5 %.

In addition to the specification of the initial openings for molten material drainage into the lower plenum it is necessary to specify conditions characterising the behaviour of crusts in subassembly positions along which materials transport will not take place initially. This means that one has to specify whether crusts and blockages in subassemblies enclosing the molten pool initially can withstand differential pressure loads. This question cannot be evaluated deterministically. However it is assumed that this question represents a problem only for crusts being built – up at the lower end of the molten pool. In radial direction crusts are supported by the mainly intact parts of the heavy reflector and the core barrel. Therefore the question about the integrity of the radial boundary of the molten pool is determined by the integrity of neighbouring structures which is assumed to be maintained under the pressure loads being established as consequence of premixing in the lower plenum.

However, the situation is different in axial direction. Here crusts have been built-up close to the lower core support structure. This structure has holes which provide the possibility of establishing differential pressure loads on the crusts directly. At the time being there is no way to evaluate that problem deterministically. Therefore two cases were considered which bound the realistic behaviour: In one case one should assume that these blockages behave like a solid body with sufficient strength and in one other case one assumes that the blockages cannot withstand differential pressure loads and that permeability along these cross sections is as if 30 % of the cross sections of the wholes in the lower core support plate become available for materials transport and pressure wave propagation, but on a delayed time scale.

Table 2.1 Molten pool and enclosing crusts data for core melt initiator: LOOP (at Δt_{PR} after pool formation onset)

	Dim.	S/R5 m3.1 rel.D	S/R5 m3.1 rel. F	MAAP	MELCOR 1.8.3 SKWU	MELCOR 1.8.3 FZK/INR
T Δt_{PR}	h:mm.ss	4:36 no HR	4:05 * 1475 *	5:38 3780	5:32 4700	Total time 27800
Molten pool data: • composition	t	98	54,1	110	80	55
UO$_2$	t	71	42.8	81	78	46
ZrO$_2$	t	27	12.3	12	1	0.7
steel	t	-		13	-	0.4
Zr	t	-		14	1	8
• average temp. (or temp. Range)	K K	2770–2873	2840	2500-3100	2800	
maximum temp.	K	2873	2873	3100		2700
Crusts state&shape[1] Erosion rates	-	SS, fx	SS, fx	SS, f	SS, c	-
In radial direction (heavy reflector)	cm/s	-	-		-	
in axial direction lower core support grid	cm/s	-	-	0		
Vapor volume above molten pool						
Pressure temperature	MPa K	0.3 2750	0.42 1370	0.3 1570	0.33 2565	0.4 1600

-?- : no reliable value extractable,
n.a. not available up to report setup

[1]SS – solid, PS – porous, f – flat, c – curved, fx – flat in each channel

S/R5 calculation stopped due to steam overheating, to be continued.

Table 2.2 Status of structures in the immediate vicinity of crusts enclosing the molten pool for core melt initiator: LOOP (temperatures, molten and/or residual thicknesses)

	Dim	S/R5 m3.1 rel.D	S/R5 m3.1 rel. F	MAAP	MELCOR 1.8.3 SKWU	MELCOR 1.8.3 FZK/INR
Upper core plate and support columns	K	Not modeled	2300 1200	n.a.	2250	2000
Heavy reflector						
Upper third temperature residual thickness	K cm	--- ---	1000 initial	n.a. initial	1200 -	1200 initial
Middle third temperature residual thickness	K cm	--- ---	800 initial	800-1700 0 – initial	1350 -	1250 initial
Lower third temperature residual thickness	K cm	--- ---	500 initial		1850 -	1750 initial
Core barrel temperatures						
upper third middle third lower third	K K K		560 500 450	Com-bined with heavy reflector	950 950 950	900 900 900
Lower core support structures						
Temperature	K		490	480	1273	1273
residual thickness	cm		Initial	initial	0	initial

-?- : no reliable value extractable,
n.a. not available up to report setup

Core melt initiator: LOOP

Table 2.3   Thermohydraulic state of reactor vessel volumes and the reactor coolant system for core melt initiator: LOOP

	S/R5 m3.1 rel.D	S/R5 m3.1 rel. F	MAAP	MELCOR 1.8.3 SKWU	MELCOR 1.8.3 FZK/INR
reactor vessel downcomer and loop nozzles		$p = 0.42$ $T = 430$ $\alpha_{liq} = 0$	$P = 0.3$ n.a. n.a.	$p = 0.33$ $T = 800$ $h_{liq} = 0$	$P=0.4$ $T=750$ $h_{liq}=0$
Reactor pressure lower plenum					
temperature pressure remnant water level		420 0.42 $\alpha_{liq} = 0,8$ 2	< 500 0.3 2,2	410 0.33 1,23	1100 0.4 1.4
RPV upper dome		$T = 430$ $\alpha_{liq} = 0$	$T = 1550$ $h_{liq} = 0$	$T = 835$ $h_{liq} = 0$	$T = 680$ $h_{liq} = 0$
Piping Loop					
hot leg single triple		658K,α_{liq}=0.1 860K, α_{liq}=0	1220K,h_{liq}=0 570K, h_{liq}=0	970K,h_{liq}=0.3 550K, h_{liq} = 0	1020K, h_{liq}=0 600K, h_{liq} = 0.
steam gen. single tubes triple		580K, α_{liq}=0 -----	n.a. n.a.	n.a. n.a.	590K, h_{liq} = 0 580K, h_{liq} =0
cold leg single triple		430K, α_{liq}=0 440K, α_{liq}=0	520K, h_{liq} =0 470K, h_{liq}=0	455K, h_{liq} = 0 460K, h_{liq} = 0	460K, h_{liq} = 0 440K, h_{liq} = 0
pump single U-leg triple		420K 424K, α_{liq}=0.5		415K h_{liq} = 1.95 415K, h_{liq} = 1.55	410K h_{liq} = 2.0 410K h_{liq} = 1.8
Pressurizer surge line		430K - 588K	620K h_{liq} = 1.5	T_{liq}=400 T_{vap}=630 h_{liq} = 9.9	900K h_{liq} = 0

-?- : no reliable value extractable,
n.a. not available up to report setup

Pressure value in [MPa], temperature in [K], and liquid volume fraction [-]

Core melt initiator: LOOP

Table 2.4   Characteristic temperature levels of reactor coolant system enclosures for core melt initiator: LOOP

	Dim	S/R5 m3.1 rel.D	S/R5 m3.1 rel. F	MAAP	MELCOR 1.8.3 SKWU	MELCOR 1.8.3 FZK/INR
reactor vessel lower plenum	K		420	410	420	420
reactor vessel shell region						
lower third	K		440	n.a.	520	520
middle third	K		450	n.a.	580	620
upper third	K		460	n.a.	640	640
upper support plate	K		681	n.a.	750	900
reactor vessel upper dome	K		550	n.a	600	610
Piping Loop						
hot leg single	K		1300	1165	820	920
triple	K		1200	505	550	600
steam gen. single	K		580	566	580	590
tubes triple			590	570	570	585
cold leg single	K		-	490	470	470
triple			470	470	470	440
Pump single	K		-	n.a.	420	410
U-leg triple	K		425	n.a.	420	410
pressurizer	K		538	670	430	620
Surge line			1400			

-?- : no reliable value extractable,
n.a. not available up to report setup

Core melt initiator: LOOP

Table 2.5   Molten pool and enclosing crusts data for core melt initiator: LBLOCA (surge line break) (at Δt_{PR} after pool formation onset)

	Dim.	S/R 5 m3.1 (Rel. F)	MAAP	MELCOR 1.8.3 SKWU	MELCOR 1.8.3 FZK/INR
t	h:min	0:53	1:30	1:01	Total time
Δt_{PR}	s	1200	3721	2000	3200
molten pool data:	t	122 (138)	110	60	45
• composition					
UO_2	t	94	84	56	40
ZrO_2	t	28	9	1	0.3
steel	t	16	14	-	0.4
Zr	t	(ICARE: HR)	17	3	4.3
• average temperature	K	-	2500 - 3100	2700	
maximum temp.	K	2859 2873	3100		2300
crusts state and shape[1]	-	SS, fx	SS, f	SS, c	-
erosion rates					
in radial direction (heavy reflector)	cm/s	0.0027 (ICARE)	0.02	-	
in axial direction lower core support grid	cm/s	0	0		
vapour volume above molten pool					
pressure	MPa	0.21	0.3	0.13	0.18
temperature	K	2780	2500	2400	1500

-?- : no reliable value extractable,
n.a. not available up to report setup

[1]SS – solid, PS – porous, f – flat, c – curved, fx – flat in each channel

Table 2.6   Status of structures in the immediate vicinity of crusts enclosing the molten pool for core melt initiator: LBLOCA (surge line break), (temperatures, molten and/or residual thicknesses)

	Dim	S/R 5 m3.1 (Rel. F)	MAAP	MELCOR 1.8.3 SKWU	MELCOR 1.8.3 FZK/INR
upper core plate and support columns	K	1740 - 1910	n.a.	2400	2000
Heavy reflector					
upper third temperature	K	1700	800	1100	1400
residual thickness	cm	initial	initial	-	initial
middle third temperature	K	>2000	800 - 1700	1400	1200
residual thickness	cm	initial	0 - initial	-	initial
lower third temperature	K	1900	550	1000	1200
residual thickness	cm	initial	initial	-	initial
core barrel temperatures					
upper third	K	1100	combined	540	570
middle third	K	1200	with	535	560
lower third	K	900	heavy reflector	530	550
lower core support structures					
Temperature	K	630-1020	420	1273	1273
residual thickness	cm	initial	initial	0	initial

-?- : no reliable value extractable,
n.a. not available up to report setup

Core melt initiator: **LBLOCA (Surgeline Break)**

Table 2.7   Thermohydraulic state of reactor vessel volumes and the reactor coolant system for core melt initiator: LBLOCA (surge line break)

	S/R5 m3.1 (Rel. F)	MAAP	MELCOR 1.8.3 SKWU	MELCOR 1.8.3 FZK/INR
reactor vessel downcomer and loop nozzles	p = 0.21 500K - 800K	p = 0.3 n.a. n.a.	p = 0.13 580K h_{liq} = 0	P = 0.19 590K, h_{liq}= 0
reactor pressure lower plenum				
temperature pressure remnant water level	390K 0.215 2	< 450K 0.3 2	380K 0.13 0.9	400K 0.19 1.3
reactor pressure vessel upper dome	460K	n.a.	720K	620K
Piping Loop				
Hot leg single triple	1600K, α_{liq} =0 1000K, α_{liq} =0	n.a. n.a.	1500K,h_{liq}=0.3 1050K, h_{liq}=0	890K, h_{liq}=0 630K, h_{liq}=0
steam gen. single tubes triple	550K, α_{liq} =0 550K, α_{liq} =0	n.a. n.a.	--- ---	550K, h_{liq}=0 550K, h_{liq}=0
cold leg single triple	480K, α_{liq} =0 470K, α_{liq} =0	n.a. n.a.	500K, h_{liq} = 0 490K, h_{liq} = 0	530K, h_{liq}=0 530K, h_{liq}=0
pump single U-leg triple	480K, α_{liq}=0.7 450K, α_{liq}=0.9	n.a. n.a.	390K,h_{liq}=0.73 400K,h_{liq}=0.08	450K,h_{liq}=0.9 450K,h_{liq}=1.0
Pressurizer surge line	600 615	n.a. n.a.	590K, h_{liq} = 0	590K, h_{liq}=0

-?- : no reliable value extractable,
n.a. not available up to report setup

Pressure value in [MPa], temperature in [K], and liquid volume fraction [-]

Core melt initiator: **LBLOCA (Surgeline Break)**

Table 2.8   Characteristic temperature levels of reactor coolant system enclosures for core melt initiator: LBLOCA (surge line break)

	Dim.	S/R 5 m3.1 (Rel. F)	MAAP	MELCOR 1.8.3 SKWU	MELCOR 1.8.3 FZK/INR
reactor vessel lower plenum	K	400	420	400	410
reactor vessel shell region					
lower third	K	470	n.a.	450	480
middle third	K	670	n.a.	500	520
upper third	K	650	n.a.	550	540
upper support plate	K	560	n.a.	700	750
reactor vessel upper dome	K	525	n.a.	570	580
Piping Loop					
hot leg single	K	900	n.a.	1000	890
triple	K	670	n.a.	720	580
steam gen. single	K	550	n.a.	550	550
tubes triple		560	n.a.	550	550
cold leg single	K	530	n.a.	515	520
triple		540	n.a.	535	520
Pump single	K	550	n.a.	400	390
U-leg triple	K	550	n.a.	410	390
pressurizer	K	600	n.a.	600	600
surge line	K	615			

-?- : no reliable value extractable,
n.a. not available up to report setup

Core melt initiator: **LBLOCA (Surgeline Break)**

Table 2.9   Molten pool and enclosing crusts data for core melt initiator: SBLOCA
(at ΔtPR after pool formation onset)

	Dim.	S/R5 m3.1 (Rel. F) [epr2*]	S/R5/ m3.2 irs [epr2#]	MAAP	MELCOR 1.8.3 SKWU	MELCOR 1.8.3 FZK/INR
T	H:min.	4:43	4:35	9:24	3:12	Total time
Δt_{PR}	S	722	1777	7740	3500	10800
molten pool data: • composition	T	43.0	83.7	110	47	32.5
UO_2	T	31.9	55.2	83	40	26
ZrO_2	t	11.1	10.7	15	7	1.5
steel	t		(1.3 ucpl)	16	-	0.2
Zr	t		0.8	12		4.8
• average Temp.	K	2818	2873	2500 - 3100	2750	2600
Maximum Temp.	K	2873	2975	3100		
Crusts state and shape [1]	-	SS, fx	SS fx	SS, f	SS, f	-
erosion rates						
in radial direction (heavy reflector)	cm/s	-	-	0,01	-	-
in axial direction (lower core support grid)	cm/s	-	-	0,02		-
Vapour volume above molten pool						
Pressure	MPa	0,28	0,22	0,3	2,2 (?)	0.5
temperature	K	2688	2727	2300	1945	2000

-?- : no reliable value extractable,
n.a. not available up to report setup

[1]SS – solid, PS – porous, f – flat, c – curved, fx – flat in each channel

*Data from S/R5 only for the EPR-2 initial conditions, Pool has not yet reached one of the envelopings, calc continued.

Data from S/R5 only for the EPR-2 initial conditions.

Table 2.10 Status of structures in the immediate vicinity of crusts enclosing the molten pool for core melt initiator: SBLOCA (temperatures, molten and/or residual thicknesses)

	Dim.	S/R5 m3.1 (Rel. F) [epr2*]	S/R5/ m3.2 irs [epr2#]	MAAP	MELCOR 1.8.3 SKWU	MELCOR 1.8.3 FZK/INR
upper core plate and support columns	K	2100 1000	2570 1100	n.a.	2000	1750
heavy reflector						
upper third temperature residual thickness	K cm	1190 initial	1424 initial	n.a. initial	1200 -	1050 initial
middle third temperature residual thickness	K cm	890 initial	1400 initial	700-1700 0 – initial	1200 -	1250 initial
lower third temperature residual thickness	K cm	480 initial	540 initial	n.a. initial	700 -	1200 initial
core barrel temperatures						
upper third middle third lower third	K K K	475 450 420	700 650 450	combined with heavy reflector	730 730 650	980 980 960
lower core support structures						
temperature residual thickness	K cm	450 initial	397 initial	500–1700 0 – initial	1273 0	1273 initial

-?- : no reliable value extractable,
n.a. not available up to report setup

Core melt initiator: **SBLOCA (46 cm^2)**

Table 2.11 Thermohydraulic state of reactor vessel volumes and the reactor coolant system for core melt initiator: SBLOCA

	S/R5 m3.1 (Rel. F) [epr2*]	S/R5/ m3.2 irs [epr2#]	MAAP	MELCOR 1.8.3 SKWU	MELCOR 1.8.3 FZK/INR
Reactor vessel downcomer and loop nozzles	p = 0.28 T = 580 α_{liq} = 0	P=0.22 T = 623 α_{liq} = 0	p = 0.3 T = n.a. h_{liq} = 0	p = 2.2 T = 600 h_{liq} = 0	P = 0.5 T = 500 h_{liq}=0
reactor pressure lower plenum					
temperature pressure remnant water level	410 0.29 2.2	398 0.22 1.99	< 450 0.3 2	490 2.2 1.7	480 0.5 1.5
reactor pressure vessel upper dome	790-870	770-960	n.a.	T = 605	1080

Piping   Loop
 Hot leg   single
                   triple
 	
 steam gen. single
 tubes: triple
 	
 cold leg   single
                   triple
	2000K, α_{liq}=0 1700K, α_{liq}=0
	
	 390K, α_{liq}=0 -?-
	
	 520K, α_{liq} =0 500K, α_{liq} =0
		1520K 805K
		
		 396 515
		
		 591 403
			1200K, h_{liq} = 0 ? K, h_{liq} = 0
			
			 400K 450K
			
			 n.a. n.a.
				590K,h_{liq}=0.05 522K, h_{liq} = 0
				
				 --- ---
				
				 610K, h_{liq} =0.3 490, h_{liq} = 0
					950K, h_{liq}=0 900K, h_{liq}=0
					
					 480K, h_{liq}=0 480K, h_{liq}=0
					
					 800K,h_{liq}=0.1 800K, h_{liq}=0

Pump single U-leg triple	410, α_{liq} = 0 460, α_{liq} = 0	397, α>0.9 397, α>0.7	n.a. n.a.	500K, h_{liq}= 2.9 470K, h_{liq}= 2.5	520, h_{liq}=2.0 630. h_{liq}=1.0
Pressurizer Surge line	1100 1500	1250 1470	n.a.	650 h_{liq} = 0	T =420 h_{liq}=0

-?- : no reliable value extractable,
n.a. not available up to report setup

Pressure value in [MPa], temperature in [K], and liquid volume fraction [-]

Core melt initiator: **SBLOCA (46 cm^2)**

Table 2.12   Characteristic temperature levels of reactor coolant system enclosures for core melt initiator: SBLOCA

	Dim	S/R5 m3.1 (Rel. F) [epr2*]	S/R5/ m3.2 irs [epr2#]	MAAP	MELCOR 1.8.3 SKWU	MELCOR 1.8.3 FZK/INR
reactor vessel lower plenum	K	410	398	<500	600K, $h_{liq} = 0$ p = 2.2	450
reactor vessel shell region						
lower third	K	410	450	n.a.	490K	600
middle third	K	420	454	n.a.	2.2	680
upper third	K	420	460	n.a.	1.7	700
upper support plate	K	560	515 - 610	n.a.	605K	1200
reactor vessel upper dome	K	520	541	n.a.		660
Piping Loop						
hot leg single	K	1200	787	1100	590K, h_{liq}=0.05	790
triple	K	600	450	450	522K, $h_{liq} = 0$	680
steam gen. single	K	400	397	390	-?-	430
tubes triple	K	-?-	516	450	-?-	430
cold leg single	K	-?-	506	n.a.	610K, h_{liq}=0.3	650
triple	K	560	443	n.a.	490K, $h_{liq} = 0$	500
pump single	K	550	396	n.a.	500K, h_{liq}=2.9	470
U-leg triple	K	560	546	n.a.	470K, h_{liq}=2.5	450
Pressurizer surge line	K	630 1200	668 1437	n.a.	650 $h_{liq} = 0$	480

-?- : no reliable value extractable,
n.a. not available up to report setup

Core melt initiator: **SBLOCA (46 cm^2)**

3 Short description of premixing codes and status of validation

3.1 The TRITHYD-application of the MC3D-code

MC3D is a compressible semi-implicit Eulerian multiphase flow computer code developed by CEA (Grenoble) [1, 2, 3]. It is based on a common kernel (including inputs and outputs, a balance and transport equation solver, time step management,...) and on several applications. The set of continuity, momentum and energy equations is solved by a semi-implicit method. The momentum equations are written in a non-conservative form on a staggered mesh in such a way that new time level velocities are expressed as function of new pressures and old other fields. Using that result the velocities can be eliminated from the mass and energy equations. They are written in a conservative form on cell-centered control volumes. For the options used in reactor calculations for the present report all equations are discretized using the first order donor-cell method. The non-linear system of equations is solved by a Newton-Raphson iteration procedure.

Molten material coolant mixing in experiments and in the late phase of a PWR severe accident can be studied with a three field (TRITHYD: liquid water, vapour, fuel droplets) or a four field (PREMEL:liquid water, vapour, fuel droplets, fuel jet with surface tracking) application. For all EPR-calculations we used the three field application. Nearly in all cases it is assumed that the molten material is discharged from porous regions in the failed structure. That means that no compact jet is formed to enter the water pool. Another reason not to use the four field application is that the status of verification and validation is not as sophisticated as in the case of the three field application.

Each field can exchange momentum and energy with the other fields. The exchange of mass is limited to the fields of water and steam. Mass and heat transfer are coupled by a thermal balance on the liquid vapour interface. Melt droplets can undergo fragmentation, which is described through an interfacial area transport equation. The pressure is uniform within one cell. The viscous diffusion has not been taken into account and heat transfer to structures is excluded. Radiation heat transfer is restricted to the cell considered.

During application of MC3D-TRITHYD to premixing experiments like QUEOS [4], FARO [5], and PREMIX [6] problems appeared, which are related to numerical difficulties, simplified modelling of physical phenomena and insufficient precision of knowledge of experimental boundary conditions. To get more insight into numerical characteristics of MC3D calculations a serie of test cases were investigated. Results are reported in [7]. For the present calculations the version 3.1 (September 1997) was used including some changes made by IRS, which are partly described in [7]. The QUEOS experiments, which give low evaporation rates at low pressure (1 bar) and do not cover the phenomena of fragmentation can be calculated with satisfying precision for the first 0.2 s as shown for QUEOS12 in Figure 3.1. For later times a large pressure peak is calculated caused by water pushed into the cross-section outlet. The FARO-experiments at high pressures like the L-14 test (50 bar) defining the international standard problem ISP-39 [8] can be recalculated to give a satisfactory pressure curve using an initial melt drop diameter of 7 mm (see Figure 3.2). The total surface of fragments found at the end of the experiment is underestimated.

All calculations for the EPR are done at a low pressure level of 2.5 bar, so validation of the code for low pressure experiments becomes very important. PREMIX is an experimental program to investigate mixing behaviour of hot alumina melt which is discharged into water at low pressure levels [6]. All calculations for 1 bar experiments show that a large vapour bubble is created around the penetrating melt. Water is pushed strongly away from the melt

reducing interaction and leading to an early blocking of the outlet cross-section. Those effects are not seen in the experiments. A lot of calculations were made changing boundary conditions and code parameters to cover a variety of unknown experimental conditions and poorly modelled physical processes. The result is that vapour bubble expansion and strong vapour outlet blocking are generic effects in the calculation of low pressure experiments with large vapour production. This is confirmed by first calculations for FARO low pressure experiments like L-27 and L-28. The reason is the large difference in density between water and vapour. The mass of 100 g vapour needs place of 167 kg water (1 bar). If the transport of vapour from the mixture zone to the outlet cannot be described with high precision, the balance of vapour production and removal from the interaction zone can lead to an overestimation of vapour in the interaction zone pushing away water. That leads to some isolation of hot melt from cold water reducing premixing.

To overcome the problem of outlet blocking, an additional boundary condition is introduced around the outlet. Water is released at the top of the test chamber and the outlet is not disturbed by intense two phase flow. The amount of water released is some measure how strong water is removed from the interaction zone and how far we are from experimental conditions. It was seen that it is very important to simulate the fast radial expansion of the interaction zone, which was observed in the experiment. To reach such strong radial expansion is difficult with the present modelling. Three actions were taken to reproduce the experimental observations:

- smearing the melt jet by expanding the diameter by a factor of two
- start with large particles
- reduce the surface tension by a factor of about ten

So we start with a spray of large particles which have strong momentum coupling with its environment and high fragmentation rates due to low surface tension. This helps to transport more melt droplets in radial direction. The melt evaporates water at those locations resulting in some counter-pressure for the big bubble around the spray type jet. The graphics given in Figures 3.3 and 3.4 show the pressure curve and the integrated steam release dependent on time in comparison with the experimental curves of PM13 [9]. The good agreement of the calculation with those experimental findings is achieved by choosing the initial melt droplet diameter to 2 cm and using a droplet-droplet heat transfer model. About 110 kg water left the vessel during 0.5 s in the calculation, which is a lot for the short time. 220 kg water were missing after the whole experiment.

Main results relevant for the reactor calculations are:

- the displacement of water is overestimated
- the release of vapour from the mixture zone seems to be not correctly described
- the effect is non-conservative, because it leads to a stronger separation of melt and water reducing thermal interaction during premixing
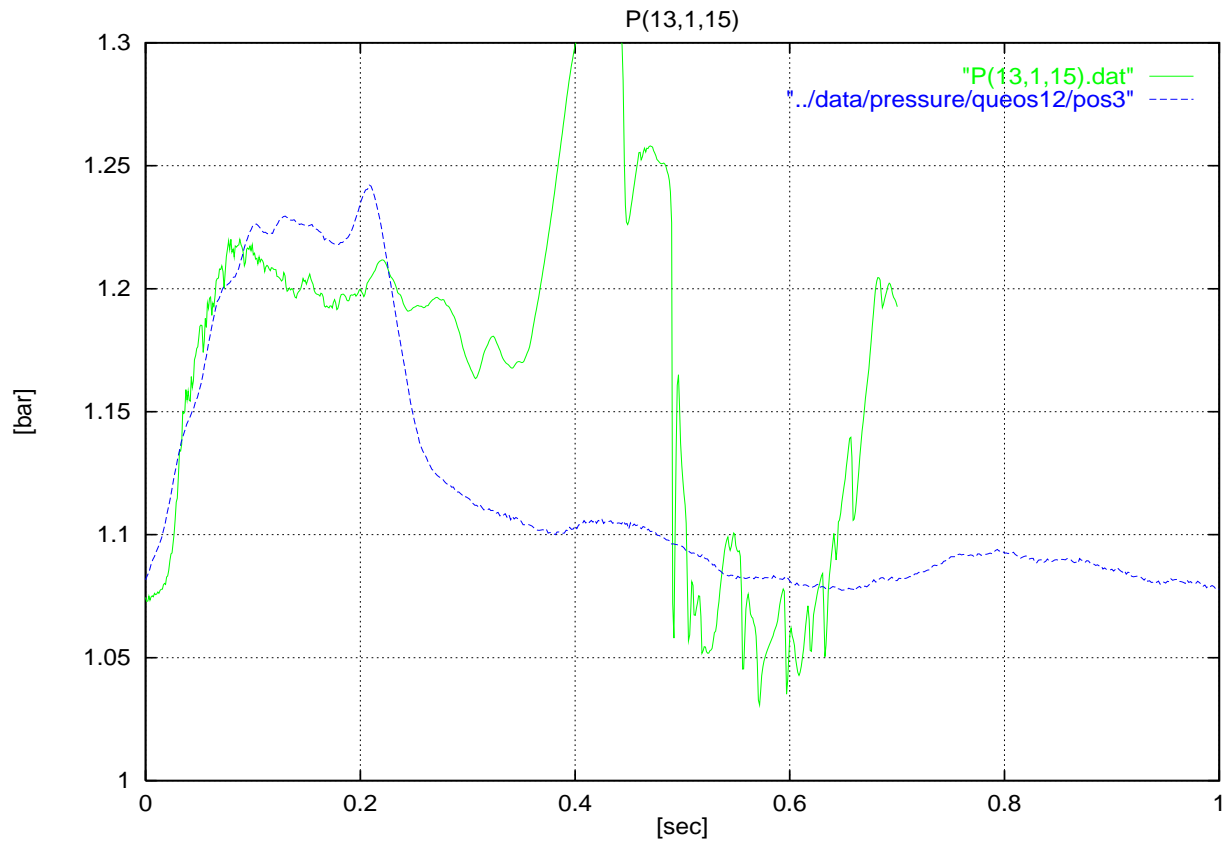
Figure 3.1   Calculated (P(13,1,15).dat) and measured pressure curve in QUEOS12
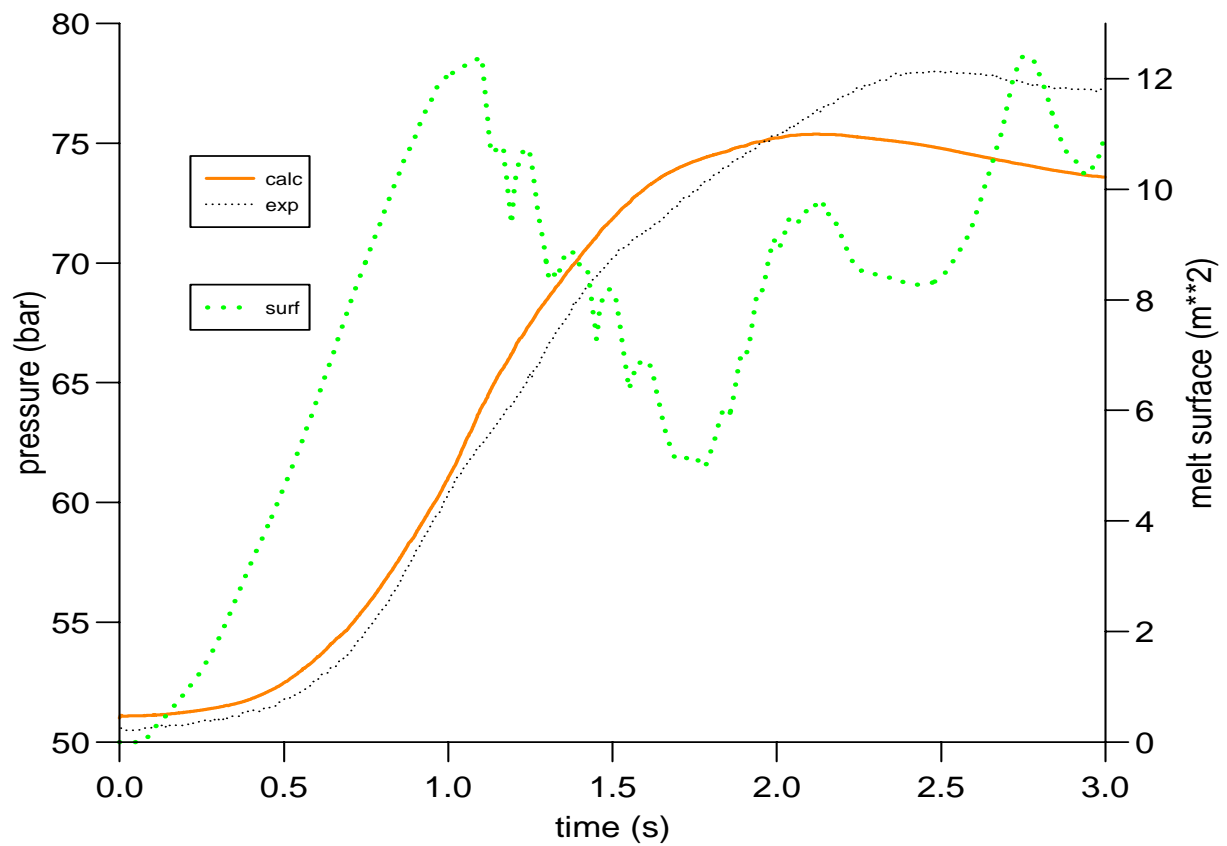

Figure 3.2   Pressure in the gas dome and total heat transfer surface for FARO L-14
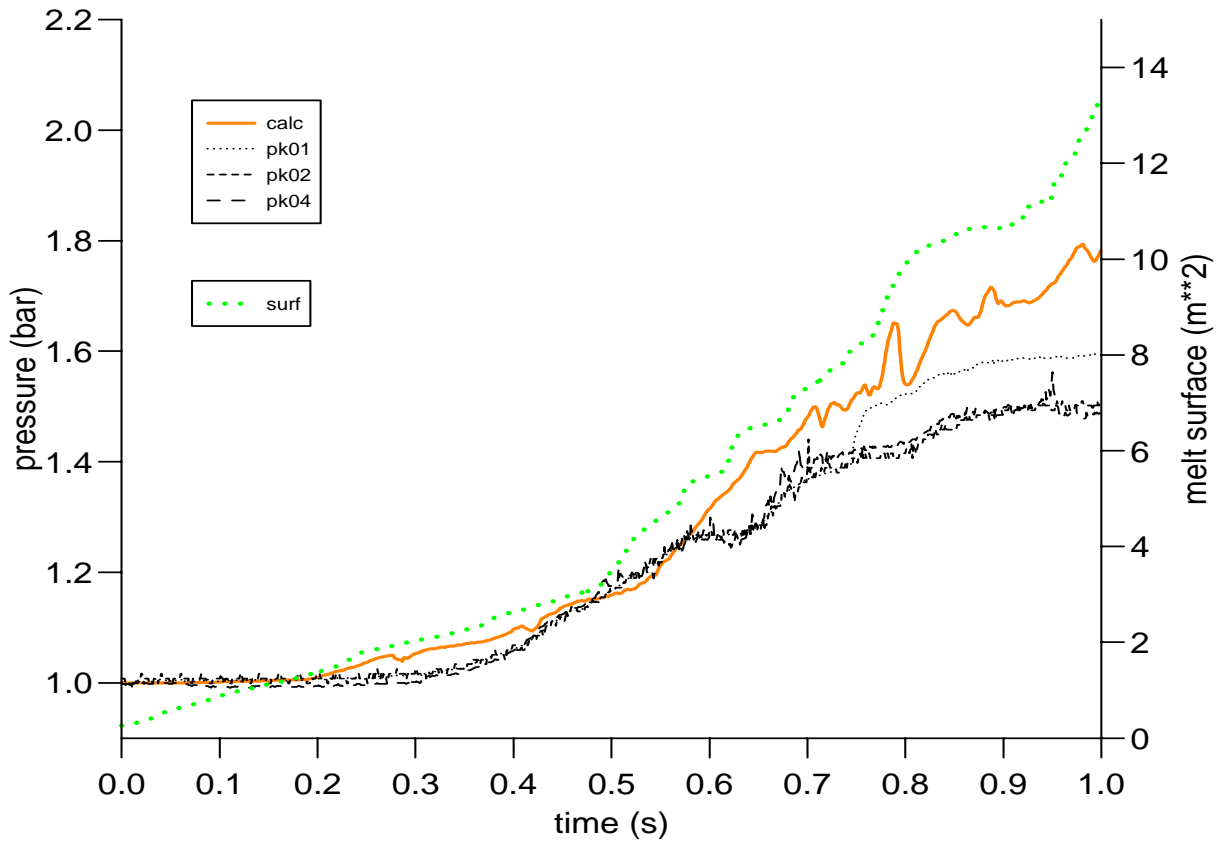
Figure 3.3　Pressure above initial water level and melt surface for PREMIX PM13 with water sink at the top
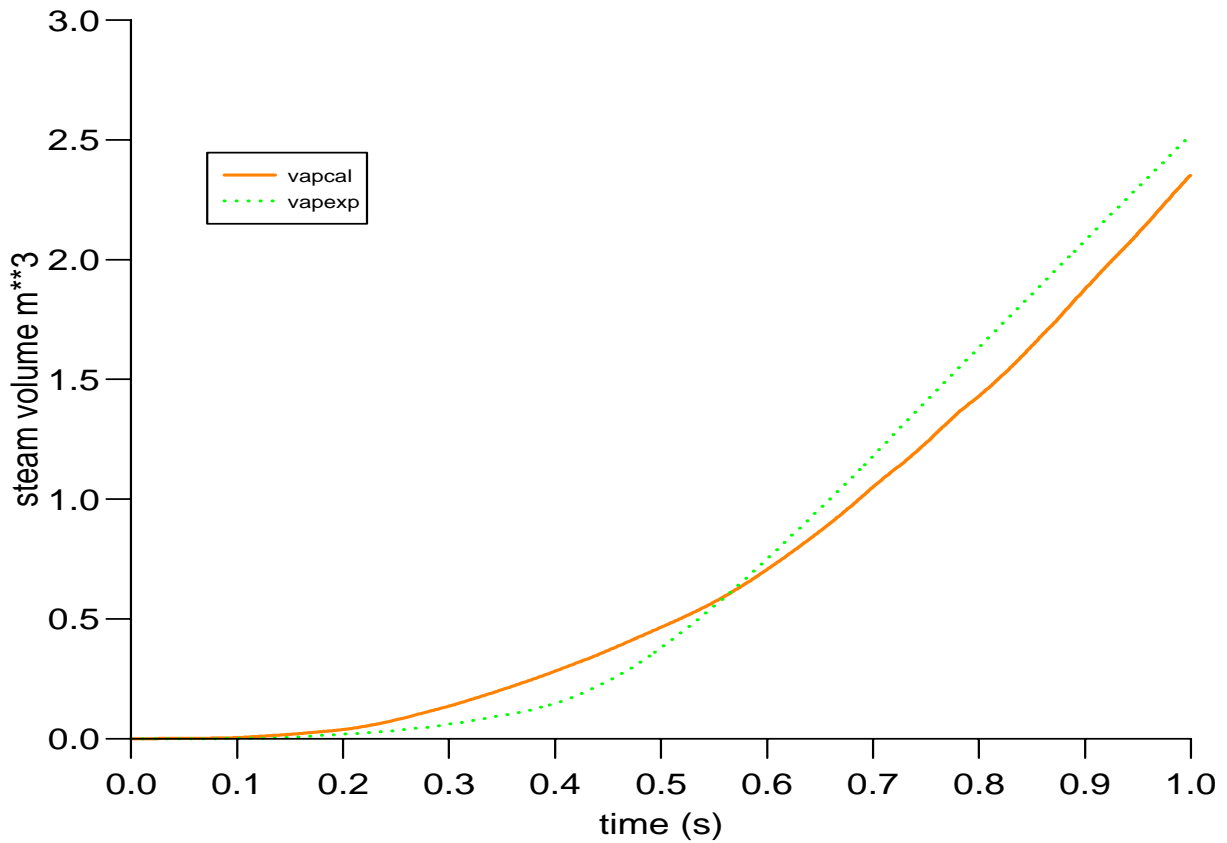

Figure 3.4　Integrated vapour volume released from the venting pipes for PREMIX PM13 with water sink at the top

3.2 MATTINA

The MATTINA (formerly IVA-KA) multifluid code [10-15] is being developed at the Forschungszentrum with the aim to analyse the premixing phase and - later - the propagation and expansion phases of steam explosions. This code uses three velocity fields to describe individual motions of gas (steam and/or air), liquid water and 'corium' (non-evaporating melt and/or solid particles). Each of the fields is characterised by conservation equations of mass, momentum, energy (expressed by enthalpy), and number density of particles (drops, bubbles, solid particles). The fields are coupled by assuming one pressure locally but the fields are not necessarily in thermal equilibrium with it or with each other. The physical processes, especially exchange of heat, mass and momentum between the fields are reflected by the source terms in the conservation equations. Whenever more than one field is present, a dispersed flow regime is assumed (mainly on basis of the volume fractions) and correlations for exchange of mass, heat and momentum are applied which are appropriate for that flow regime and the actual pressure and temperature conditions. During premixing, melt dispersal including break-up of jets is a potentially important process but the corresponding modelling is still rather uncertain. Concerning drop fragmentation we are using fairly standard models, assuming the fragmentation to be finished when the melt has lost 60 % of its latent heat of melting. However, with only one field describing the corium and only one length scale for it locally, the break-up of jets can be modelled in some very crude way only. These models have to be tested in detail and to be verified against experimental data. In the present applications, corium entering water or gas filled spaces is usually assumed to be prefragmented into large drops with 5 cm diameter. Only in some cases an initial diameter of 5 mm has been assumed for comparison with corresponding MC3D calculations.

The conservation equations are solved using a simple first order spatial differencing scheme applying the donor cell approximation. Time differencing is implicit for pressure propagation and convection whereas the source terms are evaluated explicitly. Therefore time steps are automatically limited in such a way that transients of pressure or temperatures are followed closely. This sometimes leads to extremely small time steps and thus long computing times. For compensation a not too fine meshing is used with typically 10-cm widths. This, at the same time, has the advantage of reducing the undesirable effect of neglecting nonlocal heat transfer by radiation. In the present modelling, heat is transferred by radiation only within each mesh cell. This is adequate for the most important flow configurations, i.e. for melt drops floating within water under film boiling and dense aggregates of melt and water droplets with a high volume fraction of the latter. But if the melt and the water are separated by steam on the length scale of the meshing, this (most important) type of heat transfer is largely cut off. From this point of view, a somewhat larger mesh size is preferable. Of course, there is a trade off with numerical diffusion that grows with mesh size. But in the absence of steep density gradients moving across the grid, as would e. g. be the case at the forward and backward interfaces of a moving liquid slug, some numerical diffusion should be tolerable. Especially in the present application, numerical diffusion is expected to increase melt/water mixing which is conservative. Also, experience tells that e.g. cutting the mesh sizes a factor of two decreases numerical diffusion only slightly. Small mesh sizes above do not solve the problem.

From the beginning, code results have been compared with results of FARO tests then available, i.e. performed at an initial pressure of 50 bar [5]. Also, from the beginning, the calculational results have well reproduced [10, 11] the essential features of the experiments: absence of explosive pressure events and a slow pressure rise in the gas space to a long lasting pressure plateau, sometimes going through a not too pronounced local maximum at its beginning. On the other hand, amplitudes of pressure variations have initially been seriously underestimated. Still (with some fitting of input parameters) the code was the only one that blindly predicted [10] that the FARO base case test (L-11) could exceed a vessel pressure of 100 bar which it actually did (or better: would have done without the action of the pressure relieve valves). The latest state of FARO calculations is described in Ref. 14 on the example of test L-14, i.e. the International Standard Problem ISP-39 [15, 16], see also Figure 3.5: In the originally contributed calculation (Case A, performed with IVA-KA), the pressure rise started about 0.2 sec (40 %) too early, the rise rate was about correct initially, but levelled off too soon so that the local maximum was attained 0.6 sec (24 %) too early and was 25 % too low. When IVA-KA was replaced by MATTINA in which the energy equation is expressed with enthalpy instead of entropy, spurious pressure oscillations that had occurred within the melt jet after it left the release vessel disappeared and energy conservation became as excellent as mass conservation had already been. But the pressure history (Case C) didn't change much. Only after correcting a coding error that affected heat transfer from melt drops to water droplets, the pressure rise rate agreed with the experiment for a longer time before levelling off too early (and rather abruptly) so that the maximum now occurs 0.9 sec (36 %) too early, but is only 17 % too low (Case E).

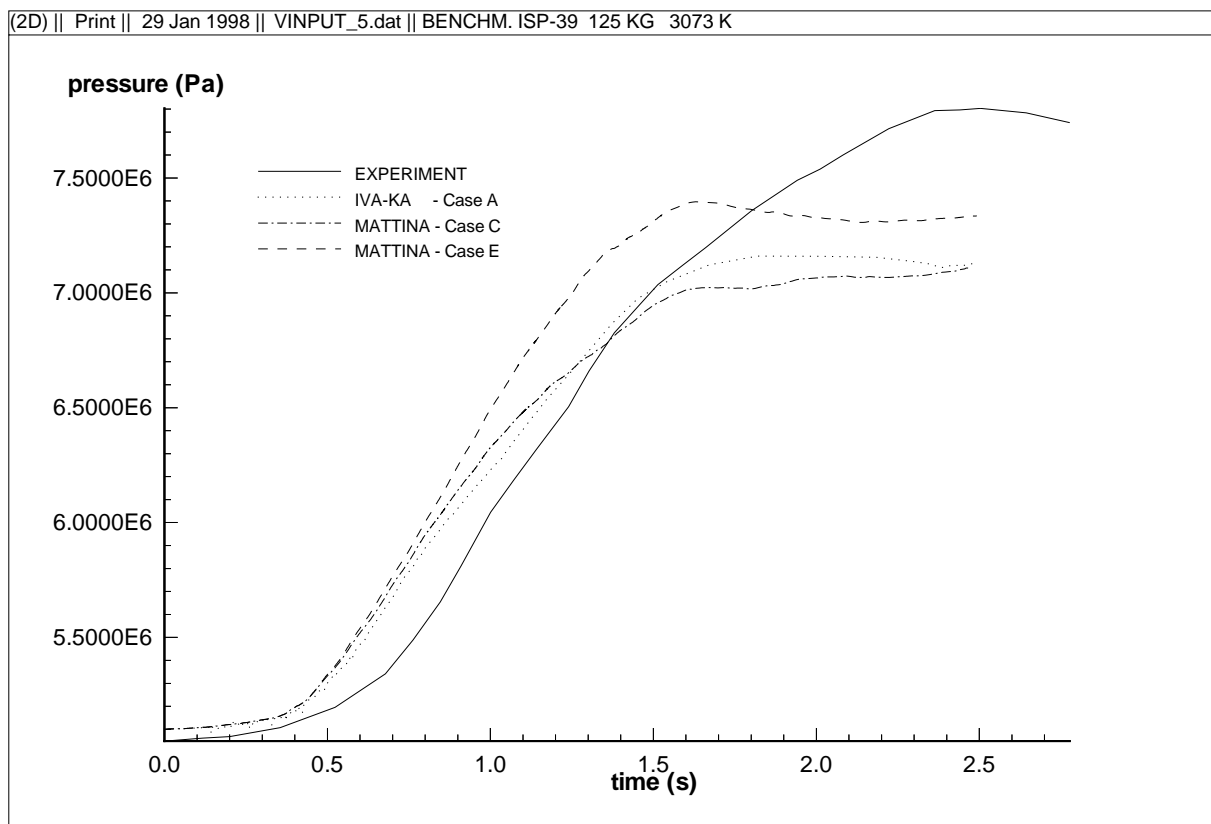(2D) || Print || 29 Jan 1998 || VINPUT_5.dat || BENCHM. ISP-39 125 KG   3073 K

Figure 3.5   Experimental and calculated pressure histories of FARO L-14

In the experiment, the first pressure maximum occurs at 2.4 sec. That the pressure doesn't rise until that time in any of our calculations might have to do with the fact that the melt is collecting on vessel bottom after 0.9 sec and that our heat transfer models are not appropriate for the melt-water configuration attained under these circumstances. On the other hand, the pressure rise starts too early in all our calculations. This may be due to the numerical diffusion that smears the leading edge of the melt jet on its 1.12 m fall towards the water surface.

Further verification was done with the QUEOS experiments [4, 13] that have been performed especially for this purpose. For minimising unknown initial and boundary conditions, these tests are performed with (large numbers of) hot solid spheres. In order to obtain test cases relevant for steam explosion conditions, high sphere temperatures and high solid volume fractions at entry into the water have been aimed at. Simulations of these tests with IVA-KA and MATTINA have shown very good agreement with experimental data [11, 13-15] if initial conditions of the particle entry into the water have been represented in the calculations as close to the experimental conditions as possible. For cold spheres (test Q-8) the effect of the momentum transfer from spheres to water when impinging onto it, was reproduced well in a qualitative sense, while the momentum transfer apparently was underestimated somewhat (too low pressure amplitudes, too short times) [13, 15]. For hot spheres (especially test Q-12 performed with 16.600 molybdenum spheres at 2300 K), the pressure histories under water and in the gas space as well as the steam flow rate were well reproduced [11, 13-15]. In calculation K [14, 15], the pressures remain somewhat too high after the main transient. This is due to assuming saturated water throughout in the beginning. Actually there was some water subcooled by more than 10 K at the bottom of the vessel. When this was taken into account in calculation V [13, 14], pressures agreed with the measured ones for a long time (0.7 sec). The agreement between experiments and calculations was similarly good for the distributions of spheres, gas and water in space [13-15]. This implies about correct motions of the leading edge of the particle cloud and that blockage of the steam vent opening by liquid water was not obtained in the calculations in accordance with the experiments. On the other side it is true that the completely different shapes of the particle clouds in tests Q-8 (cold) and Q-12 (hot) are not due to the different interactions after entry into the water but to the different conditions of entry that have been taken over from the experiments. Still, the code obviously is able to describe about correctly the multiphase flows caused by cold and very hot spheres in water. The second case also shows that the heat transfer is described about correctly and that the code is able to represent subcooled water in a reasonable way [13-15].

Simulating the steam and gas flow rate in the vent pipe is subject to additional difficulties: Firstly, gas flow starts already prior to the impact of the particles on the water due to the gas being pushed down from the delivery channel by the falling particles, the heating of the atmosphere above the water by them and, possibly, some evaporation caused by radiation to the water surface. This, of course, is not observed in the calculations that start at the time of particle impact on the water. Secondly, the quite complicated piping including some measurement devices results in an apparent pressure loss coefficient that isn't constant with time. In most cases this coefficient is high in the beginning, attains a minimum at about the time of maximum pressure (and flow) and then it increases again. All these values are higher than the steady-state value determined in the experiment. Fortunately, the pressure losses in the vent pipe are not modelled by a pressure loss coefficient in MATTINA but by geometrical obstructions (permeabilities < 1) that apparently have roughly a similar effect as the experimental setup. Only the (slow) increase of the apparent pressure loss coefficient after the pressure and flow maximum does not occur in the calculations. This might be (part of) the explanation of the calculated flow rate mostly being too high after the pressure maximum. But it was not considered reasonable to counteract this effect by parametrically increasing the

flow obstructions (decreasing the permeabilities) in the calculations. Similarly, the maxima of pressure and flow rate could be raised or lowered (in opposite directions) by varying (adjusting) the 'orifices.' This has not been done. The orifices have been chosen on the basis of the minimum of the apparent pressure coefficient.

In order to observe the effects of the falling particle mass on the flow rate prior to the contact with the water that was discussed above, a complete simulation of experiment Q-12 has been performed in which the release of the spheres from the sliding doors 1.3 m above the water surface was simulated [14-15] (case R). Here one must consider that the spheres initially form a layer less than 5 cm high on the sliding doors. Due to the finite opening time of these, the spheres would form an about 24 cm high column, 1.3 m below at water impact. With the hot spheres, there apparently occurs some (not fully understood) sticking so that the spheres have formed an about 53 cm high cloud in the experiment. In calculation R, the particle cloud was about 83 cm long when impacting the water, partly due to the finite opening time of the particles, but mostly due to numerical diffusion. This had a serious impact on the calculated pressures and flow rates. Above all, the pressure maximum in the gas space and correspondingly the maximum of the flow rate became too low. Apparently the gas 'chimney' through which the particles had entered the water in the experiment and in calculations K or V and which had allowed the steam created within the water to flow upwards (opposite to the particles) quite freely has not been created as effectively by the more elongated and therefore less dense particle cloud in calculation R. The only result that is better in this calculation is the (expected) earlier start of the gas flow. (Due to the strong numerical diffusion, evaporation even starts too early). But considered all in all, even this simulation doesn't look too bad when taking into account that it doesn't rely in any way on information on the particle entrance conditions taken from the actual experiment.

In a further step, experiment Q-48 has been simulated. This is an experiment in which the local void fraction has been measured with many probes in two horizontal lines 65 mm apart that crossed the centre of the test vessel at a height of 40 cm. The test has been performed with 10 kg of molybdenum spheres at 2000 K in a jet with 100 mm diameter and with saturated water. Here again the simulation started with a sphere column that was assumed in accordance with the experiment just above the water surface. As was to be expected, leading front penetration, pressure rise and the distribution of particles in the multiphase mixture where quite close to the experimental findings. The steam flow rate agreed with the measurement in the maximum but was somewhat too high later on, because the pressure losses were too low. The calculated local void conditions were compared with the experiment in two small volumes, one in the centre of the test vessel and the other one at a radius of 15 cm from the centre. Initially the calculation reproduced correctly that the void almost jumped to one in the centre immediately and rose more gradually at the outer position. But after about 0.2 sec both calculated values were close to one while the experimental values were between 0.4 and 0.5. So the void was overestimated by about a factor 2 during about half of transient. The comparison becomes slightly better when taking into account that actually the water was slightly subcooled (up to 2 K at the bottom) in the experiment. One can conclude that the void distribution is very sensitive to details of the modelling and that deviations from the experimental values are observed. It should be noted that this void condition is expected to have a strong influence on the 'efficiency' of steam explosions. Therefore it is used to decide whether corium present in the neighbourhood is to be considered as premixed or not – if such a decision is required.

The situation is much less satisfactory in the case of PREMIX [6] experiments. Here a straight forward simulation leads (until now) to completely wrong results. It is, e. g. observed that the melt penetrates for quite some time (0.2...0.4 sec) into the water without much pressure rise and a slow rise of the water surface. This phase is then followed by a steep pressure rise. In a standard simulation, however, the pressure would rise gradually from the very beginning and the water surface would rise besides the melt jet, thus blocking soon the initially 20 cm high vapour space between water and melt generator. This then prevents that steam can escape into the annular space besides the melt generator so that water is pushed into that gap. This is partly due to the fact that a 'standard' simulation does not describe properly the rather complicated (and not too well known) conditions of initial melt release and melt-water contact. In this case, the wrong behaviour has partly been avoided by assuming a slow start of the melt ejection and by spraying sideways the initial part of the melt as it is observed in the experiment. With such modelling the flow path towards the venting lines was blocked by water only intermittently. In this context it might also play a role that the actual situation is really three-dimensional while axial symmetry is assumed in the calculations. So one shouldn't expect too much from the simulations. But in addition (and one could say: in spite of that), the pressure rises much less steeply than in the experiment and still, after about 0.7 sec, the inlet to the venting lines (1.8 m above the initial water level) is blocked by liquid water which does not occur before 1.3 sec in the experiment (at one of the four vent lines initially). At 0.7 sec, the pressure is underestimated by about 40 % and the steam flow by about 55 %. An obvious explanation for such underestimation would be a too small heat transfer area (melt drop surface). In the calculation described here, we assumed an initial particle size of 60 mm in the melt 'jet' (similar to the orifice diameter) and relied on the code to describe the break-up into smaller drops. As a result we obtain the 'jet' with 60 mm particle diameter and particles of 6...7 mm diameter in the surrounding. This doesn't look unrealistic.

This problem needs further evaluation and at the moment it is not possible to judge on the fitness of MATTINA for premixing studies on the basis of comparisons with the PREMIX experiments. But a general conclusion is (until now) that the code always underestimates pressure built-up.

4   Geometry and boundary conditions for premixing calculations

To apply fuel coolant interaction codes like MC3D and MATTINA, geometry of the reactor pressure vessel has to be simplified strongly. Only main structure components important for the calculations are taken into account: the reactor pressure vessel wall up to coolant inlet and outlet pipes, heavy reflector and core barrel, lower core support plate and the flow distribution plate. There is one calculation in three dimensions only, all other cases are done in a two dimensional axial symmetric geometry. The spherical part (radius of about 2.7 m) of the reactor vessel forming the lower plenum is presented by steplike cylindrical walls. The important positions of structure components are given in Table 4.1. The lower core support plate has a volume porosity of 0.33 and a permeability of 0.33 in axial direction. The flow plate about 60 cm below that support plate is simulated by a single horizontal wall with a permeability of 0.39. In the 2D-calculations vessel inlet and outlet pipes are simulated by annular openings of the reactor vessel with a permeability of 0.16 representing the real cross sections of inlet and outlet nozzles. Coolant outlet is arranged above coolant inlet. At the beginning of the calculation the water level is located at the upper edge of the lower support grid. It is assumed that the core is totally molten and a pool of about 110t of corium (3000 K) is formed, blocked by the lower core support plate. The size of the failed region in the lower core support plate or the heavy reflector/core barrel depends on the cases to be considered. The thermodynamic properties of the molten corium are given in Table 4.2 using MC3D or MATTINA. Ambient pressure in the whole system is 2.5 bar initially and liquid water and vapour are assumed to be saturated (401 K). At the inlet and outlet openings a pressure boundary condition of 2.5 bar is used. That boundary condition is not changed during the whole transient. To see the influence of the system pressure an additional calculation for a specific case was performed with an enhanced system pressure of 4.5 bar.

4.1   MC3D-calculations

Figure 4.1 shows geometry and meshing used for MC3D 2D-applications. Calculations for simple test cases and premixing experiments have shown that the grid should be as fine as possible to limit numerical diffusion effects and to represent the governing equations more precisely. For MC3D we use 50 grid points in radial and 60 in axial direction. A fine meshing of 5 cm is used in the lower plenum, where the interaction takes place. In the upper part of the calculational region a much coarser mesh is taken. Due to limited computer resources the mesh of the 3D-application cannot be so fine. In radial direction 21 grid points and in axial direction 25 grid points are defined. 180° symmetry is assumed and the total circumference is devided into 16 segments. The four coolant inlet nozzles and the four coolant outlet nozzles are arranged in the 16 segments corresponding to the EPR design. In the region, where first interactions take place, a 5 cm discretisation in radial and a 10 cm discretisation in axial direction is used. The r-z-meshing is shown in Figure 4.2.

Investigating QUEOS [1] and PREMIX [2] experiments results depend strongly on the pressure loss at the outlet of test vessels. To investigate the influence of pressure loss at reactor vessel inlet and outlet parametric calculations with and without a pressure loss coefficient at open boundaries were done. There could also be a pressure loss in the narrow gap, where the downcomer is connected to the lower plenum. This effect is evaluated by another parametric calculation.

Pressure loss coefficient along the perforated flow distribution plate in the lower plenum can be estimated to give 5.3 for single phase flow [3]. Because such value is not validated for a multi-component multi-phase flow and there are no experiments for the global influence of a perforated plate on premixing a broad parametric investigation with different pressure loss coefficients was done.

Table 4.1   Positions of structures in the simplified EPR geometry

Structure	Axial Position (m)
Central bottom of reactor vessel	0.000
Flow plate	1.000
Lower edge of lower support grid	1.588
Upper edge of lower support grid	2.030
Upper edge of heavy reflector	6.755
Lower edge of coolant inlet	8.190
Upper edge of coolant inlet	8.970
Total height of calculational region	9.750
	Radial Position (m)
Radius of flow plate	1.750
Inner radius of heavy reflector	1.882
Outer radius of core barrel shell	2.145
Inner radius of reactor vessel	2.435

Table 4.2   Properties of Corium

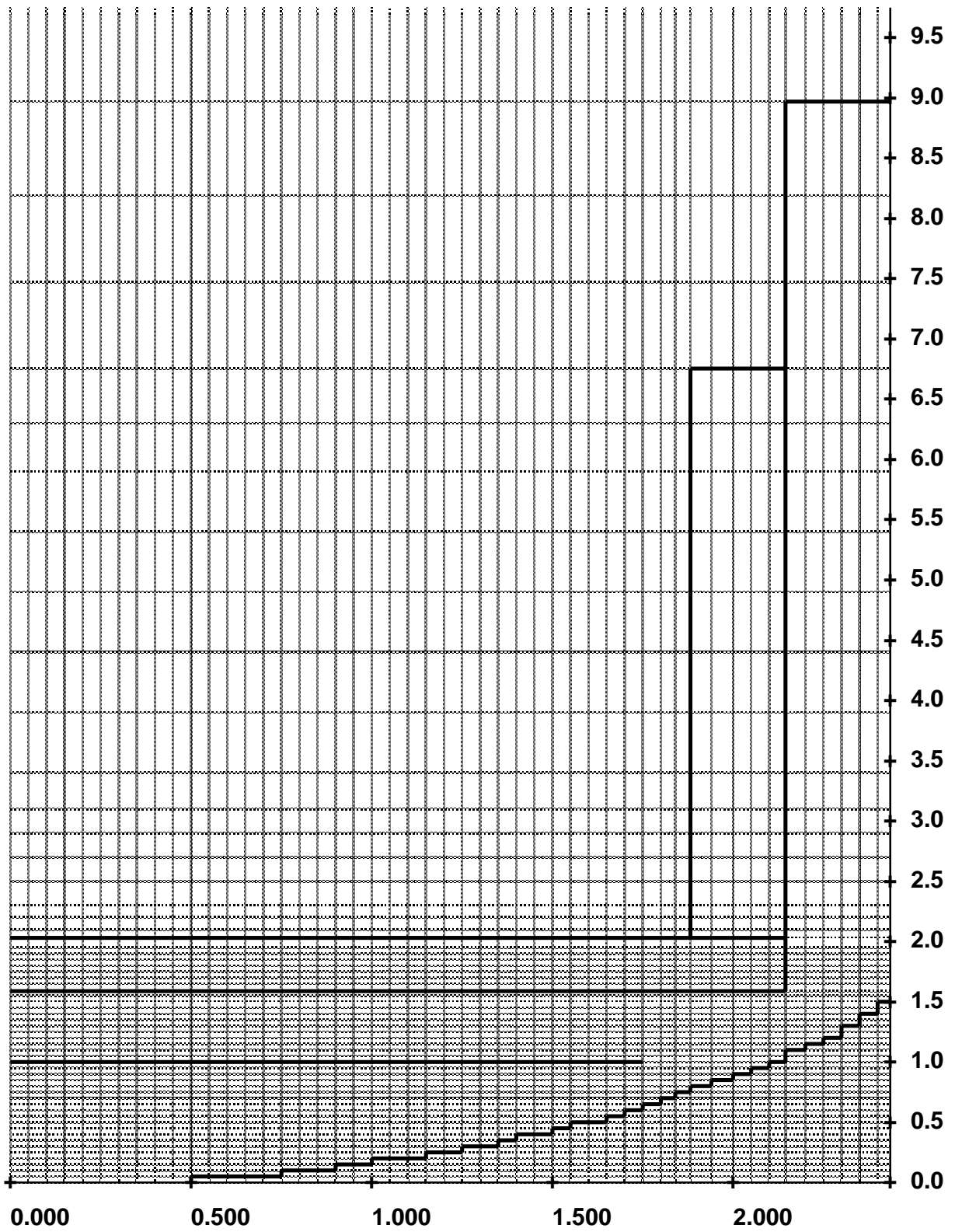| Code		MC3D	MATTINA
Density at 3000 K	(kg/m^3)	8000	7847
Thermal energy at 3000 K	(kJ/kg)	1547	1394
Solidus temperature	(K)	1955	2747
Thermal energy at solidus	(kJ/kg)	680	843
Liquidus temperature	(K)	2775	2747
Thermal energy at liquidus	(kJ/kg)	1430	1248
Cp at solidus	(J/(kgK))	430	420
Cp at liquidus	(J/(kgK))	520	579
Heat of fusion	(kJ/kg)	750	405
Surface tension	(N/m)	0.45	0.53

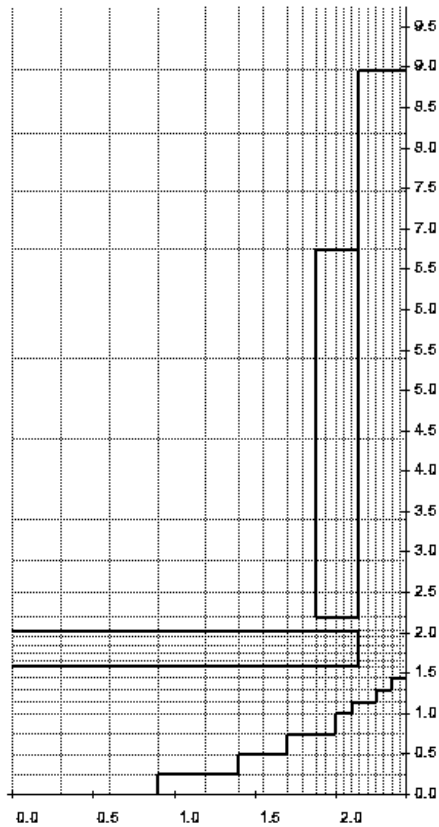Figure 4.1   Geometry and mesh for MC3D 2D-calculations

Figure 4.2   Geometry and mesh for MC3D 3D-calculations

4.2   MATTINA-calculations

Figure 4.3 shows the meshing used in the standard MATTINA calculations. The main difference to the MC3D meshing is that the cells used in the lower plenum and up to the upper surface of the lower core support plate have mostly dimensions of 10 cm in each direction as compared to 5 cm in the standard MC3D mesh. Above the lower core support plate, the axial division is equal in both meshings, but for MATTINA the width of heavy reflector and core barrel is represented by only three cells in radial direction and that of the downcomer by four cells (which applies in the lower plenum as well as far as it is concerned). The case shown here implies a sideways penetration of heavy reflector and core barrel shortly below the surface of the melt pool (the 5 % porosity may not show up in the figure). Figure 4.4 shows the lower part of the calculational domain in more detail, indicating as well where water (shaded) and melt (cross-hatched) are assumed initially.

36
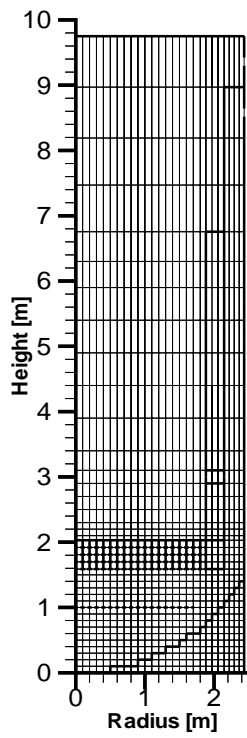
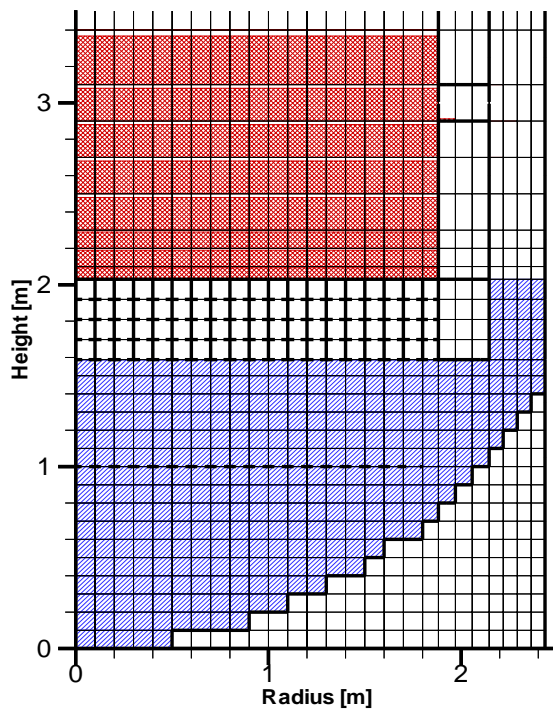Figure 4.3   Calculational mesh used for MATTINA

Figure 4.4   Calculational mesh used for MATTINA (detail and initial material
distribution)

37

The white lines at the top of the cells containing melt indicate that a volume fraction of $\alpha_3 = 0.9$ was assumed for the melt. Thus the total amount of melt assumed here is 107.7 t and that of the water is 17.3 t with 15.6 t in the lower plenum. The hydrostatic pressure surplus at the bottom of the melt pool is $\Delta p = \rho \, \alpha_3 \, g \, h = 7847.0 \times 0.9 \times 9.81 \times 1.37 \, \text{Pa} = 0.95 \, \text{bar}$.

5 Integral values for characterization of the premixing state

Premixing covers the interaction of melt with water before steam explosions might occur. There is an effective limit for the surface contact area between melt and water, because steam production causes the water to be displaced from the mixture region. This effect limits the amount of melt that could be involved efficiently in an explosion. Premixing calculations can be used to determine the maximum thermal energy input into the coolant. The distribution of melt and coolant in space can also influence how efficient an explosion could be, once it becomes triggered.

First of all the premixing state can be described qualitatively by the volume fraction distribution of melt and water in the lower plenum. The upper level of the lower plenum is defined at the lower edge of the core support grid. The development of pressure with time gives information about the strength of the interaction between melt and water. To compare different calculations and to estimate the probability and the efficiency of a steam explosion we define integral values, which characterize the premixing state. We use key values, which are evaluated as function of time:

- sum of mass and energy of melt in all cells with water volume fractions greater than 0.1 (premixed mass and energy)
- average volume fraction of water considering all cells with water volume fraction greater than 0.1 and melt volume fraction greater than 0.01
- amount of melt in the lower plenum
- amount of water in the lower plenum

The definition of premixed mass and energy is based on a very low value of the water volume fraction. The reason for that conservative evaluation is that calculation of low pressure premixing experiments results in a strong overestimation of voiding around the penetrating melt as described in Chapter 3. If the code would be more validated for low pressure experiments a water volume fraction limit of about 0.4 would be more reasonable. It is difficult to evaluate quantitatively whether it is too conservative to compensate the effect of excessive water displacement by using the limit value of 0.1. The integral values of water and melt available in the lower plenum give no information about the mixing state, but they are representative for the general potential of steam explosions.

6 Results of premixing calculations in case of axial melt relocation

6.1 MC3D – Results using the TRITHYD-application

6.1.1 Base case calculation

As base case for axial fuel relocation into the lower plenum, filled with saturated water at 2.5 bar, coherent failure of the molten pool crust with a radius of 0.45 m is assumed corresponding to about 14 cross sections of a subassembly. In that region the permeability of 0.33 of the lower core support plate forms the total cross section available for melt outflow, which is driven by gravity of a 110 t molten pool of corium. As initial droplet diameter the large value of 5 cm is used representing the order of magnitude of the holes in the support grid. For the flow plate at 1 m height in the lower plenum the pressure loss coefficient is set to zero. It limits the flow at that axial height, only. The droplet-droplet heat transfer coefficient for heat transfer from molten corium particles to water droplets is set to 3000 W/m^2/K derived from recalculations of experiments. The surface tension of corium droplets is set to the standard value given in Table 4.2 of Chapter 4.

Figures 6.1 – 6.8 show the initial conditions and the development of volume fractions of melt and water during the transient. The maximum problem time is 3 s. Until that time the premixing process has gone through a maximum and levels out at low values, as can be seen from transient mixed mass and energy curves (Figure 6.10). Material volume fraction plots show that a vapour bubble is created around the penetrating corium and water is pushed into the downcomer. After some time the vapour bubble reaches the orifice between downcomer and lower plenum and vapour escapes together with water in the direction of the coolant inlet. At the flow plate (axial level of one meter) some melt accumulates due to the reduction of flow. At the end a pool of melt develops at the bottom of the lower plenum and is covered by some amount of water in the outer radial zone.

Pressure variations are considered in more detail at two different locations: at the central bottom of the plenum and at the orifice from the downcomer to the lower plenum (Figure 6.9). The pressure at the bottom shows a smooth behaviour until about 0.65 s. Then strong oscillations are calculated. The reason for these oscillations is that the corium starts to fill up respective plenum nodes. Filling of cells with a nearly incompressible medium is a general numerical problem of multi-phase multi-component codes leading to strong pressure oscillations. In average the pressure rises by about 1 bar, where the largest part comes from the hydrostatic pressure of corium in the lower plenum. The pressure in the orifice is lower generally and does not show numerically caused oscillations. The maximum of premixing appears at about 0.7 s and reaches an energy value of 2.1 GJ equivalent to 1.4 t of corium (Figure 6.10). A few smaller peaks are found later in the transient. The first maximum is characteristic for all axial melt release scenarios. The process is determined by the competition between melt release into compact water and water displacement by evaporation. At the end evaporation dominates to separate melt from water. In Figure 6.11 the average water volume fraction in the mixing zone ($\alpha_{water} \geq 0.1$ and $\alpha_{melt} \geq 0.01$) is given depending on time. Corresponding to the maximum in premixing values around 0.6 are reached, later this value reduces to 0.3. In the same Figure the total melt surface is plotted. It starts at 430 m^2 due to the initial porosity of 0.1 for the melt pool of the molten core. A maximum of 630 m^2 is reached during the premixing process, then the melt surface area decreases, because the corium accumulates at the bottom of the plenum to become compact again. The reason for the increasing surface at the beginning is not fragmentation but formation of droplets through the porous plate with an initial diameter of 5 cm. In addition the void fraction at the surface of the large corium pool changes strongly (see Figure 6.1 and 6.5 indicating rather different melt

surfaces not reacting with water). Fragmentation as consequence of melt coolant interaction is very weak with a minimum diameter of about 3.5 cm. Figure 6.12 shows the transient development of water and melt inventory in the lower plenum. The melt is released with a nearly constant rate of 5.6 t/s and there is no strong feedback from pressure build up in the plenum. Water is pushed away by vapour produced during the interaction. At the end about 7 t of water remain in the lower plenum above the corium pool thus forming stratified conditions of the two liquids.

corium volume fraction
Time: 0.000000
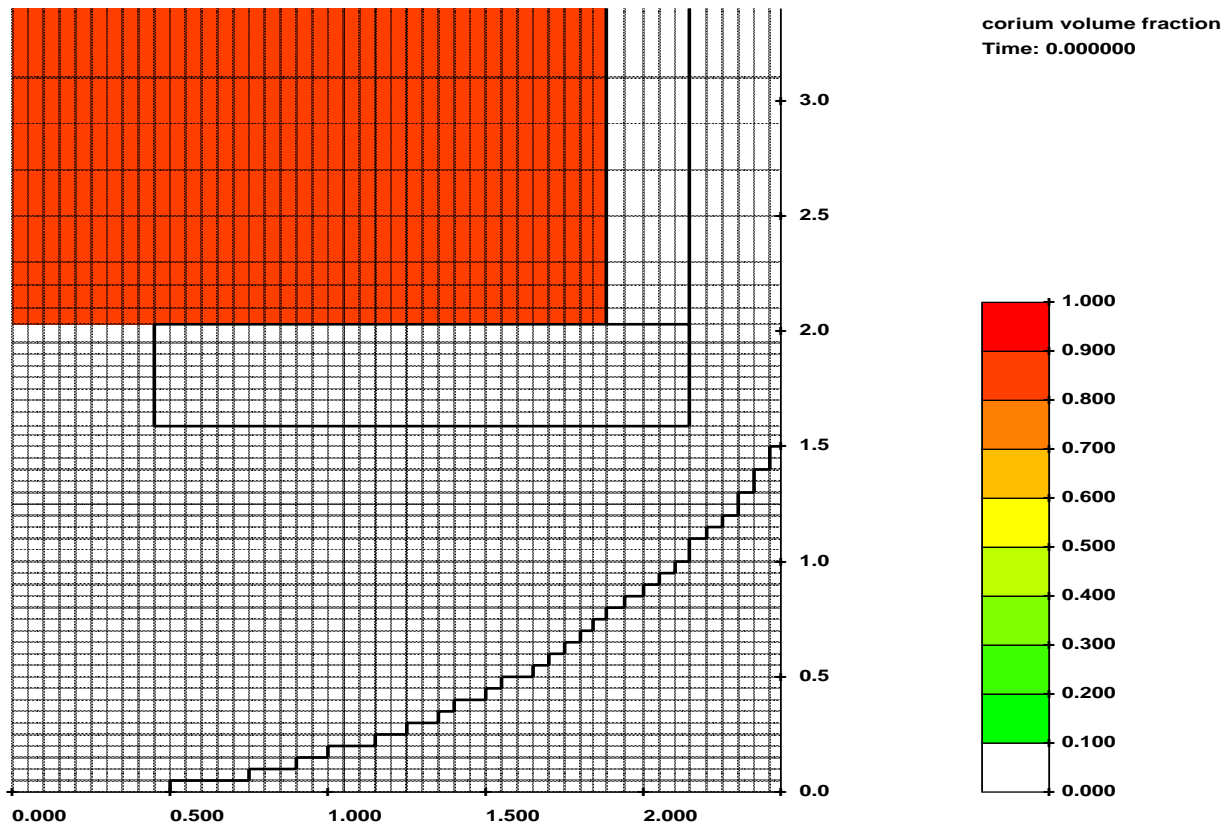
Figure 6.1 Initial volume fraction of corium

water volume fraction
Time: 0.000000
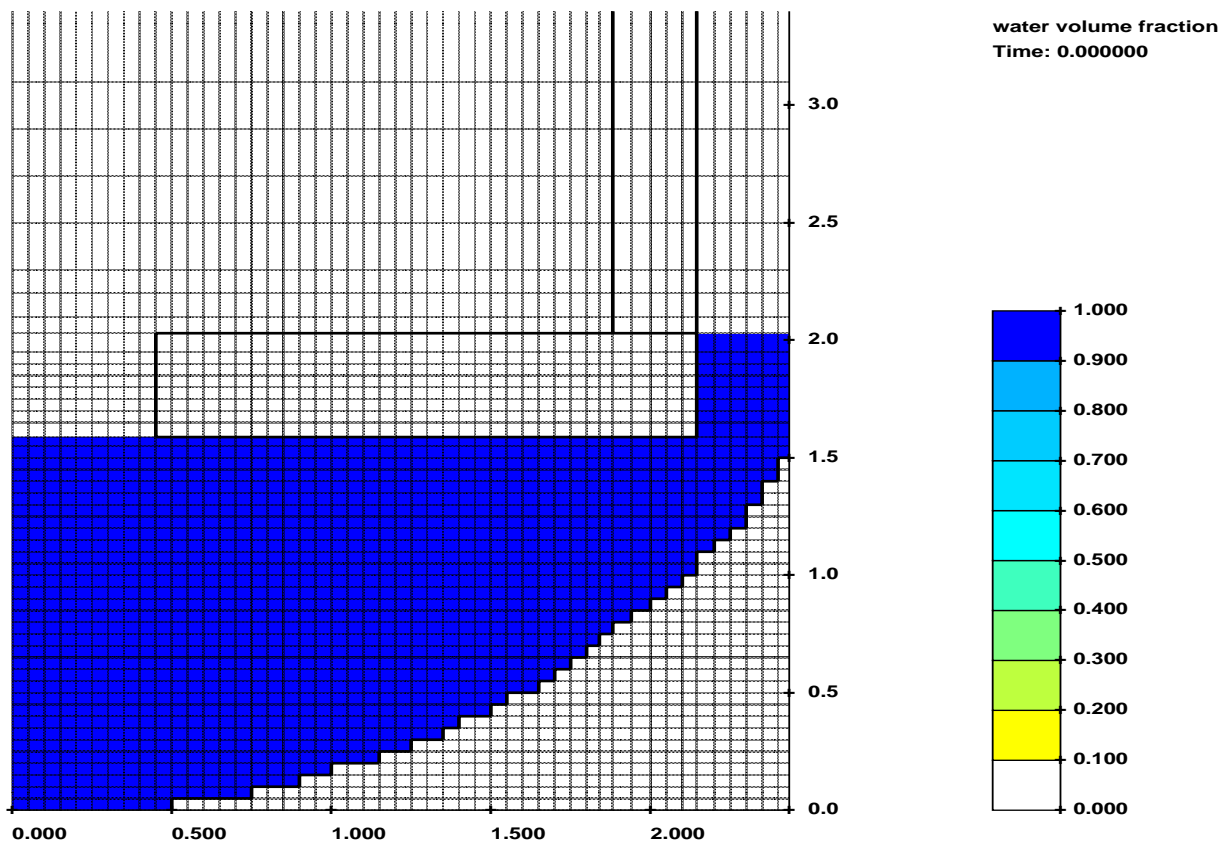
Figure 6.2 Initial volume fraction of water
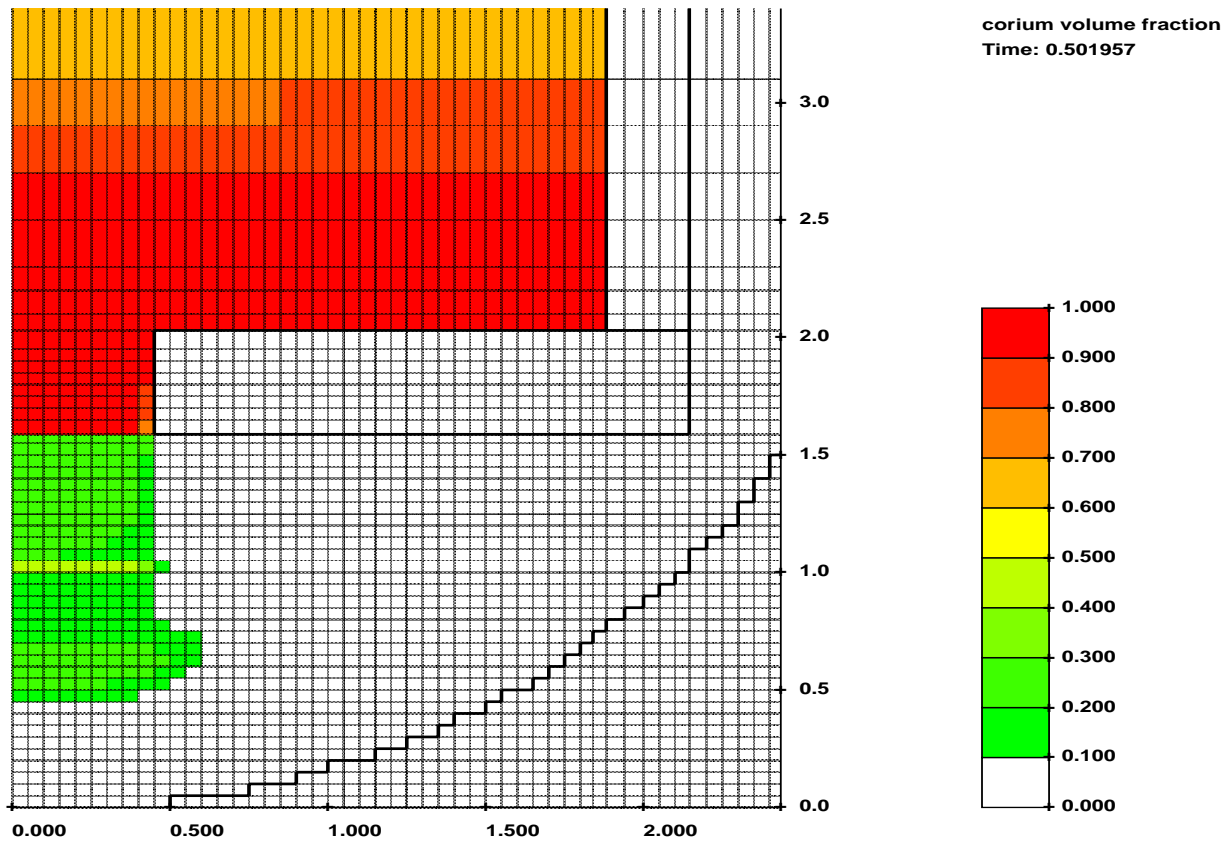
Figure 6.3 Volume fraction of corium at 0.5 s
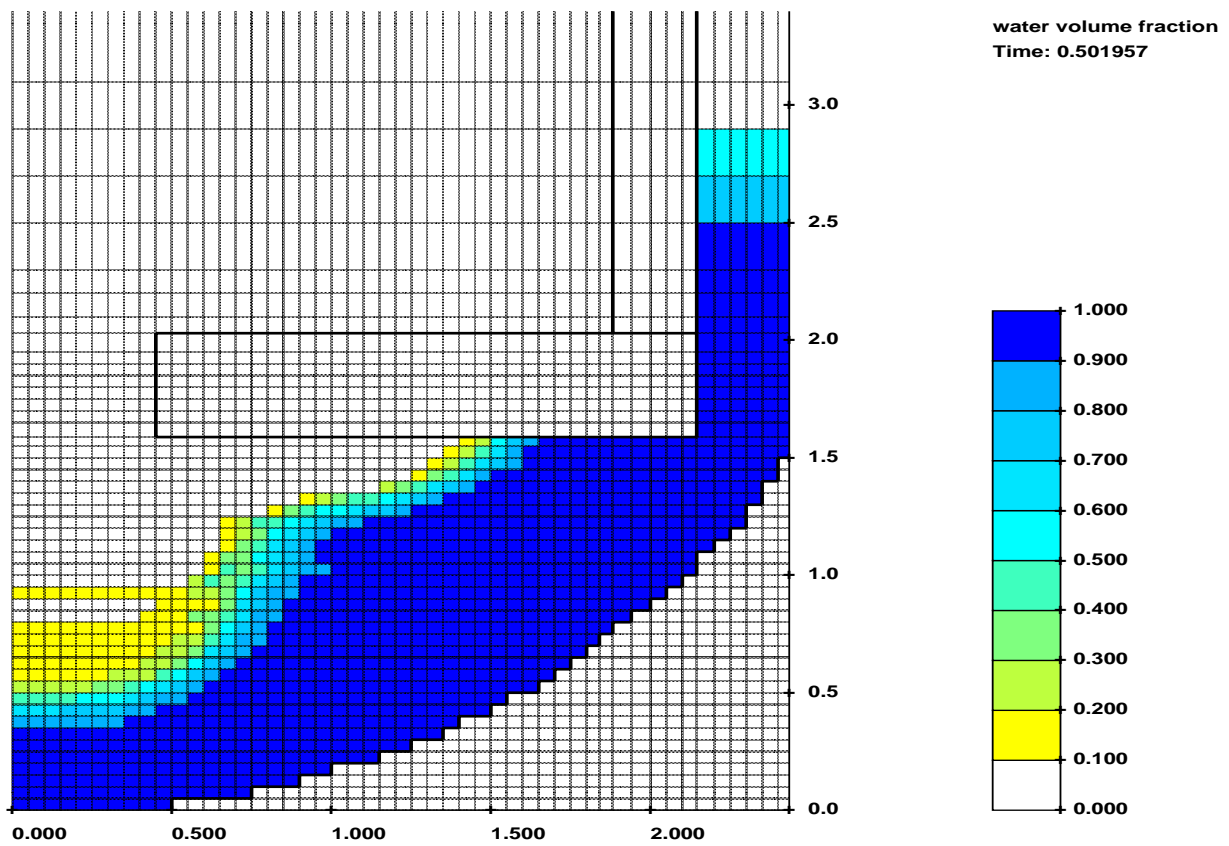
Figure 6.4 Volume fraction of water at 0.5 s
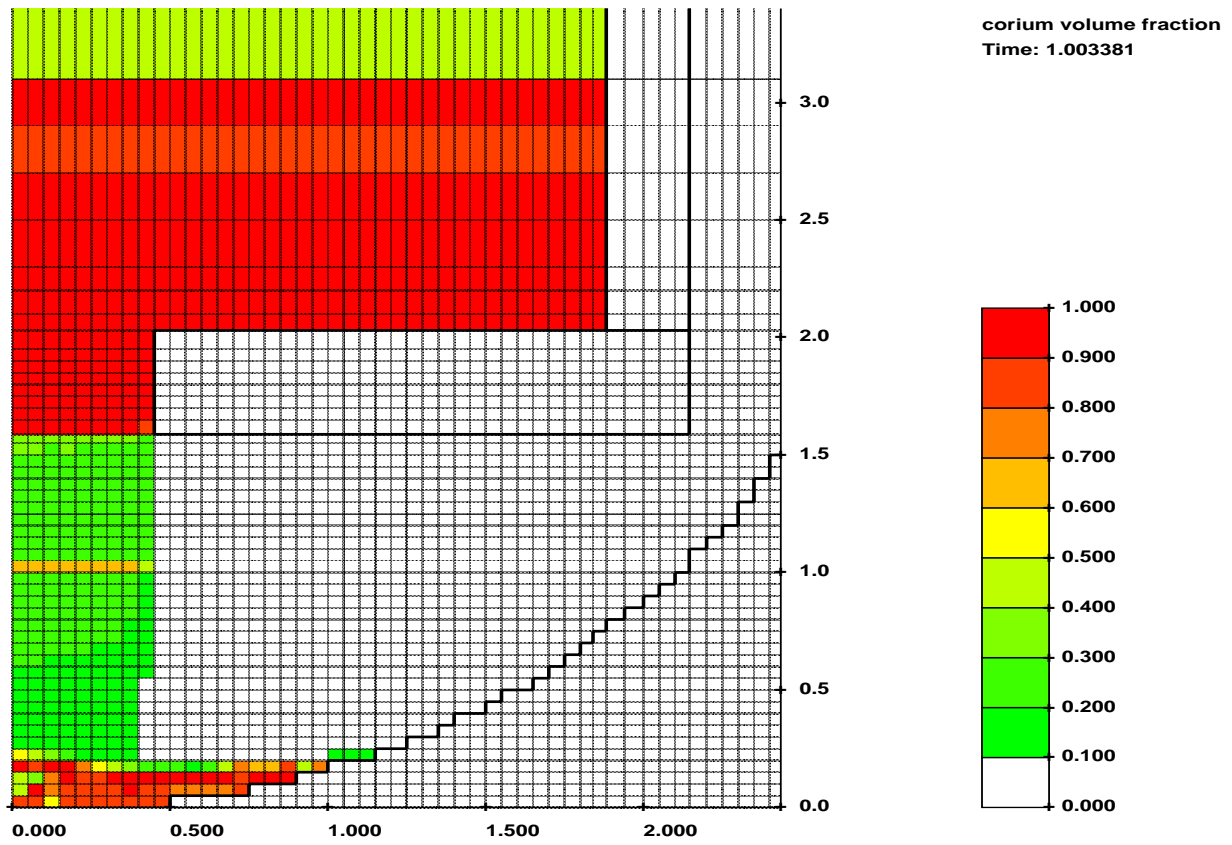
Figure 6.5 Volume fraction of corium at 1.0 s
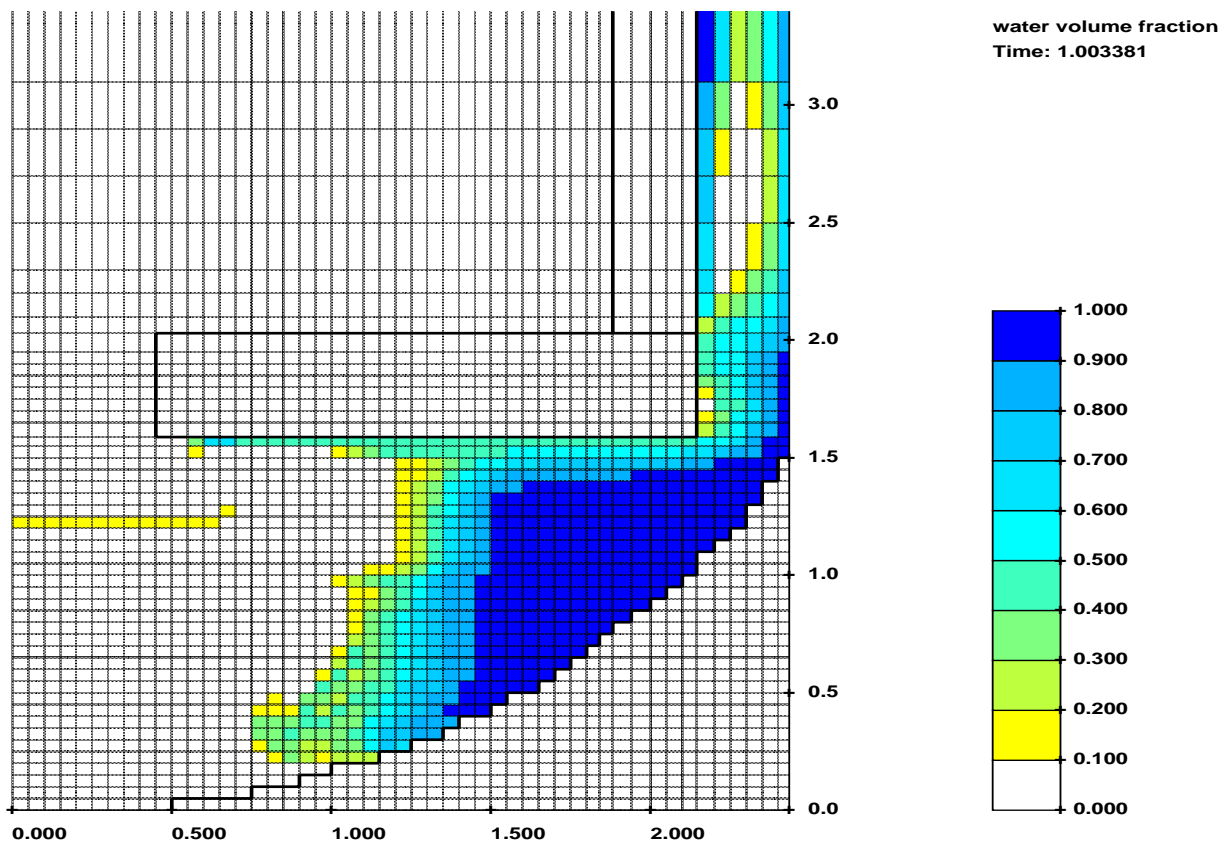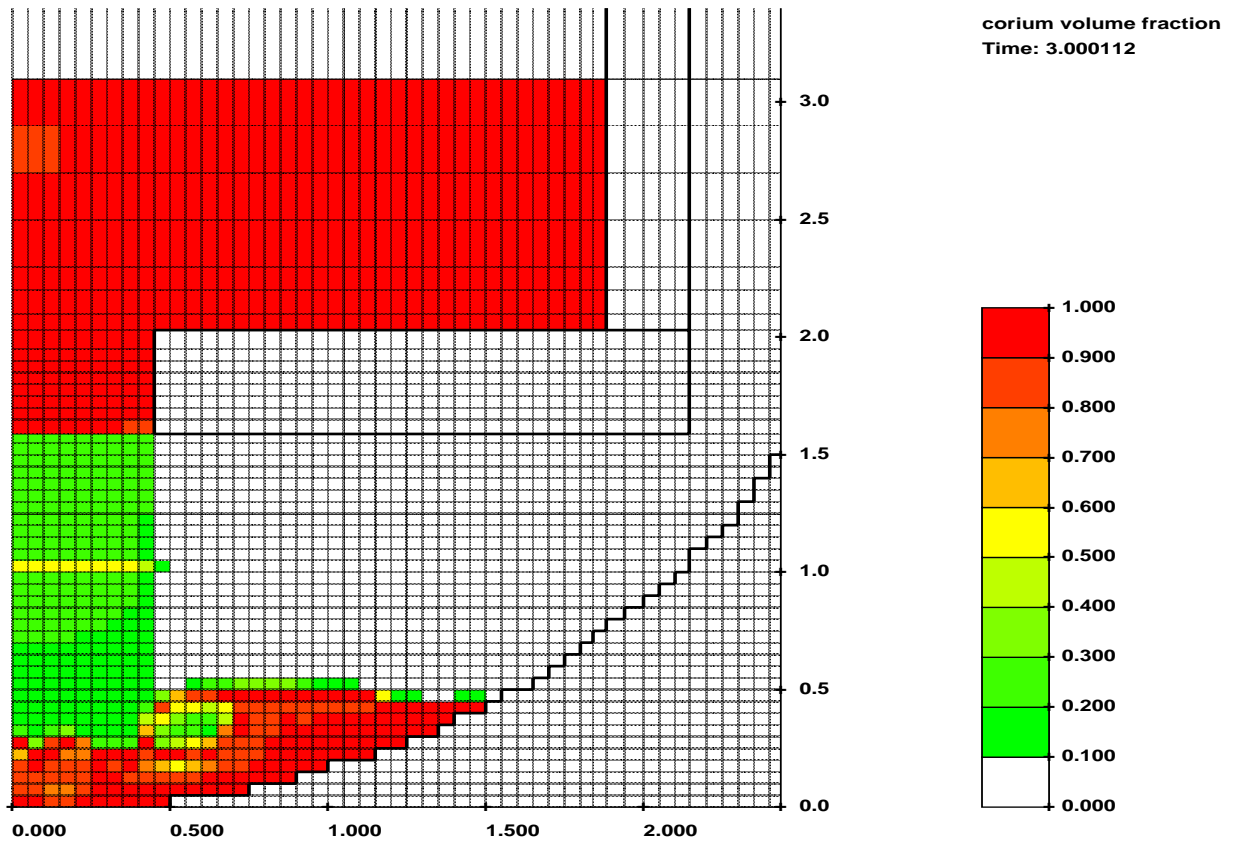

Figure 6.6 Volume fraction of water at 1.0 s
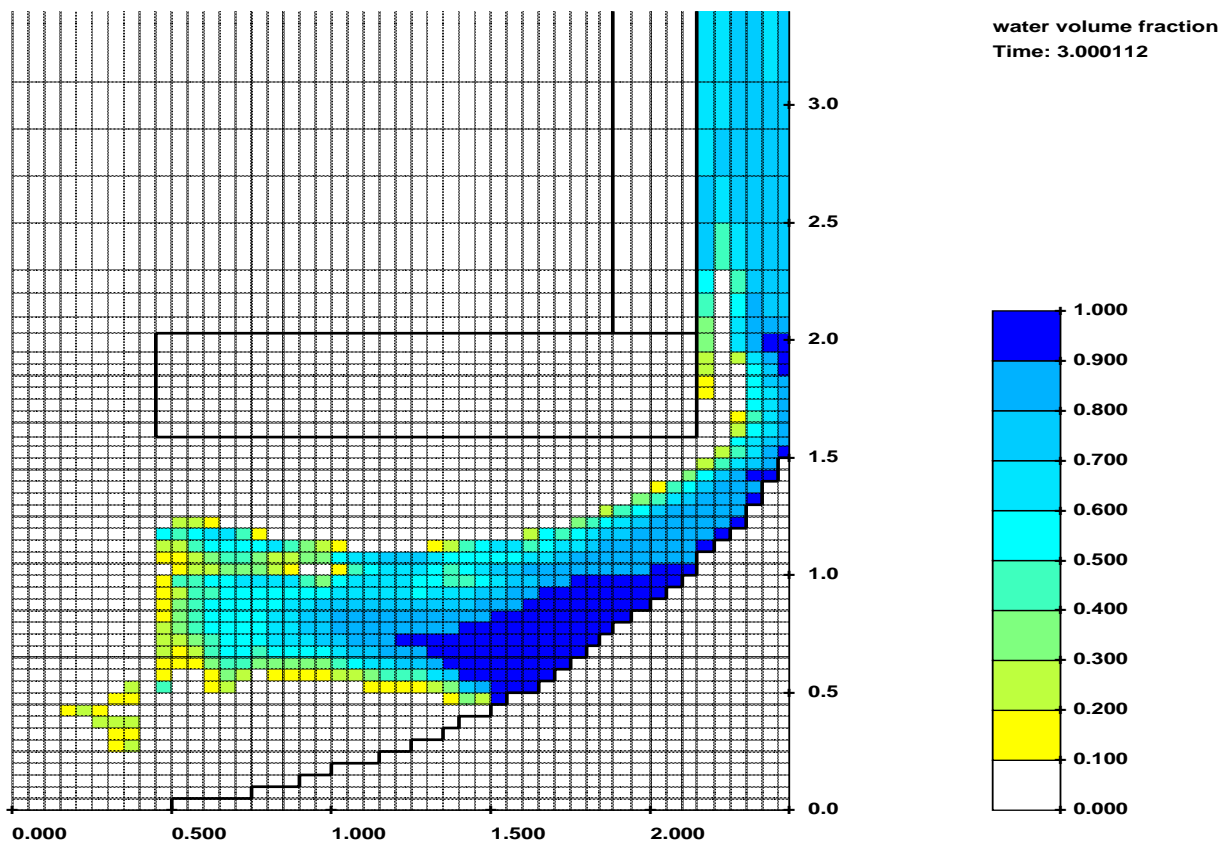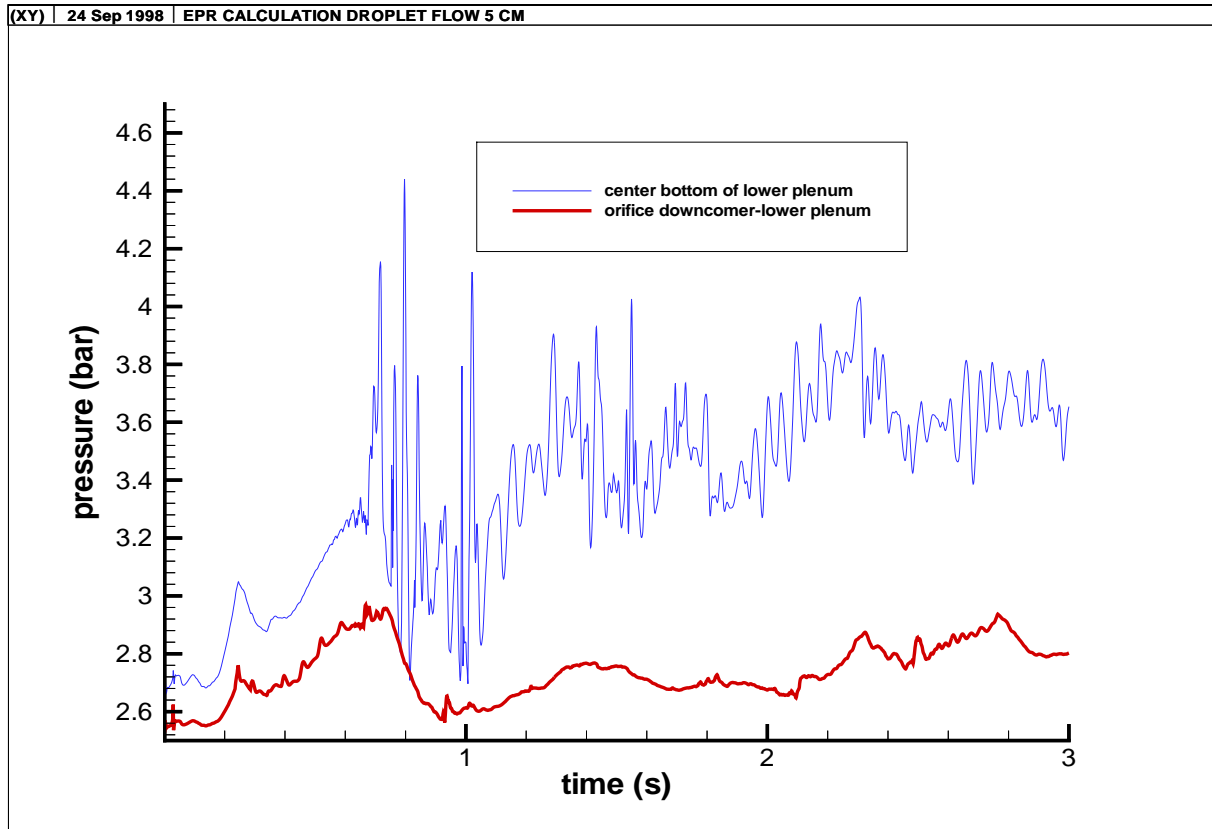
45

Figure 6.7 Volume fraction of corium at 3.0 s

Figure 6.8 Volume fraction of water at 3.0 s

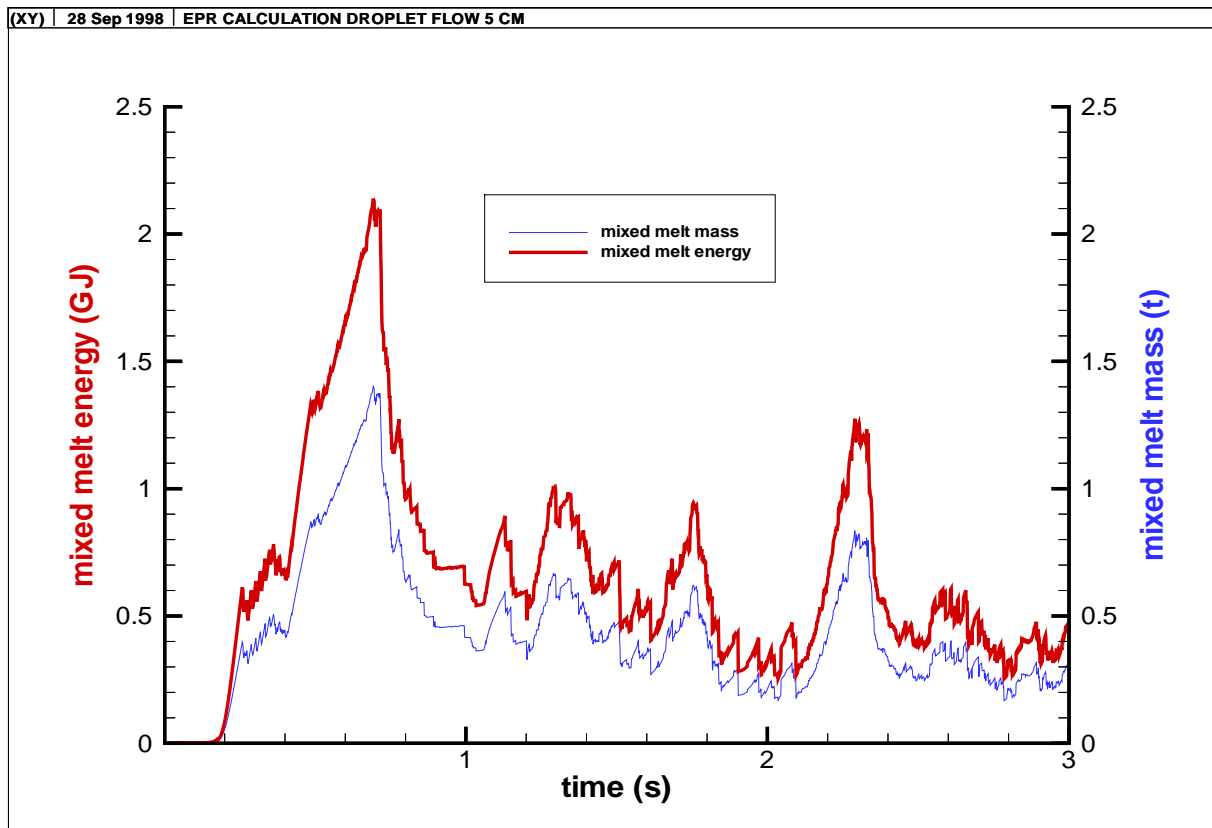Figure 6.9 Pressure at different locations in the lower plenum

Figure 6.10 Premixing data for the 0.1 limit of water volume fraction
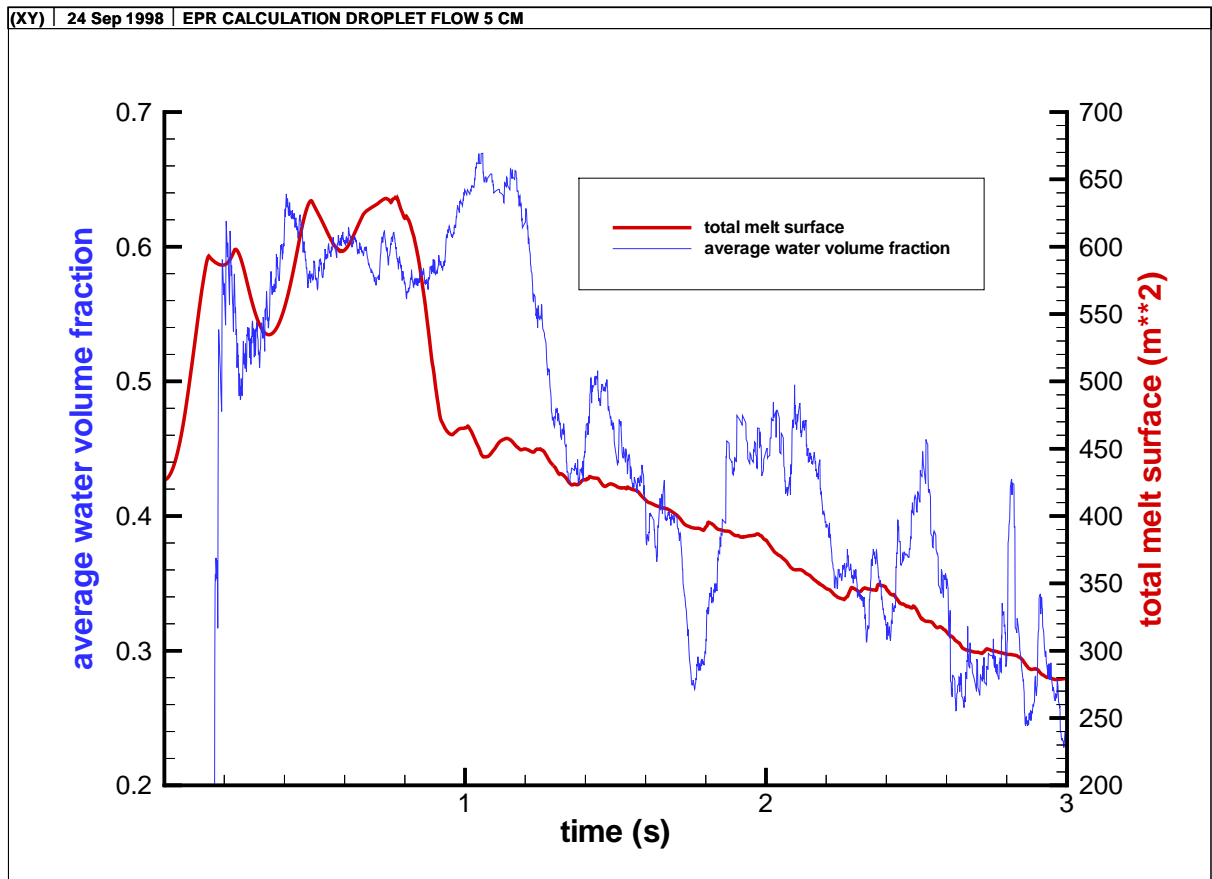
Figure 6.11 Total melt surface and average water volume fraction in the mixing zone
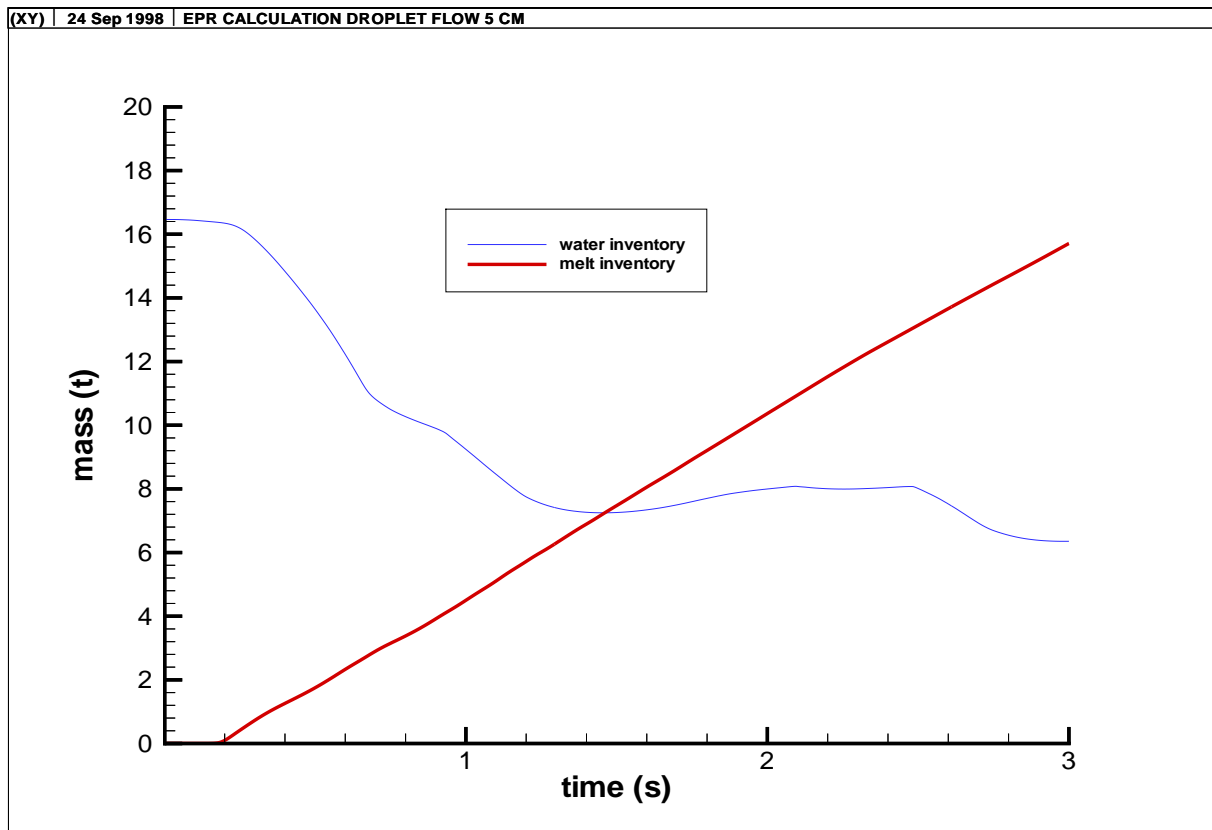
Figure 6.12 Lower plenum inventory of melt and water

6.1.2 Parametric analyses

In a first step the influence of fragmentation properties of the corium jet falling into water is investigated. Four cases are compared:

- 5 cm droplets, base case as previously described
- 2 cm droplets, all other parameters like base case
- 0.5 cm droplets, all other parameters like base case
- 0.5 cm droplets, but starting with a compact jet which is released from a central hole with a radius of 25 cm giving nearly the same release area as the other cases with porous outflow

Pressure curves at the orifice between downcomer and lower plenum are shown in Figure 6.13. The thin curves representing the two cases with initial particle size of 5 mm are similar and have a much higher maximum than the curves for the other two cases. The 5 mm particles make a much stronger interaction due to the large heat transfer surface. The difference between the compact jet and the shower of small particles is not large. One reason is that MC3D (TRITHYD) does not have a detailed jet break up model. Melt leaving a filled cell is described as droplets with the initial diameter of 5 mm until the receiving cell is nearly filled and becomes compact, too. So jet break up is driven by numerical diffusion at the melt front and the strong vapour flow created at the front by melt droplet-water interaction. The vapour flow destroys the compact behaviour of the melt. The differences between the base case and the case with 2 cm droplets are caused by the difference in heat transfer area. The reasons given for the different behaviour of the pressure curves hold for the premixed thermal melt energy, too (Figure 6.14). The stronger vapour production for small droplets leads to stronger displacement of water, which results in less premixing and less water in the mixing zone (Figure 6.15). Water leaves the lower plenum more quickly with smaller melt droplets, which can be seen from the water inventory in the plenum versus time given in Figure 6.16. The corium inventory in the lower plenum is shown in Figure 6.17 dependent on time. The melt release rate is strongly reduced at the beginning by the strong pressure build-up for small droplets interacting with water. Later on, when the pressure levels out, the melt release rate is similar for all cases considered.

One case was simulated, in which the crust failure above the lower core support plate propagates in radial direction to evaluate consequences of an increasing melt release rate during premixing. It is assumed that at 0.5 s the radius of the melt release area increases from 0.45 m to 0.85 m representing an area corresponding to about 49 subassembly positions. The pressure curves at the end of the downcomer (Figure 6.18) show that the corium additionally released needs some time to reach the water which was displaced by the already released melt. After contact the interaction leads to a pressure peak, which is about 0.5 bar higher than the first maximum. The interaction of the additional melt gives much higher premixing energies with peak values of nearly 3 GJ (Figure 6.19). But also in that case the premixing energy levels out at small values at later times. The reason for the large premixing event is that the additional melt release area is much greater than the initial one. To get strong premixing large amounts of corium have to enter the water during a time period in which the water cannot be displaced by vapour production.

To get more realistic results for PREMIX experiments the surface tension of the melt was reduced from 0.45 to 0.04 N/m. The surface tension reduction gives stronger drag and fragmentation to get more radial melt distribution. Calculations of the PREMIX experiments were done with 2 cm particles, so we will compare the base case, but using 2 cm as initial

droplet size, with a case with surface tension reduction. We see the same effect as observed in the PREMIX cases. The pressure and the premixed energy is shifted, but the changes are not really large when considering the over-all result (Figures 6.20 and 6.21).

To evaluate the importance of ambient pressure at the beginning of the fuel coolant interaction a calculation was done assuming 4.5 bar as initial pressure and water under saturation conditions. Figure 6.22 shows the various pressure differences related to the initial system pressure. The pressure rise is very similar for the two cases and no large differences are observed. This is also valid for the premixed melt energy, where only a small increasement in use of high pressure is calculated.

In the following the influence of pressure loss coefficients at inlet/outlet is investigated. In a first case the feedback from an assumed pressure loss coefficient of 10 at all coolant inlets and outlets is analysed. Because strong vapour production and pressure build-up emphasize the effect of pressure loss coefficients, the case is compared with the base case, but using 5 mm as initial droplet diameter. The pressure curves (Figure 6.24) start to differ after the vapour starts to escape from the lower plenum into the downcomer. At that time vapour flow at the boundaries becomes significant. Prior to that time, the water level rises in the downcomer and the vapour flow is low. All vapour produced is enclosed in the vapour bubble as long as the orifice between downcomer and lower plenum is totally blocked by water. There is no significant feedback from the pressure loss at the top boundaries to the value of premixed melt energy (6.25). Assuming a pressure loss at the orifice between downcomer and plenum we suspect that the water blockage is maintained for a longer time. A case with a pressure loss coefficient of 1 is compared with the base case. The influence on the results is very small. There is a small pressure shift at the beginning, but nearly no effect concerning the premixing state (Figure 6.26 and 6.27).
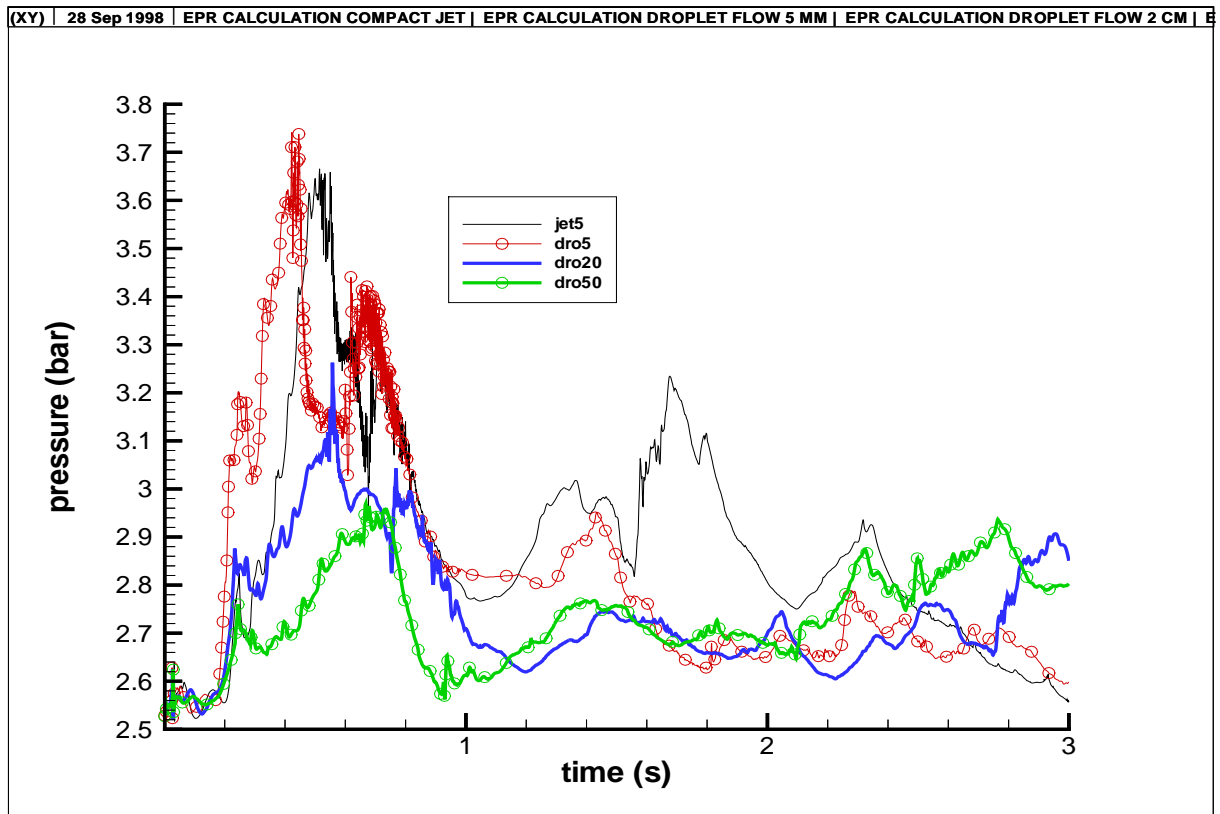
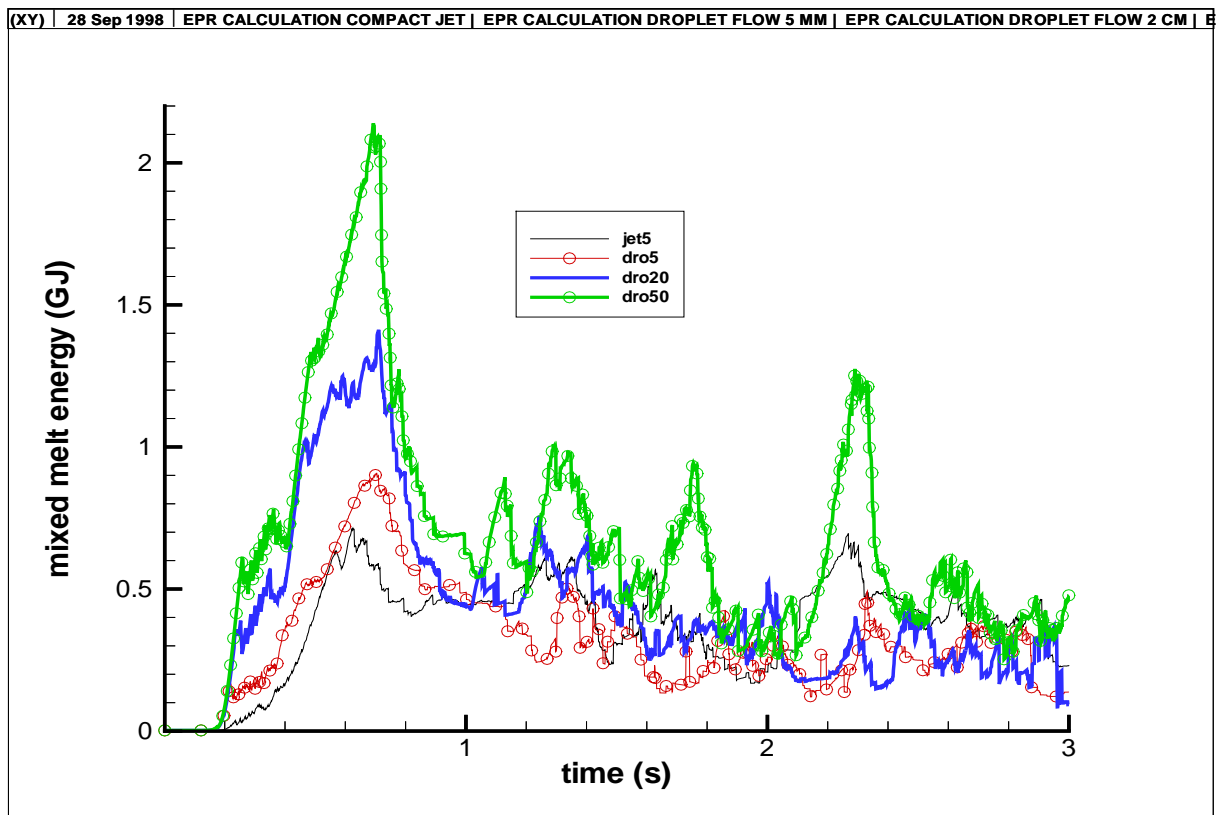Figure 6.13 Pressure at the orifice of downcomer-lower plenum

Figure 6.14 Premixing data for the 0.1 limit of water volume fraction
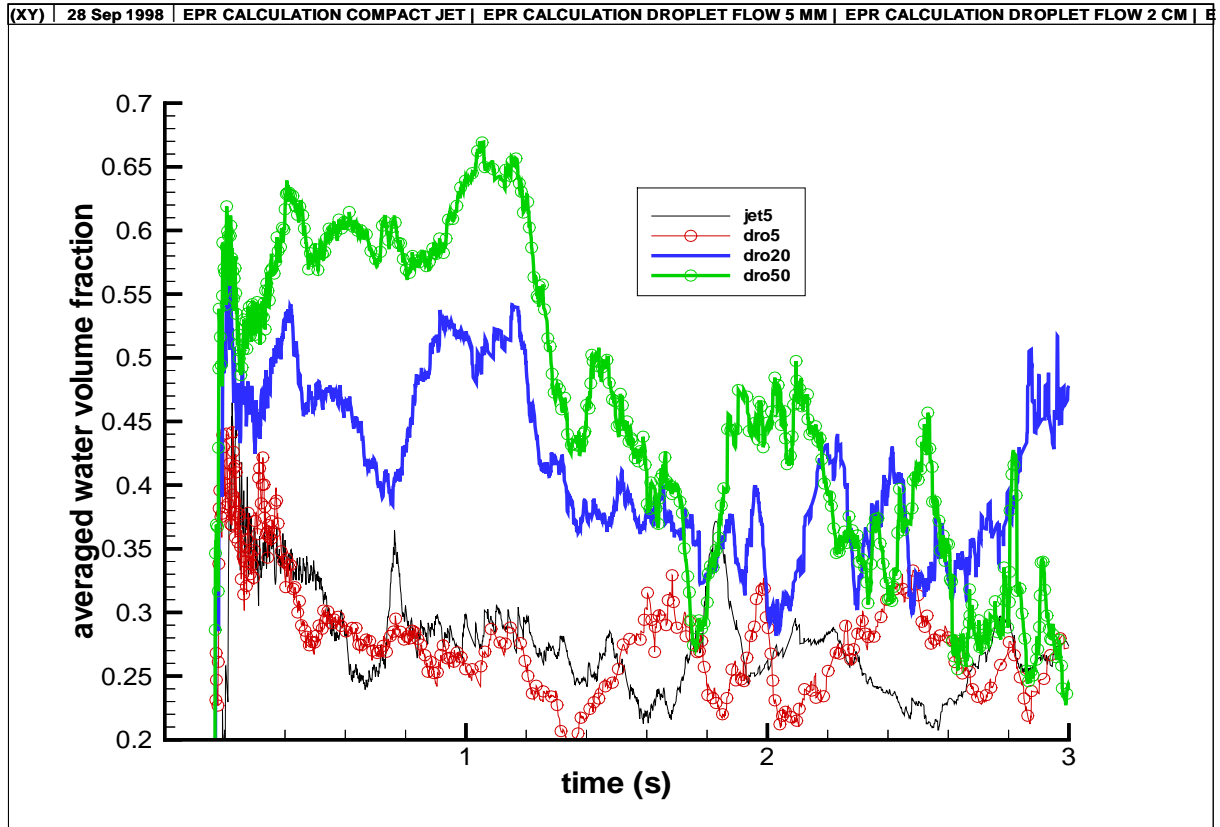
51

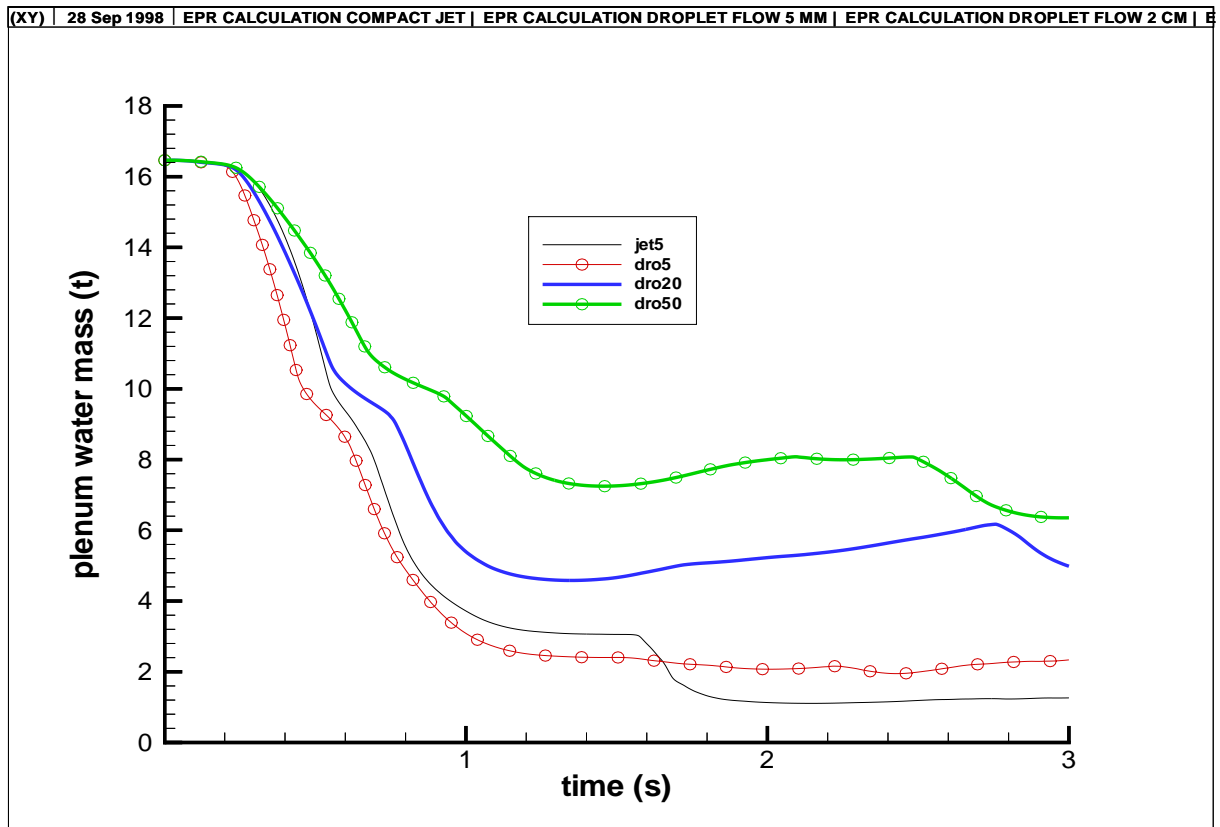Figure 6.15 Average water volume fraction in the mixing zone
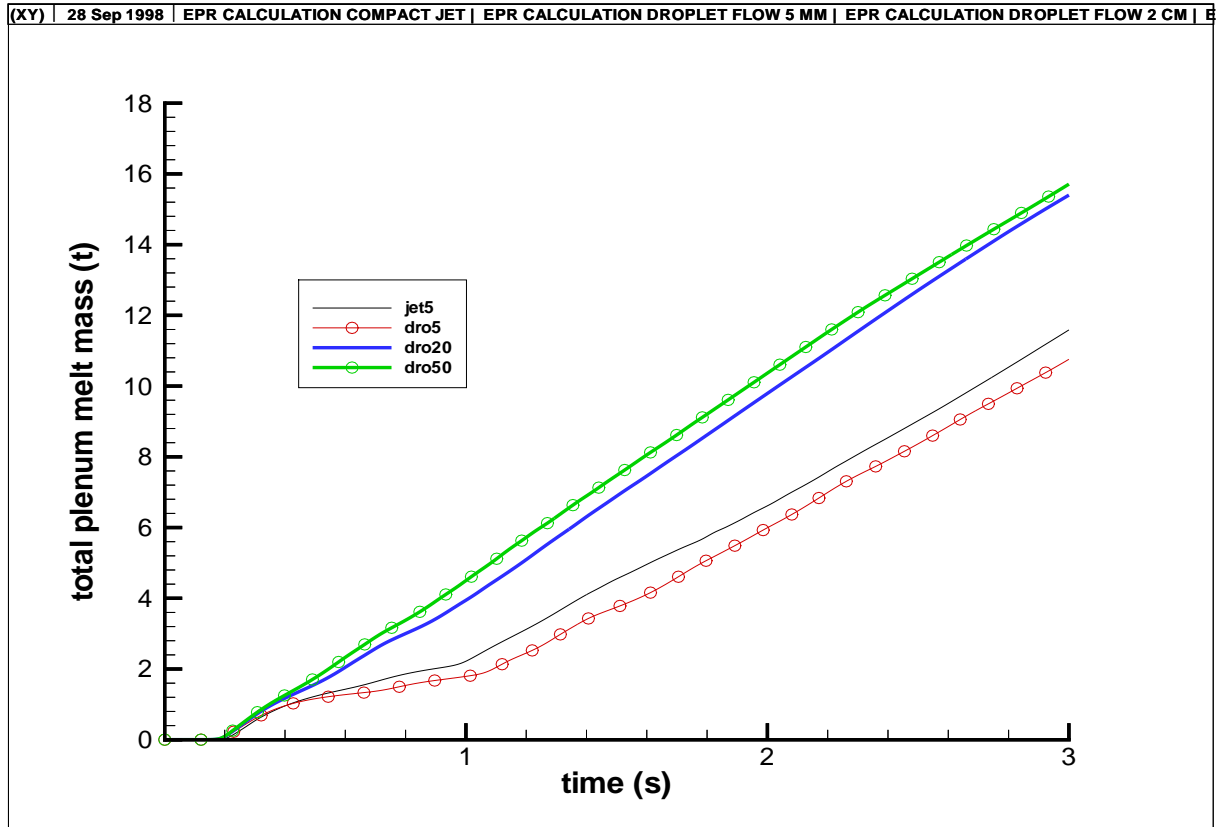
Figure 6.16 Lower plenum inventory of water

Figure 6.17 Lower plenum inventory of melt

Figure 6.18 Pressure at the orifice of downcomer-lower plenum

Figure 6.19 Premixing data for the 0.1 limit of water volume fraction

Figure 6.20 Pressure at the orifice of downcomer-lower plenum

Figure 6.21 Premixing data for the 0.1 limit of water volume fraction

Figure 6.22 Difference pressure at the orifice of downcomer-lower plenum

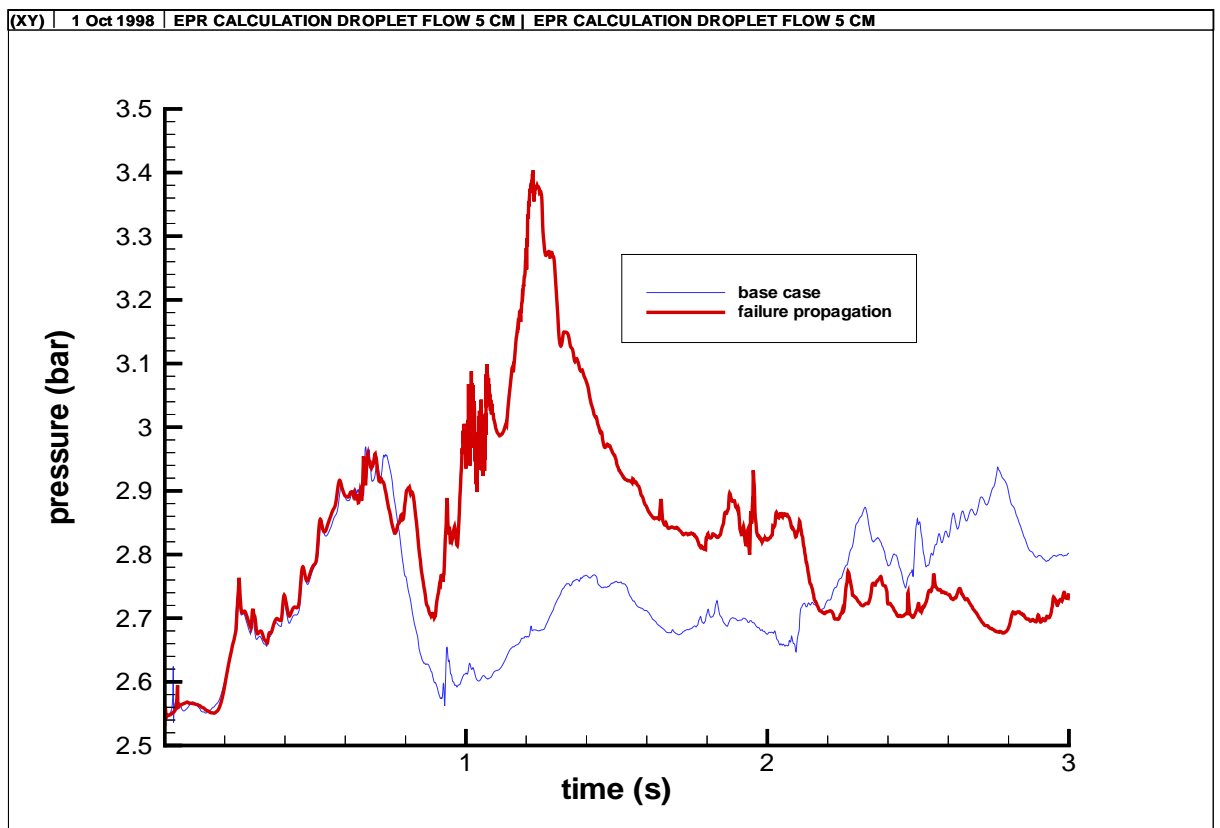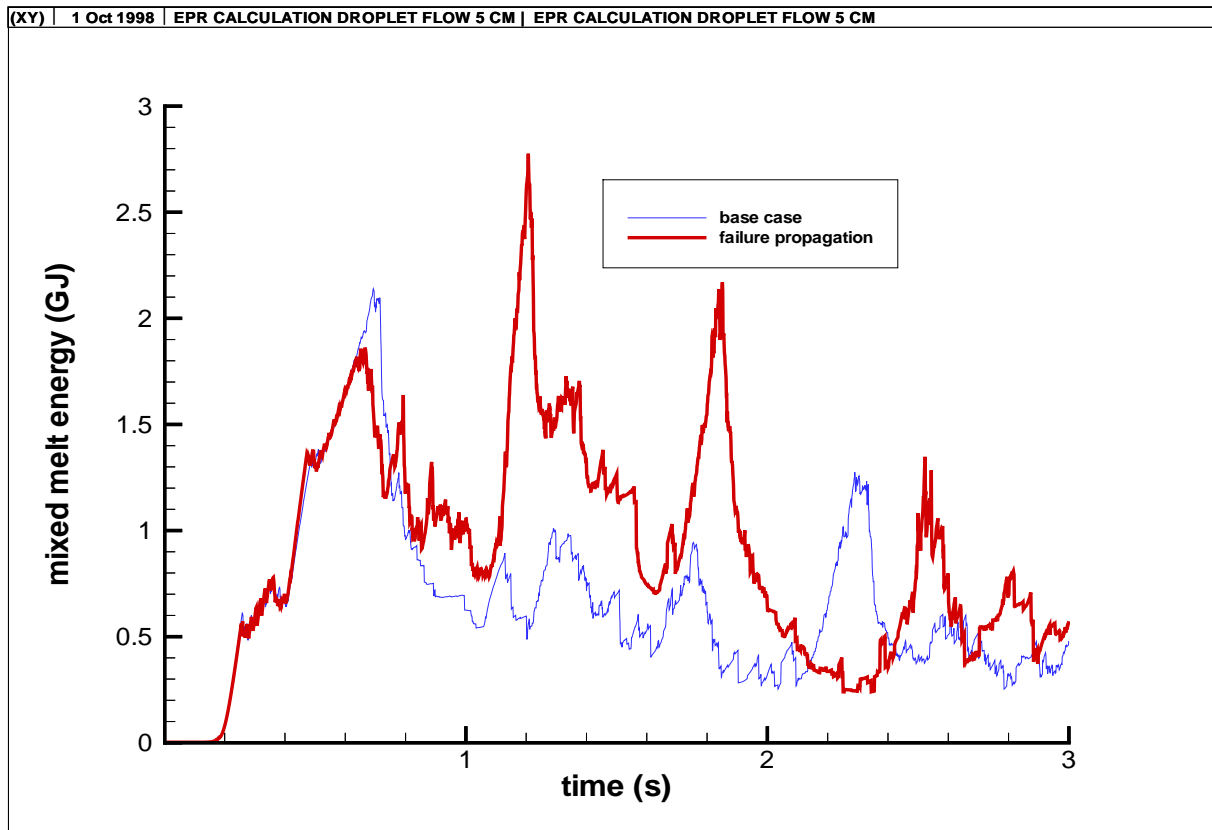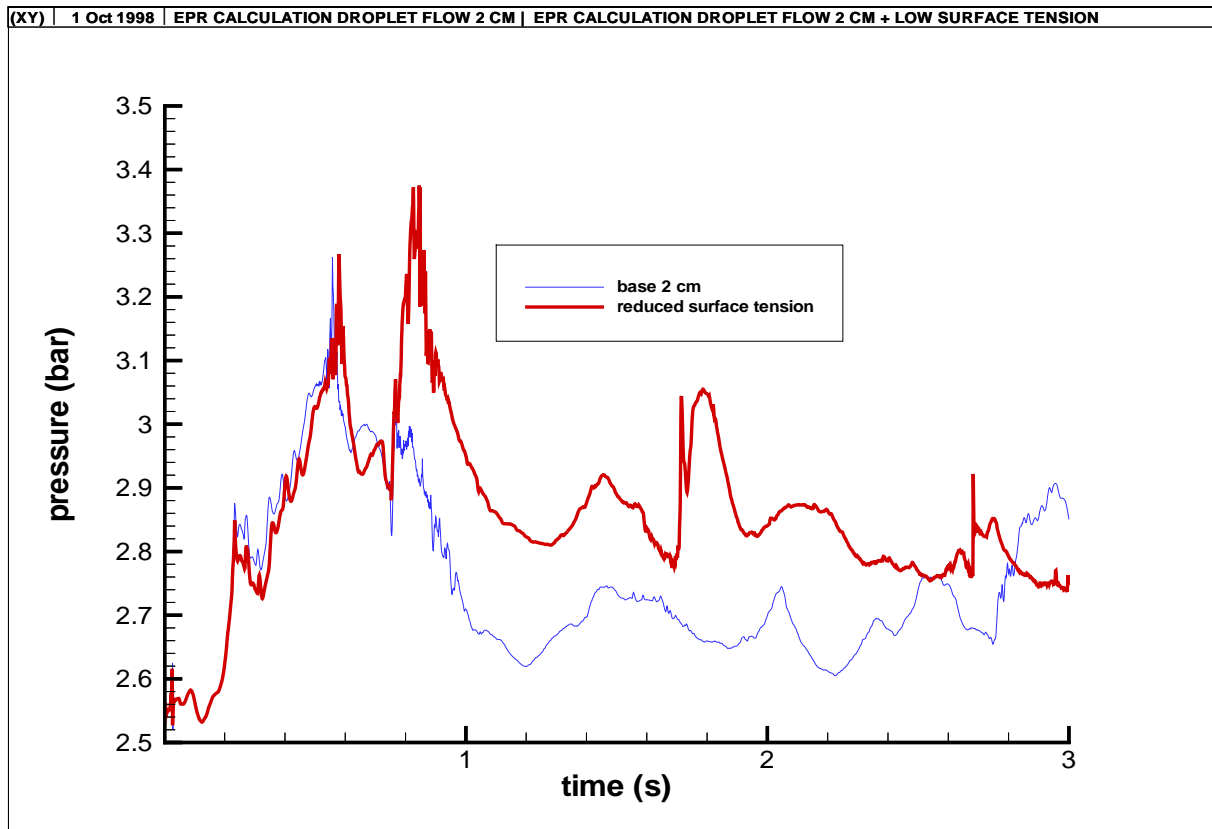Figure 6.23 Premixing data for the 0.1 limit of water volume fraction

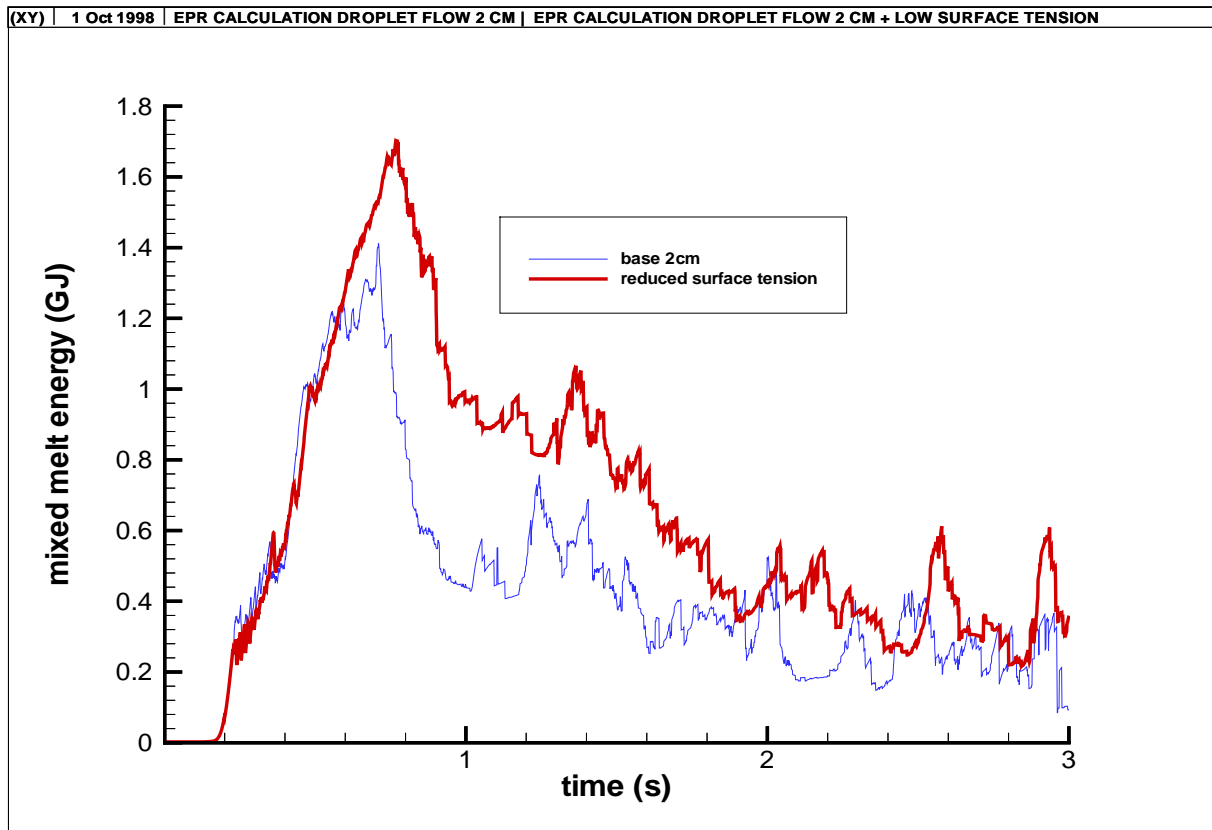Figure 6.24   Pressure at the orifice of downcomer-lower plenum

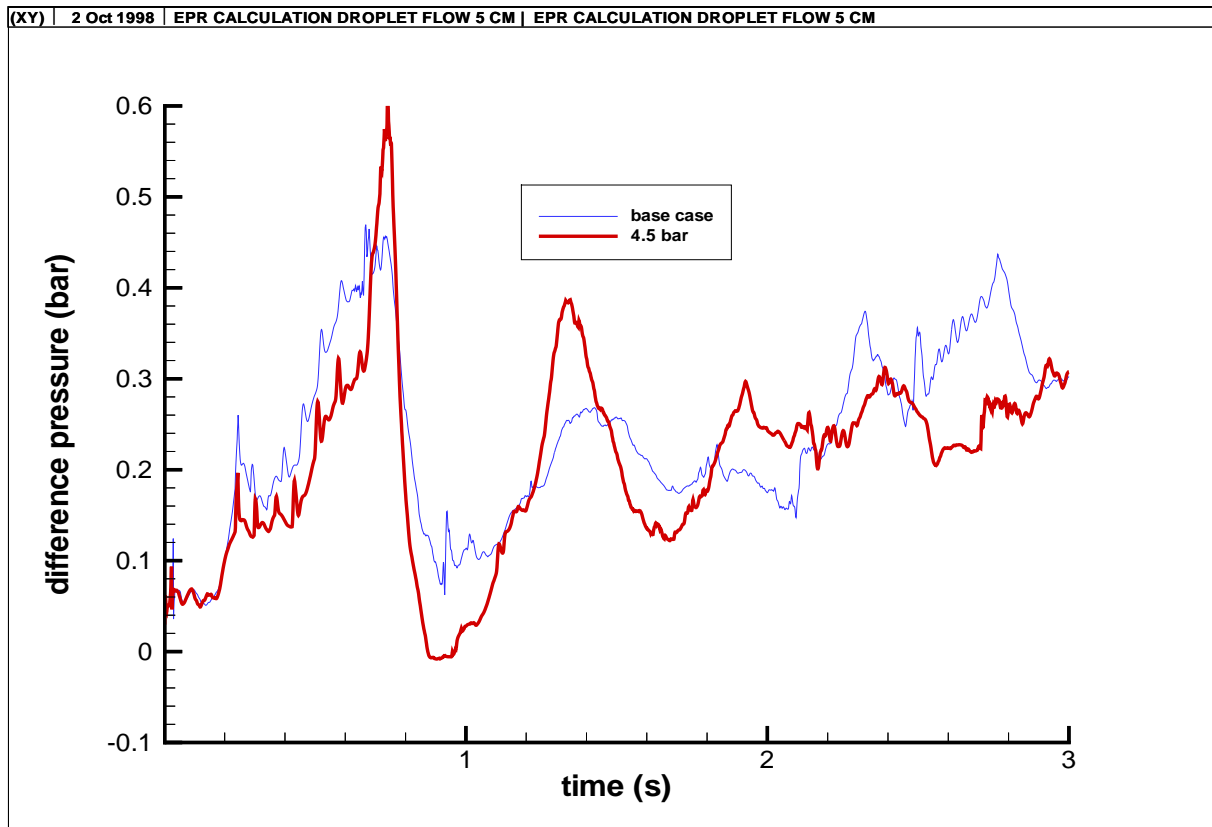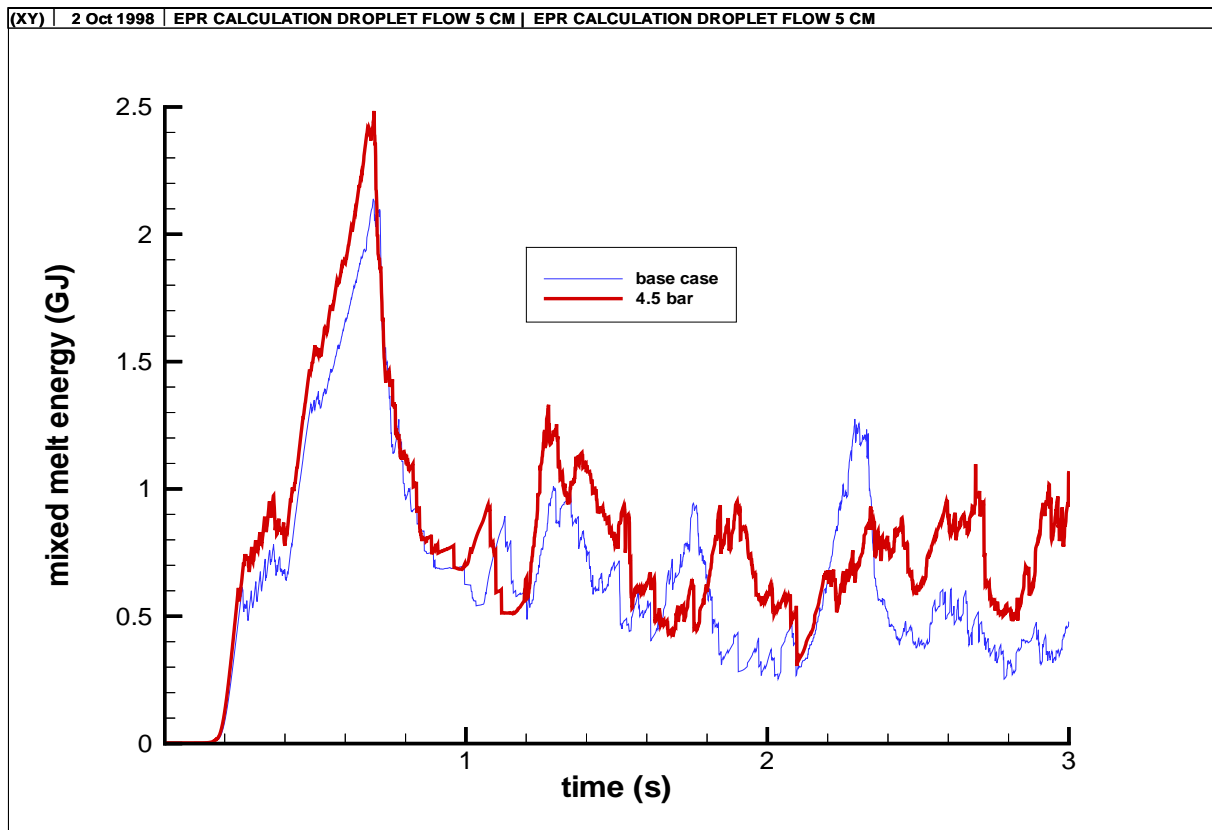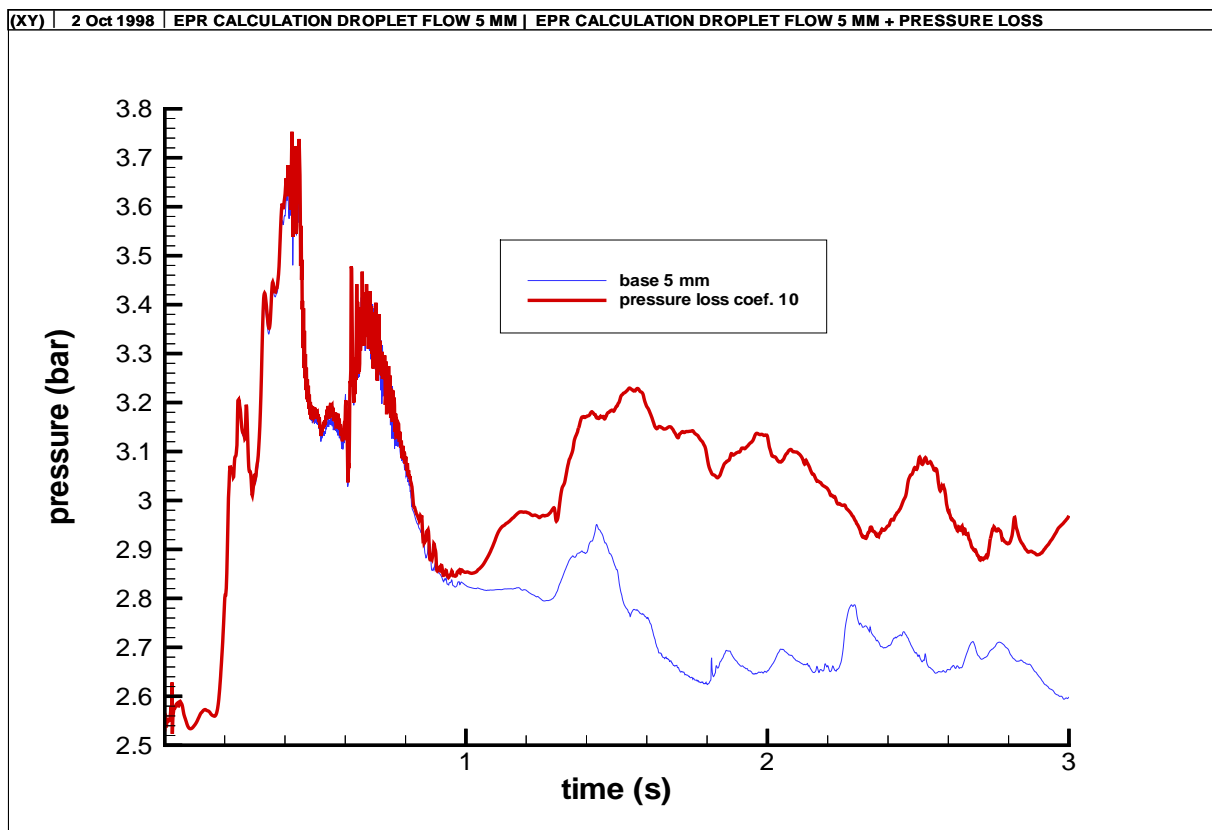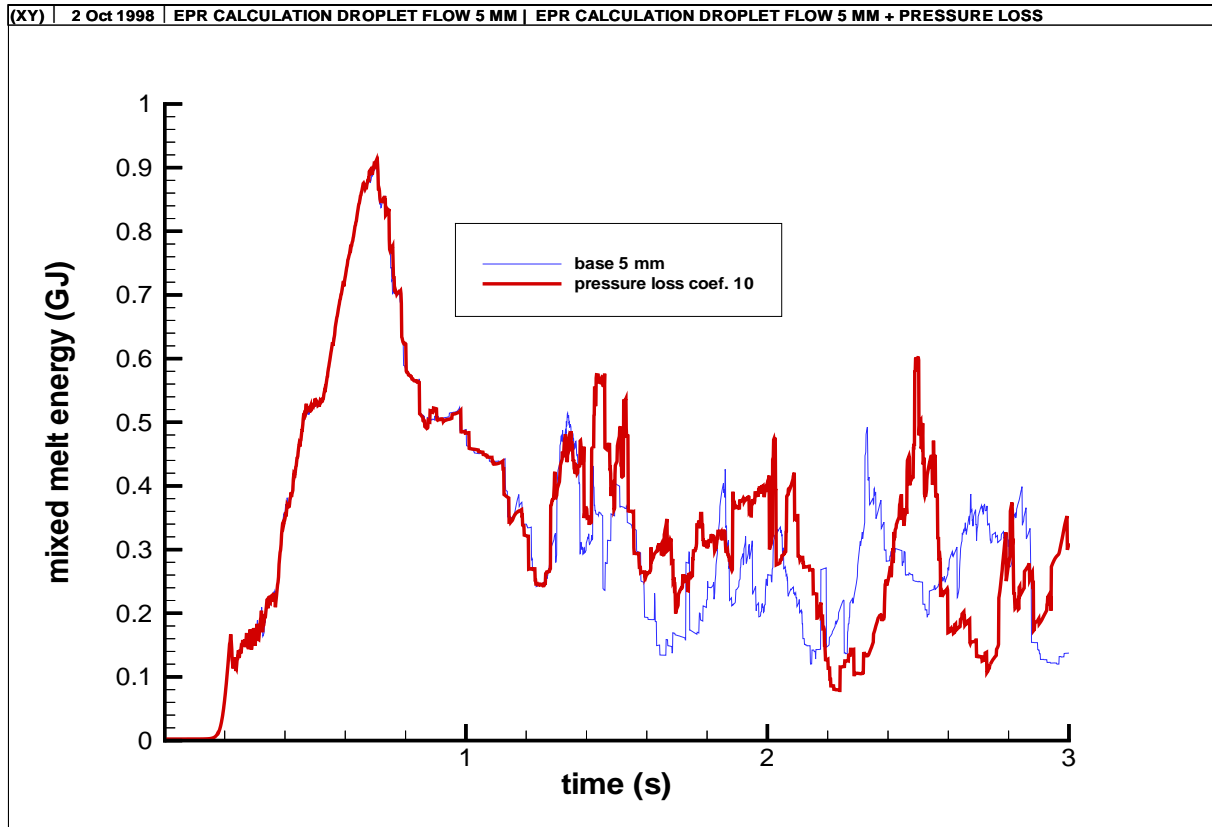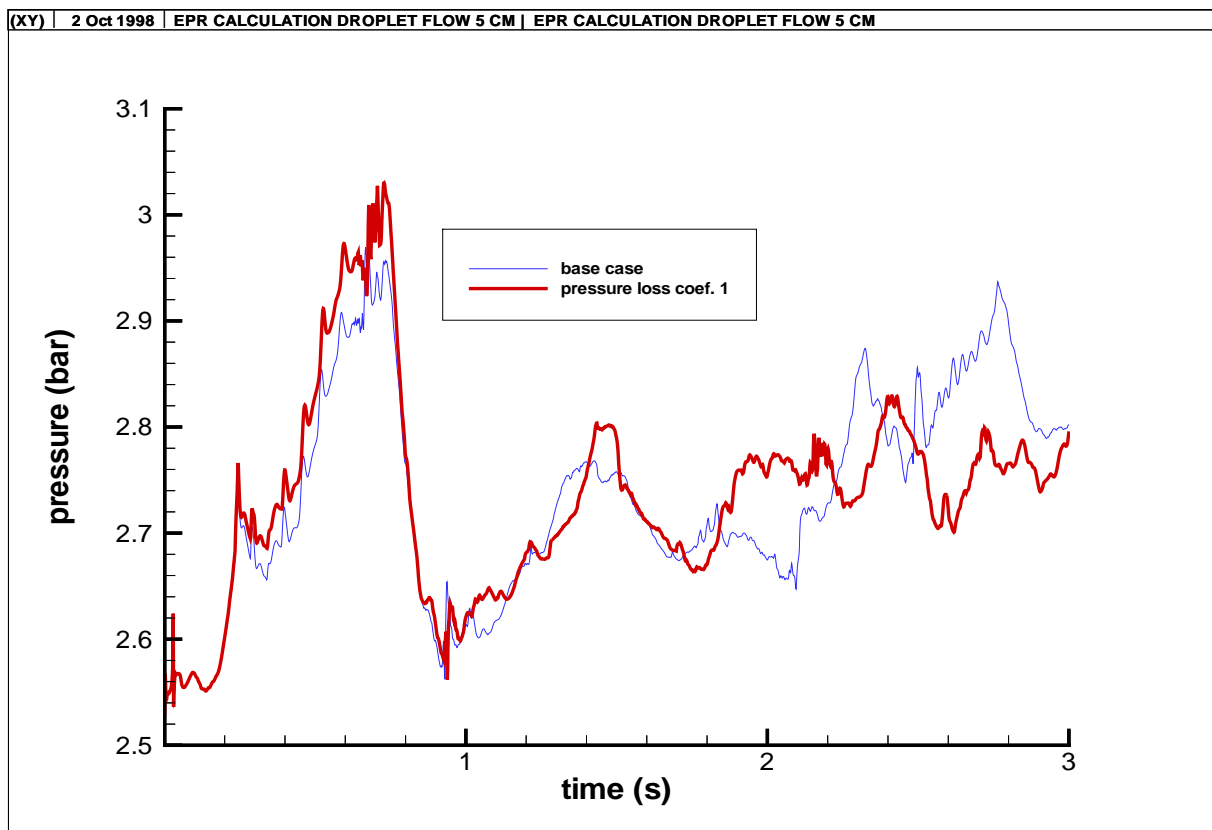Figure 6.25 Premixing data for the 0.1 limit of water volume fraction

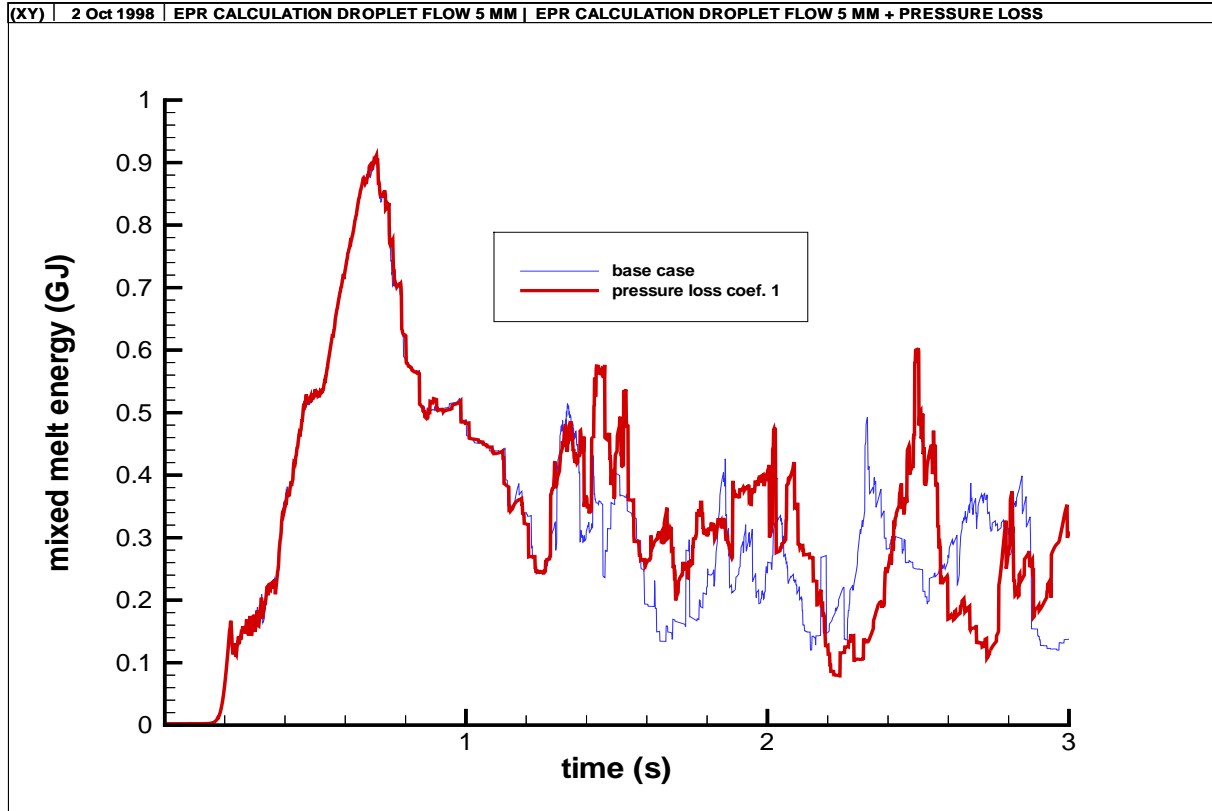Figure 6.26 Pressure at the orifice of downcomer-lower plenum

Figure 6.27 Premixing data for the 0.1 limit of water volume fraction

6.1.3 Influence of the flow plate loss coefficient

Figure 6.28 shows the geometry of the flow plate which is located below the core support grid. Within the figure the slashed area is representative for the plate geometry. Because holes of the plate have different diameters estimation of the loss coefficient becomes difficult because in literature only values for plates with uniform holes are available. However, differences of the holes diameters are small and one can estimate a loss coefficient λ between 5.0 and 5.5 (Idelchik, [3]). In the base case the loss coefficient is set to zero. In this chapter results of simulations with loss coefficients of 5.3 and 10 are presented and compared to the base case. The increase up to a value of 10 has been chosen because it cannot be excluded that the hole diameters become smaller due to partial freezing once core melt spreads out in radial direction.
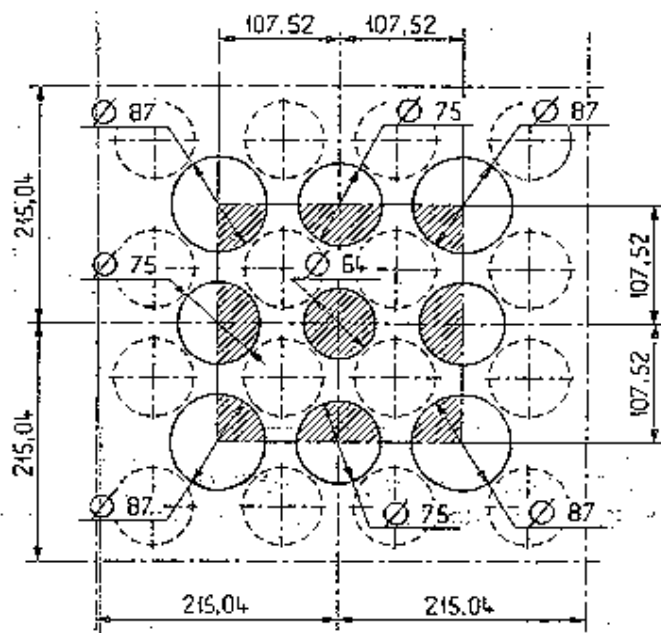
Figure 6.28: Geometry of flow plate

The largest influence of flow plate resistances on melt premixing is observed in case of an axial melt release through the core support grid. In these scenarios a crust failure at the bottom of the molten pool is assumed. The leak area is placed in the core center with a radius of 45cm and a porosity of 0.33. Geometry and spatial grid resolution are chosen the same as for the base case.

Figure 6.29 shows water and melt distributions for different loss coefficients 3s after crust failure. Differences are small. In all cases the melt has penetrated through the flow plate and has reached the bottom of the vessel. Due to evaporation the water is relocated from the lower plenum into the downcomer.

In all cases only small amounts of the core melt have left the computational area. In the lower plenum nearly the whole water is relocated into the downcomer or has left the vessel. Differences in between the calculations concern the increased spreading of melt over the flow plates surface and the amount of water in the lower plenum which is slightly increased in case of $\lambda=0$.

The influence of the flow plate can be explained as follows:

If the hot melt comes in contact with water in the lower plenum evaporation results in a pressure increase which relocates water into the downcomer. The flow plate acts as a barrier for the melt to reach the water below. The penetration of the plate by melt is dependent on λ. Increasing λ results in longer time scales and leads to stronger fragmentation of the melt. This influences evaporation and premixing.

Considering the pressure in the downcomer (Figure 6.31) the effect of the plate loss coefficient becomes obvious. Until the melt front reaches the plate differences are negligible. The pressure increases if the melt front has reached the water surface. Then evaporation of water starts and a first pressure maximum of 4.3bar is reached at 0.3s. If the melt hits the flow plate the melt surface is reduced by coalescence. This reduces the evaporation rate and the pressure decreases. The pressure increases again when the melt has passed the plate and contacts the water below. The time delay between first contact of the plate and its penetration depends on λ. The pressure amplitude which is reached after the melt has passed the plate is a function of melt particles diameter and melt flux passing the plate.
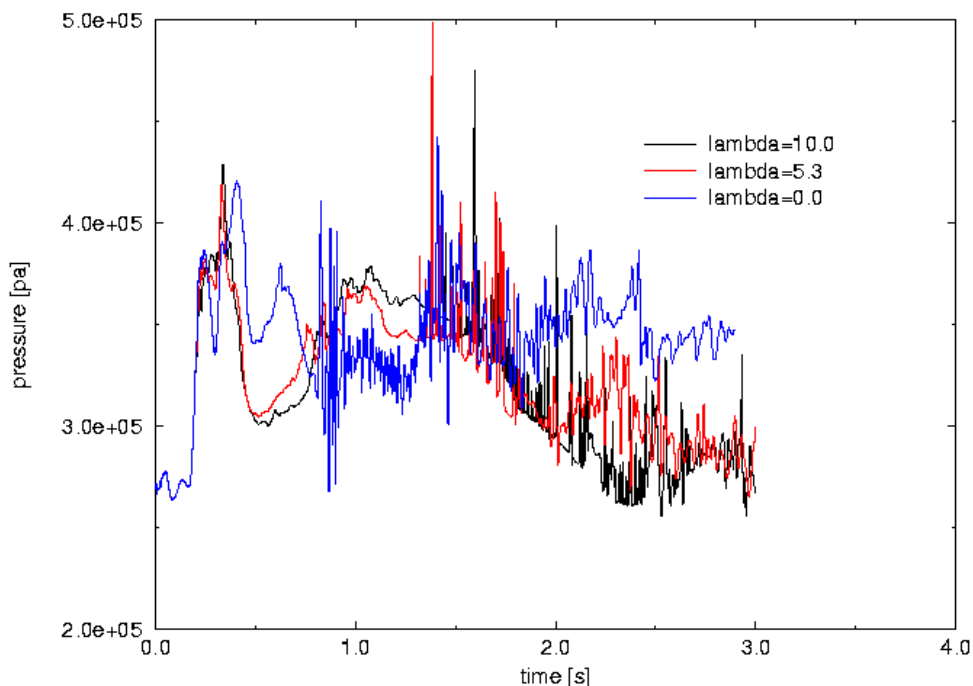
Figure 6.30: Pressure in lower plenum at different plate loss coefficients

In the present configuration the only dependence of importance is the one of the particle diameter by which the evaporation rate of water is determined.

At $\lambda=0$ a second pressure maximum of 3.4bar at 0.7s is calculated. In case of $\lambda=5.3$ (10.0) values of 3.5bar (3.6bar) at 1.1s (1.2s) are reached. After this maximum the pressure decreases towards values close to the initial pressure because more and more water is removed from the lower plenum into the downcomer.

Considering the pressure in the lower plenum (Fig. 6.30) the curves at times t>1s are very noisy which result from numerical problems concerning packing when the melt reaches the bottom of the lower plenum. At the lower position of the downcomer the pressure is increased by 0.6 bar in average in accord with the additional hydrostatic pressures of water and melt. Until 0.8s pressures in lower plenum and in downcomer are nicely correlated. Later on

60

calculated pressures in the lower plenum are influenced by numerical problems due to packing.

The release of melt from the pool into the lower plenum is mainly influenced by the pressure distribution near the leak. Pressure increases in the lower plenum mean reduction of the melt flux. So the time gradient of the melt mass accumulated in the lower plenum (Fig. 6.34) and the pressure in the lower plenum are anticorrelated.

The melt needs around 0.2s to reach the lower plenum by passing the core support grid. Then until 0.6s there are only small differences between the various cases. Then up to 1s at $\lambda=0$ the melt flux decreases because its average pressure is below the other cases. At times larger than
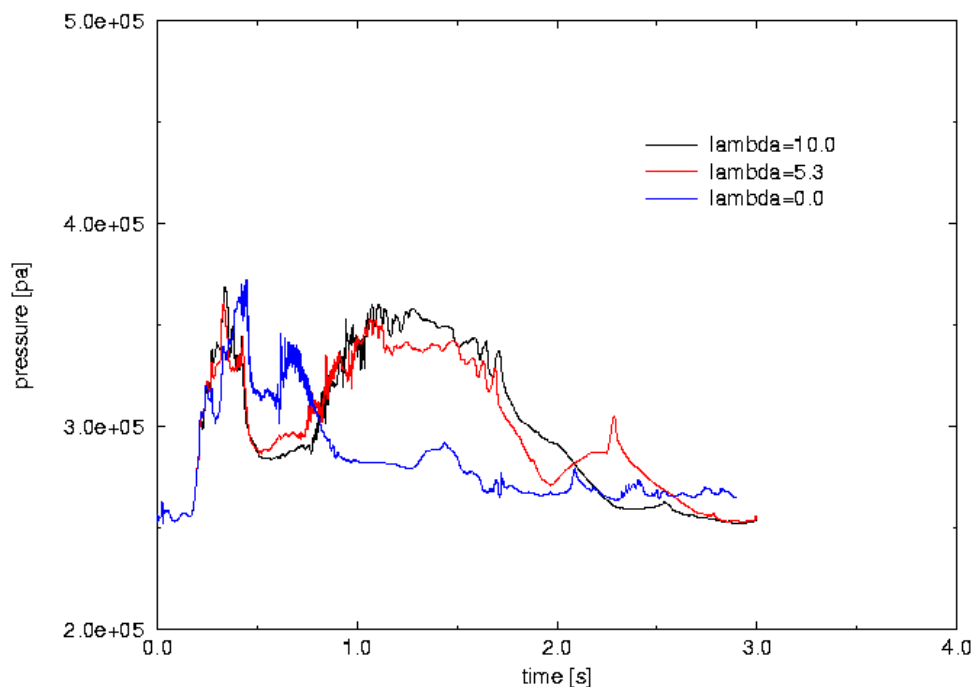
Figure 6.31: Pressure in downcomer at different plate loss coefficients

2s the release of melt equalises in all cases because the pressure in the lower plenum tends towards the initial one. After 3s between 10 tons and 13 tons of melt with an internal energy of 15-18GJ are accumulated in the lower plenum (see Fig.6.34, 6.35 and Table 6.1).

Considering the premixed melt mass and energy the influence of the flow plate by pressure loss becomes obvious (see Fig. 6.32 and 6.33). In case of $\lambda=0$ a maximum of premixed melt mass of 0.6 tons with an internal energy of 0.9GJ is calculated. The maximum is reached at 0.7s. Assuming $\lambda=10$ 1.1 tons of melt with an energy of 1.4GJ are in premixed condition. The maximum is reached at a later time of 1.3s. After having reached the total maximum the premixed energy decreases but particularly in case of $\lambda=5.3$ (which is the reference design value) between 2s and 3s local maxima of the same magnitude are calculated. This means that

61

the time interval where a steam explosion might occur is enlarged and also the potentially involved thermal energy becomes larger.
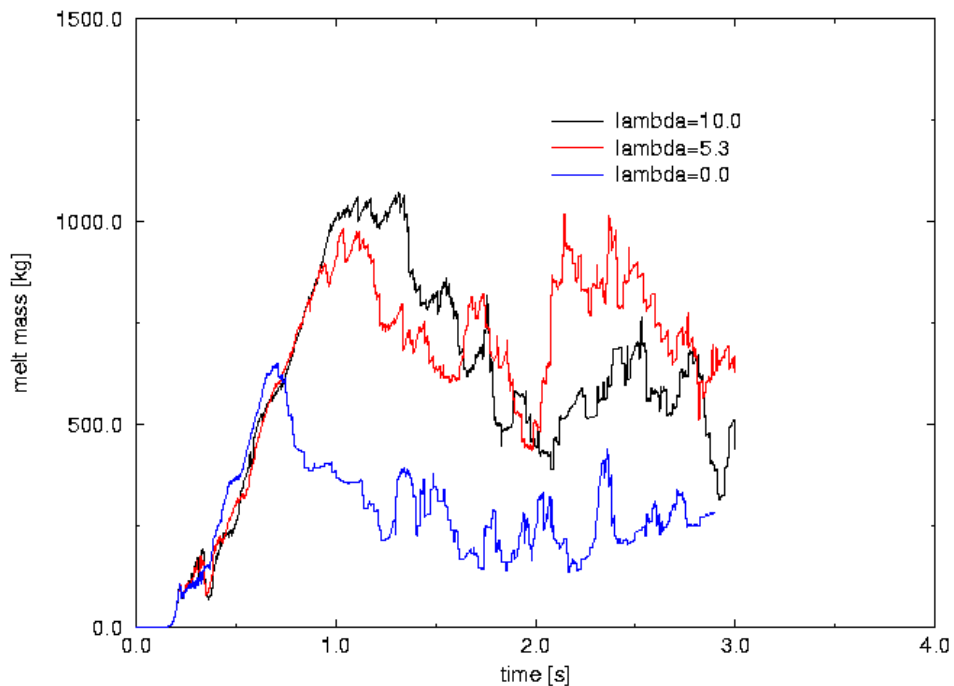
Figure 6.32: Premixed melt mass in lower plenum at different plate loss coefficients

On the other hand the mass of water in lower plenum (Fig. 6.36) decreased significantly in case of $\lambda=5.3$ and 10.0. at t>1.2s. At t=3s in case of $\lambda=0$ 2.2 tons of water are still in the lower plenum. Assuming $\lambda=5.3$ or 10.0 only 0.4 tons of water are calculated.

Figure 6.37 shows the averaged volume fraction of water in lower plenum which is in premixed condition with melt. Between 0.6s and 1.2s where the maxima of premixed melt are calculated the averaged water volume fraction varies between values of 0.25 and 0.33. After 1.2s the dependence from the loss coefficient is not clear. One can only state that the averaged water volume fraction varies around 0.25.

Table 6.1 presents a comparison of water-, melt- and vapor balances of the different cases. For $\lambda=5.3$ and 10.0 after 3s the total water inventory in the vessel is reduced to about 1t compared to 6.5t in the case without any pressure loss of the plate. At this time the released mass of melt varies between 10t and 13t. Only small amounts of the melt are blown out of the vessel (between 1kg and 13kg). Another interesting fact is the significant increase of melt surface in case of $\lambda=10.0$. The melt surface is presented here as difference between the maximum and the initial value. This is done because most of the melt is located in the pool. The melt pool is penetrated by gases and therefore the model assumes a surface of the melt within the pool. Assuming the pool doesn't change very much during the scenario time of 3 s

the just mentioned difference is close to the surface of melt which is removed out of the pool into the lower plenum.
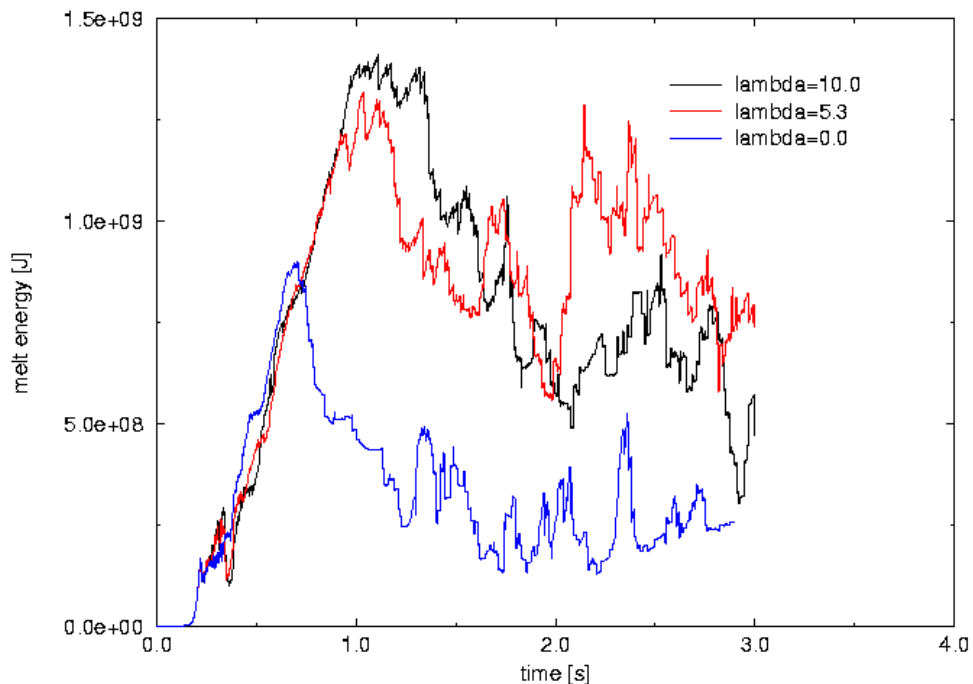
Figure 6.33: Premixed melt energy in lower plenum at different plate loss coefficients

There are two possibilities to explain the increase of melt surface. The first one is an increase of fragmentation when the melt penetrates through the plate. The second possibility is a contact of melt with water when the melt has penetrated over the plates surface and has reached its verge. Because the time dependence of the melt surface is nearly a plateau function between 1s and 3s it seems evident that the first possibility is the more probable mode because the melt needs more than 1s to reach the verge of the plate.

The pressure loss of the plate enforces the interaction between water and melt which leads to an increased evaporation. The produced mass of vapor which is very close to the mass of vapor blown out of the vessel increases from 114 kg in case of $\lambda=0$ by a factor of more than two to 280kg at $\lambda=10$.

In summary one can draw the following conclusions:

The existence of the flow plate results in an increased premixing by fragmentation of the melt. The premixed melt energy is enlarged by 50% from 0.9 GJ up to 1.3 GJ ($\lambda=5.3$; design conditions). The maximum is reached later and further maxima with similar amplitudes are calculated later into the transient. The existence of the flow plate increases the probability and most probably the strength of a steam explosion if it might occur.

Table 6.1　　Influence of flow plate loss coefficient in case of axial melt release

	Initial state	λ=0.0	λ=5.3	λ=10.0
		t=3s	t=3s	t=3s
Total water	18.2t	6.6t	1.2t	1.4t
-in lower plenum	16.1t	2.2t	0.4t	0.4t
-in downcomer	2.1t	4.4t	0.8t	1.0t
Evaporated water	0.0t	0.1t	0.2t	0.3t
Water lost	0.0t	11.5t	16.8t	16.5t
Total melt	109.8t	109.8t	109.8t	109.8t
-in lower plenum	0.0t	10.2t	13.0t	10.0t
		15.5GJ	18.0GJ	14.8GJ
-melt lost	0.0kg	1.1kg	10.4kg	13.1kg
Premixed melt	0.0t	0.6t (0.6s)	1.0t (1.1s)	1.1t (1.3s)
Melt surface max-surf(t=0)	0m^2	2350m^2 (1.4s)	2550m^2 (1.2s)	4150m^2 (2.7s)
Total vapor	201.6kg	209.2kg	182.7kg	179.4kg
Lost vapor	0.0kg	114.3kg	259.5kg	280.6kg
Pressure	2.6bar	4.2bar [1]	4.4bar [1]	5.0bar [1]

[1] short time scale fluctuation caused by packing

6.2   MATTINA

6.2.1   Base case calculation

The base case is the same as described for MC3D: distributed axial outflow of melt through the lower core support plate (LCSP) in a central region with 45 cm radius. The porosity of this area is 0.33 and the initial particle diameter is assumed to be 5 cm in rough agreement with the size of the holes in the LCSP. In this case the free volume within the LCSP outside the central melt outflow area is assumed not to be available for flow. The central region through which the melt is released is initially filled with steam.

Penetration of the melt into the water leads to a first pressure transient which reaches about 4.2 bar and is about 0.2 sec wide. (For illustrations see Section 6.3 in which these results are compared with the corresponding MC3D results.) When this event starts, the melt mass in the lower plenum is still below 100 kg, but the surface is suddenly increased significantly by break-up of the large drops. Although the event is quite limited and is even not able to stop the melt flow into the lower plenum, it is determining for the further course of events. Above all, the pressure remains higher than 3 bar from then on and liquid water is pushed into the downcomer so that no vapour can escape there. This causes the pressure level to rise to values between 3.5 and 3.7 bar in the period from 1 sec to 2 sec. It returns to the initial pressure only when, after 2 sec, most of the liquid water has been removed from the pressure vessel so that again steam can be vented.

In spite of the increased pressure level, the melt continues to flow into the lower plenum all the time with a rate of typically 3.7 t/sec. Only after 2 sec the rate increases to about 7.7 t/sec but that has no significance because then practically no water has remained in the pressure vessel.

- The events can be summarised as follows:
- Pressurisation starts at 0.175 sec with a peak of about 4.3 bar
- Pressure remains high (up to 3.7 bar) until 2.2 sec
- Melt flows continuously into the lower plenum at a rate of about 3.7 t/sec
- Only 10 % of water left in lower plenum after 1 sec
- Practically no water left in lower plenum after 1.2 sec
- Only 10 % of water left in reactor pressure vessel after 2 sec
- Practically no water left in reactor pressure vessel after 2.2 sec
- At 2.2 sec there are about 8.2 t of melt in the lower plenum.

The initial pressure event also very effectively separates the water from the melt so that very little mixing occurs. There is only one transient mixing event between 0.6 and 0.8 sec leading to 800 kg of mixed melt. The thermal energy in this melt amounts to 0.9 GJ only. According to the assumptions used in MATTINA for corium, most of this mass would already be frozen so that it would not be available for a steam explosion. It might however be that the core melt in an accident case contains enough metallic zirconium to keep the corium liquid (and thus prone to fine-scale fragmentation and steam explosions) until the much lower melting point of zirconium is reached. There is, however, an important effect of the thermal interaction on the mean specific heat content of the mixed melt and in addition this thermal interaction causes a low mean water volume fraction in the mixture. This would suggest a low 'efficiency' of a possible steam explosion. But as such detailed calculational results are not sufficiently reliable

at the moment, we do not pursue this argument. It is clear that after about 1 sec no further significant mixing can occur because no water is available in the lower plenum

6.2.2 Parametric analysis

First the influence of the flow plate in the lower plenum was studied by performing calculations with and without that plate which, here again, is simulated as a geometrical restriction (local porosity) only without an explicitly simulated pressure loss (without pressure loss coefficients). It turns out that the velocity of descent of the melt particles is lower below the flow plate than it is above. Furthermore, the thermal interactions (pressurisation events) are slightly stronger without flow plate and consequently the maximum amounts of the mixed melt mass are smaller in that case. The effect of the flow plate increases with the intensity of the thermal interactions, e.g. with the melt mass involved. The effect on the intensity of thermal interaction events described above might be due to a separation of the lower plenum into two compartments with a pressure event developing only in one of them (most probably the upper part) with the melt in the other part not being involved.

In further parametric studies the area of outflow was increased beyond the 0.21 m^2 that result from the failure radius of 45 cm chosen for the base case. Such large failure areas are considered as overly pessimistic and the results are, therefore, not reported here in detail. In general terms it is found that the intensity of the pressurization events and the maximum values of mixed melt mass increase with the rate at which melt is released from the core region. But this does not lead to arbitrarily large values because an opposing effect is observed when the sustained pressure developing in the lower plenum exceeds about 6...7 bar: in that case the integrity of the melt pool is lost as it is penetrated by steam from below. This does not necessarily mean that the flow of melt into the lower plenum is stopped. Rather an instability develops and steam penetrates locally in the centre or at the outer rim of the failure area while melt continues to flow down in the remainder of the failure area. However, this penetration, i.e. the existence of a hole in the melt pool, means that it can no longer be accelerated effectively (as a slug) by a possibly developing steam explosion, because the explosion pressures themselves would escape (at least partly) through that hole. Of course, details of this also depend on the assumptions made concerning the melt pool.

6.3   Comparison of MC3D and MATTINA results

To have some direct comparison between the two codes applied to the EPR-FCI-problem some results are compared for the base case described in Section 6.1.1 and 6.2.1. In both calculations the same initial conditions are used, but the mesh in MATTINA is coarser (about a factor of 2) in the important interaction zone (see Section 4.2). Figure 6.38 shows the pressure at the bottom of the lower plenum. During the first intensive contact of corium with water a small pressure peak appears with MC3D. With MATTINA the first interaction is much more violent and gives a pressure peak of 4.5 bar compared to 3 bar from MC3D. The reason is a stronger local fragmentation due to MATTINA modelling. Generally the pressure is higher with MATTINA during the first 2 s. The onset of strong oscillations defines the time when a compact melt accumulates at the bottom. That happens about 0.3s later in MATTINA and the oscillations have much larger amplitudes.

The tendency to higher pressures is also seen in the downcomer pressure. Figure 6.39 shows the pressure at the lower end of the downcomer for MC3D and the pressure at the upper molten corium level for MATTINA. The first small differences are due to the hydrostatic pressure of water in the MC3D case. Generally the pressure is higher for the MATTINA calculation. The stronger pressure in case of MATTINA due to a more violent interaction

leads to less premixing. The thermal energies given in Figure 6.40 are more than a factor of two smaller what concerns their maximum values.

Lower thermal energy in the mixing zone could have two reasons: lower corium temperatures or smaller mixed melt mass. As seen from Figure 6.41 the main reason in the present comparison is the smaller amount of mixed melt mass in case of MATTINA. In the late phase the lower temperatures of melt in MATTINA becomes more dominating and the difference between the two curves is not as large as in the thermal energy curves. In the MATTINA calculation only one maximum appears and the mixing energy tends to zero for the late phase, which is not the case in the MC3D calculation.

The average water volume fraction in the mixing zone (Figure 6.42) is much lower for the MATTINA case. It increases at the end of the calculation where nearly no melt is available as seen from Figure 6.40. The high pressure events in MATTINA lead to a reduction of the melt release rate by acting as counter pressure to the hydrodynamic pressure at the bottom of the corium pool (Fig. 6.43). A large difference between the results of the two codes is related to the transient water inventory in the lower plenum (Figure 6.44). With MATTINA all the plenum water is displaced after 1 s, while with MC3D about 7 t of water are retained together with about 16 t of melt in a stratified configuration.

As general conclusion of the comparison for the base case of axial melt relocation we can say that MATTINA calculates a more violent interaction when the melt poures into water by stronger melt droplet fragmentation leading to higher pressures and stronger water depletion effects.

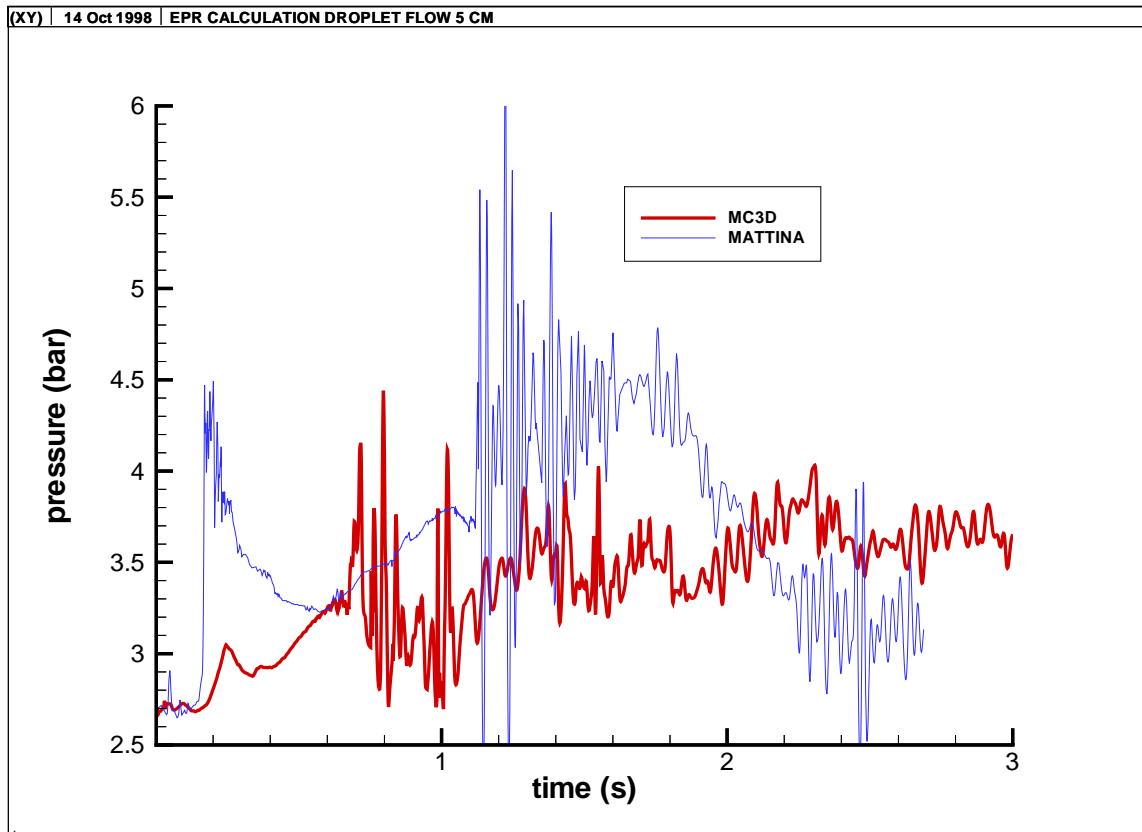Figure 6.28 Pressure at the bottom (center) of the lower plenum
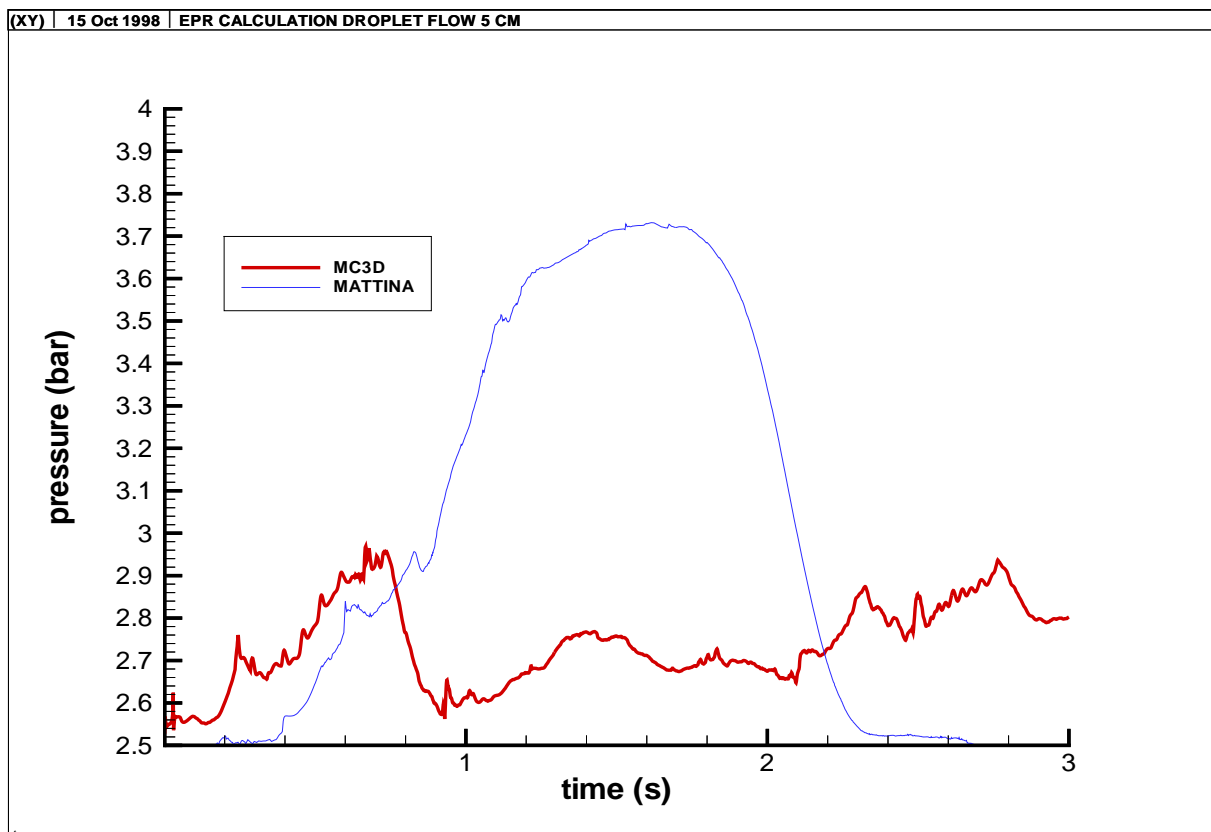
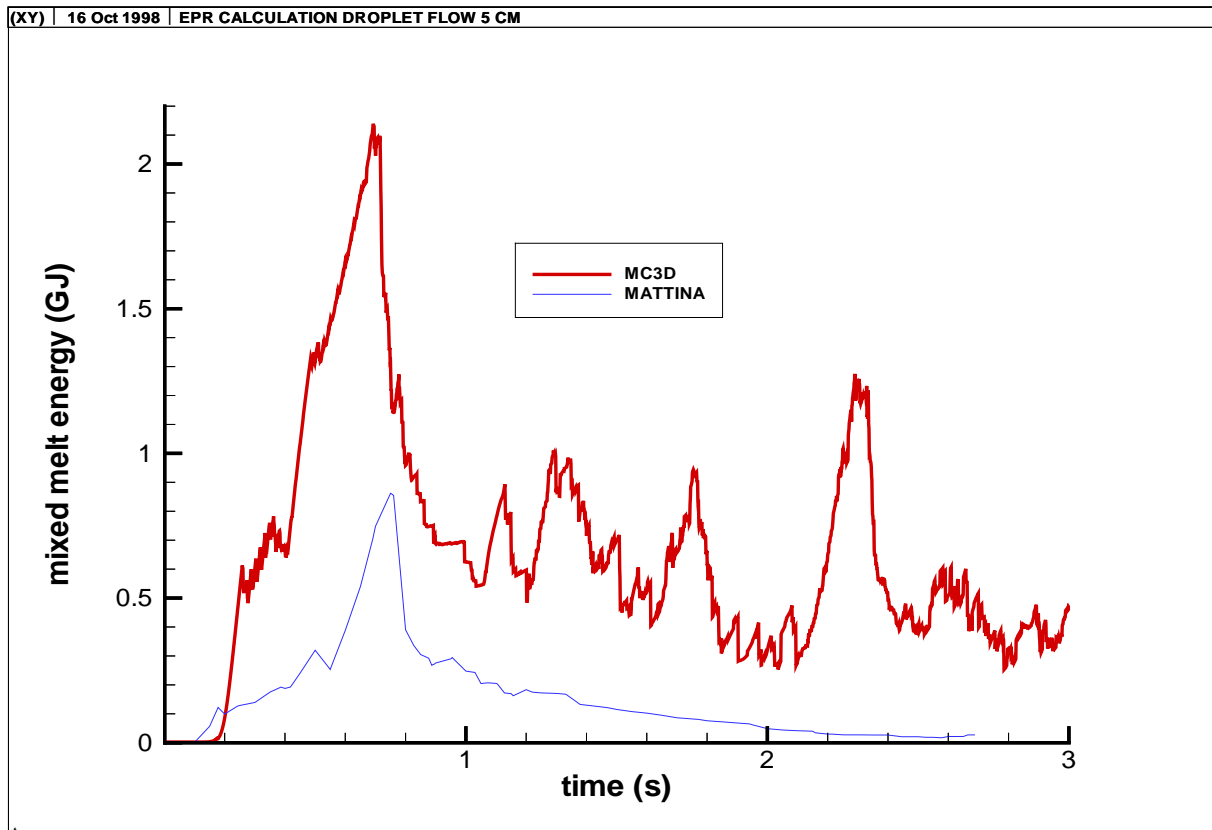Figure 6.29 Pressure in the downcomer

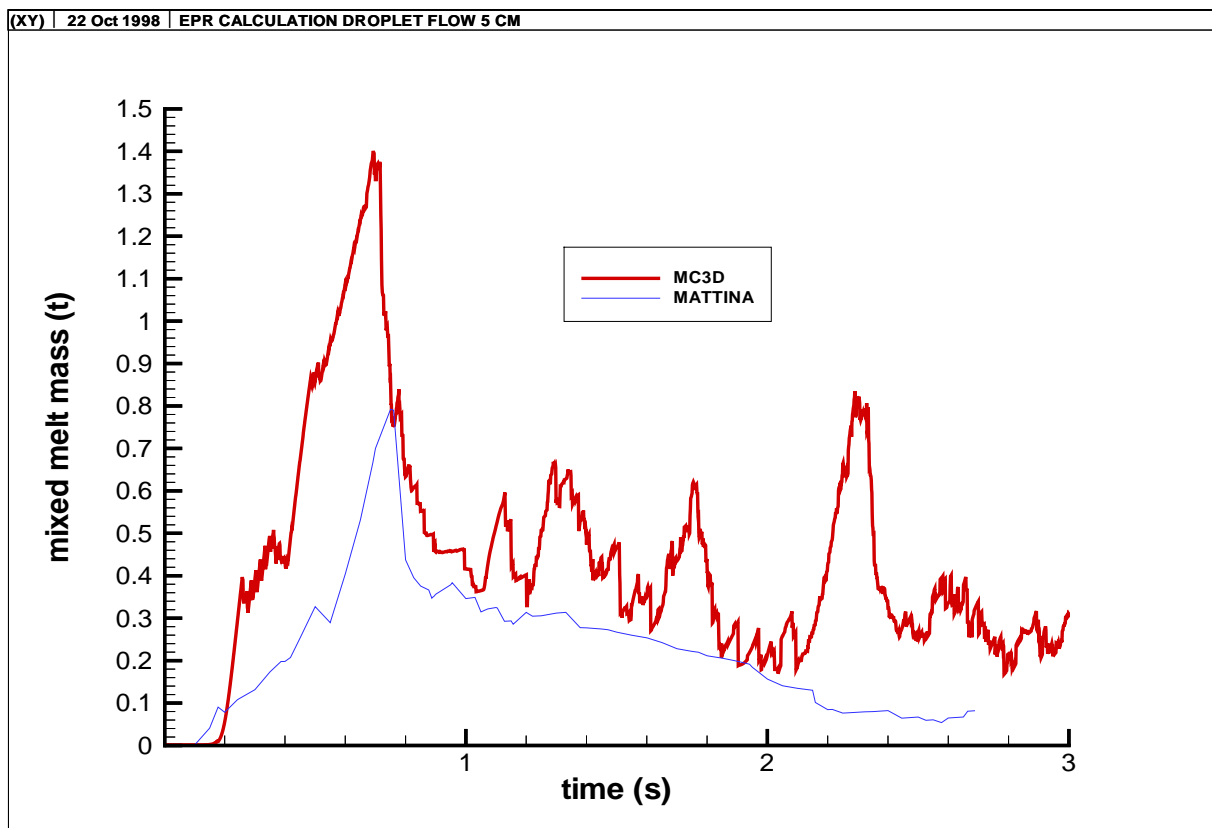Figure 6.30 Premixing data for the 0.1 limit of water volume fraction

Figure 6.31 Premixed melt mass for the 0.1 limit of water volume fraction
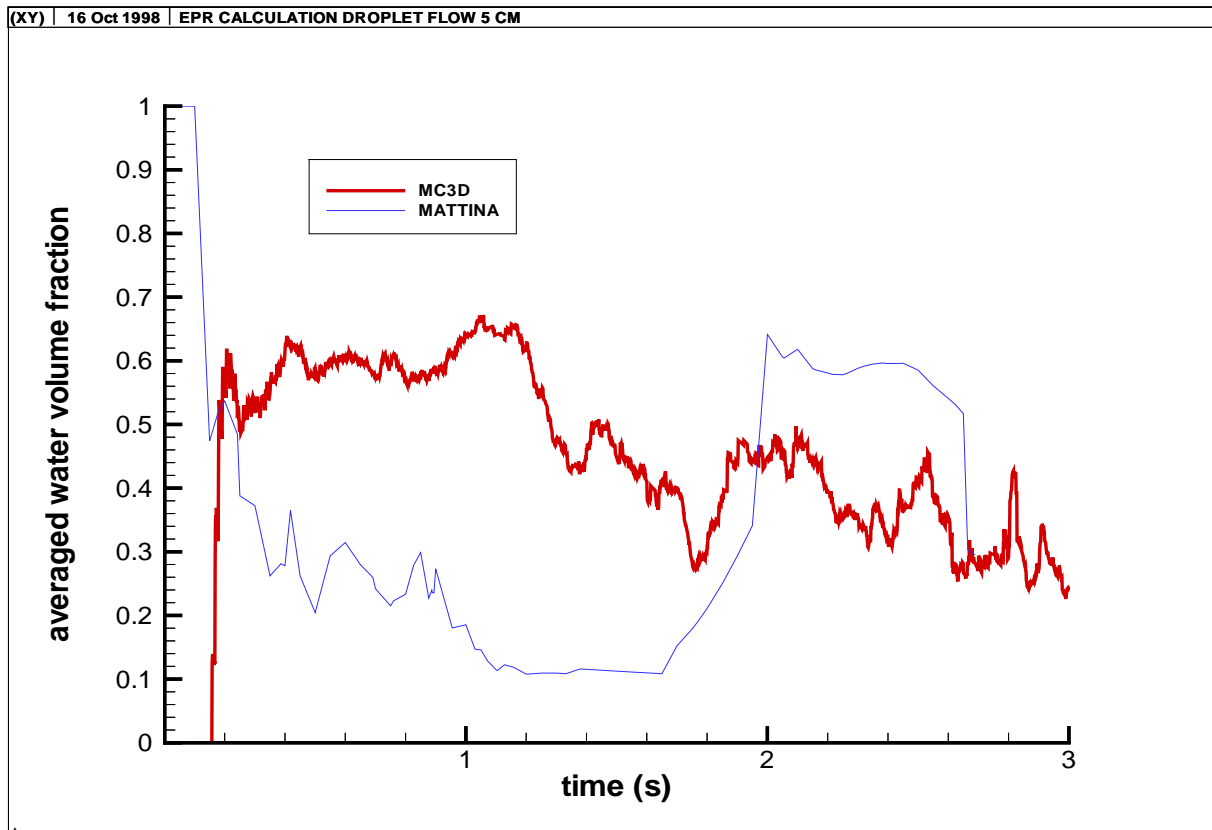
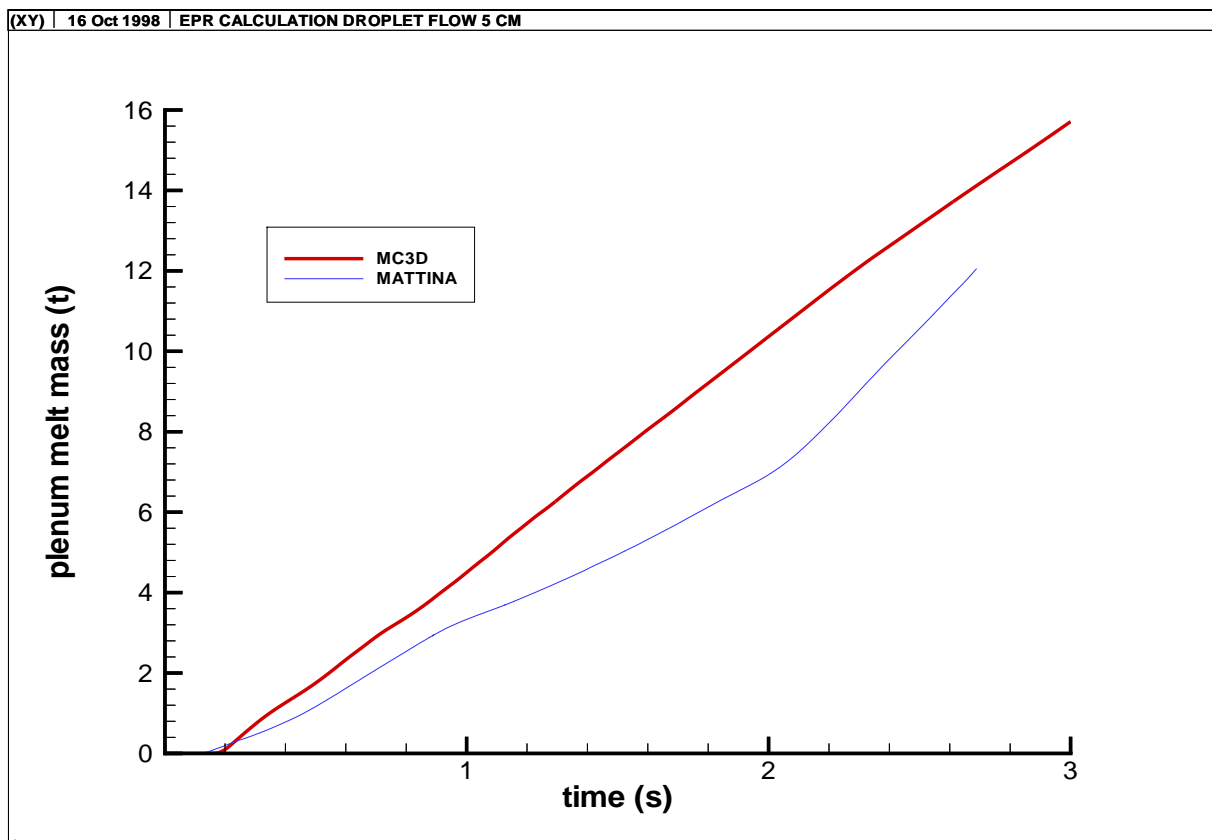Figure 6.32 Average water volume fraction in the mixing zone
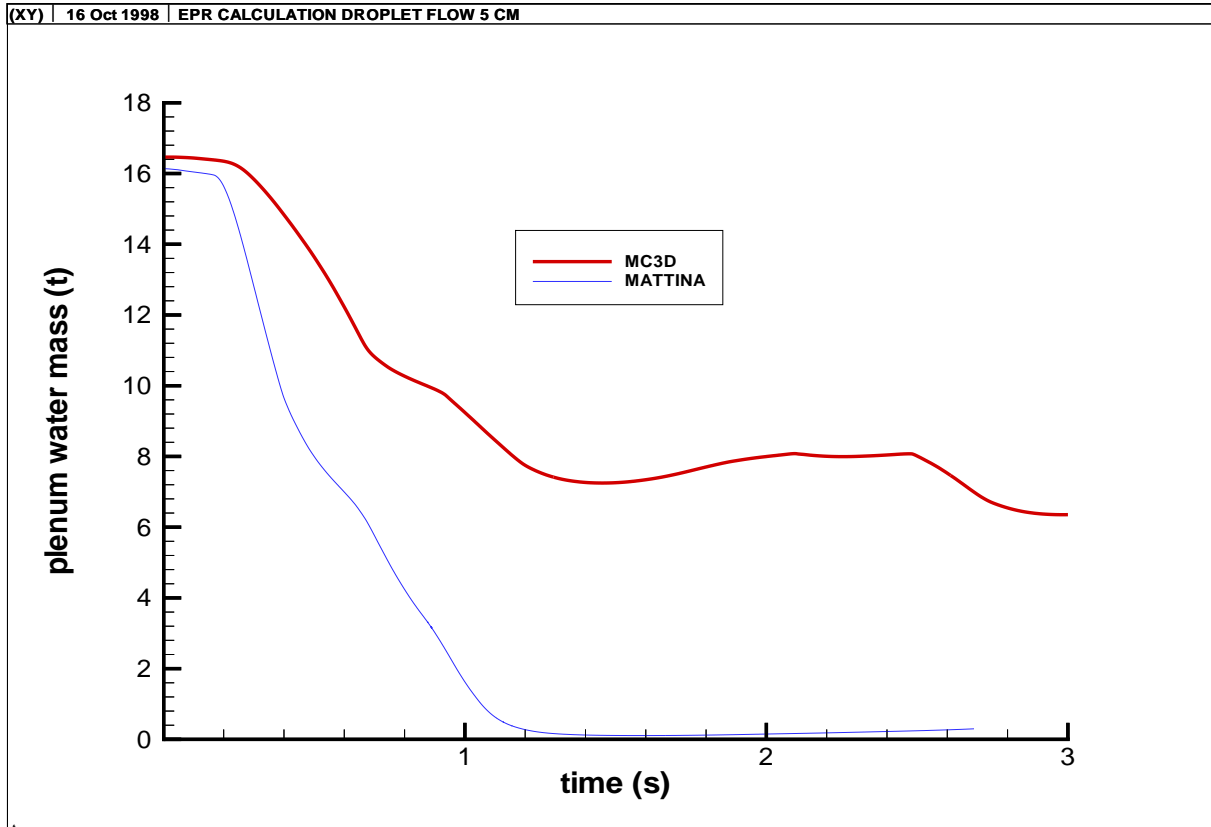
Figure 6.33 Lower plenum inventory of melt

Figure 6.34 Lower plenum inventory of water

7 Results of premixing calculations in case of radial melt relocation

During a core meltdown accident of the EPR it is most probable, that the heavy reflector melts at its radial periphery. This is a consequence of the occurrence of the maxima of the heat flux near the surface of the molten pool inside the heavy reflector.

Since it is rather expensive to perform three-dimensional simulations of fuel-coolant interactions, axisymmetric problems have been considered mainly, in order to cover a sufficient amount of different outflow scenarios and to perform a few parameter variations. However, one 3D-simulation was performed as well.

The most important drawback of the 2D approach in the frame of radial leakage scenarios is the implication of a radial leak across the whole perimeter of the heavy reflector, which is certainly not realistic. The only justification in applying this approach is the hope to get conservative estimates of the premixed masses and energies, because of the large area of the leak, and, consequently, the large outflow rates of the melt.

It should be emphasized however, that, due to the large numerical diffusion of first order space and time approximations used in the MC3D code, an inherent tendency of separation of melt and water by steam in the calculated flow fields exists. The influence of this effect on the premixing quantities can hardly be assessed without comparison with calculations with higher order methods, which are not available. It is however probable, that the separation of melt and water reduces the premixed mass and energy significantly. As discussed in section 5 definition of integral values characterising the premixing state attempts to compensate this known difficulty of the calculations.

7.1 MC3D – Results using the TRITHYD-application

In this section, results of some MC3D simulations of radial outflow scenarios with the triphasique (TRITHYD) application of the code will be given. The most probable failure mode of the heavy reflector is a melt-through failure in the upper heavy reflector region surrounding the melt pool. Therefore as base case of the 2-D simulations

1. a leak area of 5 % ($\equiv$ 0.138 [m^2]) in the upper part of the heavy reflector, closely below the surface of the molten pool, is assumed. The identification number[1] of this case is (145.16:49). The initial particle diameter of the fragmenting melt is assumed to be 5 mm. The pressure loss coefficient of the flow plate in the lower plenum of the reactor vessel is assumed to be 0.

Since it is not possible to extract the exact location of the failure of the heavy reflector from severe accident analysis codes like SCDAP/RELAP, the cases of a small and a large leak at the bottom of the heavy reflector, directly above the lower core support plate, are also investigated. Consequences of the small leak have been analyzed applying a 3-D coarse mesh approach and a respective 2D approach. The two considered leak areas of the 2D-simulations were

2. 5 % ($\equiv$ 0.182 [m^2]) (Identification: 146.16:18) and

3. 25 % ($\equiv$ 0.91 [m^2]) (Identification: 146.15:37), respectively.

---

[1] cf. table 1.1 in the summary

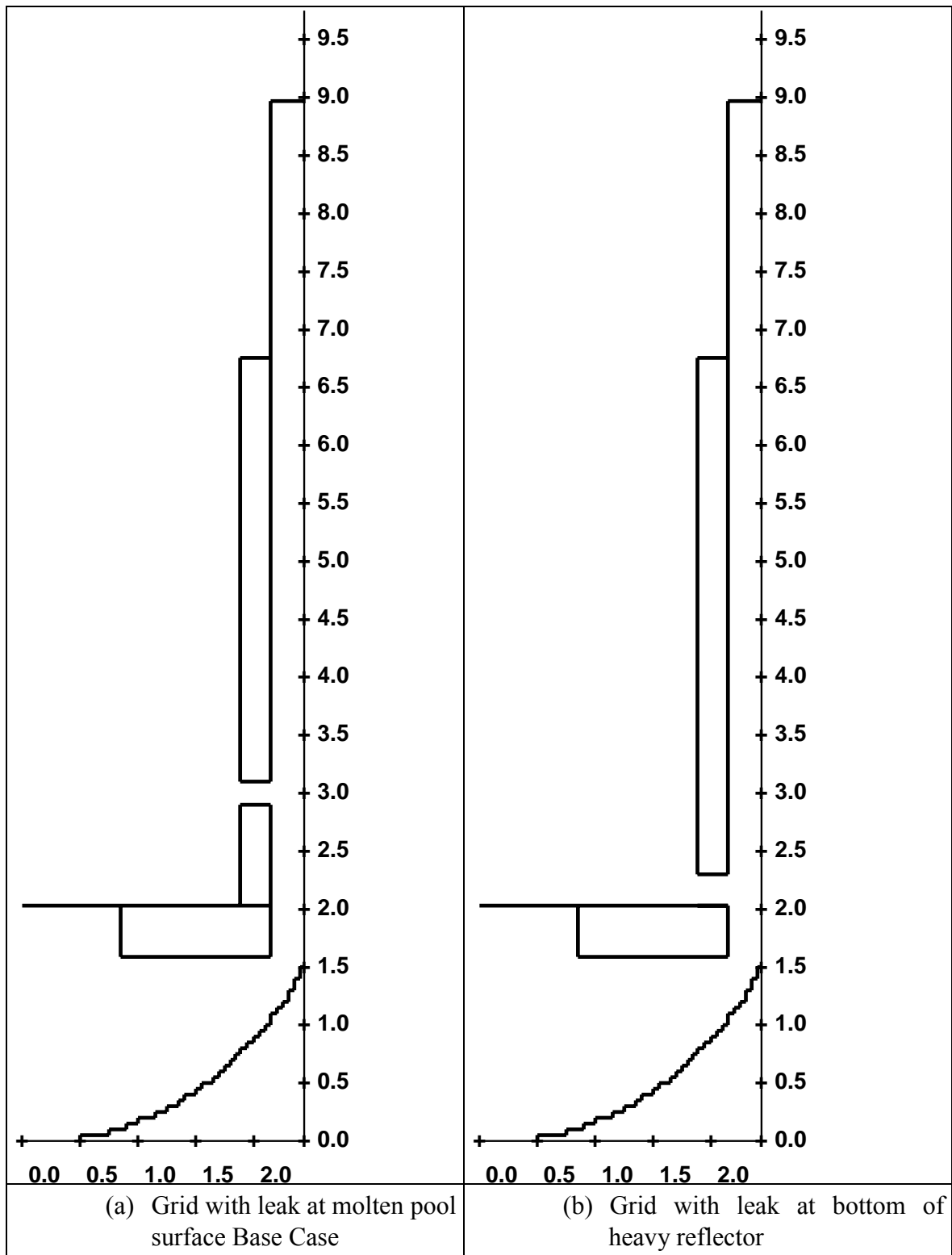| (a) Grid with leak at molten pool surface Base Case	(b) Grid with leak at bottom of heavy reflector

Figure 7.1 Geometry

Figure 7.1 shows the computational grid for the top and bottom leakage scenarios. The number of grid lines is 50 x 60.

In additional two runs the initial particle diameter of the fragmenting melt and the pressure loss coefficient of the flow plate were varied. These two runs were

4. 5% leak in the lower heavy reflector, with 50 mm initial particle diameter (Identification: 160.10:121), and

5. 25% leak in the lower heavy reflector, with a pressure loss coefficient of the flow plate of 10 (Identification: 209.14:10).

Finally (6.) an axisymmetric calculation with the coarser grid of the three dimensional simulation was performed. The basic outflow scenario of this simulation corresponds to the 5% leak in the lower heavy reflector. The pressure loss coefficient of the flow plate was 5.3 in this case. The identification number of the axisymmetric, coarse grid simulation is (265.09:00).

7.1.1 3-D calculation

The essential difficulties in performing 3-D calculations with MC3D are the limited central memory space and very long computation times. Using the IBM-SP256 at the University of Karlsruhe a maximum of 8000 cells is possible. A radial melt outflow scenario with a simulated time of 5s would take around 4 weeks of cpu time. As cpu time increases with n^2 where n is the number of cells it was decided to use a maximum of 4000 cells. The presented 3D scenario was calculated with 3840 cells. Simulating a problem time of 5s took around 150 cpu hours.

In Figure 7.2 the grid is presented. The resolution is 20*8*24 cells. The intention of the grid spacing is to have a good resolution in regions with strong melt-water interactions. So the downcomer has the same radial discretization as the presented fine grid of the 2-D simulations while in regions apart from the position of melt release a coarser grid is used. In circumferential direction symmetry is assumed.

Figure 7.3 shows geometrical positions of the reactor inlet and outlet nozzles. Each of them are represented by one cell in circumferential direction.

The position of melt release through the heavy reflector is placed in the first cell above the core support grid at z=2.03m. The height of the leak is 0.07m. The circumferential position of the leak is between 335 and 0 degrees (see Figure 7.1.2), so that one cell wall is opened for the release of melt. The porosity is set to 0.635. The effective free channel area is equivalent with the presented 2-D cases where the leak is smeared over the whole circumference with a porosity of 0.05.The effective leak area is 0.182m^2. The initial diameter of melt particles created by fragmentation is assumed to be 5mm.

The initial distributions of water and melt and at 1s after beginning of melt release are presented in Figure 7.4. The jet melt hits the wall of the reactor vessel, where it is divided into a small part flowing against gravity while the main part flows down the wall into the lower plenum. When the melt comes in contact with water (note: the initial position of water level is just below the leak) evaporation occurs by which the water is pressed into the downcomer. A circumferential displacement of 180° compared to the leak position is preferred.

At t=5s (Figure 7.5) around 2/3 of the water has left the lower plenum via the downcomer. The residual water is mainly located in lower parts of the vessel. At this time the melt has reached nearly the lowest position of the lower plenum. The fronts of water and melt remain nearly separated at all times in the transient. As shown later the premixed melt mass is small compared with the total amount of melt in the lower plenum.

At t=3s only small amounts of melt are located in the downcomer. During the total simulation time around 15% of the released melt is blown out.
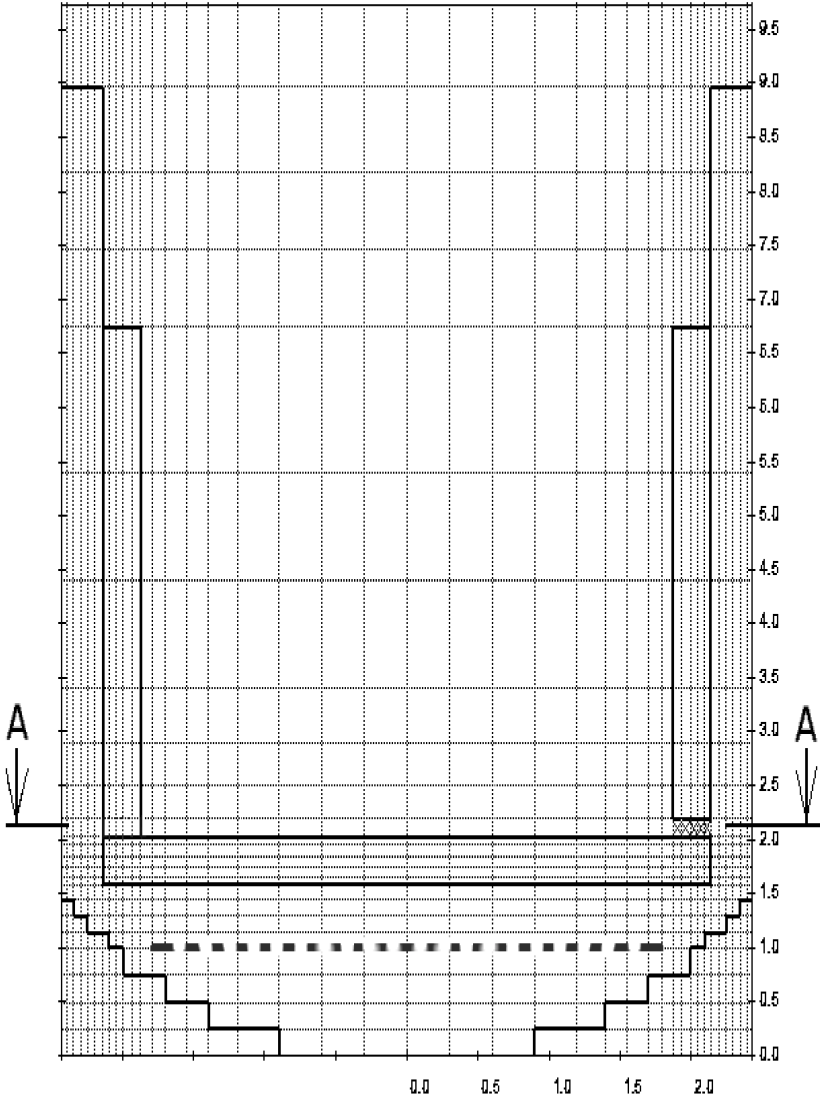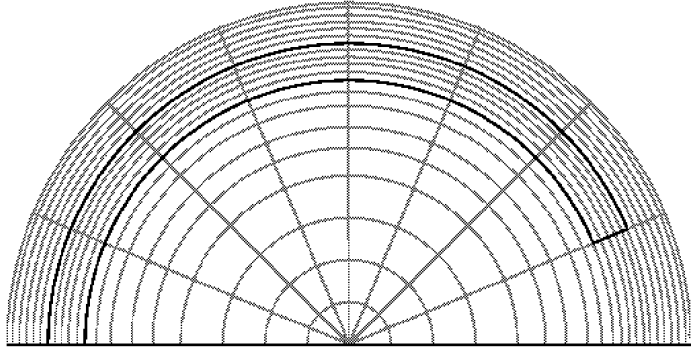

View A-A

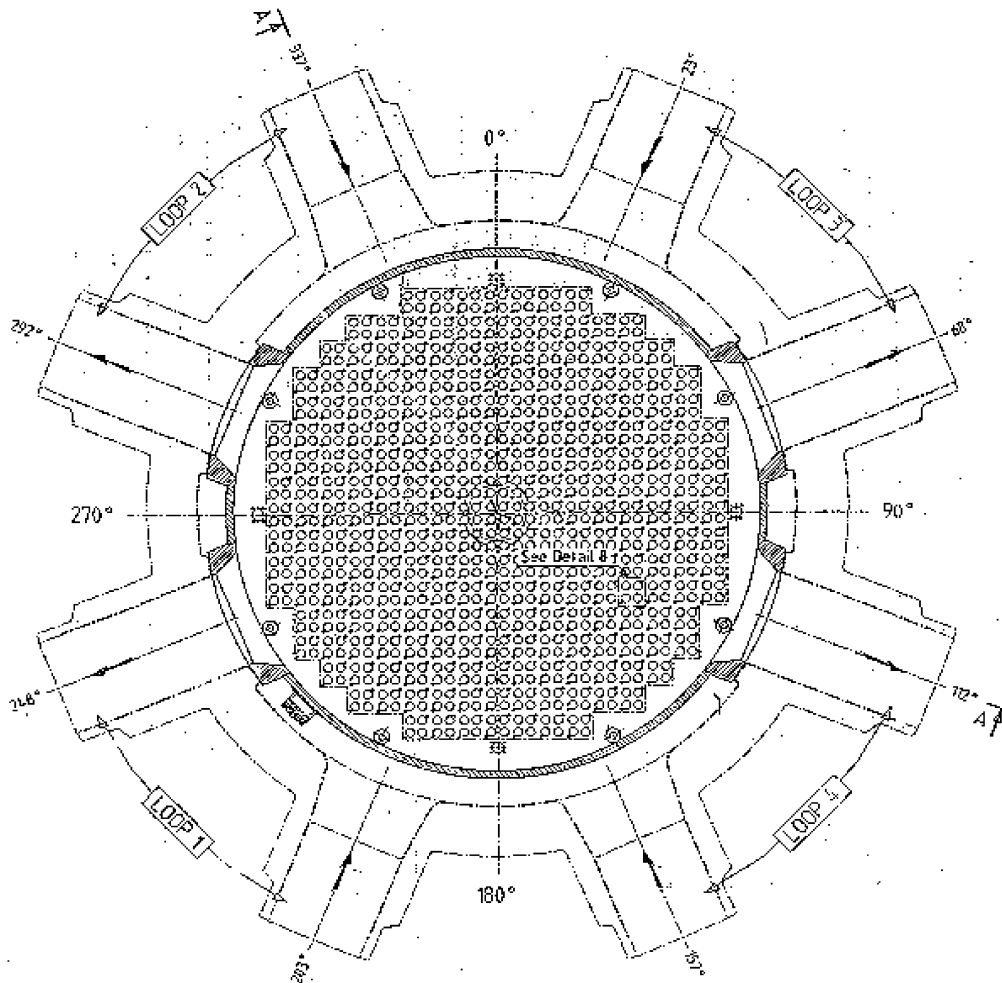Figure 7.2   Nodalization for 3D calculations

Figure 7.3   EPR configuration of inlets and outlets

The circumferential distributions of water and melt are presented by Figure 7.6. The vertical position of the plotted distribution is the level of the flowplate. At t=1s the melt firstly reaches this location . The water begins to move towards the dowcomer displaced in circumferential direction by 180^0 to the position of the leak. At t=3s the melt has spread over more than 2/3 of the circumference. The melt is mainly located near the walls. Only at locations near the leak there is a tendency of radial spreading and enhanced premixing with water. At the end of the scenario at t=5s the melt has spread over the whole circumference.Now the melt is (at this vertical level) completely located at the walls. As mentioned before all pictures show a separation of water and melt.

Figures 7.7 and 7.8 shows the pressure time dependencies in lower plenum and in downcomer. For comparison a 2-D scenario using the same coarse grid and another one using a fine grid are also plotted (see section 7.1.2).

The pressures are –for the same scenario- well correlated when different locations are considered. Pressures in lower plenum are larger because of a hydrostatic surplus. Pressures calculated with a 2-D simulation show more intensive fluctuations. The occurrence of packing problems and other numerical difficulties have more relevance for the whole domain because of the lower number of cells. It is not surprising that the amplitude of peaks is in general higher. There is one exception in the downcomer between 0.7s and 1.8 seconds where the pressure in 3-D seems to be more disturbed. This is because the location where the pressure is

76

plotted is very close to the position of the leak where the melt is released. In 2-D the leak is smeared over the whole circumference so that the effect of packing is reduced when the melt reaches the wall of the vessel.
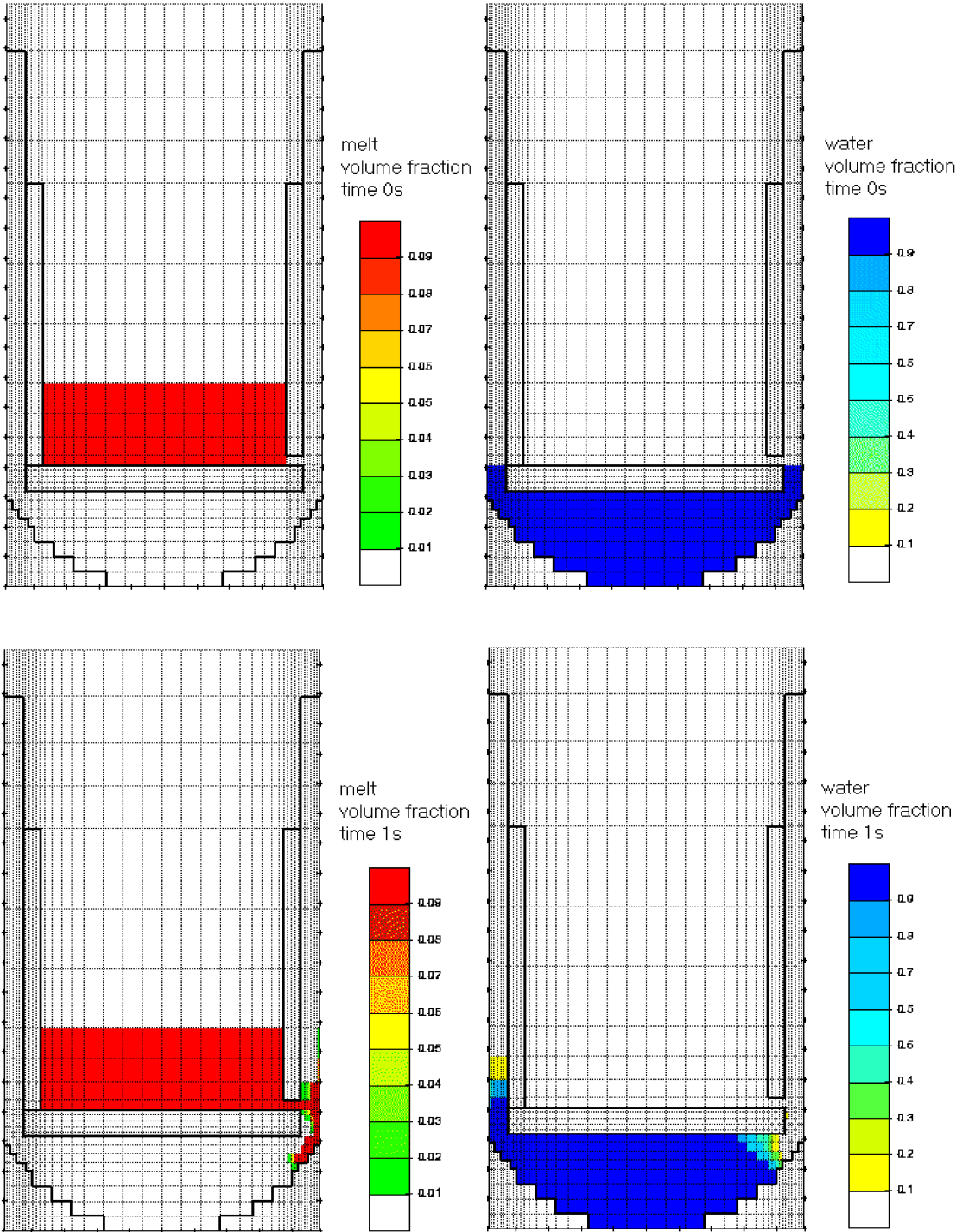
Figure 7.4   Water and melt distribution at t = 0s and t = 1s, 3-D radial release scenario
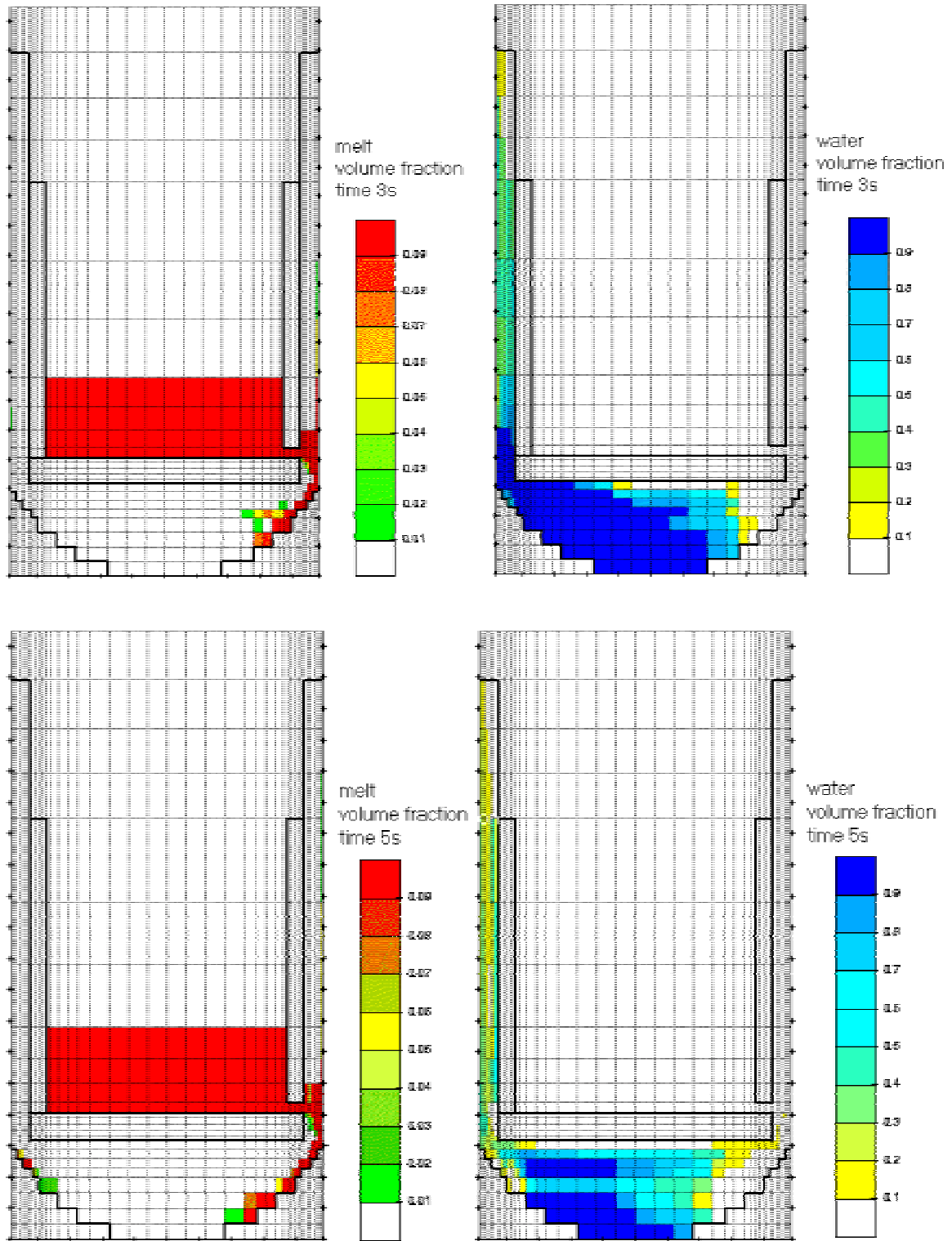
Figure 7.5   Water and melt distribution at t = 3s and t = 5s, 3-D radial release
            scenario

The correlation between the different scenarios is poor. The 2-D pressures show oscillations
at a time scale of 1-2s which cannot be observed in 3-D. In 2-D case of radial melt release the
water in lower plenum is completely enclosed by melt. The water has no possibility to leave
the vessel without a counter flow with melt in the opening of the downcomer. This causes the
just mentioned oscillations.

78

melt volume fraction

0.00 0.01 0.02 0.03 0.04 0.05 0.06 0.07 0.08 0.09 1.00

water volume fraction

0.00 0.10 0.20 0.30 0.40 0.50 0.60 0.70 0.80 0.90 1.00
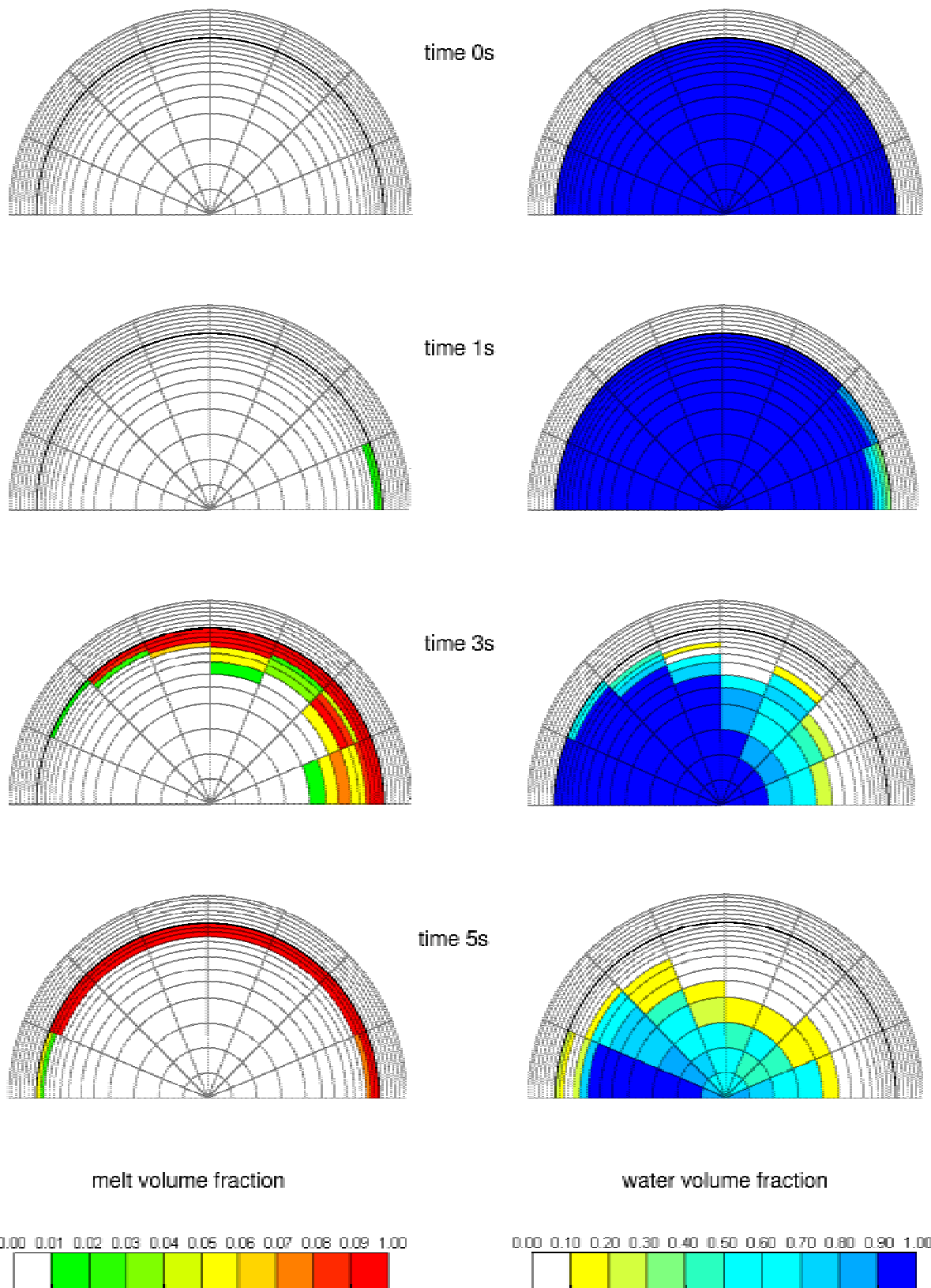
Figure 7.6   Melt and water distributions at vertical level of flow plate in lower plenum

Figure 7.7   Pressure in lower plenum
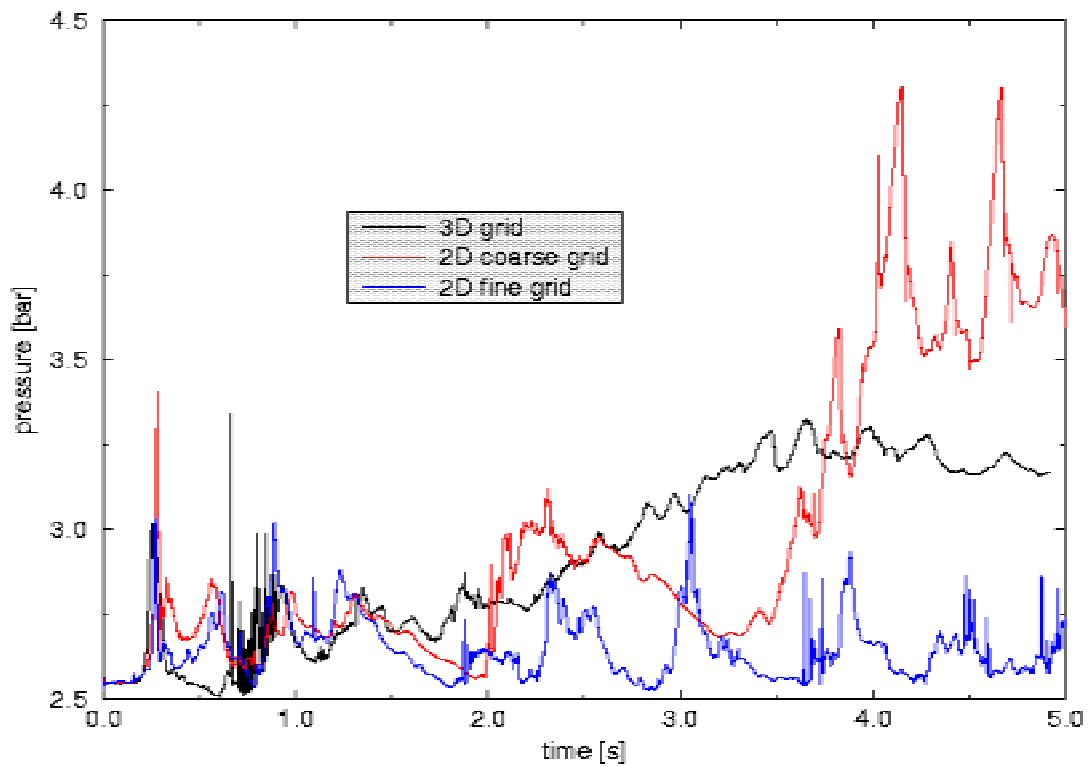
Figure 7.8   Pressure in downcomer

80
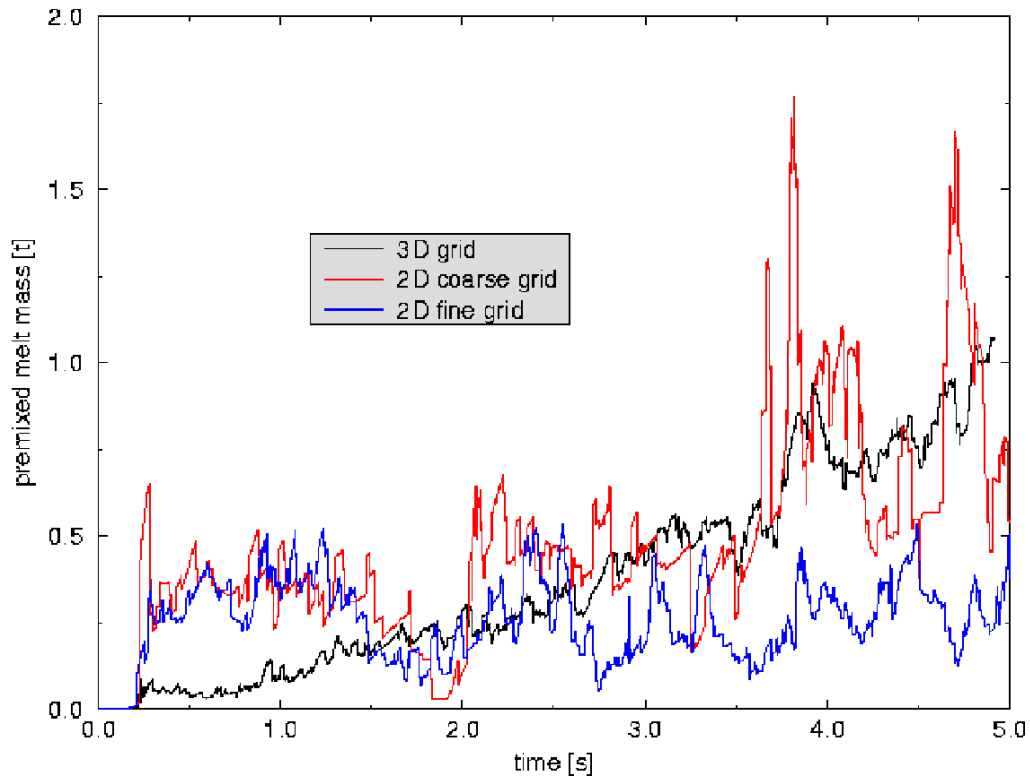
Figure 7.9   Premixed melt mass in lower plenum
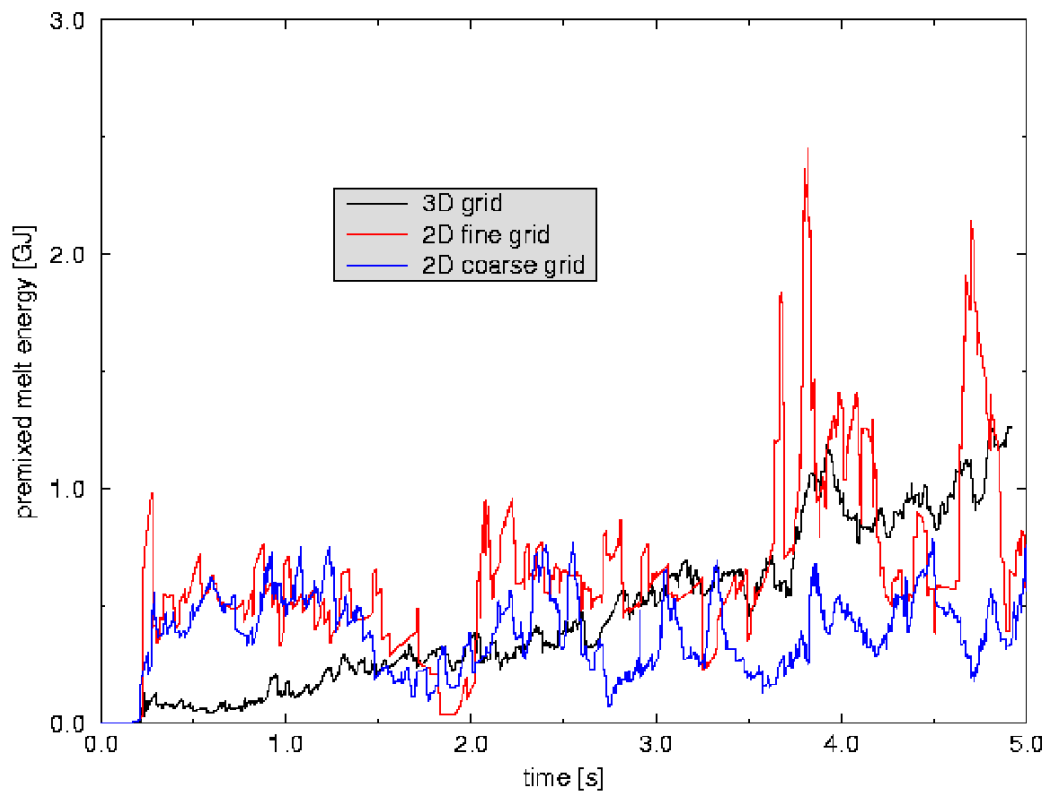
Figure 7.10   Premixed melt energy in lower plenum

81
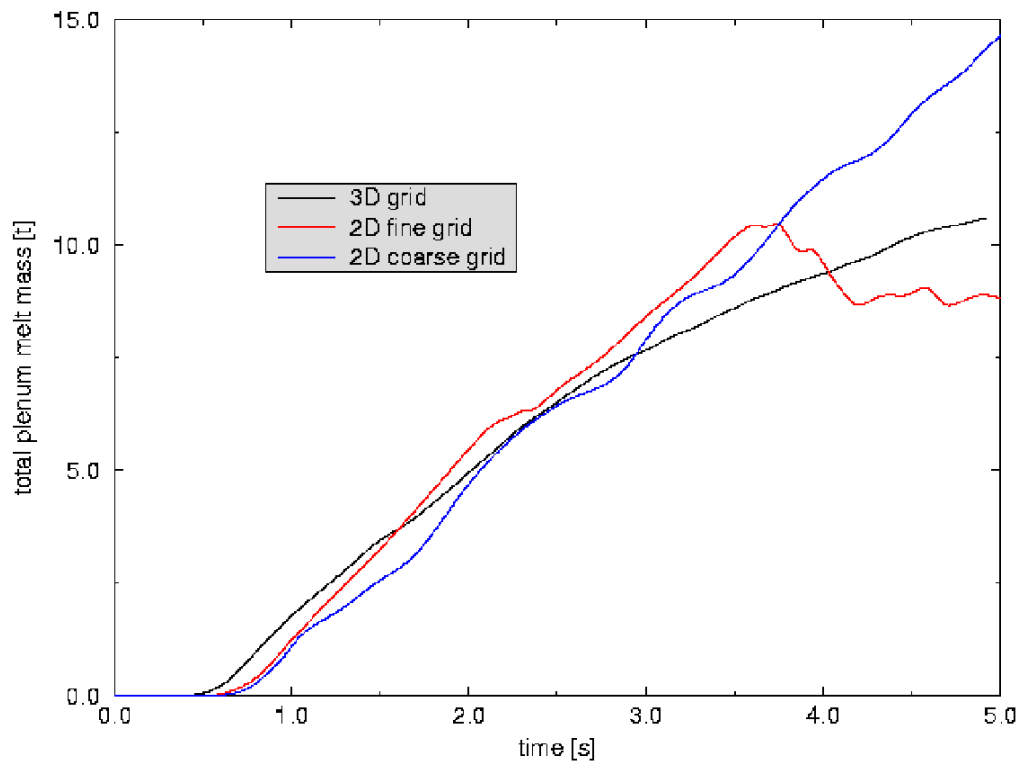
Figure 7.11   Total melt mass in lower plenum
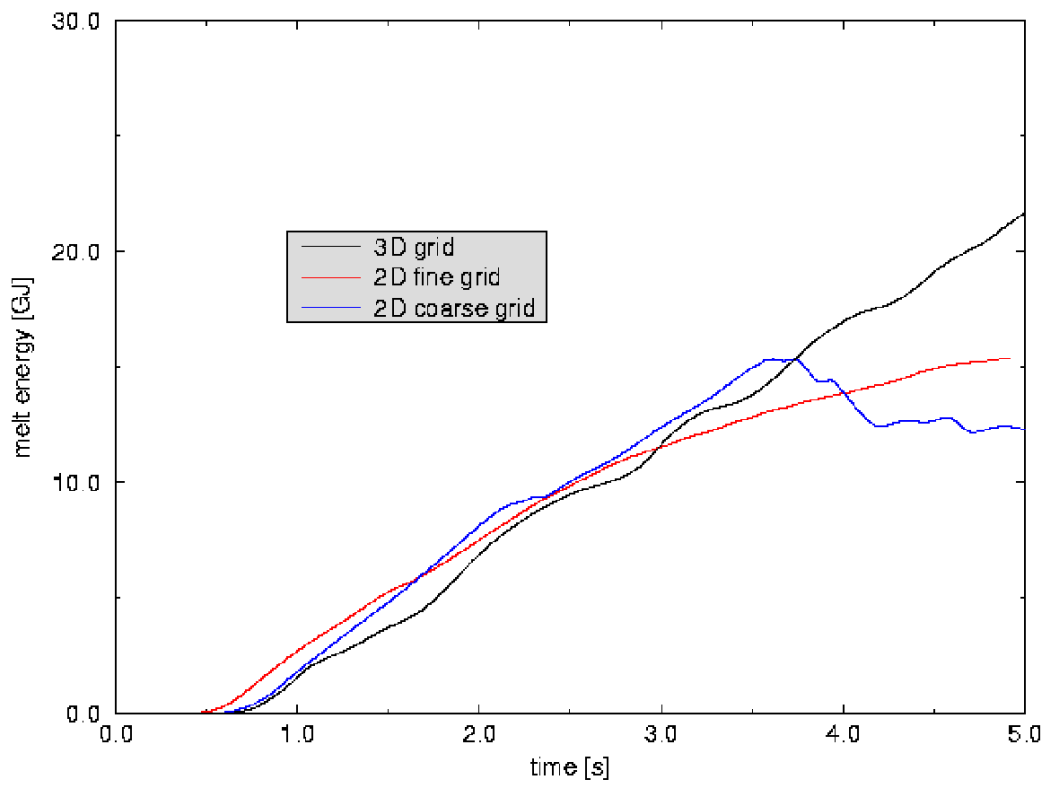
Figure 7.12   Total melt energy in lower plenum
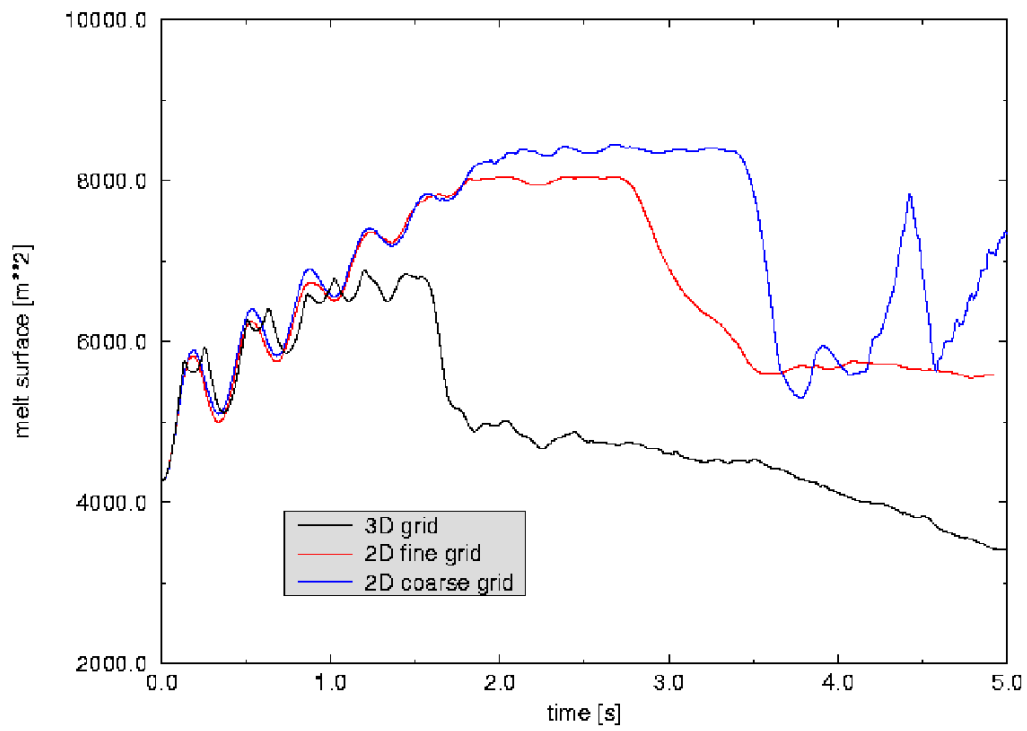
Figure 7.13   Total melt surface in reactor vessel
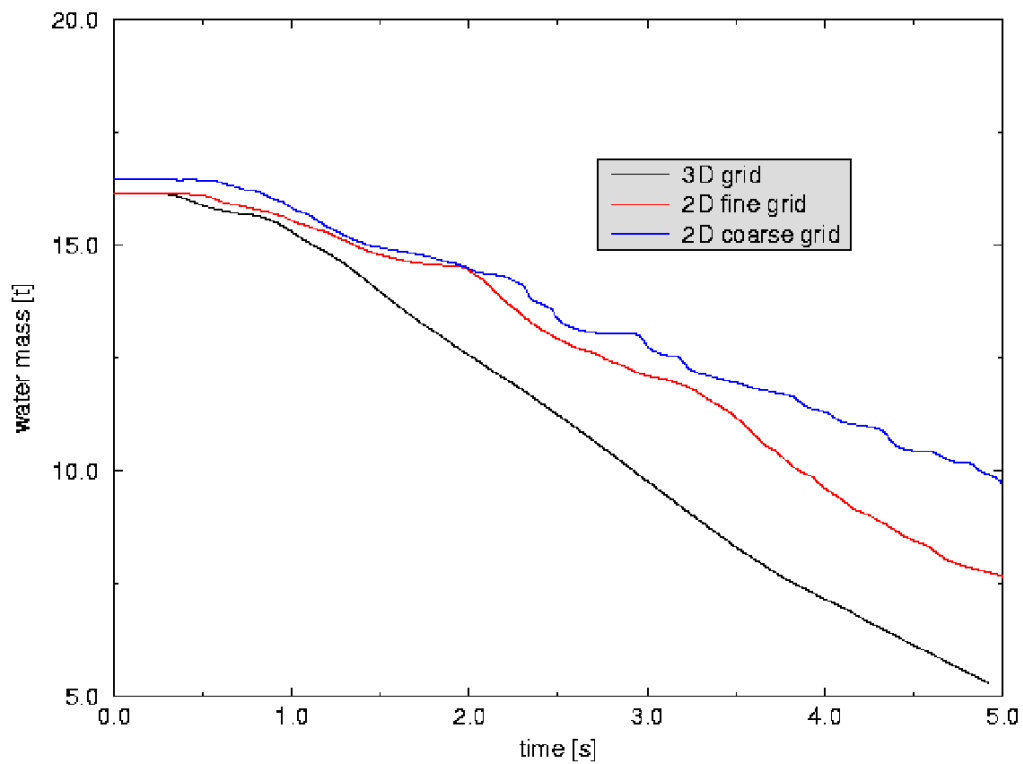
Figure 7.14   Water mass in lower plenum

83
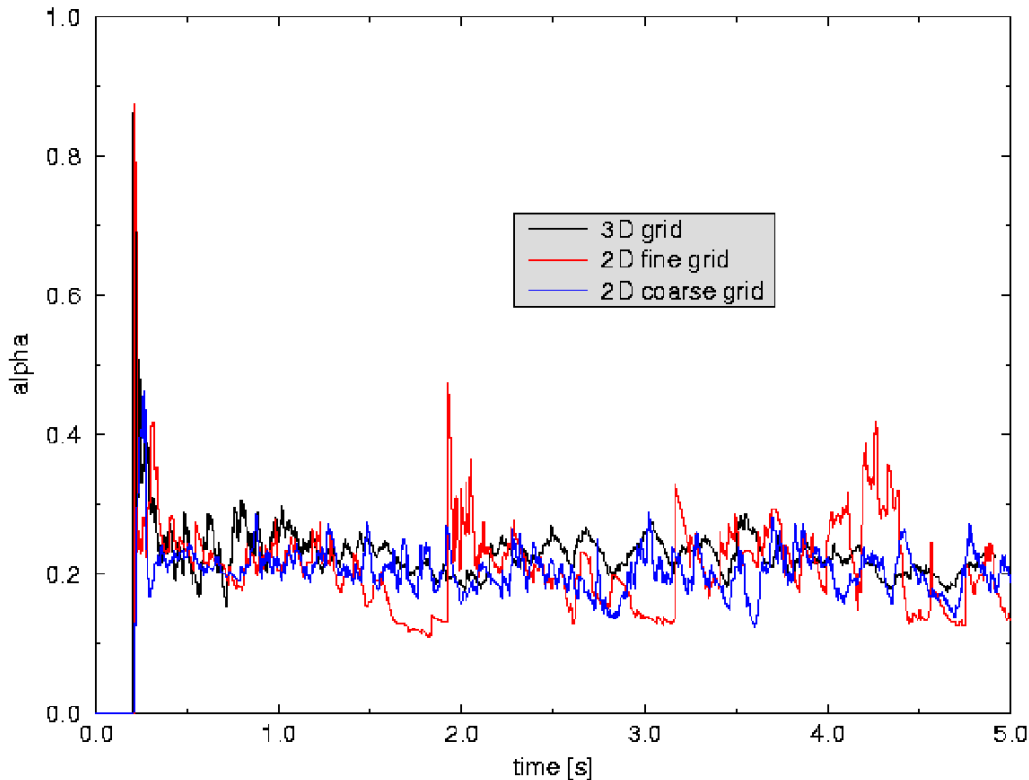
Figure 7.15   Averaged water volume fraction in lower plenum

Within 3-D the pressure reaches its maximum of 3.5bar at 3.2s (2-D with coarse grid: 6.1bar at 4.2s in lower plenum) and then slowly decreases down to its initial level. This behaviour is similar to experimental observations from FARO or PREMIX. At times larger than 4s the differences between 2-D with coarse grid and 3-D become rather large. This can be understood because in 2-D the melt reaches the lowest part of the lower plenum that leads to very strong numerical packing problems. The pressure increases at t>4s within the 2-D scenario with a coarse grid. This leads to a penetration of steam into the melt pool and causes some interactions which are reflected in fluctuations in pressure, premixed melt mass etc. at times between 4s and 5s. However, it should be mentioned that maxima which occur within peaks are generally coupled with numerical difficulties. Their physical relevance is doubtful.

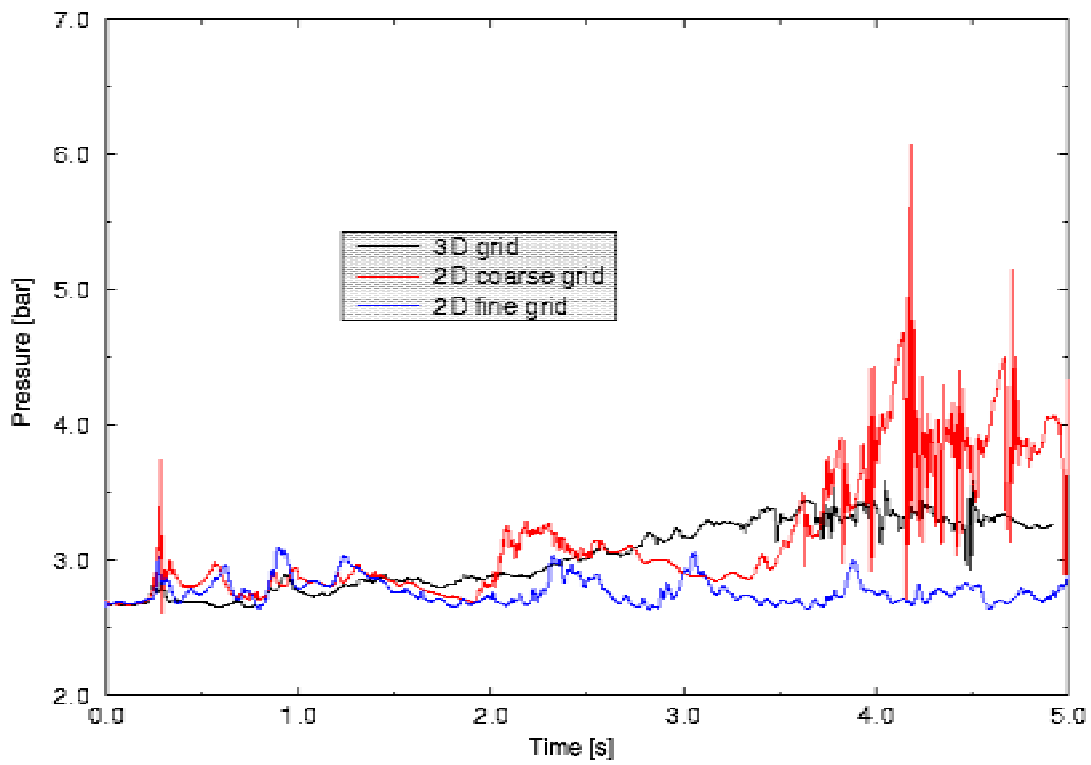A similar behaviour is shown by the premixed melt mass and energy (Fig. 7.9 and 7.10). In 2-D the time dependence is dominated by high frequency oscillations and long time scale oscillations at frequencies of 0.5-1Hz.

In 3-D the maximum of premixed melt mass is reached at 5s (1.1 tons) with an internal energy of 1.2GJ. Tests with a simulation time up to 8s have shown that the total maximum is reached at 5s and then a slowly decrease of values characterising premixing is calculated.

The 2-D cases are very similar concerning premixing until 2s. Then differences are increasing. The overall maxima are 1.8 t of melt with an enthalpy of 2.4GJ for the 2-D scenario and a coarse grid and 0.5 t of melt with an enthalpy of 0.7GJ in case of the fine grid.

The release of melt (see Figure 7.11) is quite similar in all cases. After 3.5s the melt release decreases in case of 2-D with coarse grid because of the significant pressure increase in the downcomer. Up to 5s between 8t (2-D coarse grid) and 15t of melt (2-D fine grid) are released. The internal melt energies are in the range of 12GJ to 22GJ (Figure 7.12).

84

It should be mentionend that the melt release rate is anticorrelated with the pressure in the lower plenum and in downcomer. If pressure increases the release of melt decreases. Because of the strong pressure increase at times greater than 3.5s in 2D the release rate becomes negative which means that melt moves from the lower plenum into the downcomer or back into the melt pool.

Another interesting fact is the total melt surface (Figure 7.13). At t=0s all the melt is located in the pool and penetrated by gases. So a non negligible melt surface of more than 4000m^2 is calculated. By fragmentation of the released melt the surface increases. The oscillations of the melt surface are caused by coalescence because the melt contacts with walls especially the stairway like wall structures in the lower plenum or by numerical effects if the melt front reaches new cells not yet filled with melt.

The two graphs of the 3-D and the 2-D scenario with coarse grid are similar up to 3.5s. A maximum of around 8000m^2 is calculated. At times above 3.5s coalescence becomes important and the melt surface decreases. At times between 4s and 5s the 2-D scenario with coarse grid shows some oscillations depending on the breakthrough of vapor into the pool.

Comparing the different 2-D scenarios concerning the melt surface strong grid dependencies can be recognized. A coarser grid has the tendency to treat a water-melt mixture as a more disperse flow so that a greater melt surface is calculated. Therefore the fine grid leads to a smaller maximum value of 6300m^2 for the surface.

The existence of water is necessary to trigger steam explosion. The possibility for this event decreases when the water becomes rapidly removed from the lower plenum. Figure 7.14 presents the total water mass in the lower plenum. The small difference of the initial value between 3-D/2-D-coarse grid and 2-D with fine grid depends on the grid spacing in radial and vertical direction.

In case of the 3-D simulation the water is removed fastest because there is a free way via the downcomer cross-section circumferentially displaced by 180^0 against the leak position in the heavy reflector. Within a 2-D simulation the water is enclosed by melt and there is more resistance to leave the lower plenum due to the established counter current flow. At the beginning of melt release around 18t of water are in the lower plenum. After 5s between 5.2t (3-D) and 9.8t (2-D fine grid) are blown out of the vessel (see also Table 7.1.)

For premixing it is also interesting to know the volume fraction of water for regions with water-melt interaction. In Figure 7.15 the averaged water volume fraction for cells with premixing in the lower plenum is given.The differences between the scenarios are small apart from the fact of oscillations in case of the 2-D simulations. In general the averaged water volume fraction moves between 0.2 and 0.3 without significant tendencies.

A comparison between the 2-D scenario with coarse grid and 3-D is shown in Table 7.1. Results of a MATTINA-2D calculation are included which are discussed later in chapter 7.6.

The mass of lost water which is released via the downcomer inlet nozzles doesn't differ very much in both cases (10.4t/9.3t). One can draw the conclusion that the amount of water in the downcomer must be 2.6t in 3-D and 1.2t in 2-D. The mass of melt which is blown out via the downcomer amounts to 1.7 t (3-D) and 1.1t. This is in the order of 15% of the total amount of melt in the lower plenum.

Table 7.1   Comparison of different radial release scenarios

	Initial state	MC3D—3D	MC3D—2D	MATTINA—2D
		t=5s	t=5s	t=5s
Total water	18.2t / 17.8t [a]	6.8t	8.1t	12.6t
-in lower plenum	16.1t	5.2t	7.7t	12.6t
-water lost	0.0t	10.4t	9.3t	5.2t
Total melt	109.8t / 107.6t [a]	108.2t	108.7t	102.1t
-in lower plenum	0.0t	10.2t 14.8GJ	8.8t 12.3GJ	2.6t (4.5s) 2.4GJ (4.3s)
-melt lost	0.0t	1.7t	1.1t	5.5t
Premixed melt	0.0t	1.1t (5.0s) 1.2GJ (5.0s)	1.8t (3.8s) [b] 2.4GJ (3.8s)	1.2t (5.0s) 1.0GJ (4.8s)
Melt surface max-surface(t=0)	0m^2	2300m^2 (2.1s)	4200m^2 (3.0s)	1280m^2 (5.0s)
Melt release rate		2.4t/s	3.9t/s	3.2t/s
Total vapor	201.6kg	203.7kg	108.8kg	93.9kg
Lost vapor	0.0kg	685.1kg	929.6kg	not available
Pressure	2.6bar	3.6bar (4.2s)	6.1bar (4.2s) [b]	3.8bar (2.7s; 5s)

[a] initial state MATTINA   [b] short time scale fluctuation caused by packing

According to the melt surface in 2-D the mass of vaporised (and blown out) water is 40% higher than in the 3D-simulation. It is astonishing that in 3-D the total mass of vapor in the vessel is not very different from the initial value. One explanation is the decreased possibility of contact between water and melt because the melt is located near the leak and water gets separated very fast from the melt. So the temperature of vapor is closer to its initial value. As the pressure has increased after 5s (from 2.6bar to 3.3bar in downcomer, see Fig. 7.8) a nearly unchanged value of the total mass of vapor is possible. In 2-D it is impossible for the vapor to

leave the vessel through the downcomer without passing close to the leak. Therefore its temperature must be closer to the melt temperature .

Following conclusions can be drawn:

Considering radial melt release scenarios there is no possibility to avoid 3-D simulations because otherwise water in the lower plenum gets enclosed by the draining down melt. This is felt somewhat unrealistic but represents most probably a conservative estimate related to premixing conditions.

Within 2-D scenarios oscillations at time scales of 1-2s are observed which are apart from reality. Switching to 3-D leads to a reduction of fluctuations with short time scale which is indicative for less numerical difficulties. In case of 3-D water and melt are separated faster.

It is clear that a 3-D simulation has to be preferred but improvements are necessary because of the uncertainties within physical modelling and the numerical diffusion caused by donor cell method. Therefore 2-D simulations still have their merits to evaluate trends dependent on different open parameters as axial height of failure location and size of the failure cross-section.

7.1.2   Axisymmetric base case calculation

As base case, the outflow scenario with a 5% leak in the upper part of the heavy reflector (145.16:49) was considered. This case was calculated with an initial diameter of melt droplets of 5 mm and a zero pressure loss coefficient for the flow plate in the lower plenum.

- ***Melt relocation and evolution of the flow fields***

Figure 7.6 shows the melt and water inventory in the lower plenum region of the reactor vessel. For comparison, the values for the two bottom leakage scenarios (cases 2., 3. from above) are plotted together with the base case. More details of the bottom leak calculations will be given in the section dealing with the parametric analyses. As one can expect, the small leak in the upper part of the heavy reflector (base case) leads to the smallest melt outflow rate and evaporation, and the large leak in the lower part to the highest rates. Figure 7.17 shows the melt energy in the lower plenum region. The energy in the plenum region is nearly proportional to the melt mass, and approximately a linear function of time. Its value after 10 s varies from 9.7 GJ in case of the small top leak, over 42.3 GJ (small bottom leak) to 75.9 GJ in case of the large bottom leak.

Figure 7.8 shows the evolution of the flow fields of the base case by plotting the volume fractions of melt and water in the lower part of the reactor vessel at the selected times 3 s, 6 s, and 9 s, respectively.

It can be seen, that the relocating melt leaving the downcomer flows downwards along the perimeter of the lower plenum of the reactor vessel. Due to the small driving pressure the outflow rate of the melt is only small. 9 s after the start of the melt relocation, the melt has not yet reached the bottom of the vessel and a lot of water still remains above the melt in the lower calotte.
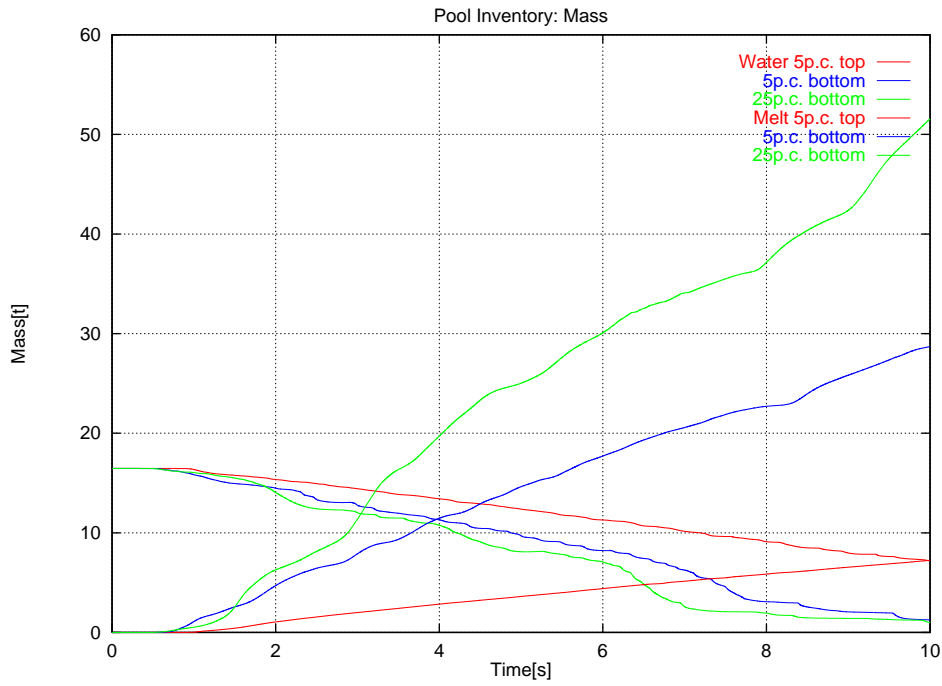
Figure 7.16 Masses in the pool region
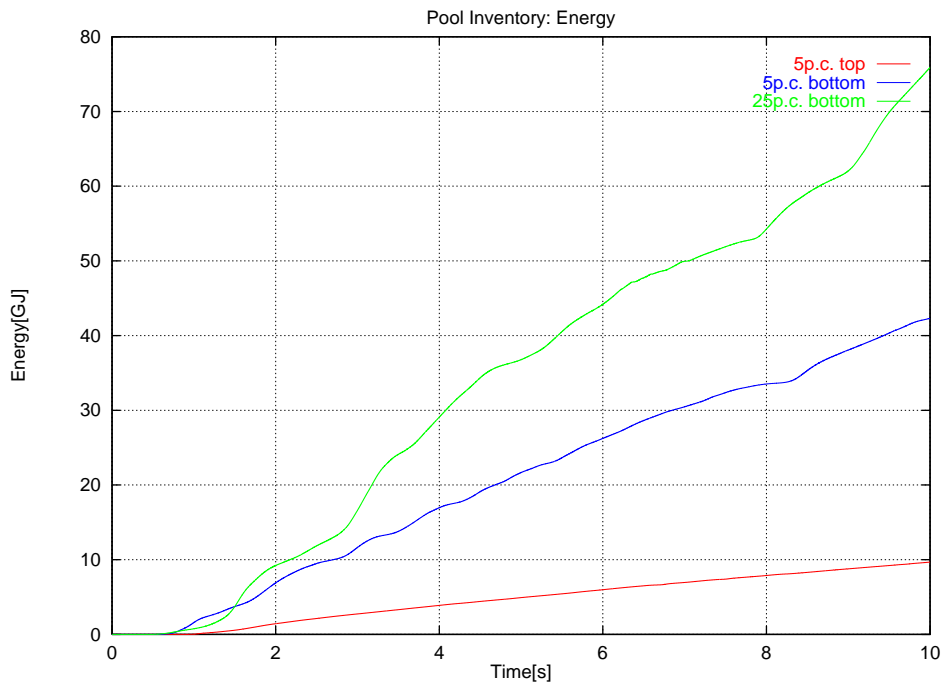
Figure 7.17 Melt energy in the pool region
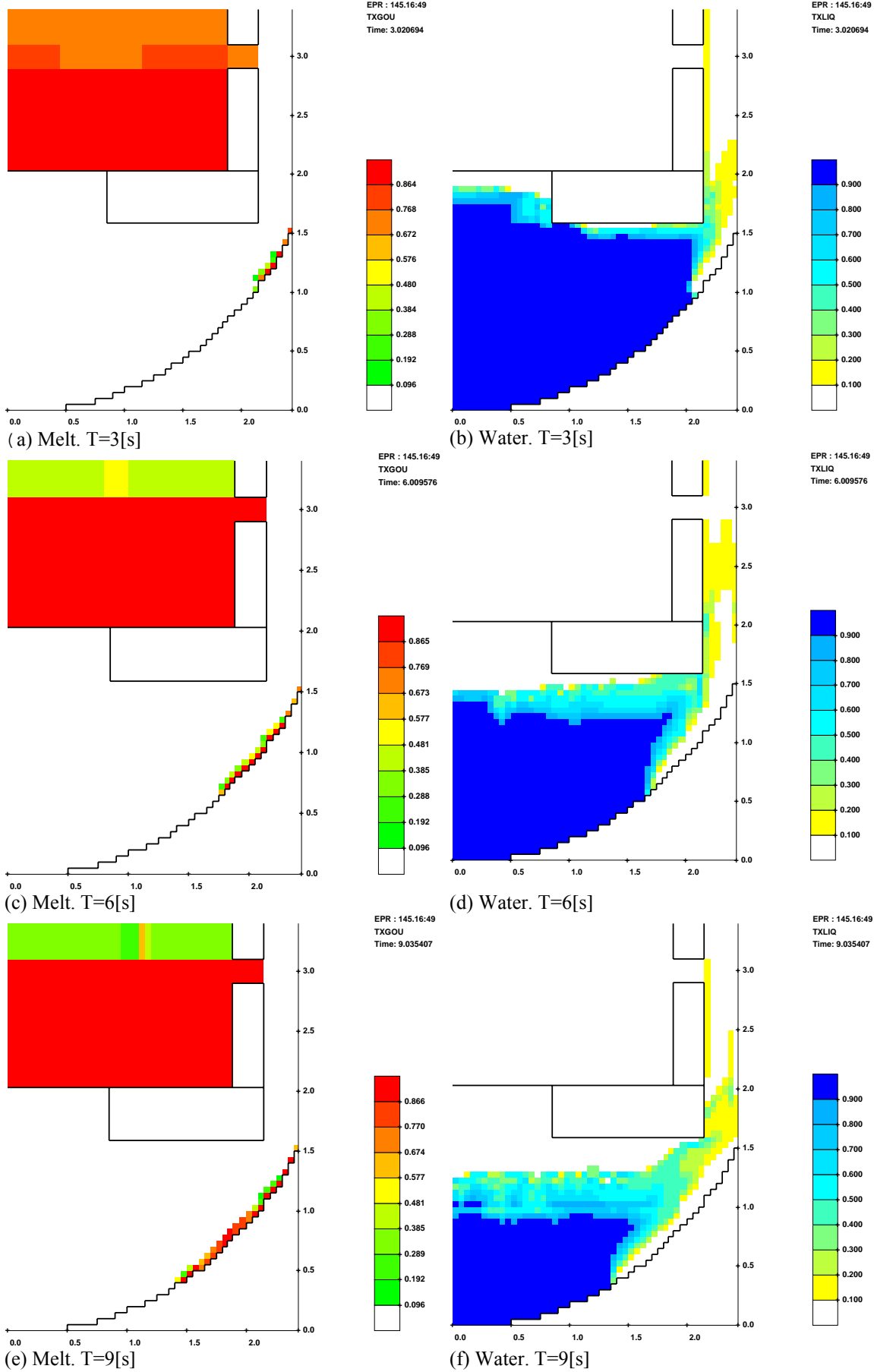
Figure 7.18 Volume fractions. Base case: 5p.c. top leak

-   *Evolution of the pressures*

Figure 7.9 shows the pressures at the bottom of the reactor vessel and the outer edge of the lower core support plate for the base case (1.) with the small leak in the upper heavy reflector and the two bottom leak scenarios(2., 3.).

It can be seen (see Fig. 7.9), that in case of the small leak at top the pressure rise is very small (less ≈ 0.1 bar). In case of the small leak at bottom the peak pressures in the first 6 seconds don't exceed 3.1 bar, after 6 s the pressure level rises a little bit, but the peak values stay below 3.6 bar. In case of the large bottom leak the pressure rise is the highest one, but only some peak values at the bottom of the reactor vessel go above 4 bar.

The pressure level at the outer edge of the lower core support plate (see Fig. 7.9) is generally a little bit smaller.

-   *Evolution of the premixing quantities*

Figure 7.10a-b shows the premixed melt and energies as functions of time for the base case and the two bottom leak scenarios. The premixed melt masses are a function of the melt outflow rate and increase with increasing flow rate. The peak values are about 0.4-0.5 t in the base case, about 0.5-0.7 t in case of the small bottom leak, and about 0.8-1.0 t in case of the large bottom leak. The corresponding peak values of the premixed energies are 0.5-0.6 GJ, 0.7-1.1 GJ, and 1.2-1.5 GJ, respectively.

Figure 7.11 shows the premixed water volume fractions as functions of time. The volume fractions of premixed water oscillate for the different leakage scenarios around 0.2.
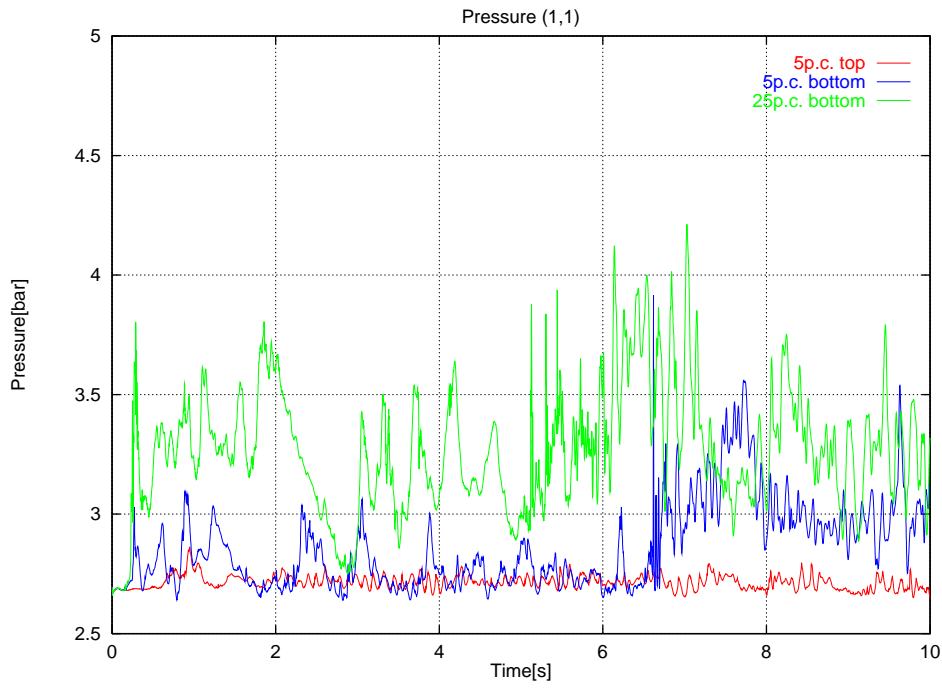
(a) Pressures at bottom of vessel
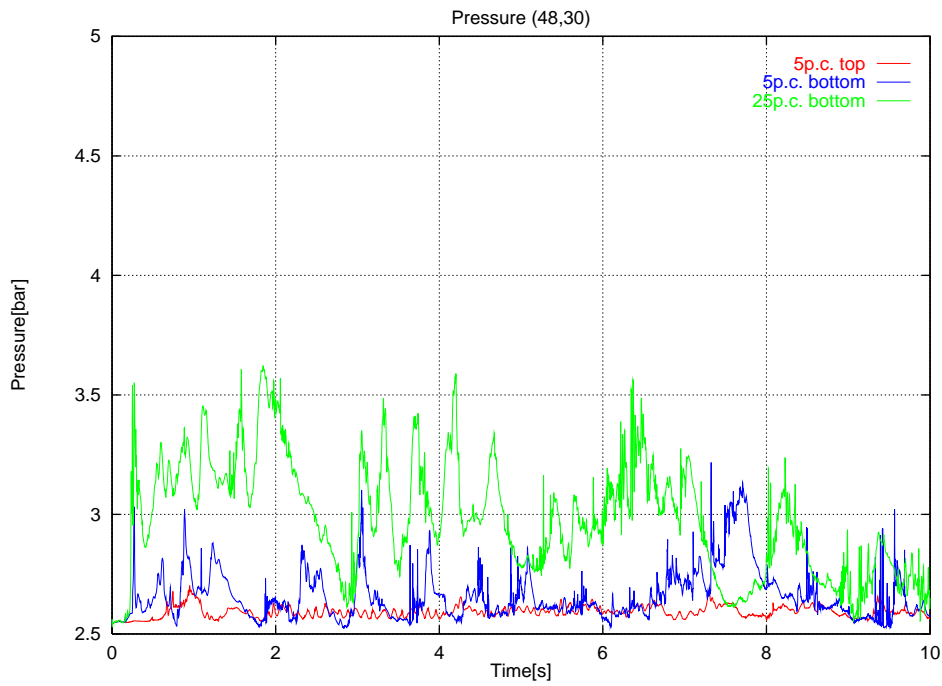
(b) Pressures at outer edge of support plate

Figure 7.19 Pressures of base case and lower leakage scenarios

91
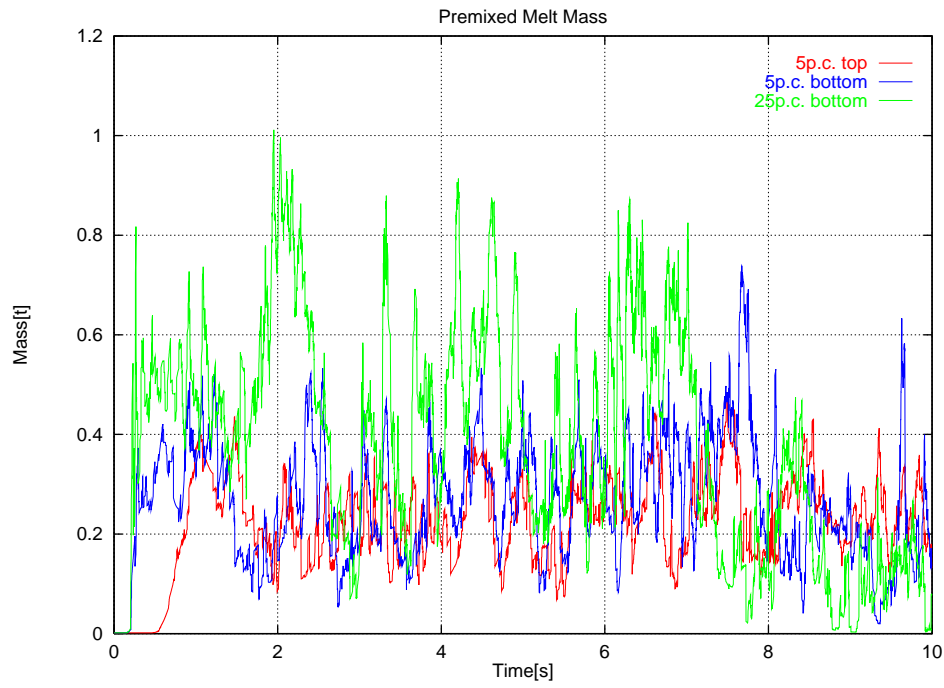
(a) Premixed melt mass
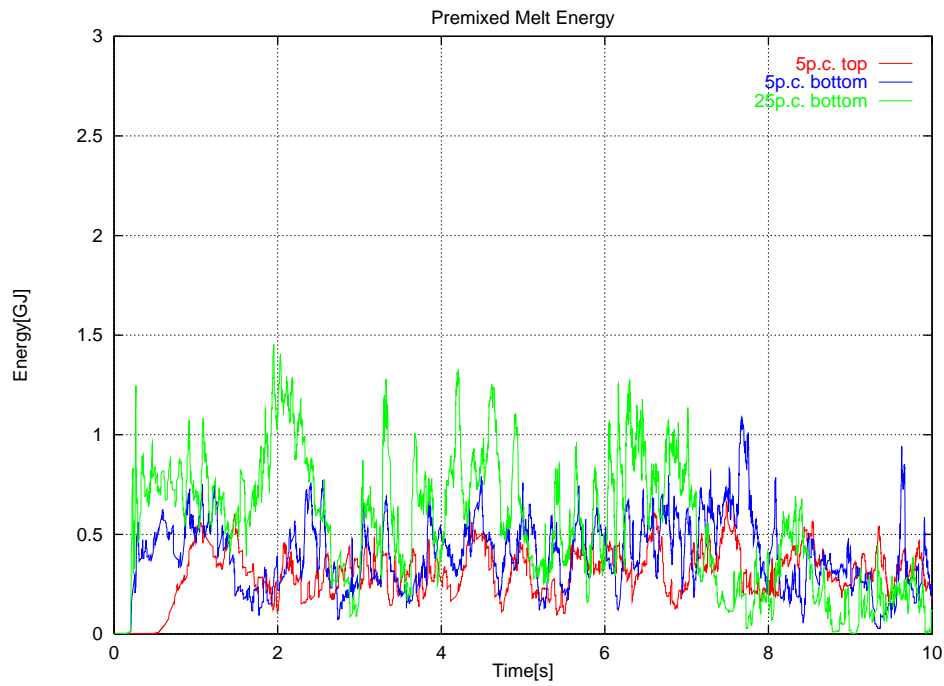
(b) Premixed melt energy

Figure 7.20 Premixed melt mass and energy. Base case and lower leakage
scenarios
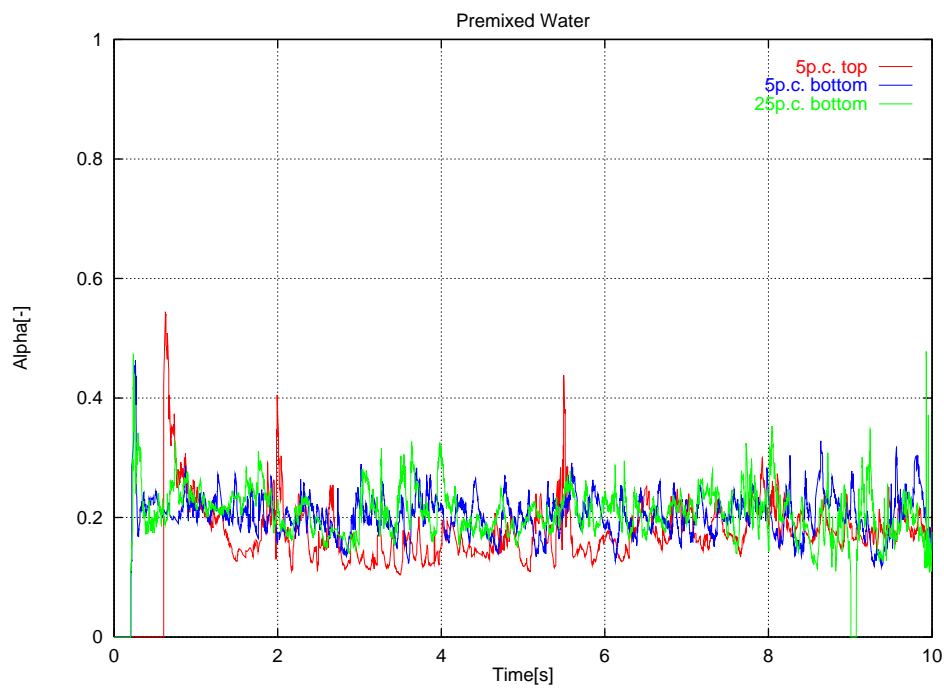
Figure 7.21 Premixed water volume fraction. Base case and lower leakage scenarios

7.1.3   Parametric analyses

Some details for the bottom leak scenarios will be given here and the influence of initial particle diameter and pressure loss coefficient of the flow plate in the lower plenum will be discussed.

Bottom leak scenarios

Figures 7.12a-f show the evolution of the flow fields for the small (5p.c.) bottom leak by showing the volume fractions of melt and water in the lower part of the reactor vessel at the selected times 3 [s], 6 [s], and 9 [s], respectively.

It can be seen that due to the higher hydrostatic driving pressure of the melt pool, a significantly higher amount of melt as in the base case flows out of the heavy reflector. 9 s after the start of the calculation, a pool of melt has been build up in the lower plenum and only little water flows above this melt pool.

The figures 7.13a-f show the evolution of the flow fields for the large (25p.c.) bottom leak by presenting the volume fractions of melt and water in the lower part of the reactor vessel at the selected times 3 s, 6 s, and 9 s, respectively.

This case has the highest outflow rates. 9 s after the start of the calculation, a large pool of melt has been build up in the lower plenum and most of the water is evaporated at this time.
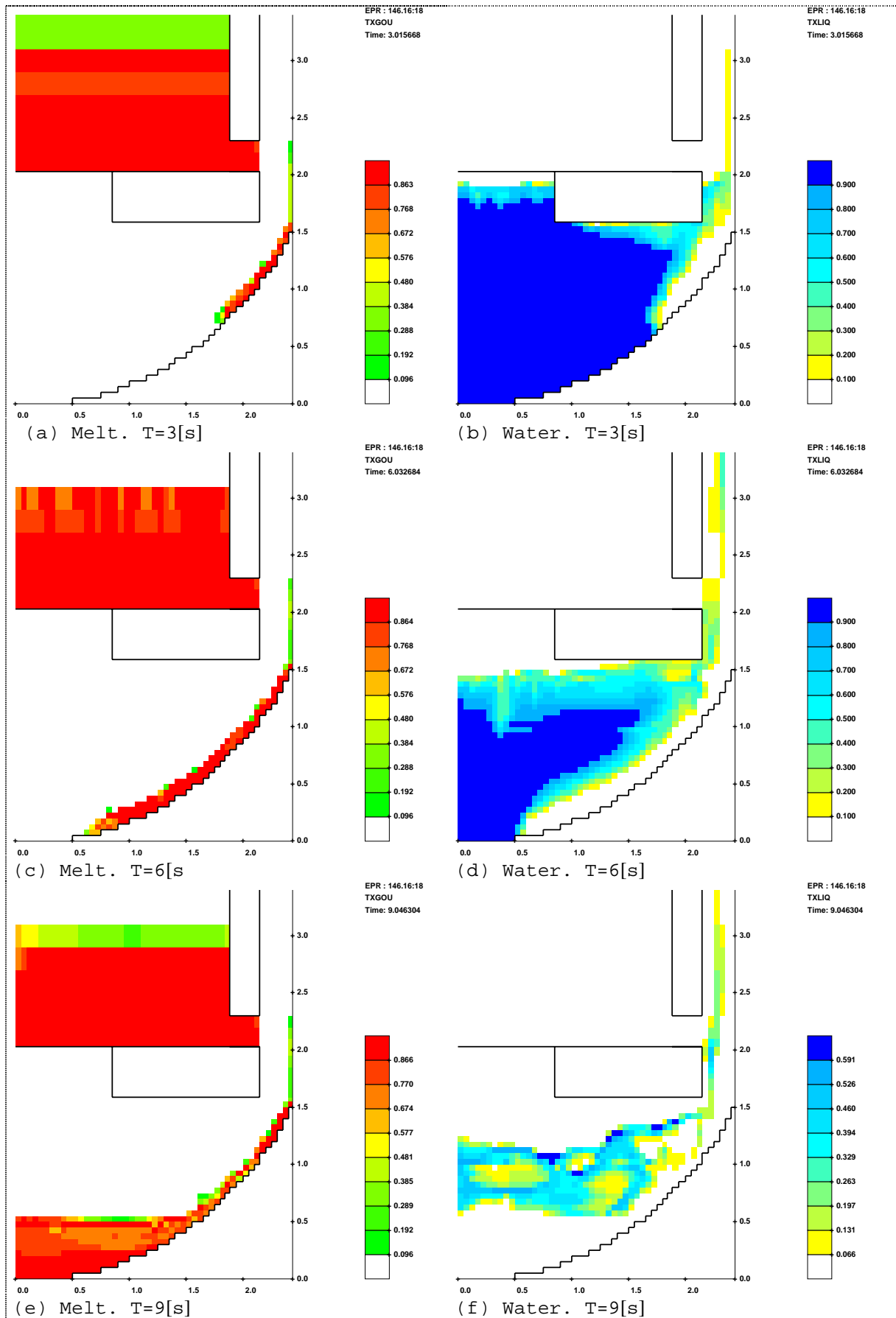
Figure 7.22 Volume fractions. 5p.c. bottom leak.
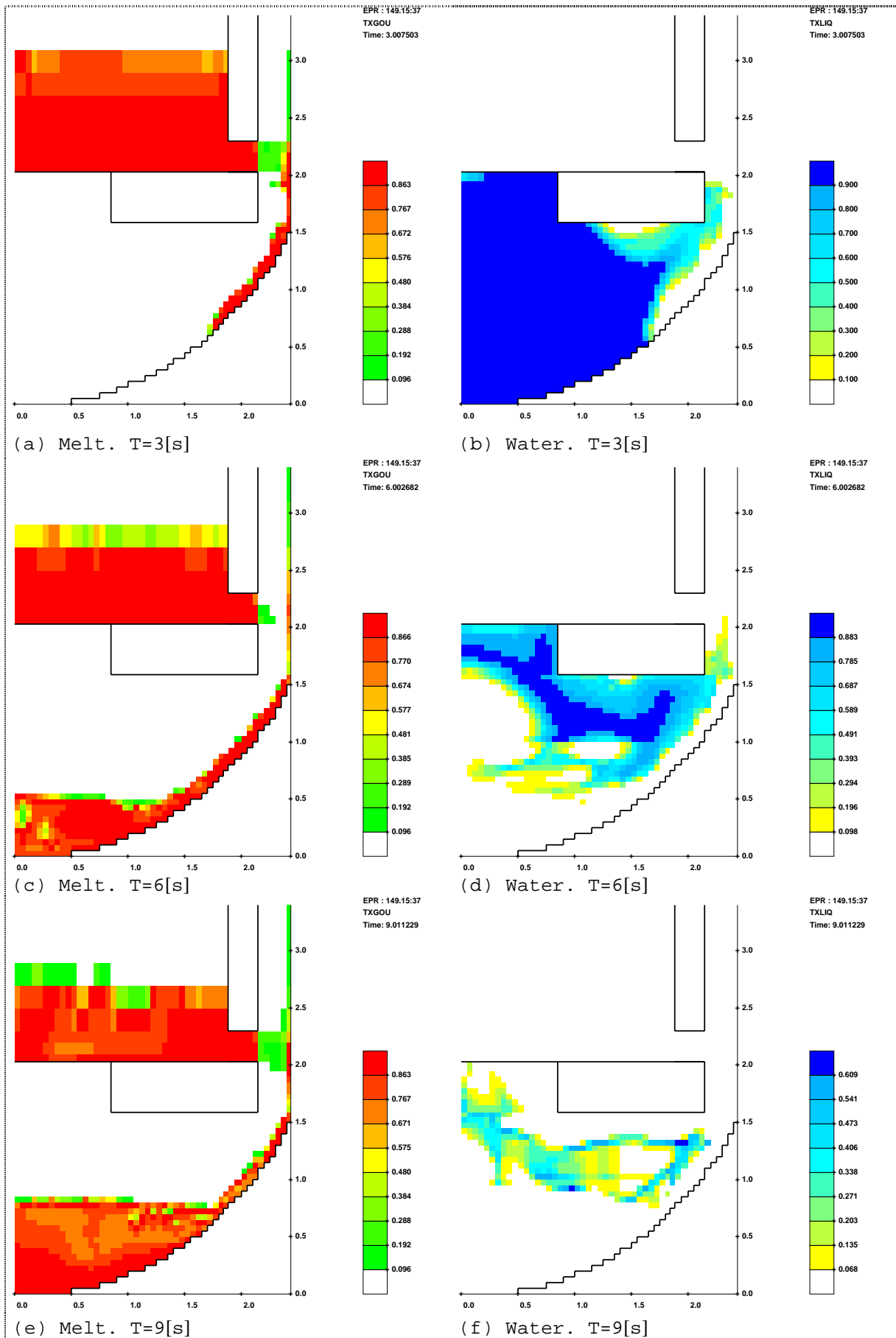
Figure 7.23 Volume fractions. 25p.c. bottom leak.

96

- *Variation of the initial particle diameter*

One important parameter of the simulations is the initial particle diameter of the fragmenting melt. It influences directly the heat transfering surface of the melt. This parameter variation is performed for the small (5%) leak at the bottom of the heavy reflector.

- *Evolution of the flow*

Figure 7.14 shows the melt and water inventory of the pool for 5 [mm] and 50 [mm] initial particle diameter. Obviously only small differences exist in the melt flow rate. Looking at the water inventory of the pool, it can be seen that the evaporation rate is almost the same up to 6 s. Then the larger initial particle diameter results in a weaker evaporation[2] of the water.

Figure 7.15 shows the corresponding melt energy inventory in the pool. Since the melt energy is proportional to the melt mass in the pool, only little differences exist between the large and the small particle diameter case.

Figure 7.16 shows the melt surface as function of time for the small and the large initial particle diameter. The melt surface of the 50 mm diameter case is up to a factor of 10 smaller than of the 5 mm case. Therefore one would expect a *significantly* lower evaporation of water in case of the large particle diameter. The reason why this is not the case is most probably a strong separation of water and melt by steam in both cases, which reduces the influence of the particle surface upon the heat transfer from melt to water.
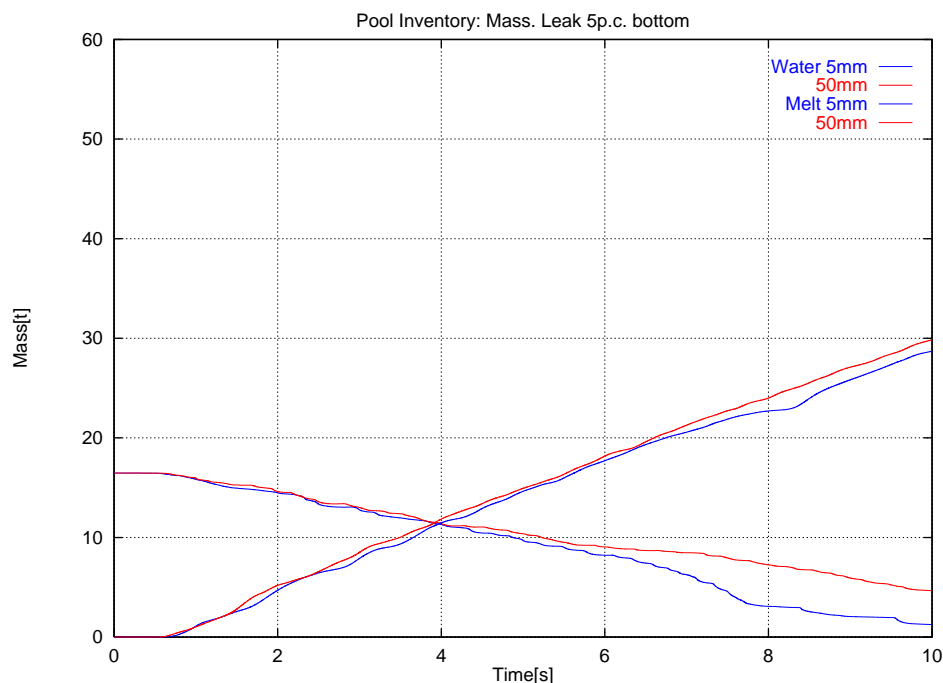
Figure 7.24 Masses in pool region. 5 mm and 50 mm initial particle diameter

---

[2] Precisely: a lower rate of water leaving the pool region.
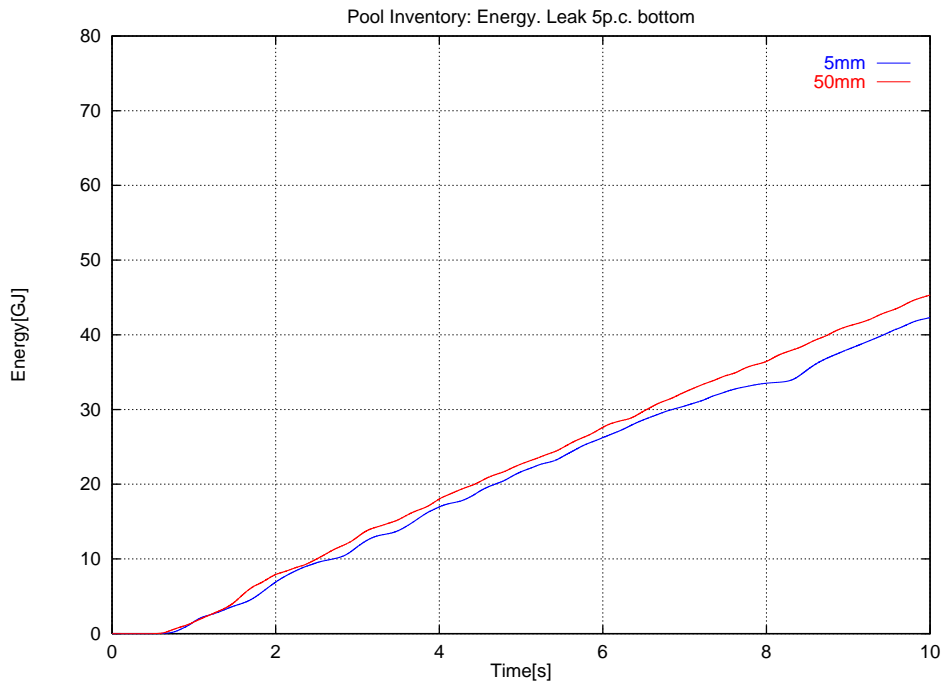
Figure 7.25 Melt energy in pool region. 5 mm and 50 mm initial particle diameter
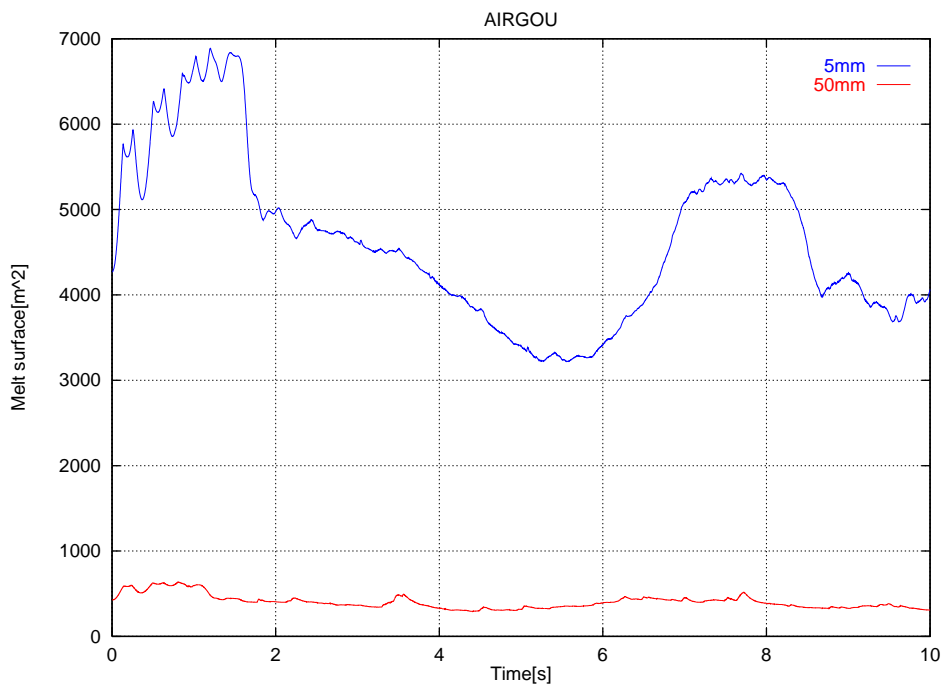
Figure 7.26 Melt surface. 5 mm and 50 mm initial particle diameter

Figures 7.17a-f show the temporary evolution of the volume fractions of melt and water. A comparison of the water volume fraction at 9 s (figure 7.17f) with figure (7.12f) shows significantly more water in the lower plenum due to the smaller evaporation rate in case of the larger initial particle diameter.
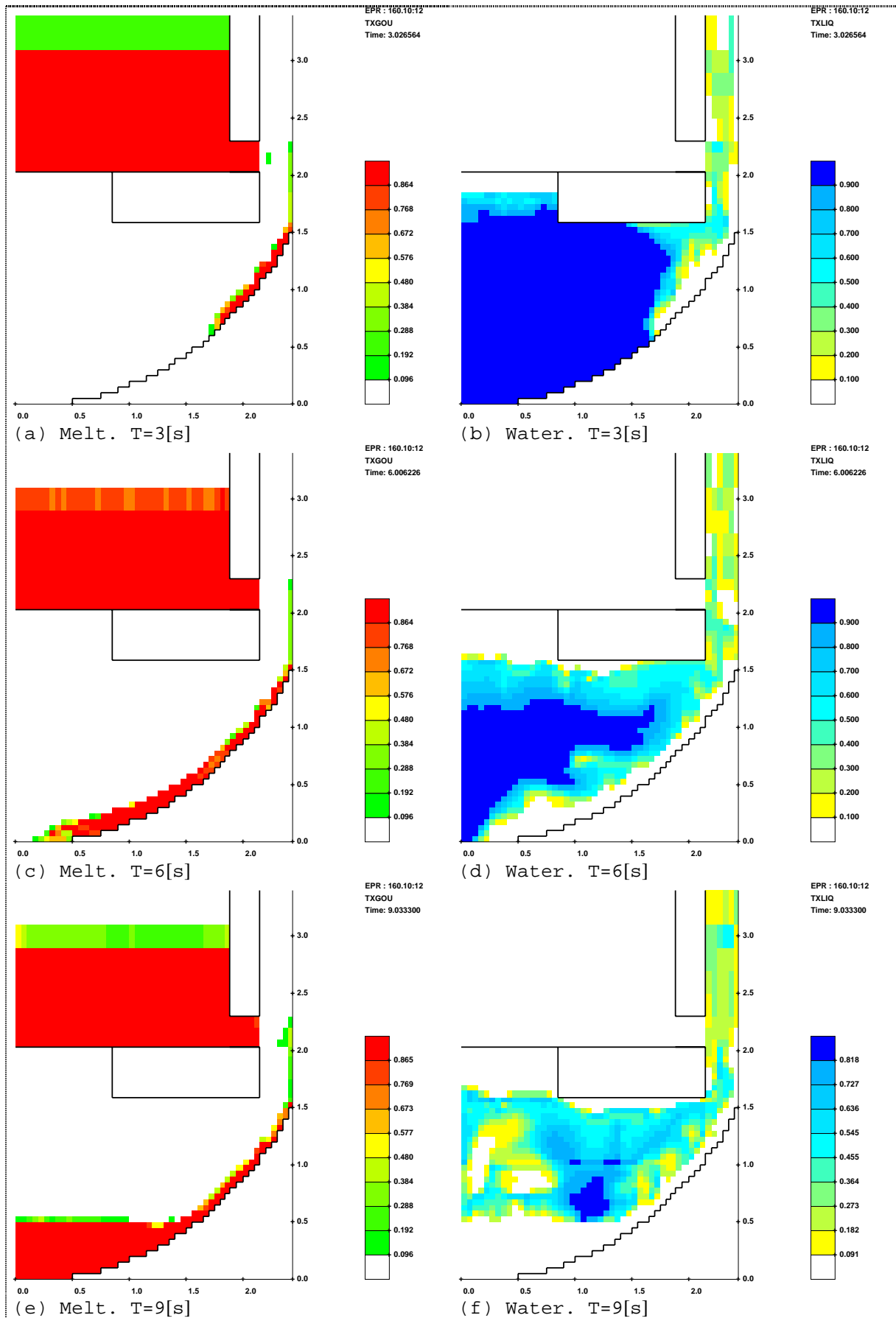
Figure 7.27 Volume fractions. 50 mm initial particle diameter.

- *Evolution of the Pressure*

Figure 7.18 shows the pressures at the bottom of the reactor vessel and at the outer edge of the lower core support plate. There are no significant differences in the pressure values for both cases.
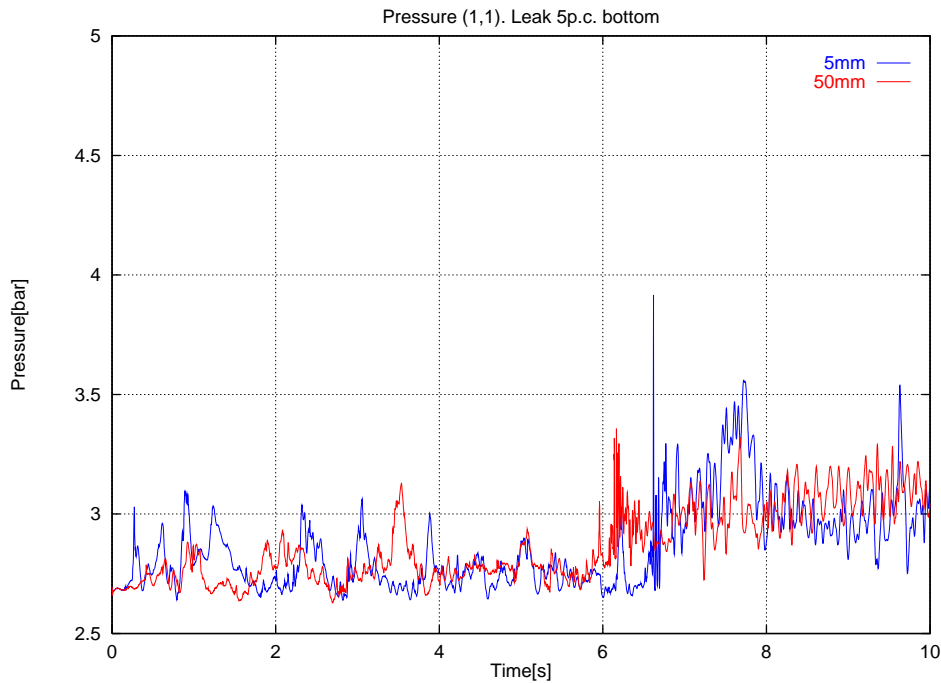
(a) Pressures at bottom of vessel
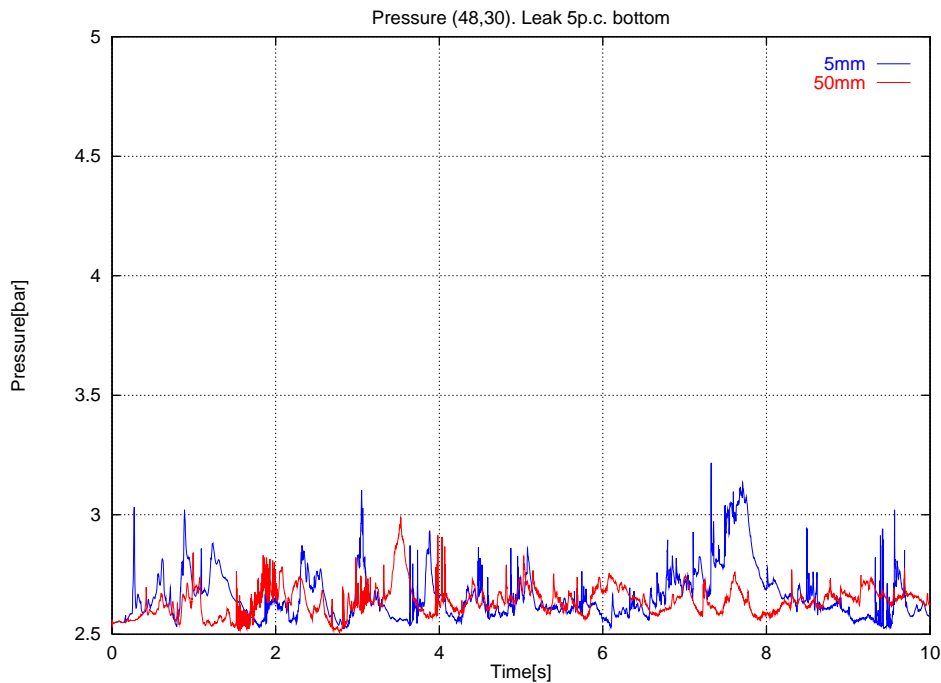
(b) Pressures at outer edge of support plate

Figure 7.28 Pressures with 5 mm and 50 mm initial particle diameter

- *Evolution of the premixing quantities*

Figure 7.19a-b shows the premixed melt mass and energy for the large and the small initial particle diameter. The premixed quantities in case of the larger diameter are higher than in the small diameter case. The peak values for the 50 [mm] case range from 1.2-1.8 t 2.1-2.7 GJ, respectively) contrary to 0.5-0.7 t (0.7-1.1 GJ, respectively) in the 5 mm case.
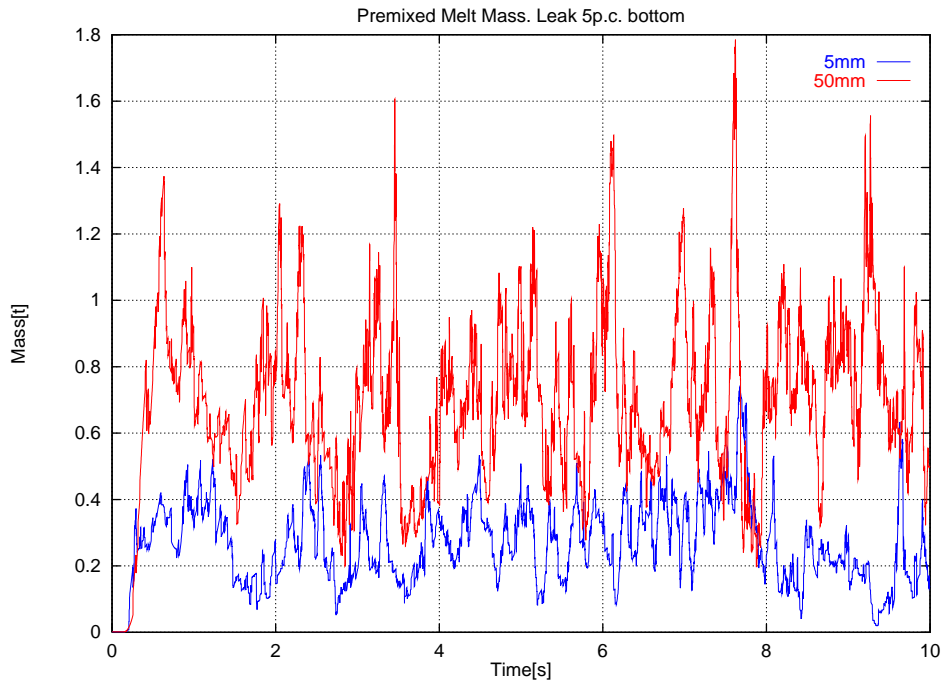
(a) Premixed melt mass
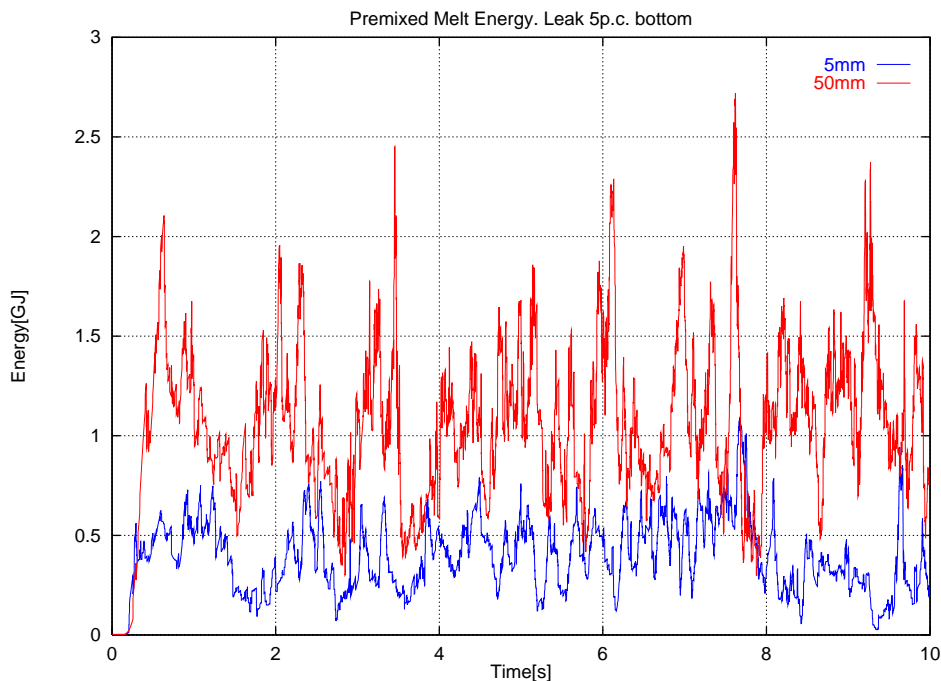
(b) Premixed melt energy

Figure 7.29 Premixed melt mass and energy. 5 mm and 50 mm initial particle diameter

The premixed water volume fractions (Figure 7.20) are significantly higher for the large diameter case during the first 2 seconds of the calculation and only slightly higher at later times.
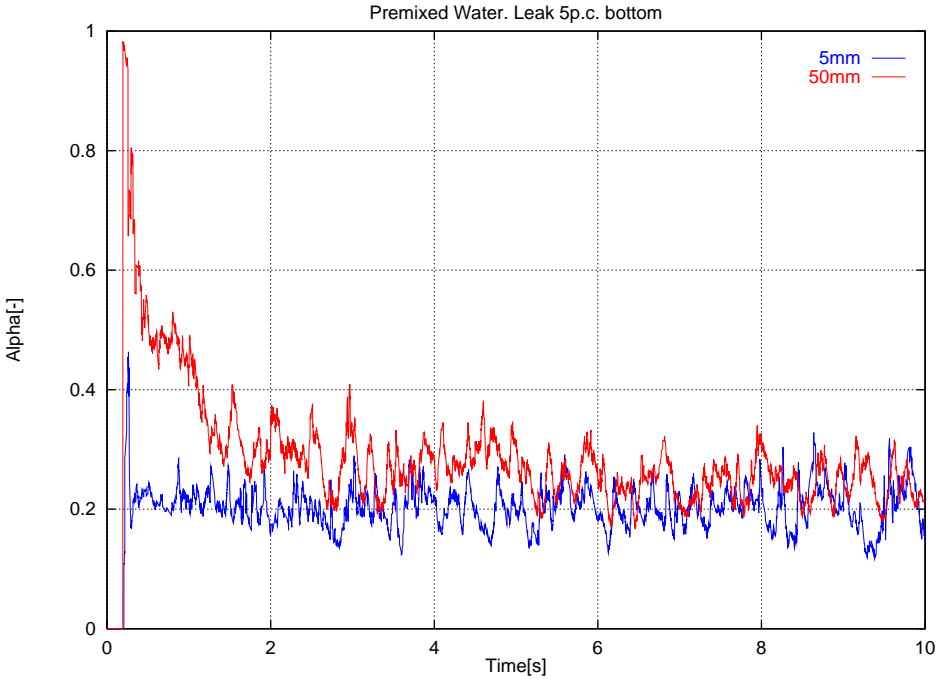
Figure 7.30 Premixed water volume fraction. 5 mm and 50 mm initial particle diameter

Variation of the pressure loss of the flow plate

Now the influence of the pressure loss coefficient of the flow plate in the lower plenum of the reactor vessel will be discussed for the case of the large (25%) leak at the bottom of the heavy reflector.

- ### *Evolution of the flow*

Figure 7.21 show the melt and water and figure 7.22 the energy inventory in the pool region for a pressure loss coefficient (zeta) of 0 and 10.

It can be seen, that for a pressure loss coefficient of 10 about 20% less melt flows out of the heavy reflector into the pool. This is a surprising result, since the evolution of the pressure (Figure 7.23) in the reactor vessel indicates only small differences for both cases. Therefore the driving pressure for the outflow out of the melt pool inside the heavy reflector, i.e. the difference between the hydrostatic pressure inside the pool and the pressure in the downcomer, should be nearly the same for both cases, and thus result in similar outflow rates.

A further investigation of this phenomenon showed, that a pressure loss coefficient of the flow plate reduces the time step of the calculation by a maximum value of about 25%. Since the numerical approximation of the underlying differential equations of MC3D is of first order in space and time, this small time step change has a significant effect upon the calculated solution: After 10 s about 20% less mass flowed out of the heavy reflector.
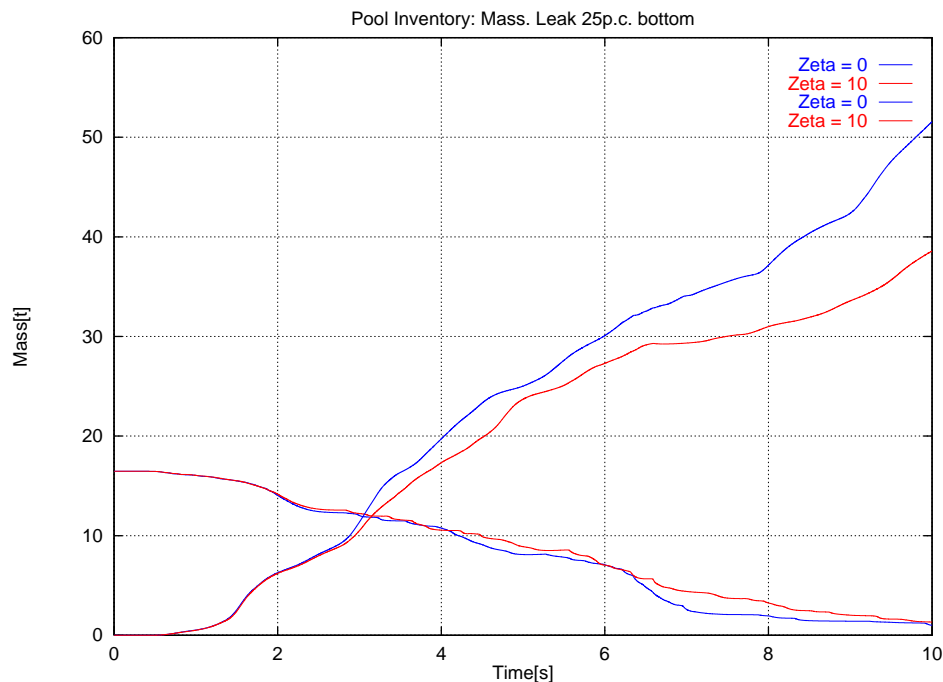
Figure 7.31 Masses in pool region. Pressure loss coefficient 0 and 10
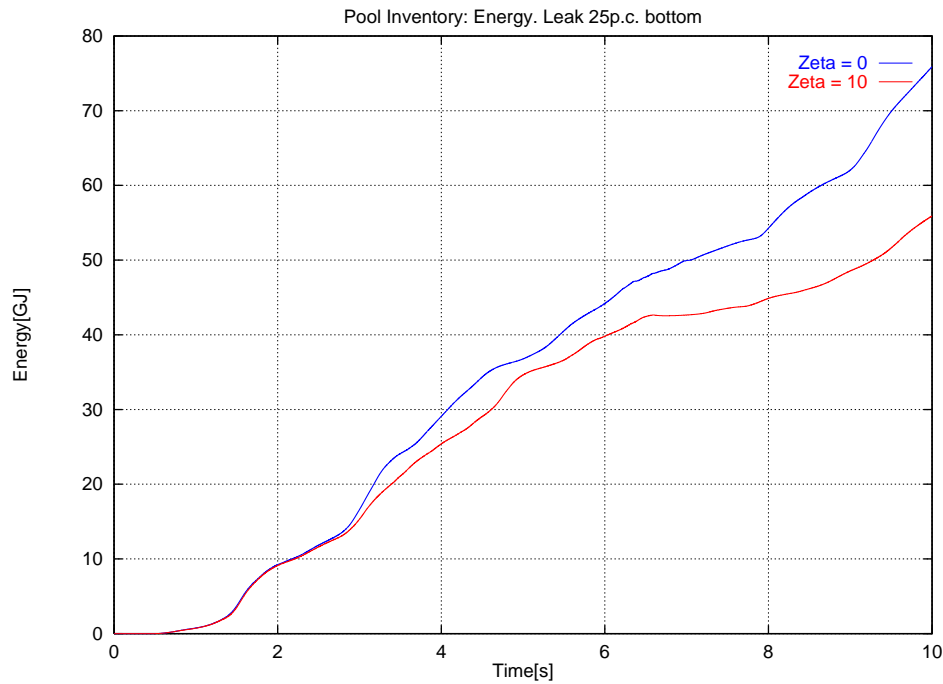
Figure 7.32 Melt energy in pool region. Pressure loss coefficient 0 and 10

- ***Evolution of the Pressure***

Figure 7.23 shows the pressures at the bottom of the reactor vessel and at the outer edge of the lower core support plate. Only small differences exist between the two cases.

The figures 7.24a-f show the temporary evolution of the volume fractions of melt and water. A comparison of figure 7.34f with figure (7.23f) shows the influence of the pressure loss coefficient by a horizontal row of cells filled with water directly above the flow plate (vertical coordinate ≈0.7 m).

- ***Evolution of the premixing quantities***

The Figures 7.25 and 7.26 show the premixed melt mass, energy, and water volume fraction. The pressure loss coefficient of the flow plate has no significant influence upon them.
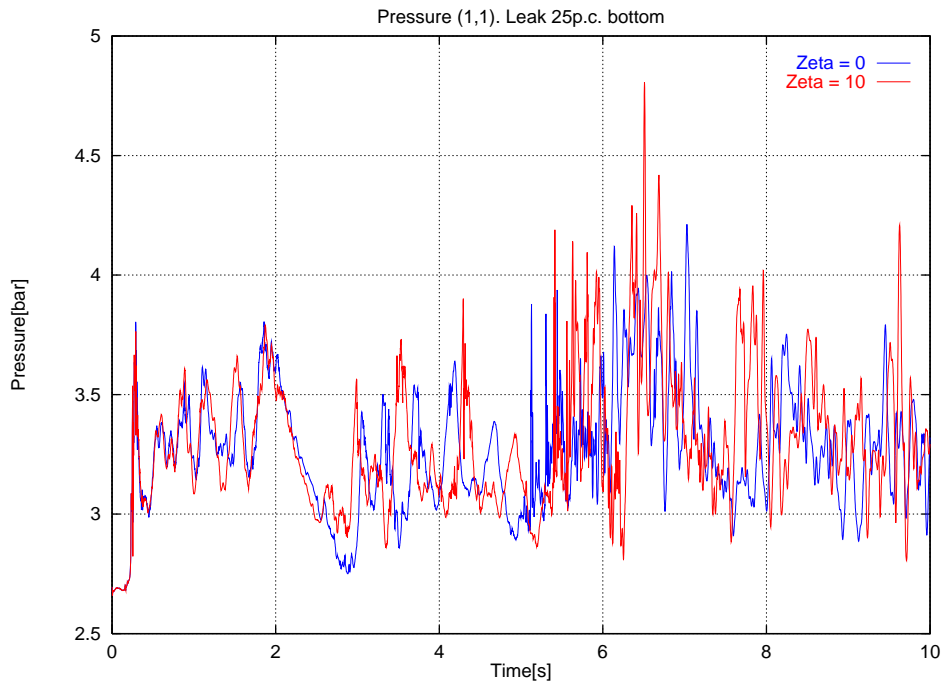
(a) Pressures at bottom of vessel
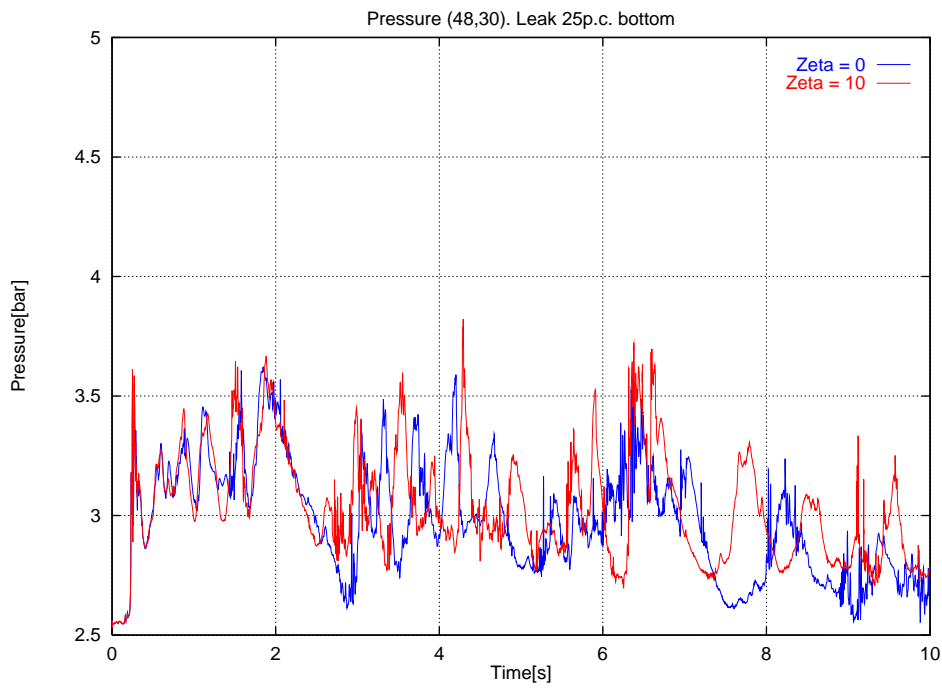
(b) Pressures at outer edge of support plate

Figure 7.33 Pressures with pressure loss coefficient 0 and 10
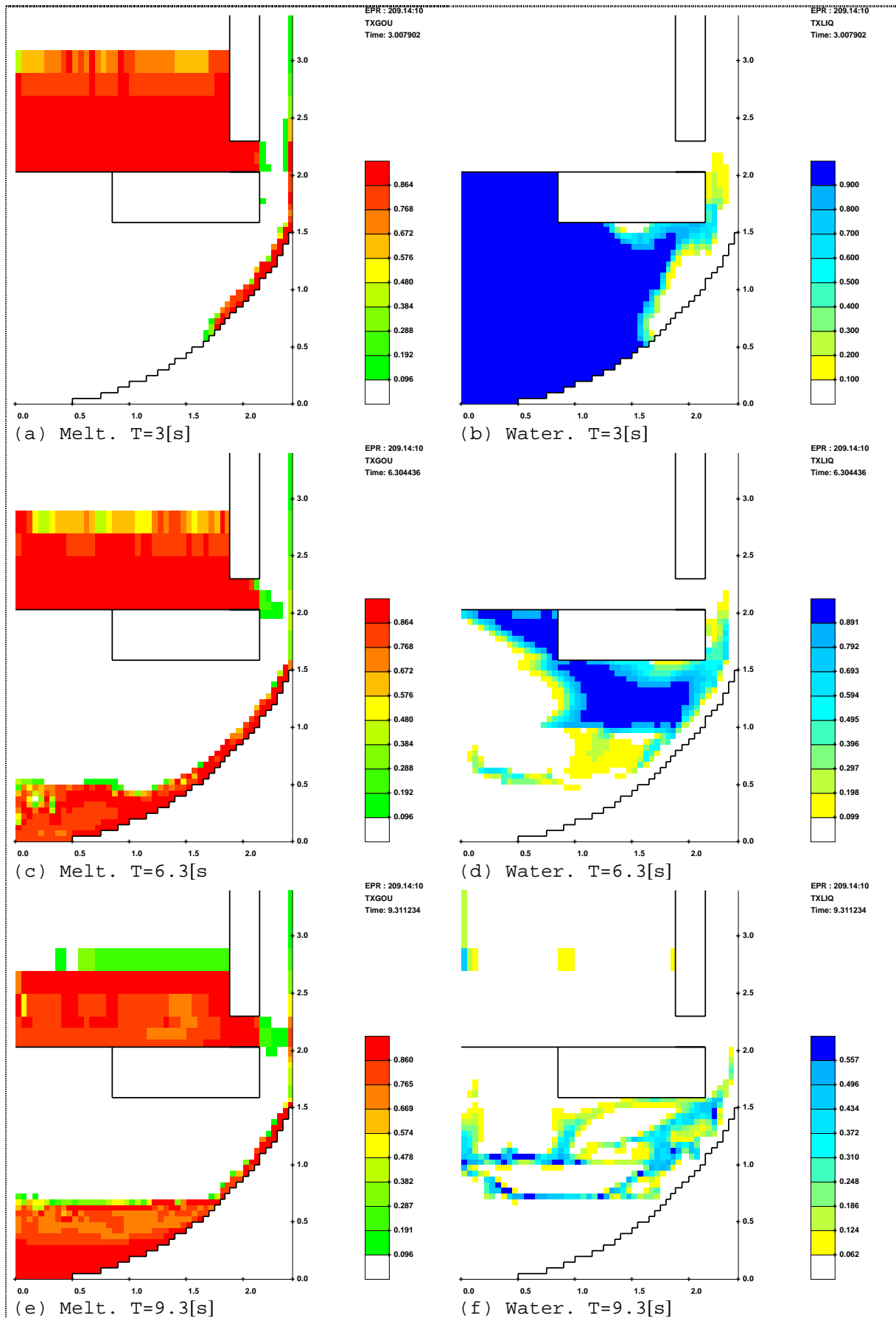
Figure 7.34 Volume fractions. Zeta = 10.
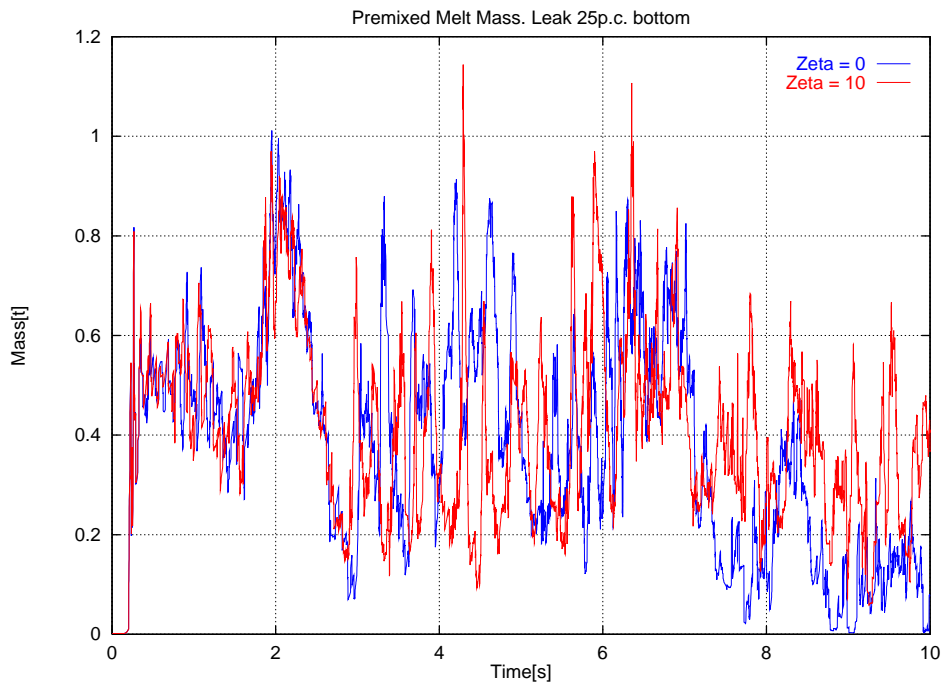
(a) Premixed melt mass
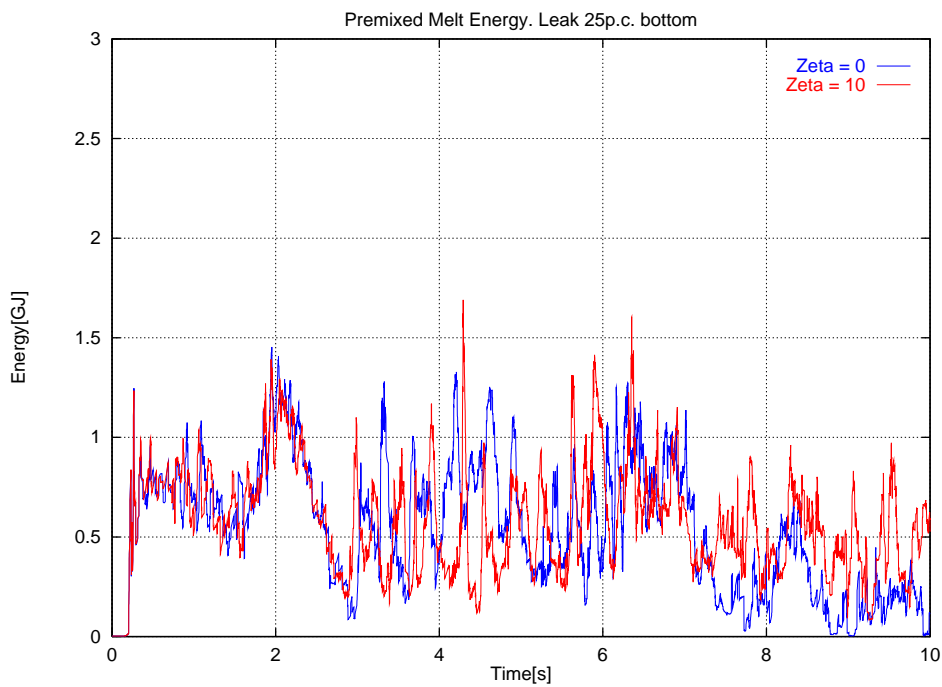
(b) Premixed melt energy

Figure 7.35 Premixed melt mass and energy. Pressure loss coefficient 0 and 10

107
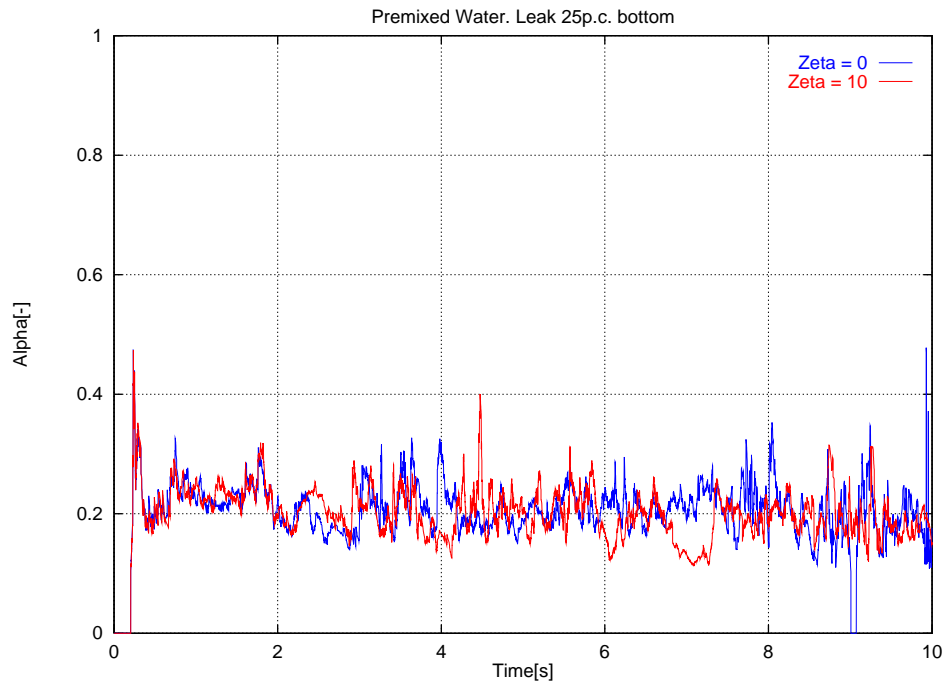
Figure 7.36 Premixed water volume fraction. Pressure loss coefficient 0 and 10

7.1.4 Coarse grid simulation

In order to assess the differences between two- and three-dimensional calculations, a two-dimensional simulation with the coarse grid of the three-dimensional simulation of chapter 7.2 was performed.

Figure 7.27a-b shows the two different grids. The grid used in the 3D simulation had to be strongly coarsened in the lower part of the problem and towards the centerline.

The coarse grid simulation will be compared with the fine grid simulation with the 5% bottom leak. Two further differences between these two simulations are the compact lower core support plate and a pressure loss coefficient of 5.3 of the flow plate in the coarse grid case. Some calculations not presented here revealed no large differences if these features were taken into account in the fine grid simulation.

The figures 7.28 to 7.30 show the mass of melt and water and the melt energy in the pool region. The most significant difference compared with the fine grid simulation is the nearly constant melt inventory in the lower plenum after about 4 s. The reason for this is the build up of a higher pressure in the lower plenum region for times greater 4 s (cf. Figure 7.31) which reduces the driving pressure difference of the melt outflow. This pressure build up could be an effect of the coarser (larger) cells filled with water, which were entered by the melt its way down the outer periphery of the lower plenum.

The figures 7.32a-f show the volume fractions of melt and water. A Comparison of 7.31a with 7.22a shows that at T=3 s the melt starts entering the large cells towards the centerline.

The figures from 7.34 to 7.36 show the premixed mass, energy, and water volume fraction. The premixed mass and energy are evidently higher in the coarse grid case. The peak values are about $1.0 - 1.8$ t and $1.2 - 2.5$ GJ, respectively.

Apart from some single peaks in the coarse grid case, the temporal evolution of the premixed water volume fractions are very similar in both cases.

Figure 7.33 shows the surface of the melt droplets. The melt surface in the fine grid simulation is distinctly smaller for times greater ≈ 1.5 s. At times larger ≈ 4.0 s, when the melt flow out of the heavy reflector stops in the coarse grid case, the two curves are not directly comparable, since it would be necessary to consider the large surface of the different amount of melt inside the heavy reflector.
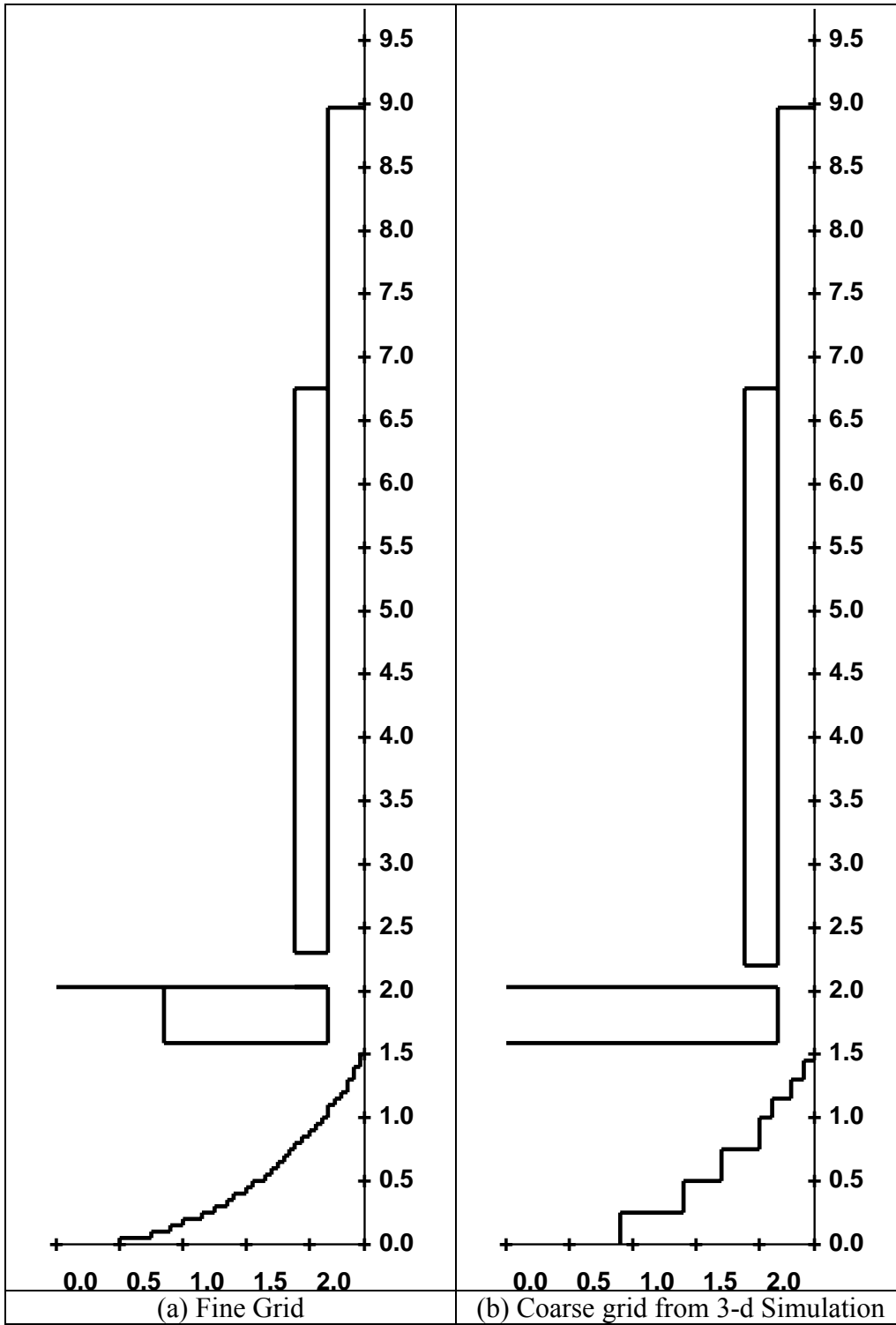
Figure 7.37 Fine and coarse grid
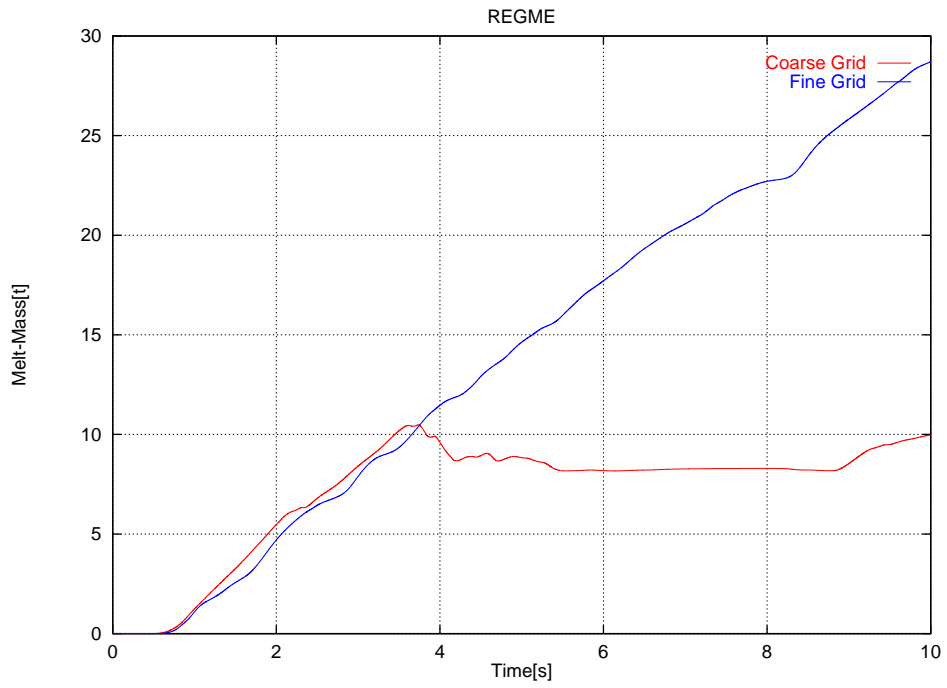
Figure 7.38 Melt mass in lower plenum region
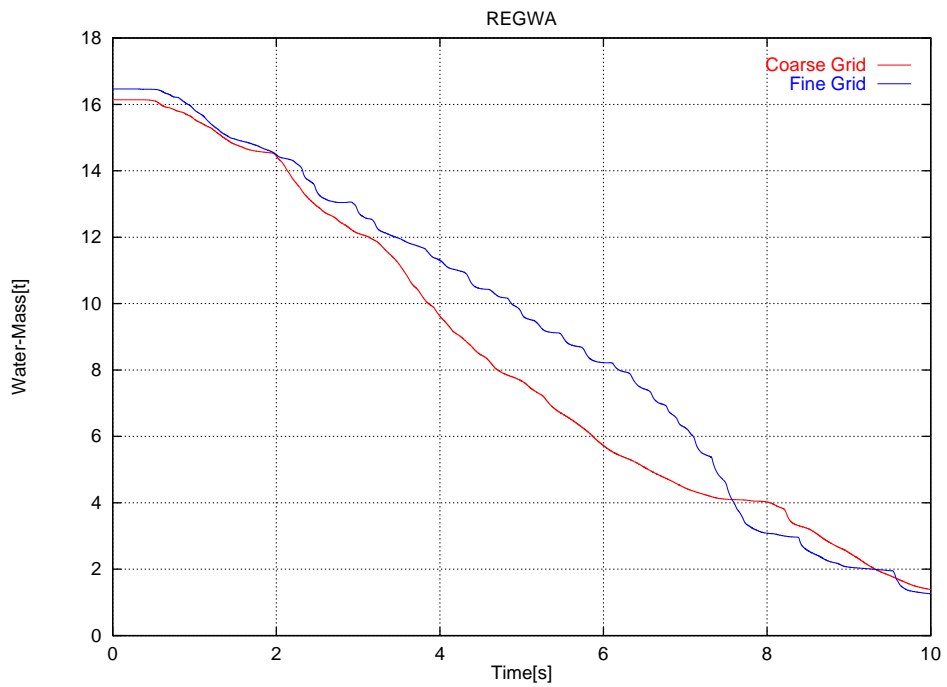
Figure 7.39 Water mass in lower plenum region
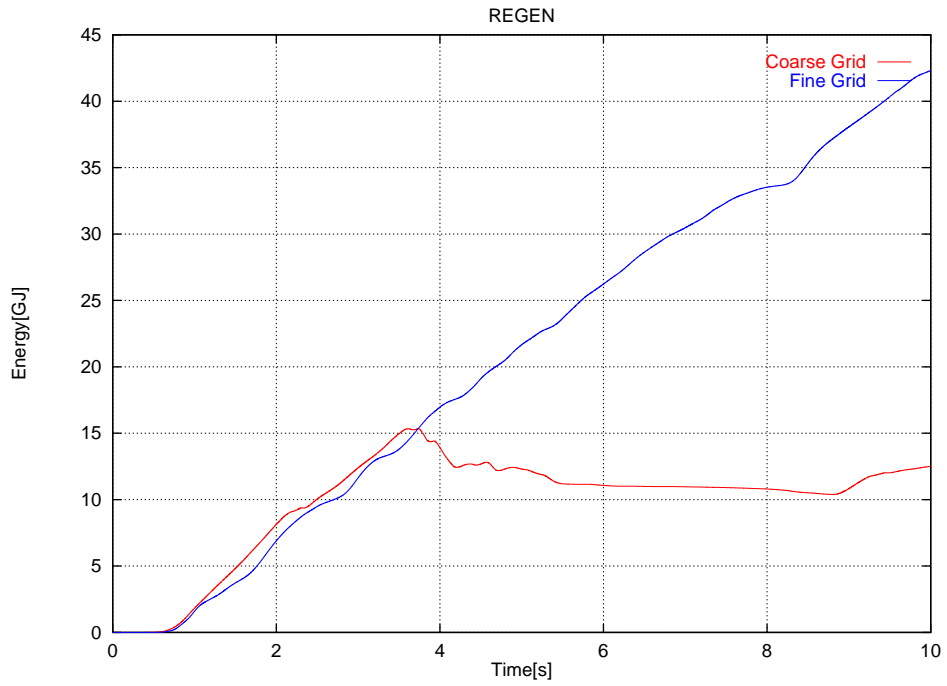
Figure 7.40 Melt energy in lower plenum region
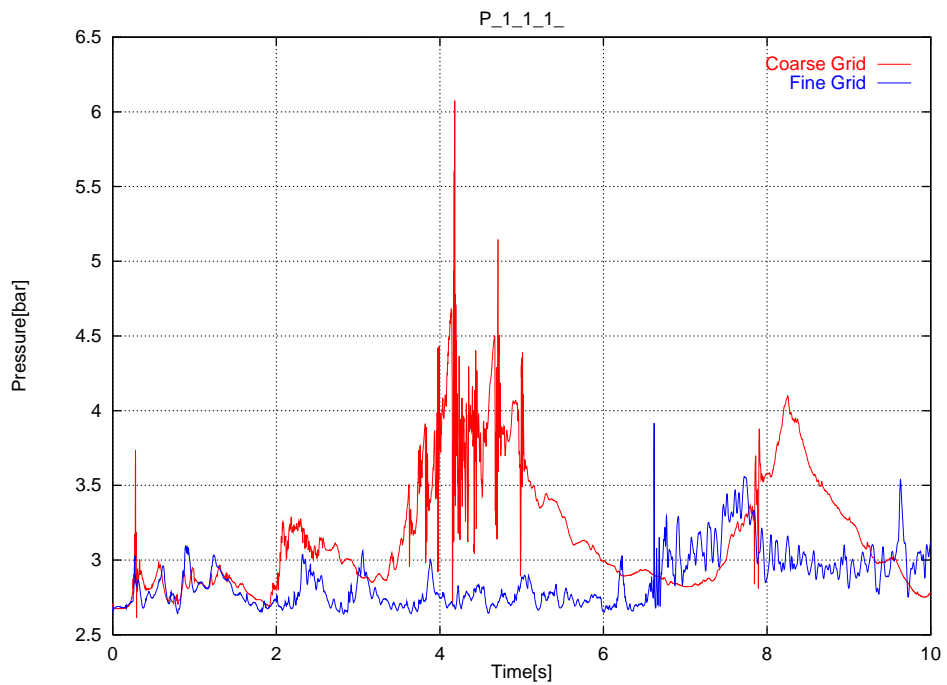
Figure 7.41 Pressure in lower plenum region
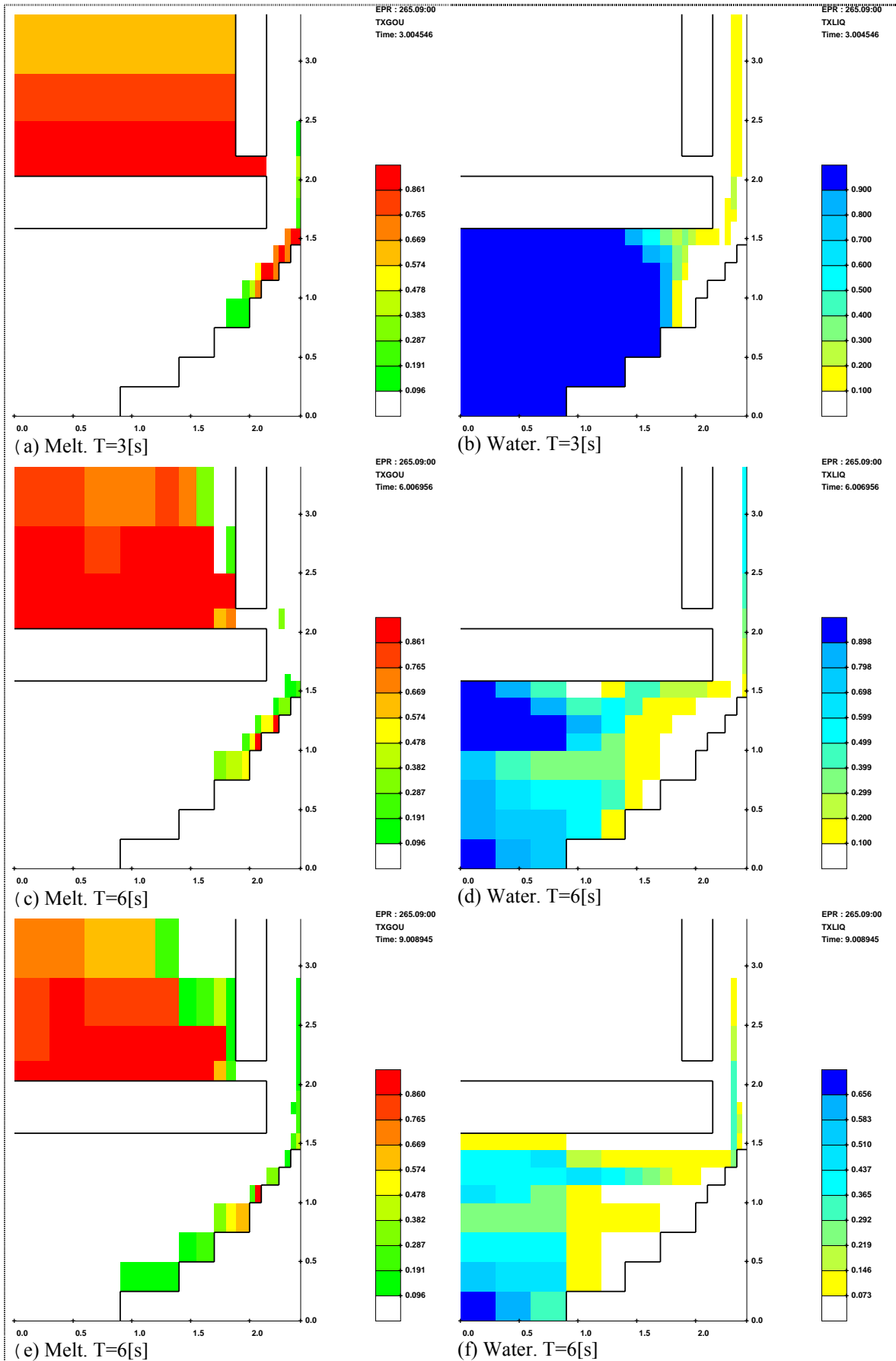
Figure 7.42 Volume fractions. Coarse grid.
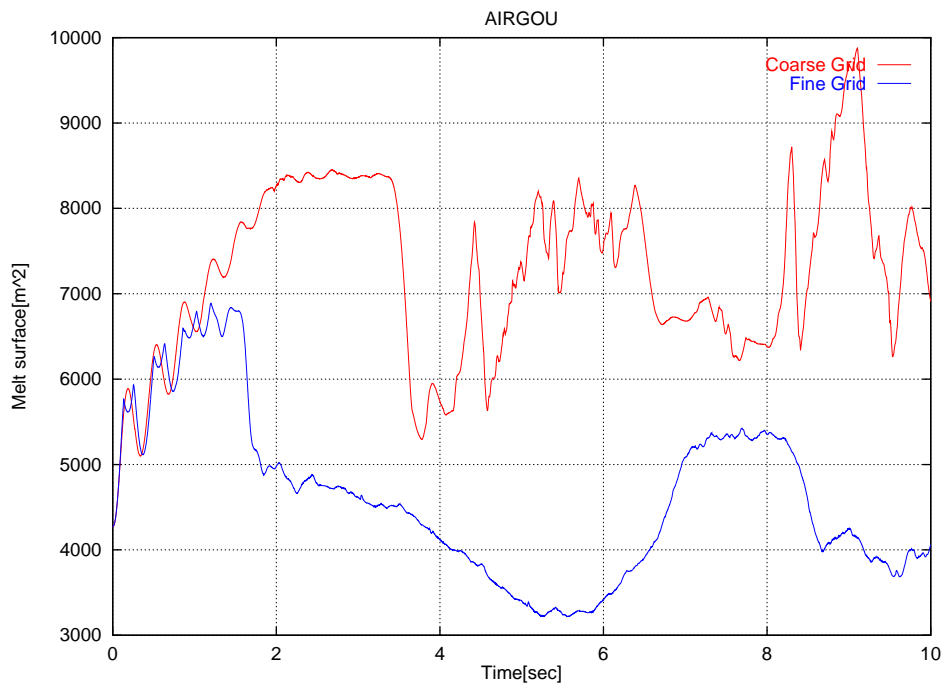
Figure 7.43 Melt surface
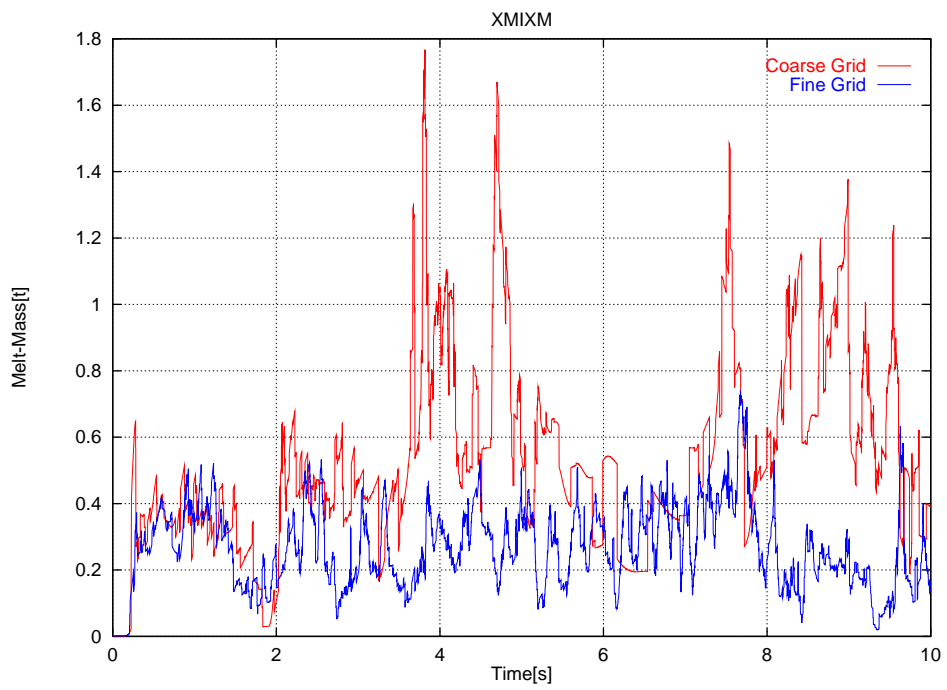
Figure 7.44 Premixed melt mass

114
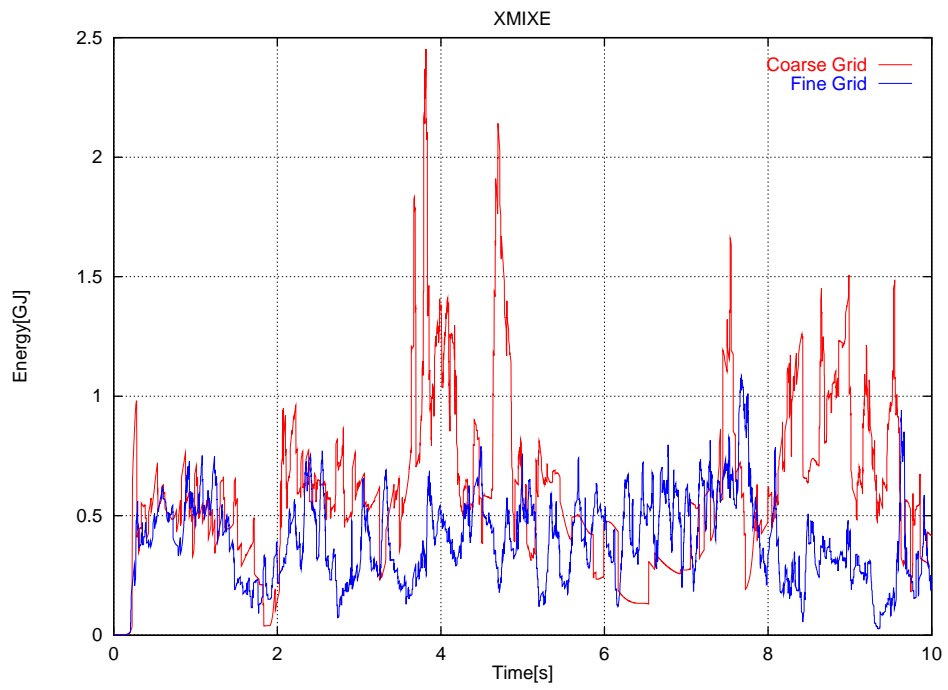
Figure 7.45 Premixed melt energy
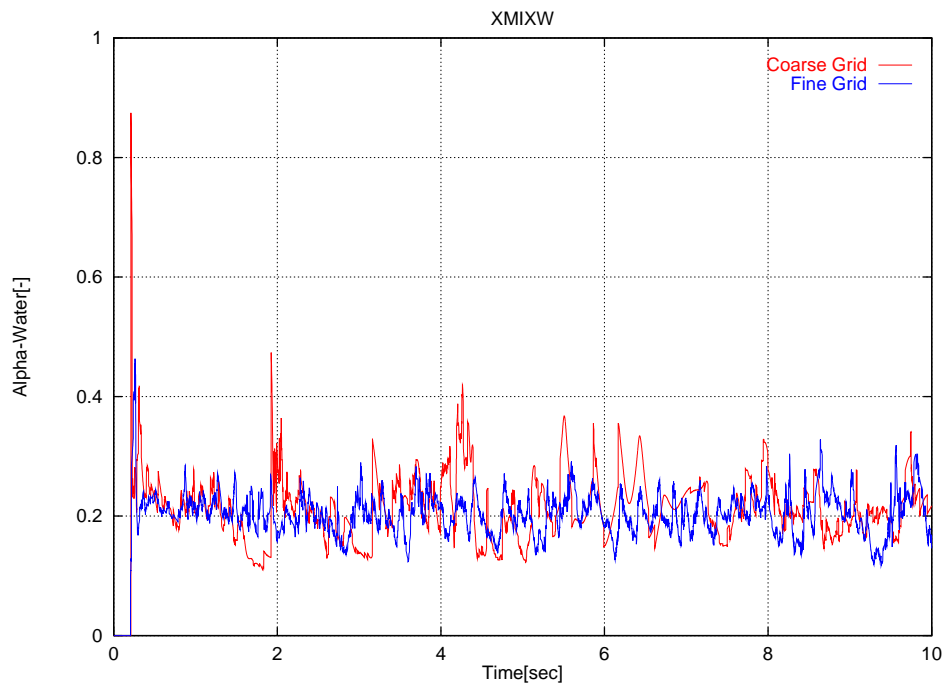
Figure 7.46 Premixed water volume fraction

115

7.1.5 Summary of the axisymmetric cases

In order to determine possible limits of the premixed energies in case of radial leakage scenarios of an EPR core melt down accident, some 2D-calculations with the MC3D computer code were performed. Three different leakage scenarios were considered:

1. a 5% (0.138 m^2) leak at the top of the heavy reflector,
2. a 5% (0.182 m^2) and
3. a 25% (0.910 m^2) leak at the bottom of the heavy reflector.

Because melting of the heavy reflector is most probable near the surface of the melt pool, the 5% top leak was indicated as base case.

Another two calculations were performed in order to assess the influence of the

4. initial particle diameter of the fragmenting melt and
5. the pressure loss coefficient of the flow plate in the lower plenum of the reactor vessel.

Furthermore(6.), in order to compare the axisymmetric simulations with the full three-dimensional one, an axisymmetric run with the coarse grid from the 3d case was performed.

The table 7.1 gives a summary of the significant parameters of the simulations. The labels will be used to identify the several runs in the following tables.

Table 7.2   Performed runs

Identification	Leak[a]	Pos. [b]	Ø[c]	Zeta[d]	Label	Note
1. 145.16:49	5%	Top	5	0	5-Top.5D.0Z	BASE CASE
2. 146.16:18	5%	Bottom	5	0	5-Bot.5D.0Z	
3. 149.15:37	25%	Bottom	5	0	25-Bot.5D.0Z	
4. 160.10:12	5%	Bottom	50	0	5-Bot.50D.0Z	
5. 209.14:10	25%	Bottom	5	10	25-Bot.5D.10Z	
6. 265.09:00	7.94%[e]	Bottom	5	5.3	5-Bot.5D.5Z.c	Coarse Grid

[a]Permeability of leak
[b]Position of leak in heavy reflector
[c]Initial particle diameter of the fragmenting melt in [mm]
[d]Pressure loss coefficient of the flow plate in the lower plenum
[e]Actually the same leak area like 5-Bot.5D.0Z

- ***Masses in lower plenum***

Table 7.3 shows the lower plenum inventory of melt and water in the lower plenum at 5 s and 10 s. The initial water mass in the pool is 16.46 t. The mean melt flow and pool water loss rates are in kg/s.

As expected, the small (5%) leak at top leads to the smallest melt outflow and evaporation rates, and the large (25%) leak at bottom to the highest ones. It should be noted, that the difference in the outflow rates between the two 25% bottom leak cases is most probable due

to slightly smaller time steps in case of the simulation with a pressure loss coefficient for the flow plate.

Furthermore it is remarkable that in case of the coarse grid simulation the melt mass in the pool is nearly constant for times greater 4 s. This is most probably a consequence of a pressure build up in the pool, which reduces the pressure difference between the downcomer and the melt pool inside the heavy reflector.

Table 7.3   Masses in pool

Run	Melt[a] 5 [s]	...10 [s]	Water[a] 5 [s]	...10 [s]	Melt flow[b]	Evap.[b]
5-Top.5D.0Z	3.6	7.2	12.4	7.2	800	1000
5-Bot.5D.0Z	14.6	28.7	9.7	1.26	3000	1600
25-Bot.5D.0Z	25.0	51.6	8.1	1.0	5400	1600
5-Bot.50D.0Z	14.9	29.9	10.3	4.66	3100	1200
25-Bot.5D.10Z	23.7	38.6	8.9	1.33	4100	1600
5-Bot.5D.5Z.c	8.8	10.0	7.7	1.39	3000[c]	1000

[a] in metric tons
[b] in [kg/s], rough mean values
[c] for times < 4 [s], $\approx$ 0 for times > 4 [s]

Energies in lower plenum

Table 7.4 shows the lower plenum values of melt energy for 5 s and 10 s. The initial energy inventory in the reactor vessel is 169.8 GJ. All energies are in GJ.

The energies in the lower plenum region are nearly proportional to the melt mass. In case of the coarse grid simulation, the energy inventory is therefore nearly constant after about 4 s.

Table 7.4   Energies in pool

Run	Energy[a] 5 [s]	...10 [s]
5-Top.5D.0Z	4.9	9.7
5-Bot.5D.0Z	21.7	42.3
25-Bot.5D.0Z	36.8	75.9
5-Bot.50D.0Z	22.7	45.3
25-Bot.5D.10Z	34.6	55.9
5-Bot.5D.5Z.c	12.3	12.5

[a] in [GJ]

Premixed Mass, Energy and Water

Table 7.5 shows the range of the maximum values of premixed melt mass and energy. Since the temporal evolution of these is of highly oscillatory nature, the range of variation is quite large.

The peak values of the premixed energies are about 2.7 GJ for the 5% leak at the bottom of the heavy reflector and an initial particle diameter of 50 mm.

Table 7.5   Premixing quantities

Run	Melt[t][a]	Energy [GJ][a]	Water[b] [-]
5-Top.5D.0Z	0.4 – 0.5	0.5 – 0.6	0.1 – 0.3
5-Bot.5D.0Z	0.5 – 0.7	0.7 – 1.1	0.1 – 0.3
25-Bot.5D.0Z	0.8 – 1.0	1.2 – 1.5	0.1 – 0.3
5-Bot.50D.0Z	1.2 – 1.8	2.1 – 2.7	0.2 – 0.4
25-Bot.5D.10Z	0.8 – 1.1	1.2 – 1.7	0.1 – 0.3
5-Bot.5D.5Z.c	1.0 – 1.8	1.2 – 2.5	0.1 – 0.4

[a]mean range of peak values
[b]mean range of variation

7.2   MATTINA-Results for the axisymmetric cases

7.2.1   Base case calculation

The base case is essentially the same as described for MC3D: Sideways outflow through heavy reflector and core barrel at the level 2.9...3.1 m assuming a permeability of 5 % so that the effective flow area at the inner face of the heavy reflector (radius 1.882 m) is 0.12 m^2. The configuration of the lower plenum is as shown in Fig. 4.4: the lower core support plate is open at the bottom and voided. (Its porosity is 33 % equal to the vertical permeabilities.) For the base case, the outflow location was chosen slightly below the pool surface (where one would expect it to be situated) in order to promote in a conservative way the outflow of melt and at the same time to cover in a conservative way the possibility that an outflow opening that is situated at the pool surface initially proceeds in downward direction during the melt release (for further discussions see 7.2.2). The initial particle radius was chosen as 5 mm which is unrealistically small but was chosen in order to compensate for the ineffective fragmentation observed in MC3D. This point as well is further discussed in 7.2.2.

When considering these calculations, however, one must keep in mind that simulating radial outflow, which actually occurs in a single azimuthal position, with a 2D code in axial symmetry is quite inappropriate. Instead of a jet of melt or a concentrated shower of droplets we are simulating here a very diluted spray of melt particles approaching the water surface. So, a deep penetration of the melt into the lower plenum is practically prevented by the modelling from the beginning. Also, the water has no free path for escaping because it is impacted by melt all around the circumference. So it cannot give way to the melt which enforces immediate interaction. Also, in this case, the representation of the lower hemisphere of the pressure vessel by steps gets an unfavourable significance: the melt coming from the downcomer will tend to settle on the horizontal steps instead of gliding down the inclined inner vessel surface towards the vessel centre. So it tends to remain in a situation in which it can be 'premixed' (following our criterion) while, in reality, it would collect in a pool on the vessel bottom and become separated from water. This effect could be avoided by simulating the force acting downhill on an inclined surface and/or the momentum exchange of melt particles with external walls. But until now such models are not available. Unfortunately this latter aspect applies as well to the 3D simulation performed with MC3D. The effect is even especially strong in that calculation because an especially coarse grid had to be used in the

lower plenum in order to keep the total number of cells in a practical range. At any rate: sideways outflow will require further studies in three dimensions with proper meshing and initial conditions.

The base case was calculated with MATTINA up to 8.6 sec. During this time no fast transients are observed. (Transient pressurisation events are not to be expected because the corium is assumed to be fragmented into small particles from the beginning and the interaction occurs at the free surface of the water.) The pressure in the downcomer reaches about 2.9 bar after 7.5 sec, see Figure 7.47. The rate at which melt enters the lower plenum is
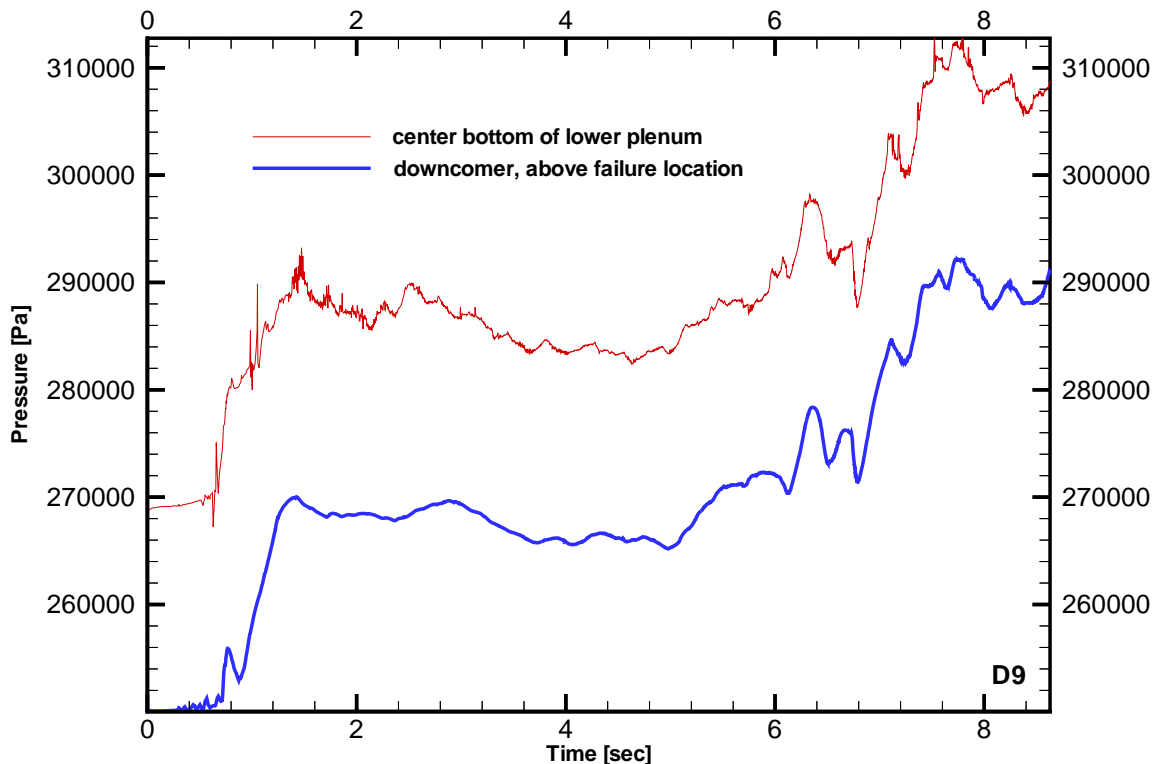
Figure 7.47 Pressure history (sideways outflow close to the top with 5 mm initial particle radius)

very low, about 270 kg/sec, see Figure 7.48. At the same time melt is carried out of the pressure vessel (into the cold leg) at a rate which is about 400 kg/sec in the beginning and increases to 1.6 t/sec in the end. This is a consequence of the thermal interaction at the water surface that produces a lot of steam which carries with it the small corium particles. As a consequence, we have after 8.6 sec about 2.1 t of corium in the lower plenum while 4.1 t have left the pressure vessel. It is also interesting to note that the total amount of 'frozen' corium determined by MATTINA is 3.2 t at that time – larger than the amount of corium in the lower plenum. This indicates that at least 1.1 t of melt are within the downcomer. While the criterion for the frozen state applied in MATTINA may not be applicable to the corium to be expected in an accident case as discussed already in 6.2.1, this large amount of 'frozen' material at least indicates that practically all the melt outsides the core area has undergone strong thermal interaction with the water and has thus lost a large portion of its thermal energy. More specifically we may consider the 'mixed' 'melt', cf. Figure 7.49. Its maximum of 1.3 t is

119

reached after about 8 sec and its thermal energy is then 0.5 GJ. This gives a specific enthalpy of 0.38 GJ/t, a value low enough so that even a corium containing metallic zirconium would be frozen completely. So there is no potential for a steam explosion. Under these circumstances it is not relevant that the 1.3 t of 'mixed' corium are not necessarily the absolute maximum. Larger numbers might be reached at later times but these masses would be frozen as well. But all this, as discussed above, is subject to the axially symmetric modelling and to assuming a small initial particle diameter.

Figure 7.48 Corium and water masses in the lower plenum (sideways outflow close to the top with 5 mm initial particle radius)

A critical point might be that large amounts of corium and water are present in the lower plenum for long times in this case, in contrast with the downward relocation scenarios. Without structures separating melt from water it is difficult to definitely exclude that some local event (an initial steam explosion) leads to more mixing. In the present case, there are 2.1 t of corium in the lower plenum at 8.6 sec and there are still 10.6 t of water present as shown in Figure 7.48 with some more (less than a ton) in the lower core support plate. However, the total thermal energy in that corium is 1.2 GJ only – a value that is still far from being potentially dangerous. In addition, again, the specific enthalpy of this mass is so low that even zirconium contained in this mixture would be solid so that no potential for a steam explosion is found.
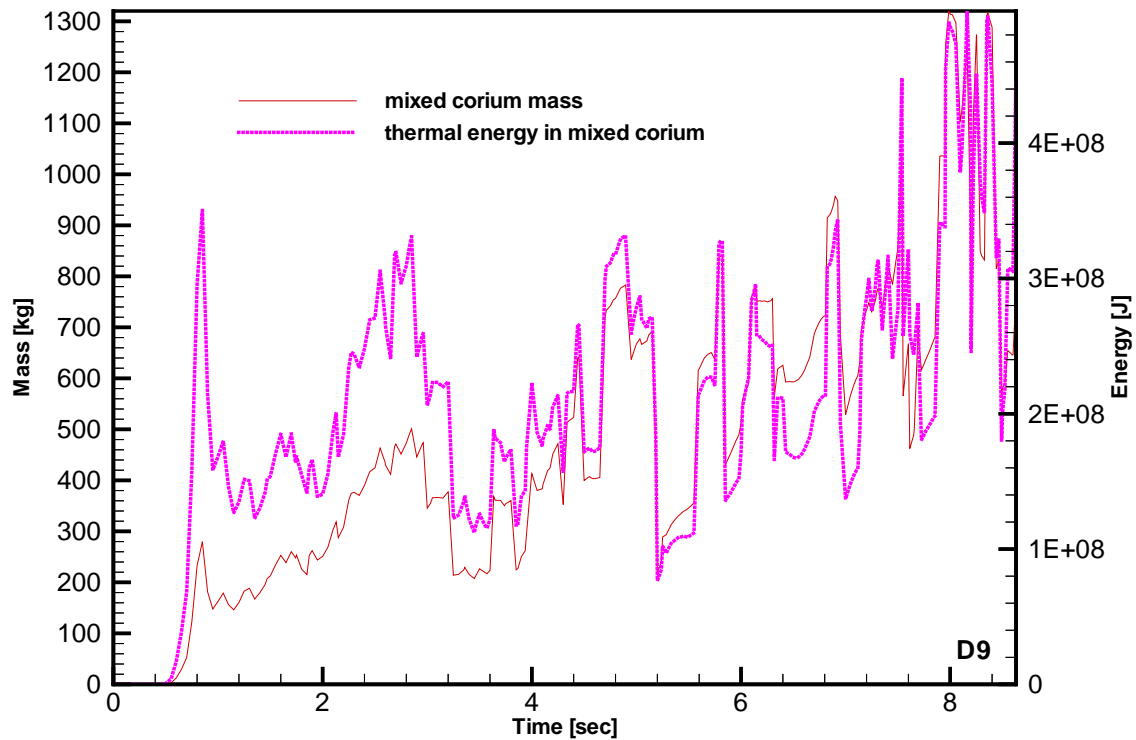
Figure 7.49 The mixed corium mass and its thermal energy (sideways outflow close to the top with 5 mm initial particle radius)

Another aspect in which this sideways relocation case differs from the downward relocation cases is the fact that a pressurisation of the melt pool occurs after 2.4 sec when the pressure balance between downcomer and core area allows some steam to penetrate through the breach into the core area. This appears to be an intermittent process and the amounts of steam must be very small because the outflow of steam into the hot leg remains lower than that into the cold leg by about an order of magnitude. Still the pressure reaches more than 4 bar in the upper part of the melt pool (about 5.2 bar at its bottom). This causes some agitation of the melt pool and a little spray of melt droplets above the failure position.

7.2.2 Parametric analysis

The base case was repeated with MATTINA assuming an initial particle diameter of 50 mm. Quite surprisingly, the results concerning the pressure are quite similar, see Figure 7.50. Obviously the melt particles are fragmented into the range of diameters below 10 mm already on their way towards the compact water. There are more abrupt pressure changes but their amplitudes are very small. Correspondingly the pressure in the downcomer oscillates a little bit but its average value is very similar to the base case. The same applies to the pressurisation of the melt pool.
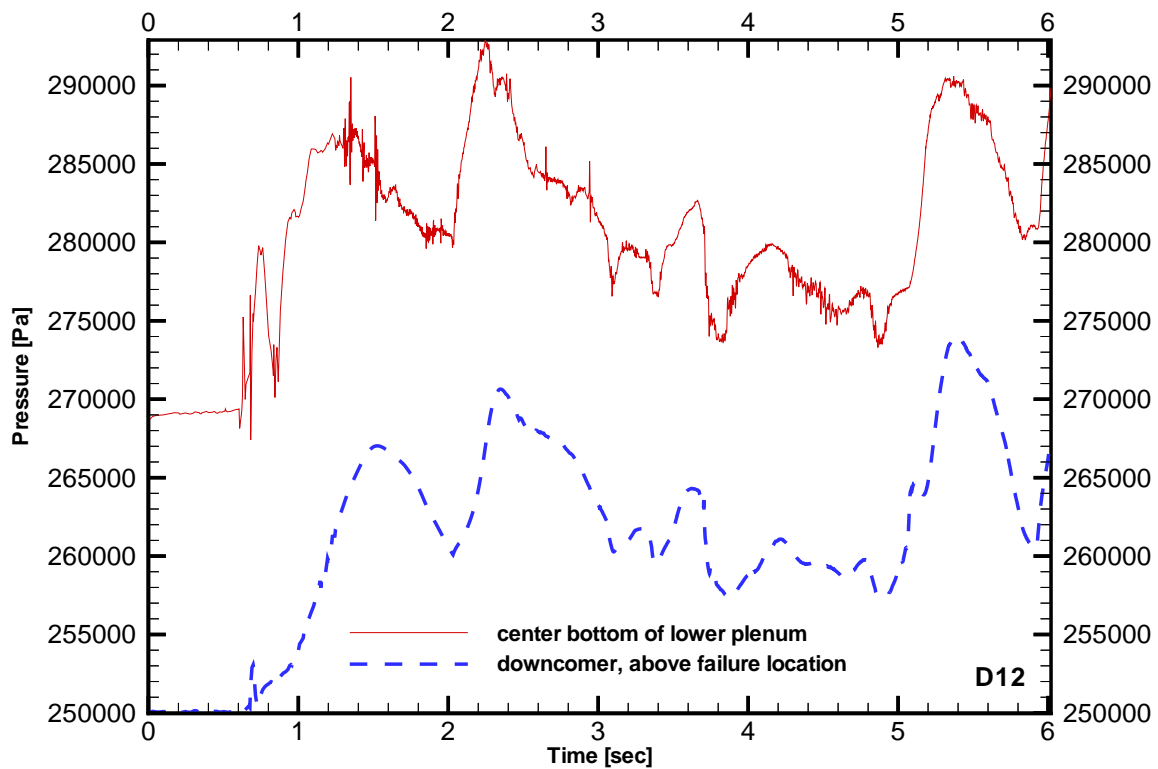
Figure 7.50 Pressure history (sideways outflow close to the top with 50 mm initial
particle radius)

The amounts of melt relocated and mixed are higher in this case, however. The case was
calculated until 6 sec and the mass in the lower plenum then amounts to 2.2 t, see Figure 7.51
(as compared to 1.1 t in the base case). The 'mixed' mass reaches almost 2 t in a narrow spike
shortly before 6 sec, see Figure 7.52. (In the base case this value was below 1 t until then.)
The enthalpy content of the mixed mass has a peak value of 1.8 GJ (Fig. 7.52) which almost
equals that of the melt in the lower plenum, 2.0 GJ. On the other hand, the removal of melt
from the pressure vessel is much less effective (0.8 t instead of 2.0 t at 6 sec) while, on the
other hand, the water is removed more quickly: the remaining mass is 10.4 t at 6 sec as
compared to 12.2 t in the base case (Fig. 7.51). So, if we extrapolate the decrease of water
mass in the lower plenum (which may not be too uncertain), we find that all the water would
have gone after 15 sec. It is very unlikely that the enthalpy of the melt in the lower plenum
can reach a possibly dangerous value, let's (cautiously) say 6 GJ, within this time. The last
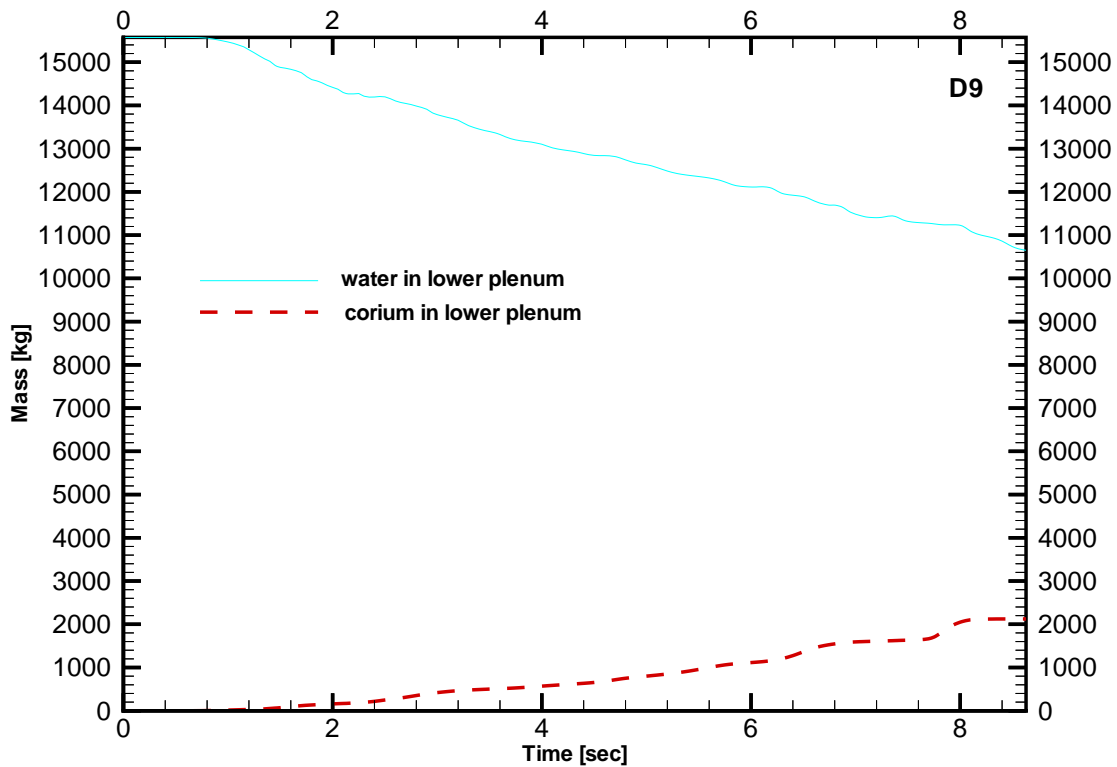assertion is based on another, more uncertain extrapolation.

122

Figure 7.51 Corium and water masses in the lower plenum (sideways outflow close
to the top with 50 mm initial particle radius)
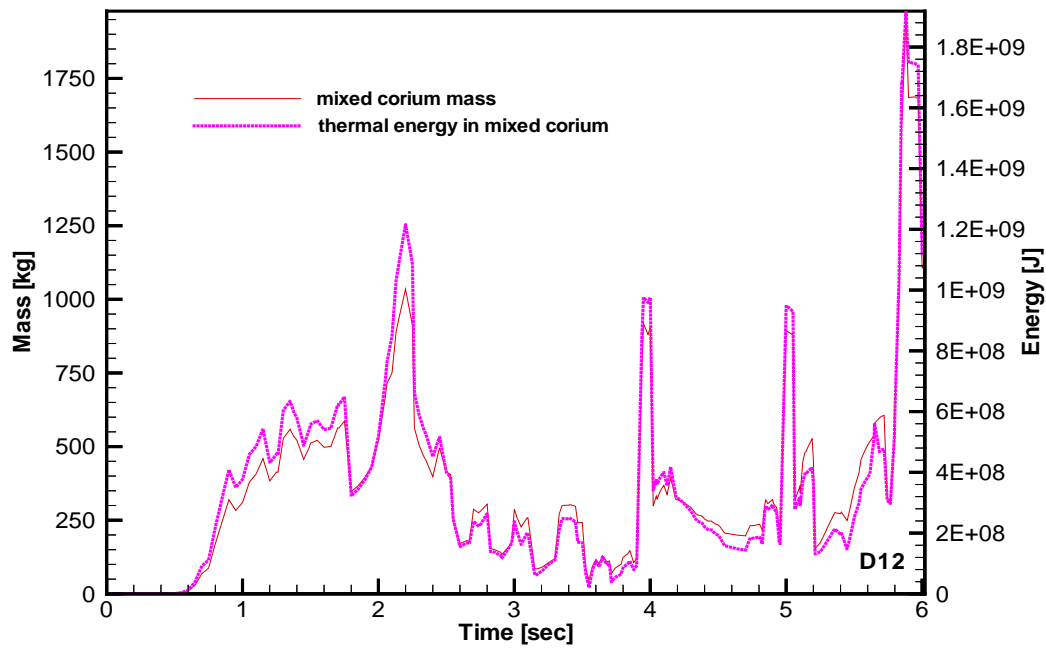
Figure 7.52 The mixed corium mass and its thermal energy (sideways outflow close
to the top with 50 mm initial particle radius)

The spatial distributions of water and corium at the end of the calculation are illustrated in Figure 7.43 which shows the volume fractions of these materials as fractions of the cell area that are dark grey for corium and shaded for water. The remaining white space represents the volume fraction of gas. In this type of graph always the corium is shown on the bottom of the cell and the water and the gas above it (in this order). But the reader should keep in mind that these three phases are always assumed to be intermixed in the code. The white space within the pool area indicates the amount of void present there that has increased in comparison with the initial state (Fig. 4.4) due to the agitation caused by steam penetrating into the melt pool. The water is concentrated in the central part of the lower plenum with some steam in the upper part of the plenum. Most of the corium in the lower plenum is collected in the unrealistic corners that are used in these simulations to describe the lower hemisphere of the vessel. Practically all the water above this corium has been blown away.
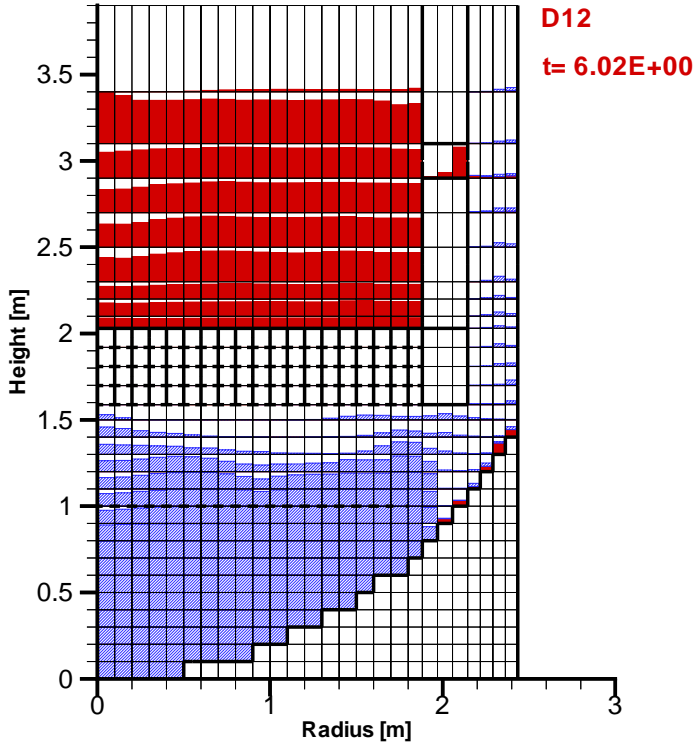
Figure 7.53 Final material distribution (sideways outflow close to the top with 50 mm initial particle radius)

Further cases were calculated with the failure location at the bottom of the melt pool like in the 3D simulation (see 7.1.1) and the calculational mesh used there. The failure area is 17 cm high (one cell) and has a permeability of 7.94 %. This gives a minimum free flow area of 0.16 m^2. The whole lower core support plate is excluded from the flow (closed). The results of the calculation with 5 mm initial particle diameter are contained in Table 7.1.1 for comparison with the MC3D calculations. The same case has again been calculated with an initial particle diameter of 50 mm, which is more conservative. This time, the larger initial particle diameter actually leads to more pronounced pressure transients and an overall stronger pressure build-up in the lower plenum and the downcomer: in the latter we have a peak with a maximum of about 5.2 bar at about 2 sec and a quasi-steady pressurisation to slightly above 4 bar between

5 and 6 sec. The mixed mass reaches a maximum of 3.4 t at 6.2 sec with a corresponding maximum in the enthalpy of 2.7 GJ. At the end of the calculation, at 8 sec, these values are already considerably smaller. Also the water mass has already decreased to 5.5 t so that no further and larger maximum in mixed melt should occur. Even the melt in the lower plenum decreases after a maximum of 4.2 t at about 4...5 sec and the enthalpy in all this mass has a maximum of 4 GJ (only) at 5...5.8 sec and then decreases to less than 1 GJ.

A similar case (failure at bottom, 50 mm initial particle diameter) has been calculated with the standard MATTINA calculational grid. This means that the failure area is 27 cm high and extends over two cells axially (with 5 % permeability). Also, in comparison taken over from the 3D calculation, the cells are larger in radial direction in the outer zones (heavy reflector, core barrel and downcomer) but considerably smaller in the central area. In axial direction, only the cells within the height of the lower core support plate are larger (4 cells within this height instead of 5), all other axial cell dimensions are the same or smaller, considerably so in the part of the lower plenum below the flow plate. The results are quite similar to the case described above. However, the transient pressure peak in the beginning is absent due to the availability of the buffer space filled with steam in the lower core support plate. (The same effect can be observed when using the MC3D-3D-grid.) Similarly the pressures at later times are more moderate (about 1 bar lower). Still, in contrast with the above case, a melt pool pressurisation occurs and less melt is transported into the lower plenum (the maximum is 2.9 t at 4.2 sec) and less melt is premixed (2.7 t at 6.5 sec). Correspondingly the maximum of the enthalpy in the mixed mass is slightly smaller: 2.6 GJ.
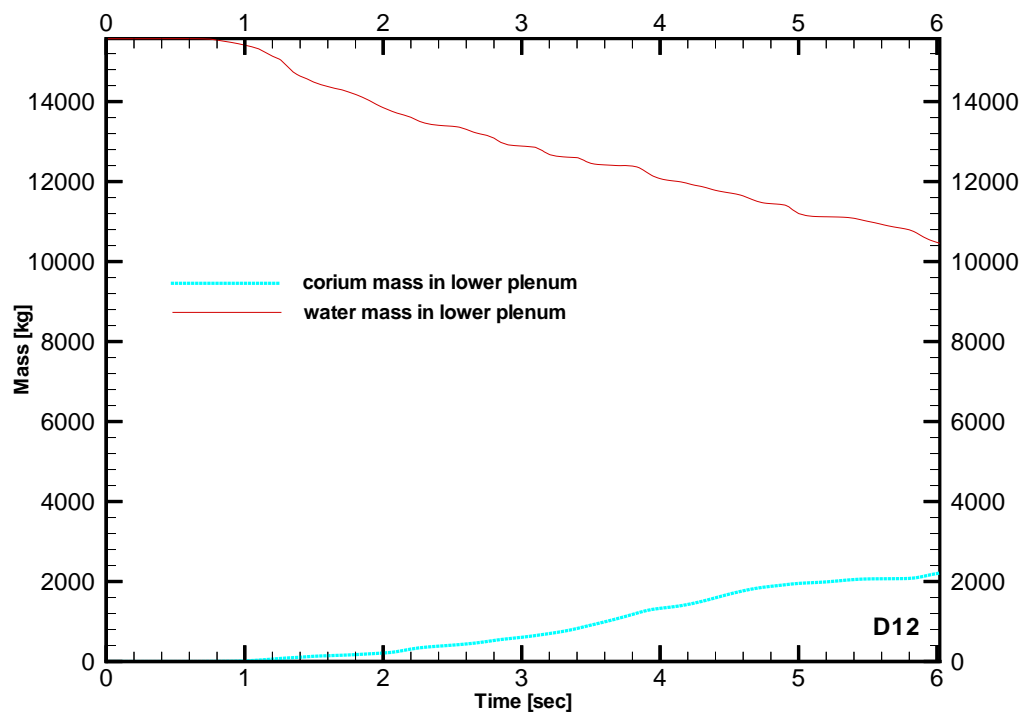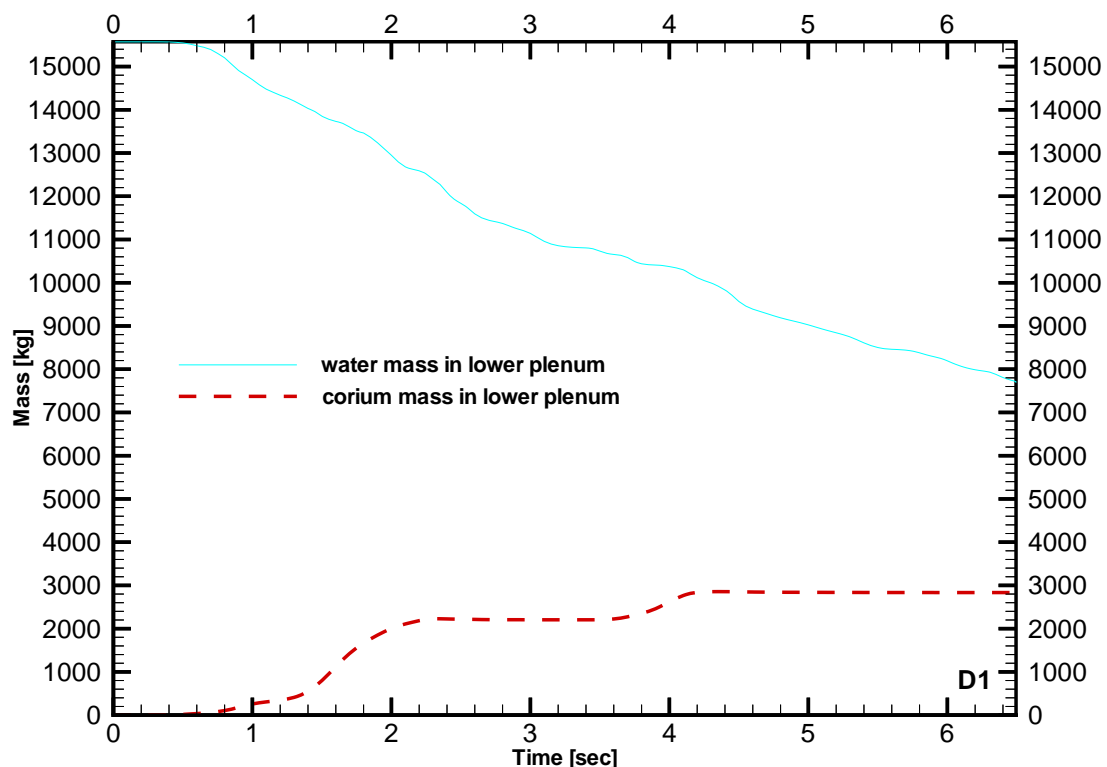

Figure 7.54 Corium and water masses in the lower plenum (sideways outflow at the bottom with 50 mm initial particle radius)

Again, in both cases with the low failure location, more melt is blown out of the pressure vessel than enters the lower plenum.

As a final parametric case, a slit from top to bottom of the heavy reflector and core barrel besides the melt pool was assumed to grow within 13.7 sec with a permeability of 1.69 %. This corresponds to a slit about 20 cm wide (but with its area distributed all around the circumference). The assumed downward growth rate (10 cm/sec) is certainly too large (too pessimistic). Here the meshing of the 3D calculation with MC3D was used with one modification: the lower core support plate was assumed to be open from below. In this case almost nothing happens until 7 sec. The pressures remain benign (essentially below 3.2 bar in the downcomer) all the time until, at 17.87 sec it starts to rise steeply. But at that time, already, only 2.6 t of water have remained in the lower plenum (plus 0.6 t within the lower core support plate). The mixed mass has gone through a maximum of 1.7 t shortly before with a maximum 'mixed' enthalpy of 0.9 GJ. Even the enthalpy of all the melt in the lower plenum peaks at only 3.8 GJ (for 4.8 t) shortly before. So, if the pressure rise that is calculated at 17.97 sec would trigger a steam explosion, that would not be a dangerous one. If not, the remaining water would be blown out of the pressure vessel and there would remain no further chance for a steam explosion.

7.2.3   Summary of MATTINA calculations for sideways outflow

The base case (high failure position, 5 mm initial particle diameter) is characterised by low melt relocation rates and intensive thermal interactions. Still the pressures remain low because the interaction always occurs at the free surface of the water. Therefore, also, more melt is swept out of the pressure vessel than can enter the lower plenum. No potential of an energetic steam explosion is found because the corium practically is frozen before sizeable amounts can accumulate within the water.

When the more realistic value of 50 mm is assumed for the initial particle size, the pessimistically determined 'mixed' corium mass reaches a maximum of 2 t with a maximum thermal energy content of 1.8 GJ. But this is still far from possibly jeopardising vessel head integrity.

The highly conservative assumption of a quite large failure just above the lower core support plate together with the conservative initial particle diameter of 50 mm lead to maximum thermal energies in the mixed corium of 2.6...2.7 GJ (depending on the meshing) which should still not pose a problem to vessel head integrity.

The assumption of a slit that opens from top to bottom (at a probably too high rate) leads to a very slow mixing with maxima of 1.7 t for the mass and 0.9 GJ for the enthalpy of the mixed mass. Within the calculated almost 18 sec, 4.8 t of corium reach the lower plenum (with 3.8 GJ of energy) but then only 2.1 t of water remain so that no efficient steam explosion is possible any more.

In these scenarios large water masses remain in the lower plenum for long times (several seconds) so that large masses of melt might be able to accumulate there. This would mean that these masses were not separated by structures and could thus be intermixed and take part in an interaction. In the base case, this concern is irrelevant because essentially all the melt accumulating in the lower plenum is already frozen. When this case is considered with an initial particle diameter of 50 mm, the effect discussed above occurs to some extent but during the time covered by the calculation the corium masses involved remain so low that no potential for vessel head failure could be derived. An extrapolation to longer times indicates

that presumably all the water will be removed before a potentially dangerous amount of thermal energy can be present (not to talk of being premixed) in the lower plenum. A similar situation is seen in the even more pessimistic case with a large failure directly above the lower core support plate and the large initial particle diameter. In the case with a slit opening from top to bottom, the calculation covers the time until the water is practically removed and no potentially dangerous situation is encountered.

The calculations here discussed do not result in situations in which a steam explosion could occur that could jeopardise vessel head integrity. With some extrapolation that can even be concluded for the long-term behaviour. But of course, all this is valid only within the modelling frame applied here, i.e. in a two-dimensional, axisymmetric description of a situation that is inherently three-dimensional.

In these investigations, no induced failure of the melt pool has been assumed. Such failure might occur if interaction pressures were able to break the crust containing the melt pool. But the pressure transients calculated here are so weak that it seems unlikely that they could break the crust. On the other hand, the pressure maxima calculated are certainly more uncertain than the general pressure development and not too much is known about the strength of the crusts. So this topic should be reconsidered when further developed tools are available in both areas of research.

7.3   Comparison of MC3D and MATTINA-Results

In Table 7.5 a comparison of results for a radial release scenario calculated by MC3D and MATTINA is presented. The details of the scenario are described in chapter 7.1.1.

Differences between MC3D and MATTINA can be explained with the stronger fragmentation of melt particles in MATTINA. Stronger fragmentation leads to an increase of the total particle surface which initiates a faster heat transfer between melt and water/steam. So MATTINA calculates a faster evaporation of water.

The most significant difference is the melt mass which is blown out of the vessel. This value is higher by a factor of 5 in the MATTINA calculation when compared to MC3D results. If the melt is released and comes into contact with water in MATTINA a stronger fragmentation occurs by which the evaporation of water is increased. Because of drag between melt particles and steam the particles have a stronger tendency to be blown out of the vessel. If the released melt particles are removed faster from the water they will vaporise less water. So MATTINA loses only 5.2 tons of water compared to 9.3t in MC3D-calculation.

The amount of melt which is accumulating in the lower plenum is also significantly smaller (MATTINA: 2.6t; MC3D: 8.8t). Therefore the melt surface is considerably smaller in MATTINA-calculation. The maximum of premixed melt is smaller by about 40% in the MATTINA-calculation.

A comparison of the pressure maxima is difficult because in MC3D the maximum occurs during a packing event. Neglecting fluctuations with short time scales MC3D calculates a pressure maximum in the lower plenum of about 4bar. This is quite close to the pressure of 3.8bar   calculated   by   MATTINA

8 Summary of premixing results

Premixing of corium pouring into residual water of the lower plenum of the EPR was investigated using two multicomponent-multiphase codes: MC3D and MATTINA. A simplified geometry including the heavy reflector, the lower core support plate and the flow distribution plate was chosen to describe the most important structure components of the reactor vessel internals. A low pressure scenario was assumed with a system pressure of 2.5 bar and a large 110 t corium pool of 3000 K located directly on the lower core support plate. The level of saturated water reaches the upper edge of the lower core support plate. Axial relocation of melt in the center of the core is considered as a compact jet or as a distributed outflow through the failed structure. Radial distributed melt displacement is simulated at the bottom or at the top of the molten pool penetrating through the heavy reflector and the core barrel shell entering the downcomer to flow down to the lower water filled plenum. The basic free cross section is assumed to be about 0.2 m^2. The sensitivity to scenarios with increasing corium outflow rates is investigated, too.

Parameter studies were done to cover a band of uncertainties. A very strong influence on the results is recognized for the variation of the initial size and the transient increase of the melt release area. The initial droplet size is a key value for the strength of the thermal melt water interaction. The pressure losses at the distribution flow plate in the lower plenum influence the mixing of corium with water considerably. The spatial discretization has a strong impact on the overall result due to the nonlinear behaviour of most of the simulated processes and the utilization of a first order scheme for the convective terms in the basic equations. Feedback of pressure losses at coolant inlet and outlet and at the junction between downcomer and lower plenum is of minor importance. Moderate variations of the system pressure give similar results. For MC3D the change in melt surface tension does not give large differences due to the used combination of fragmentation and drag models.

The maximum mass and thermal energy of premixed corium is determined by summation of all mesh cells with a water volume fraction greater than 0.1 thus attempting to compensate the strong water depletion effect observed during recalculation of experiments. The average water volume fraction in the premixing zone is calculated by summation of all mesh cells containing water volume fractions greater than 0.1 and melt volume fractions greater than 0.01.

As observed in the experiments at low pressure calculations indicate that the water of the lower plenum is displaced rapidly by vapour into the downcomer for axial and radial outflow scenarios. Radial outflows should be investigated by 3D-simulations, to avoid an artificial enclosure of water in the lower plenum. Generally premixing is intensified by large melt release cross sections, large initial droplet diameters and pressure loss in the lower plenum flow distribution plate. The conservativly oriented evaluation of all investigated cases leads to a maximum of thermal premixing energies of 3 GJ and an average water volume fraction of about 0.5 to 0.6 in the premixing zone. In the majority of the calculated cases the maximum premixing energies vary between 0.5 to 2.0 GJ and the values of the respective average water volume fraction between 0.2 to 0.5. The total amount of melt in the lower plenum can be much larger than the premixed melt mass with a considerable water inventory still available. At the end water is largely separated from a rather compact molten corium pool.

Generally the two codes show similar results. MATTINA gives lower thermal premixing energies due to stronger water displacement, which is caused by strong evaporation events after intensive fragmentation of melt droplets. The presently used MC3D version simulates a more moderate fragmentation behaviour leading to less evaporation and water depletion. Both

codes predict removal of non negligible amounts of fragmented core material into the primary circuit if radial outflow scenarios are considered.

9 Steam explosion potential, energy conversion considerations, and energy partitioning

In this chapter the likelihood of the occurrence of an energetic steam explosion, the possible energy release during such an explosion and how much of that energy might go into the kinetic energy of the core debris are discussed.

The present study is based on the scenario that melt relocates from the core area into a water filled lower plenum and partly mixes with the water. It is postulated that this leads to an energetic steam explosion that accelerates core debris against the vessel head which implies the danger of a catastrophic vessel head failure. The possibility of such an energetic steam explosion in a (hypothetical) core melt down accident has been questioned occasionally during the last years based on experimental evidence obtained in the KROTOS facility at JRC Ispra [1]. Therefore these experiments are discussed here shortly in order to show that they do not prove the impossibility of energetic steam explosions in a molten down light water reactor core (LWR) until now and probably never will do.

In this discussion we'll use the argument that an efficient steam explosion requires fast fine-scale fragmentation of the melt after the explosion has been triggered. This generally accepted picture of a steam explosion is based on numerous observations in experiments and leads e.g. to the use of the fragment size as indication of which part of the mass has 'participated' in an explosion. Typically a diameter below 200…300 μm is required in this context. One may also recall that even the melt that was involved in the quite benign steam explosions that have occurred in experiments at the Forschungszentrum (BETA V 6.2 and PREMIX 11) was found in the form of very fine fragments afterwards.

The KROTOS explosion experiments in shock tube geometry have lately been performed with two types of melt: alumina (Al_2O_3, typically 1.5 kg at 2650 K) and a model corium (80 % UO_2 + 20 % ZrO_2, typically 3 kg at 3050 K). In these experiments the Al_2O_3 shows consistently strong explosions with pressures even beyond 1000 bar and up to 2.5 % energy conversion while for some time no interactions at all were observed with corium. However, in the meantime, clearly propagating events have been obtained with the corium as well. Only the pressures were much weaker, i.e. subcritical.

These results prompted some people to suggest that actual corium would not produce steam explosions. While such a conclusion can already be questioned on the basis of earlier experimental results (e.g. MFTF Rig A and SUW tests at Winfrith [2], MDC-2 at SNL Albuquerque [3]), it remains indispensable to understand the important differences observed in the KROTOS experiments.

It now appears that a special boundary condition of the KROTOS experiments plays an important role: Due to the arrangement of furnace and test section, the melt is injected into the test section with an initially high velocity, i.e. 30 m/s. It seems furthermore that, as a consequence, alumina is broken up into relatively large drops either during its travel towards the water surface or directly beneath this surface while the corium remains an essentially coherent jet even in the water. Consequently and due to its much lower density, the alumina is quickly decelerated and does not fragment further in the water. The corium jet, on the other hand, continues to travel at a high velocity so that fine fragments are formed. This might be the explanation of the observation that corium causes strong evaporation and thus voiding of the mixing zone while alumina mixes with the water with very low void fractions. This difference in void fraction within the mixing zone is sometimes already considered as a

possible explanation of the different behaviour of the two melts. However, there are indications as well from experiments (JAERI ALPHA test STX021 [4]) as analyses (with CHYMES [5]) that high void fractions may not prevent highly efficient steam explosions.

A second point is that the corium has a very small superheat (beyond the solidus temperature which is estimated as 2850 K) in these experiments (due to the usual experimental difficulties with materials with such a high melt temperature). In addition, the finely fragmented corium loses a lot of energy during the mixing process so that it may already be frozen sufficiently for not fragmenting further when a trigger is applied. Alumina with its low solidus point (2320 K), on the other side, remains much longer subject to fine scale fragmentation. However, if the corium that is formed during an accident should actually contain a sizeable amount of metallic zirconium, this corium might remain subject to fine scale fragmentation as long as the zirconium phase remains liquid, i.e. down to 2125 K which is even lower than the freezing point of alumina. In that case the alumina experiments might be more representative of an accident situation than the present corium experiments.

It might be noted that the material property differences that seem to cause the different behaviour of corium and alumina in the KROTOS experiments will in the end (so to say automatically) be accounted for in the steam explosion analysis intended with the multifid codes that are under development presently. This applies to the density difference with its implications for deceleration, break-up and heat transfer as well as the difference in solidification temperature (and the resulting superheat).

The evaluation of the mechanical consequences of a steam explosion is ideally done with a verified steam explosion model that is able to calculate reliably the pressure development and the production of mechanical energy. In the absence of such a model, another way to estimate the mechanical consequences of a steam explosion conservatively is to apply an energy conversion factor to the thermal energy content of the melt that is considered as participating in the steam explosion. In this way one gets a value for the mechanical energy release but not for the pressures involved. Also, this procedure requires to decide somehow arbitrarily which melt is considered as participating in the steam explosion and which not. Actually, the melt involved may vary during the explosion process and no verified (or at least generally accepted) criterion is available for defining the participating mass on the basis of premixing calculations. Still such procedure was adopted for the present study because no appropriate explosion model is available while on the other hand the BERDA experiments give a criterion for upper head failure that is based on the kinetic energy in an upward moving mass of core debris. The criterion used to define the potentially interacting corium mass is described in Chapter 5.

The interacting mass and its thermal energy, of course, vary during the mixing process. Typically high values are assumed during short periods. This raises the question of how probable it is that a steam explosion is triggered during such a short period. However, triggering is such an incompletely understood process – especially under the large scale reactor conditions – that we cannot rely on triggering to occur or not during certain periods. Therefore we have to use the maximum of the thermal energy in the premixed corium during the whole mixing process.

The energy conversion factor η is defined as the ratio of the released mechanical energy to the thermal energy available in the melt that participates in the steam explosion. For simplicity we consider the total heat available at the onset of the steam explosion.

137

On the basis of unrealistic models using thermodynamic equilibrium theory such as the famous Hicks-Menzies model, one obtains upper values of 40 % for the energy conversion factor [6]. For 'real' processes often a value of 15 % is quoted as conservative (in Ref. [7] an uncertainty band from 0.1 to 0. 2 is used). This value has no solid experimental or theoretical foundation. It is rather based on a number of quite uncertain observations made in some cases with quite differing initial and boundary conditions:

- For the accident in the SL-1 reactor (Idaho, 1961) in which this reactor was destroyed by a supercritical excursion followed by a steam explosion, $\eta = 10...15$ % was estimated afterwards on basis of the few indications available [8].

- An assessment of the 'Quebec foundry incident' (Province of Quebec, early 60ies) in which about 45 kg of molten iron fell into a shallow water basin, an assessment based on the damage done to the building gave $\eta \approx 13$ % [8].

- In the experiment RC-2 (SNL, 1983/84) the EXO-FITS test stand was completely destroyed after a total of 18.5 kg of iron-aluminium thermite had been poured into water. An evaluation of the mechanical energy release gave values of 6…17 % for η. In spite of all uncertainties involved, it was stated explicitly that "a conversion ratio greater than 10% was certainly likely." [9]

In better instrumented experiments, mostly smaller values of η have been found:

- In the experiment SUW-9 (Winfrith, 1983 [2]) in which 24 kg of uranium-molybdenum thermite have been released under water in a closed pressure vessel, $\eta = 2.3$ % was measured. That result assumed that the mechanical energy could be determined from the compression of the gas in the gas space above the water. But in this experiment, the loads became so high that the lid of the vessel was lifted and some of the contents was released. Without this failure the pressure and thus the mechanical energy estimate would certainly have been higher. In addition, it is not clear that actually all mechanical energy has contributed to the gas compression. Some considerable fraction might have remained in the water as turbulent kinetic energy. So the 2.3 % are certainly a lower limit only.

- In 6 out of 7 experiments of the FITS-B series (SNL, ~1981[10]) the energy conversion factor was between 1.1 and 1.6 % if only the estimated kinetic energy of the materials that were blown apart was taken into account. To this value, about 0.5…1.0 % have to be added that went into the compression of the gas in the FITS vessel. The combination gives a maximum η of 2.5 % for FITS-8B [11]. (An erroneous evaluation of the original authors had resulted in values up to 10 %.)

- In the KROTOS tests (JRC Ispra, 1993/4) that have been performed with about 1.5 kg of alumina, the maximum η values again reached 2.5 % [12]. Also this is to be considered as a lower limit because there is practically no axial constraint in these experiments.

- In the ALPHA experiments (JAERI, 1992-4), in which typically 20 kg of iron-aluminium thermite were released into water, pressurisation of the test vessel atmosphere alone indicated energy conversion factors of 3…6 % in three experiments. In one case (STX019) the rise of one gas temperature indicated a gas compression that would have required 19.5 % of energy conversion [4].

In view of these widely scattered and mostly uncertain experimental data with doubtful relevance, i.e. transferability, and the additional difficulty to extrapolate from the medium-scale experiments to the much larger reactor scale and from simulating materials to corium, the only way to obtain reasonably reliable data for accident situations is the application of a fairly realistic steam explosion model that has been verified by comparison with the above listed evidence and further really reliable data. Such data are expected from the experimental programme ECO-1 that is to start at the Forschungsezentrum in 1999. Until now, such a model is not available. But already in 1987, Oh [13] from the University of Wisconsin has presented a partly parametric model which, when applied to the RC-2 experiment gave an energy conversion factor of 7...8 %. When applied to hypothetical accident situations in an (American sized) LWR, this model gave maximum energy conversion factors of 10...15 %.

From the theoretical side, the following considerations can contribute to our problem: as mentioned above, purely thermodynamic models of energy conversion give maximum values of about 40 %. This gives so to say the microscopic result for energy conversion within the corium-water mixture. Here we must recall that efficient energy conversion in a steam explosion requires intimate mixing of extremely fine fragmented corium with water (which in turn requires coarse premixing during a premixing phase). This means that the working fluid (water/steam) is interspersed with a large number of small particles having a density that is at least about an order of magnitude larger. Thus, when the working fluid starts to do work on the surroundings by expanding, it must at the same time accelerate these embedded particles. This increases the amount of kinetic energy that remains within the 'reaction products' but more importantly leads to an efficient dissipation of kinetic energy by turbulent dissipation. Krieg [14] has evaluated this effect and found that up to 60 % of the microscopically available work can be dissipated in that way so that only 40 % are available macroscopically to do work on the surroundings. Combining these two 'efficiencies' we find that up to 16 % of the available heat might become available as destructive work energy. Here, one might argue that the kinetic energy that is dissipated is added again to the working fluid as heat which is not taken into account in the thermodynamic model of energy conversion. Some of this heat might be converted into work again with some delay and less efficiency. So the combination of maximum theoretical conversion factors should possibly be taken as somewhat higher than 20 %.

From all this we must conclude that an energy conversion factor below 15 % cannot be defended as being conservative at the moment and that 15 % are not unrealistically high. So we will adopt this value as reference value. Besides that, we will also use a value of 30 % in order to be very conservative. However, when considering the results obtained with that choice, one should take into account that that value is with certainty very conservative, possibly too much so.

This leads to the question of how much of the total mechanical explosion energy may become instrumental to load the vessel head (energy partitioning). In the present study it is assumed that the steam explosion which occurs in the lower plenum accelerates the largely molten core material upwards so that they impinge on the upper internal structures (as far as they are still there) and on the vessel head, thus loading the vessel head mechanically. This is a conservative assumption because it includes the worst possibility for loading the vessel head with (part of) the mechanical energy of the steam explosion. At the same time this assumption gives a well defined interface between the thermo- and fluiddynamic studies of the steam explosion itself and the mechanical studies about the load carrying capability of the vessel head – allowing to perform these two studies in parallel instead of one after the other. On the other hand, any desired (and technically possible) degree of realism can be introduced into

139

this concept by using more realistic (less conservative) methods to determine that part of the explosion energy that goes into the kinetic energy of the slug. We are using here the latter term to shortly denote the materials (melt, crusts, pin debris) that are accelerated upwards without implying a certain shape or structure of this material.

This concept is not new, e.g. [7, 15], and from the very beginning it has been criticised on the grounds that (Rayleigh-Taylor) instabilities would destroy (break up) the slug in such a way that an effective acceleration was prevented. Therefore Amarasooriya and Theofanous [15, p. 300] give three reasons for still considering such a slug:

a) A major portion of the slug acceleration occurs during the initial stages of slug displacement.

b) Below-core structures would be expected to fail at the core joints stabilizing upward slug displacement against bubble-breakthrough phenomena.

c) In a realistic geometry the slug would travel by somewhat less than one vessel diameter before impacting upper internal structures.

The third point above is no longer true when considering the upper core plate and the control rod guide tubes as molten away. But the other two arguments, which are independent of each other, are quite valid.

The role that can be played by below-core structures is difficult to judge. One well defined possibility is to consider the lower core support plate (LCSP) as being accelerated together with the melt pool, neglecting its porosity. In this way the LCSP would prevent any breakup of the slug by instabilities. On the other hand, the LCSP would have to be accelerated together with the heavy reflector without their kinetic energy contributing effectively to the loading of the upper vessel head because these structures would be decelerated before the core masses impinge on the vessel head and would not cause permanent damage (plastic deformations). In addition, the core barrel would absorb explosion energy while being compressed. This possibility is further assessed in Chapter 10. It is concluded that for a mechanical energy of about 1 GJ or more fuel into the upward acceleration of the LCSP not more than 40% will be transferred into corium impact energy. Failure of the joints as suggested in point b) above [15] seems not to be likely under the geometrical conditions of the EPR.

If one now considers the acceleration of the core debris alone as a possibility to load the vessel head, the question has to be answered how much of the explosion energy can be absorbed by these masses (the 'slug'). The study performed by Theophanous et al. [7,15] results in values below 40 % without taking into account the effect of the lower core support plate. So, with the LCSP actually being present, 40 % certainly is a very conservative value and, as it agrees with the value found in Chapter 10 for the other possibility of accelerating the core debris, this is the value we'll adopt here.

If the core materials are accelerated largely independent of the lower core support plate, one has to consider the lower crust keeping the melt pool together and all still intact parts of the core below that crust including fuel pins and the lower end plates of the fuel assemblies. The crust may not remain intact during the acceleration but its pieces together with the solid structures of the lower part of the core would tend to reduce the rate of instability growth – with stronger effects on shorter wavelengths.

Still we may assess the role that Rayleigh-Taylor (RT) instabilities might potentially play by considering the purely hydrodynamic processes during the ideal acceleration of a liquid cylinder within a tube (neglecting friction). This is the situation in which RT instabilities are most effective. The pertinent facts about nonlinear growth of RT instabilities which are relevant here only, have been compiled in the Appendix A on the basis of a review paper by Jacobs [16]. It follows that such a cylinder would be penetrated fastest by an RT bubble with a wavelength (diameter) equal to the tube diameter. It is further derived in the Appendix A that a cylinder of height h is penetrated by this bubble while the liquid is travelling a distance $s_p = h^2 / (0.24\ D)$, independent of the acceleration (assuming constant acceleration). If we assume a diameter of D = 3.8 m, a liquid mass of 80 t and a density of ρ = 8000 kg/m^3, we have a cylinder height of about h = 0.9 m. This gives a distance traveled by the cylinder before it is penetrated of about 0.9 m. The question then is whether it is possible to accelerate the cylinder to a dangerous level of kinetic energy on this short distance. If we take kinetic energies beyond 0.4 GJ as potentially dangerous for the vessel head, the velocity must be at least v = 100 m/sec. Thus the required acceleration [$b = v^2 / (2s)$] is about 5000 m/sec^2 and the required pressure is 400 bar. This is well within the range of steam explosion pressures that have been observed. Even requiring a factor 2 for compensating the effect of the lower core support plate with its 33 % porosity would lead to 800 bar which are still not in a physically unreasonable range. Only the fact that such a pressure would have to act during almost 20 msec means that really strong explosions would be required and that lower head integrity were no longer assured. These questions will have to be studied further when both, premixing and steam explosions, can be modelled reliably.

In addition, the above estimates are unrealistically optimistic (they predict breakup of the liquid too early) as they disregard the fact that initially there is an induction period during which the RT bubble forms while penetrating much more slowly. Figure 8 in Ref. 16 illustrates this effect and how it can be described in an approximate but very reliable way that was first proposed by Fermi. The Figure shows this for a 2-D bubble (because only there a fully analytical solution is available), but for our purposes here it is sufficient to observe that for a dimensionless bubble amplitude (penetration depth) of α = 1.53 ($\alpha = 2\ \pi\ h\ /\ D$), the approximate solution gives about twice the (dimensionless) penetration time as application of the terminal bubble velocity throughout. This gives a factor 4 in the required travel distance. Thus s_p = 3.6 m. This is already more than half the acceleration distance available (6.35 m) and the pressures required at minimum reduce equally by a factor 4 to 100 bar and 200 bar, respectively. These pressures would have to act during about 70 msec which is not a priori implausible for subcritical pressures.

Furthermore, it has been assumed until now that the liquid initially forms a flat cylinder. Actually one has to expect in the accident case that the lower crust carrying the melt pool is somewhat convex in downward direction. Thus the height to be penetrated would be larger at the centre and the local acceleration would be lower there (same pressure – more mass). Both facts would tend to stabilise the slug.

It has been mentioned above that the distance travelled by the liquid slug before it is broken up by RT instability is independent of the acceleration (or the driving pressure) in the approximation used here. So it is very well possible to slowly accelerate a slug and to break it up prior to collecting potentially dangerous kinetic energies in it, if only the driving pressure is low enough. This can occur e.g. in numerical simulations in which only the pressures developed during premixing are considered without triggering (and modelling correctly) a steam explosion, see e.g. [17]. However, when considering such simulations, one also has to keep in mind that any mass moving large distances through a coarse calculational mesh will

be dispersed strongly by numerical diffusion as long as simple first-order difference schemes are used. An example of this is given in [18] and further discussed in Chapter 3.2 of this report.

The above discussions suggest that it is not reasonable to argue in a very general way that the formation and acceleration of a potentially dangerous slug are not possible. The outcome will very much depend on the circumstances of the case considered. But, of course, there always remains the possibility to introduce realistic considerations into the assessment of the possible kinetic energy of that slug

In experiments in which liquid was accelerated upwards in a tube, often quite early penetration of a cylinder by a large RT bubble has been observed – typically when the cylinder had travelled one height. But Seo and Bankoff [19] stress that this is due to the way in which the experiments have been conducted: Normally the liquid initially rests on a membrane that bursts when a high pressure is applied below it. But prior to breaking, this membrane tends to curve upwards thus impressing already an RT bubble with a large amplitude on the liquid before the acceleration starts. In the experiments reported in Ref. 19 this curvature was prevented by perforated plates and in one case that is reported in some more detail it was observed that a liquid cylinder initially 6.5 cm high was penetrated (or rather eroded from behind) by about 2/3 while the liquid was travelling 19 cm – almost three times its initial height.

For completeness we refer here again to a possibility that was discussed in section 6.2.2, i.e. loss of integrity of the slug before an explosion is triggered. This quite favorable process might take place above all when premixing follows the downward outflow of the core melt through the lower core support plate. Then, the pressure that develops in the lower plenum will tend to reduce the melt flow and, after eventually having become large enough, it will accelerate some of the melt upwards, possibly with steam flowing in counterflow to some melt masses still moving downwards into the lower plenum. Here the pressures are low (much lower than in an explosion) and consequently the crust that holds the pool may withstand the pressure from below so that only the melt above the initially failed cross section is accelerated and blown upwards. Once this has developed to a sufficient extent, there is no longer the danger of accelerating a slug that could jeopardize vessel head integrity because any explosion pressure developed in the lower plenum would propagate (be released) through the opening in the molten pool so that there would remain only a small pressure difference to accelerate the pool. Fortunately this occurs the earlier, the larger the melt relocation rate is because of the stronger pressure build-up. So there is a mechanism limiting the time span during which a potentially dangerous premixture can grow. This limits the thermal energy available for a possible steam explosion. The mechanism is especially effective in cases with large failure cross sections and thus melt flow rates – an additional self-limitation of premixing. We must, however, mention that we have actually observed this effect in our present simulations only when applying the code MATTINA (which tends to predict higher pressures during premixing) and when using assumptions for the melt relocation rate that we consider to be more conservative than necessary.

In summary we conclude the following:

Judging on basis of the available theoretical and experimental information, we concluded that a conservative energy conversion factor amounts to a value of 15%. But in view of the uncertainties involved, we also considered a value of 30%. As triggering of steam explosions is so little understood we could neither rely on a trigger to occur in a certain situation nor exclude it to happen in other situations. Therefore we looked for the maximum of the

premixed thermal energy during the whole mixing process and applied the conservatively estimated conversion factors to that thermal energy to get an estimate on the related mechanical explosion energies if a steam explosion might occur. This gives maximum values of the mechanical explosion energies which amount to 0.45 and 0.9 GJ, respectively. In our opinion the higher values are extremely pessimistic. In the majority of the analysed cases the respective maximum values amount to 0.075 GJ up to 0.6 GJ.

However, mechanical explosion energies do not convert directly to the kinetic energy of the core melt which is accelerated upward as consequence of the explosion energy that is transferred to the core material on top of the core support plate as a reasonable estimate. On this basis a loading energy to the upper vessel head is estimated to amount to maximum values of 0.18 GJ and 0.36 GJ, respectively. In the majority of the analysed cases these maximum values amount to 0.03 GJ up to 0.24 GJ, respectively.

10 Determination of admissible energies which the reactor pressure vessel head can withstand

To avoid conditions which may question the integrity of the reactor containment, it is required that the reactor pressure vessel head and the head bolts must not fail [1]. The BERDA program is aimed at determining the admissible energies E_{slug}, E_{plate} and E_a, Fig.10.1. By comparing these values with the maximum mechanical energy released during a steam explosion E_{expl}, it is found out whether steam explosions not lead to a failure of the reactor pressure vessel head.

The BERDA I partial program for the determination of the admissible kinetic energy E_{slug} of the core melt being hurled against the reactor pressure head has already advanced to a considerable extent. It focuses on model experiments, while numerical calculations are of supportive character only. The results determined for E_{slug} have meanwhile reached a high degree of reliability.

The BERDA II partial program for the determination of the admissible energy input E_{plate} at the core support plate is still at its beginning. Here, computation models play an important role. The results obtained up to now rather have the character of estimates. For more reliable statements to be made, further analyses and experiments are needed.

As far as the BERDA III partial program is concerned, only first ideas have been developed so far. The necessity and the detailed contents of this work still remain to be discussed.

10.1 Determination of the admissible kinetic energy Eslug of the core melt being hurled against the reactor pressure vessel head; BERDA I partial program

10.1.1 Experimental setup

In the model experiments BERDA I, the upper part of the reactor pressure vessel is simulated by models scaled down 1:10, i.e. length scale λ = 10; setup see Fig. 10.2, [2].

Due to the different temperatures of the model head (room temperature) and the reactor pressure vessel head (300 – 400 °C), slightly different stress-strain diagrams must be considered. The stresses in the diagram for the pressure vessel head are about λ_σ times the stresses in the diagram for the model head, where the stress scale $\lambda_\sigma < 1$. The influence of the strain rate mentioned below leads to an additional slight reduction of the stress scale. Based on available data a value of $\lambda_\sigma = 0.87$ is chosen. After the results of respective material studies will have been obtained, this scale may be modified slightly.

The different temperatures of the internal structures of the model (room temperature) and the internal structures of the reactor pressure vessel (600 °C and more) have a stronger impact on the stress-strain diagrams. However, this is not reflected by the chosen stress scale. Rather internal structures made of softer brass were employed in some tests. In test 16, the guide tubes of the control rods even consisted of much softer lead material.

10.1.2 Test results

Up to now, the BERDA I tests 01 through 17 have been performed. A survey of the results is given in Figs. 10.3 to 10.5. More detailed information may be found in [2 – 6], as well as in the special test reports.

As expected, the impact force of a liquid is much smaller than that of a respective solid (compare test 03 in Fig.10.3 and tests 05 and 06 in Fig. 4). The reduction factor amounts to 3–4.

As also expected, the internal structures cause a further considerable reduction of the impact force (compare tests in Figs. 10.4 and 10.5). For moderate velocities that do not cause plastic head deformations the reduction factor amounts to about 7, if the complete upper internal structures are considered. The reduction factor is assessed to be between 3 and 4, if only the upper grid is available.

During the slug impact the upper internal structures were heavily deformed and damaged, Fig.10.6. However, a careful examination of the resulting wreckage revealed that only a mechanical energy of about 0.05 MJ had been dissipated in these structures. The mechanical energy dissipated in other components can be assumed to be even smaller (since there was no permanent head deformation). However, the kinetic slug energy was between 0.5 and 0.7 MJ before the impact. Thus it can be concluded that the major part of this energy had been dissipated by the irregular flow of the liquid after the impact.

The material properties of the internal structures do not have any significant influence on the head load (in Fig.10.5 the results obtained for steel and brass structures nearly correspond to each other). Nor does the number of fractures have any strong influence (according to Fig.10.6, only a few fractures occurred in the steel structures, while a large number of fractures could be observed in the brass structures). This behavior can be understood, since the major part of the kinetic slug energy is dissipated in the liquid. This result is of big advantage for the application to the reactor. Detailed knowledge on the temperature of the internal structures during the steam explosion and the resulting material properties as well as on the extent of radiation-induced embrittlement is not required.

As evident from test 17, the previous assumption of the reactor pressure vessel head always failing earlier than the head bolts under overload conditions could not be confirmed.

For the verification of the results, the major characteristics were determined in a redundant manner. The momentum obtained from the force measured as a function of time was compared with the momentum of the liquid slug prior to the impact. It was concluded that major measurement errors do hardly exceed an order of 10 %. Visual control of the contour of the incident liquid slug turned out to be impossible. However, calculations with the finite element program ABAQUS suggest that e.g. in test 07 the slug had a rather compact form, while in test 09 the form was less compact [7]. For a better understanding of the various phenomena, the impact processes were simulated using the SimSIC computer program [8]. It must be mentioned, however, that some of the variables measured in the model experiments are applied as input data for the above computer program.

10.1.3 Transfer of the results to the reactor scale

Conversion of the test results to the reactor scale was accomplished using similarity theory. By means of the conventional basic equations (equilibrium conditions, time-independent elastic-plastic material behavior, etc.), the scales below were derived from the length scale $\lambda = 10$ and the stress scale $\lambda_\sigma = 0.87$:

displacement scale   = λ =   10

strain scale		=	1		
time scale		=	$\lambda / \sqrt{\lambda_\sigma}$	=	10.7
velocity scale		=	$\sqrt{\lambda_\sigma}$	=	0.93
force scale		=	$\lambda^2 \lambda_\sigma$	=	87
energy scale		=	$\lambda^3 \lambda_\sigma$	=	870

Of course, the basic equations and neglections assumed only allow an approximative description of the processes. Consequently, the above scales are also of approximative character. To determine the resulting deviations by way of example, the similarity experiments FLIPPER were performed; Fig.10.7, [9 – 11].

For ferritic steel, indications regarding a slight size effect were found. It may be explained by the known strain rate effect on the stress-strain diagram and can be taken into account by the respective reduction of the stress scale λ_σ. This is already taken into consideration by the given value of $\lambda_\sigma = 0.87$.

For austenitic steel a strong size effect was observed. As suggested by further indications, this is to be attributed to a size effect on the material behavior. In structural mechanics analyses, such an influence is usually not considered. When deriving the scales this effect was also not taken into account. For the given reactor problem, this neglection can be accepted, as austenitic steel is only used extensively for the internal structures. However, according to the results discussed before, the influence of the material properties of the internal structures on the head load is rather small, Fig. 5. Therefore, also the influence of the size effect of the austenitic steel on the head load is very small.

A further check of the scales could be provided by so-called SMALL BERDA tests, where the length scale with respect to the BERDA tests was 5. Consequently, with respect to the reactor the length scale was 50 [12]. However, in the SMALL BERDA tests only slugs consisting of lead spheres could be realized. Therefore, only a comparison with the BERDA I tests 01 and 02 is possible, where similar slugs had been used. Applying the scales previously derived to the results of the SMALL BERDA tests, a satisfactory agreement is obtained with the results of the BERDA I test 02.

The scales for the conversion of the test results to reactor conditions also apply to non-linear processes. However, material damage and fracture processes could not be taken into account, as adequate theoretical models do not exist. Therefore, the conversions are only performed for those model experiments BERDA I, where it is quite certain that the plastic head deformations (strains) do not cause any fracture even for reactor dimensions.

As findings regarding component fracture as a function of the component size are hardly available, only small plastic deformations are admitted at the moment. However, as soon as higher ductility will be detected in larger components, accordingly higher plastic head deformations will be accepted.

As far as the internal structures are concerned, large plastic deformations and fractures do not cause any problems. As mentioned above, these processes do not have significant influence on the head load.

10.1.4 Determination of the admissible slug energy Eslug

With only small plastic head deformations being admitted, the results of the model experiments (Figs. 10.3 to 10.5) allow the following conclusion to be drawn.

Case A: All upper internal structures are molten. According to Fig.10.4, an admissible kinetic slug energy of about 0.12 MJ can be assessed. Taking into account the energy scale, a value of about

$$E_{slug} = 0.1 \text{ GJ}$$

is obtained for reactor dimensions. If this case would be of relevance, additional tests with velocities of about 55 m/s would be recommendable. This would also help to explain in further detail the considerable scattering of the results observed under these conditions.

Case B: Only the upper support grid is available. The temperature does not exceed 600 °C by far. According to Fig.10.5, test 14, an admissible kinetic energy of 0.46 MJ is obtained. In view of the energy scale,

$$E_{slug} = 0.4 \text{ GJ}$$

is obtained for reactor dimensions. For this result to be confirmed, at least another test under conditions similar to those of test 14 is required.

Case C: All upper internal structures are available. According to Fig.10.5, an admissible kinetic energy of 0.90 MJ is obtained. The energy scale yields about

$$E_{slug} = 0.8 \text{ GJ}$$

for reactor dimensions. To confirm this result, at least another test should be performed at an increased velocity of 150 m/s. The results of test 16 suggest that the control rod guide tubes may be allowed to have very high temperatures with the material strength decreasing to a fraction of the initial values. However, this needs to be verified by means of another test with lead tubes at a velocity of 130 m/s and possibly even 150 m/s.

It should be pointed out that these results are rather conservative. When simulating the core melt impact at the head, care was taken that the liquid slug was very compact.

In case of more irregular liquid surfaces and considering dispersion effects, a considerable reduction of the impact forces and consequently increased admissible kinetic slug energies E_{slug} are expected. This is supported by test 04 where the crucible failed and the resulting liquid dispersion caused a reduction of the impact force at least by a factor of two. However, for test 16 where the crucible failed, too, a considerable reduction of the impact force could not be observed.

Furthermore, as mentioned above, only small plastic head deformations are admitted. However there are some indications that higher plastic deformations would occur before fracture not only for the BERDA head, but for the full size head. This would again increase

the admissible kinetic slug energies. E_{slug}. In addition, it should be mentioned that also minor head fractures would be tolerable.

10.2   Determination of the admissible energy input Eplate at the core support plate; BERDA II partial program

10.2.1   Computation model for rough assessment

Here, the computation model represented in Fig.10.8 is used. It is assumed that the bores in the core support plate cannot essentially reduce its loading. Thus, for this rough assessment they are neglected.

The kinetic energy E_{slug} of the core melt which is hurled upwards is (Fig.10.8a)

$$E_{slug} = \int F_0 \ ds_0 = m_0 \int a_0 ds_0$$

with the acceleration force F_0, the mean acceleration path s_0, the core melt mass m_0 and the mean acceleration a_0.

During acceleration, the geometrical form of the core melt may change. In particular, radial acceleration components may occur. They lead to a radial liquid dispersion. Thus the energy E_0 input into the core melt is higher than E_{slug} (Fig. 8a)

$$E_0 = \int F_0 \ ds_1 = m_0 \int a_0 ds_1 .$$

Due to equilibrium reasons, the applied force must be equal to the acceleration force F_0. During radial liquid dispersion, however, the acceleration path s_1 and the acceleration a_1 on the support surface of the core melt will be larger than the mean acceleration path s_0 and the mean acceleration a_0 in the core melt.

The kinetic energy of the core support plate is (Fig. 10.8b)

$$E_1 = \int F_1 \ ds_1 = m_1 \int a_1 ds_1$$

with the acceleration force F_1 required for the plate and the plate mass m_1.

During acceleration, the core barrel is compressed. The dissipated energy E_2 amounts to (Fig.10.8c)

$$E_2 = \int F_2 \ ds_1 .$$

For the transformation of this expression, the resistance force F_2 of the core barrel is assumed to be constant. Furthermore, also the pressure p_1 resulting from the steam explosion and acting on the core support plate having the surface area A_1 is assumed to be constant. Hence,

the energy fed into the plate is $E_{plate} = p_1 A_1 s_1$. When calculating E_2, the acceleration path s_1 may be substituted. This yields

$$E_2 = E_{plate} \cdot F_2 / p_1 A_1.$$

It must be noted that due to the above assumption and the resistance force F_2, which depends on the hardly known core barrel temperature, the energy E_2 can only be determined rather roughly. However, E_2 turns out to have a moderate influence only. To obtain conservative statements, either a lower estimate is applied in the further calculations or the force F_2 is neglected completely.

The admissible energy input E_{plate} at the core support plate is obtained as follows:

$$E_{plate} = E_0 + E_1 + E_2$$

The terms of E_0, E_1 and E_2 have to determined such that after the acceleration phase the core melt is moved upwards with the admissible kinetic energy of E_{slug}.

In case of an unrestricted radial core melt dispersion, the acceleration ratio χ

$$\chi = a_0 / a_1$$

above all depends on the core melt geometry. If the geometry change during the acceleration is assumed to be small, χ also describes the path ratio

$$\chi = s_0 / s_1.$$

Hence, the energies E_0 and E_1 can be expressed as multiples of E_{slug} and

$$E_{plate} = E_{slug} \frac{1}{\chi} + E_{slug} \frac{1}{\chi^2} \frac{m_1}{m_0} + E_{plate} \cdot F_2 / p_1 A_1$$

is obtained. Decomposition to E_{plate} yields:

$$E_{plate} = E_{slug} \left(\frac{1}{\chi} + \frac{1}{\chi^2} \frac{m_1}{m_0} \right) \Big/ \left(1 - \frac{F_2}{p_1 A_1} \right)$$

It should be mentioned that the deceleration of the core support plate by compression of the core barrel does not contribute to the maximum impact of the vessel head and its bolts. The cross section of the core barrel limits the force transferred to the bolts. Furthermore, this force occurs prior to the core melt slug impact against the vessel head.

10.2.2   Calculation of the acceleration ratio χ

The acceleration ratio χ resulting from radial dispersion can be calculated in good approximation using the program SING [13].

Four cases were studied. The core melt located on the core support plate had a mass of 80,000 kg in each case.

Case a: The core melt has a cylindrical form. The diameter of 3.9 m is given by the heavy reflector, the height amounts to 0.715 m. The core barrel withstands the pressure in the core melt, which results from acceleration. Then radial dispersion does not take place, i.e. $\chi = 1.0$.

Case b: Geometry as above. However, the core barrel is expanded radially and may contact the reactor pressure vessel in the lower part, i.e. radial dispersion takes place. Taking into account that also the heavy reflector will be removed radially, the program SING yields $\chi = 0.7$.

Case c: The core melt has a cylindrical form. The diameter of 3.3 m and the height of 1.0 m more or less correspond to the form of the crucible used in the BERDA I experiments, enlarged by the length scale of $\lambda = 10$. The crust enclosing the core melt does not withstand the pressure occurring during acceleration and radial dispersion takes place. The program SING yields $\chi = 0.5$.

Case d: The core melt has the form of a truncated cone. The smaller circular area of the truncated cone with a diameter of 3.0 m is located on the core support plate. The larger circular area with a diameter of 3.6 m is located 1.0 m above the core support plate. Also here, the crust on the core melt is not supposed to prevent radial dispersion. The program SING yields $\chi = 0.4$.

Changes of the geometrical conditions during dispersion (radial expansion of the core melt near the core support plate is larger than near the upper head surface) are assumed to be small and the resulting increase in χ was not taken into consideration in these analyses. Nor was the limitation of radial dispersion by the wall of the reactor pressure vessel at the latest taken into account. It is assumed furthermore, that the core melt which is hurled back in radial direction from this limitation does not contribute to the formation of a compact slug again.

It remains to be verified by detailed analyses and in particular by the model experiments BERDA II, whether or not these and other assumptions made above comply with the processes occurring. Planning of these experiments has been completed. The constructional modifications of the BERDA facility required have already been specified and the respective orders are being placed at the last quarter of 1998. First results are expected for 1999.

10.2.3 Rough determination of the admissible energy input Eplate

By means of the formula derived in Sec. 10.2.1, the admissible energy input E_{plate} at the core support plate can be determined. The admissible kinetic energy E_{slug} depends on the state of the upper internal structures according to Sec. 10.1.4, cases A through C. The acceleration ratio χ depends on the core melt configuration encountered on the core support plate and partially on the behavior of the core barrel according to Sec. 10.2.2, cases a through d.

In a first computation series, the mass of the core support plate is assumed to be half of the core melt mass, $m_1 = 0.5\ m_0$, which more or less corresponds to the actual situation.

In a second computation series, about half the mass of the heavy reflector is added to the mass of the core support plate, $m_1 = m_0$. Hence, it is assumed that about half of the heavy reflector

and the core support plate are accelerated in upward direction, while the other half is able to back out due to the high temperatures and the resulting low strength.

For simplicity, the axial resistance force F_2 is neglected. As a result, E_{plate} is slightly underestimated.

The results are listed in Table 10.1. It was postulated that in case A the moderate, admissible kinetic energy of the upwards hurled core melt causes a moderate pressure during acceleration only, which is not sufficient for a radial expansion of the core barrel. This means that the combination A/a is relevant, while A/b is irrelevant. In case B the higher admissible kinetic energy of the upward hurled core melt is probably sufficient, in case C it is certainly for radial expansion of the core barrel. Consequently, the combination B/a is probably irrelevant and the combination C/a is certainly irrelevant.

It should be stressed again that these assessments need to be confirmed by the model experiments BERDA II.

If one assumes that at least the upper grid is available, the most conservative result is

$$E_{plate} = 1.0 \text{ GJ}.$$

It applies for the unlikely case wehre the core melt covers the whole upper surface of the core support plate. In addition it is based on the conservative result for E_{slug}.

On the other hand, however, it must be pointed out, that the given values for E_{plate} are rough estimates only. As already mentioned, detailed analyses and in particular the BERDA II model experiments are required for more reliable statements to be made.

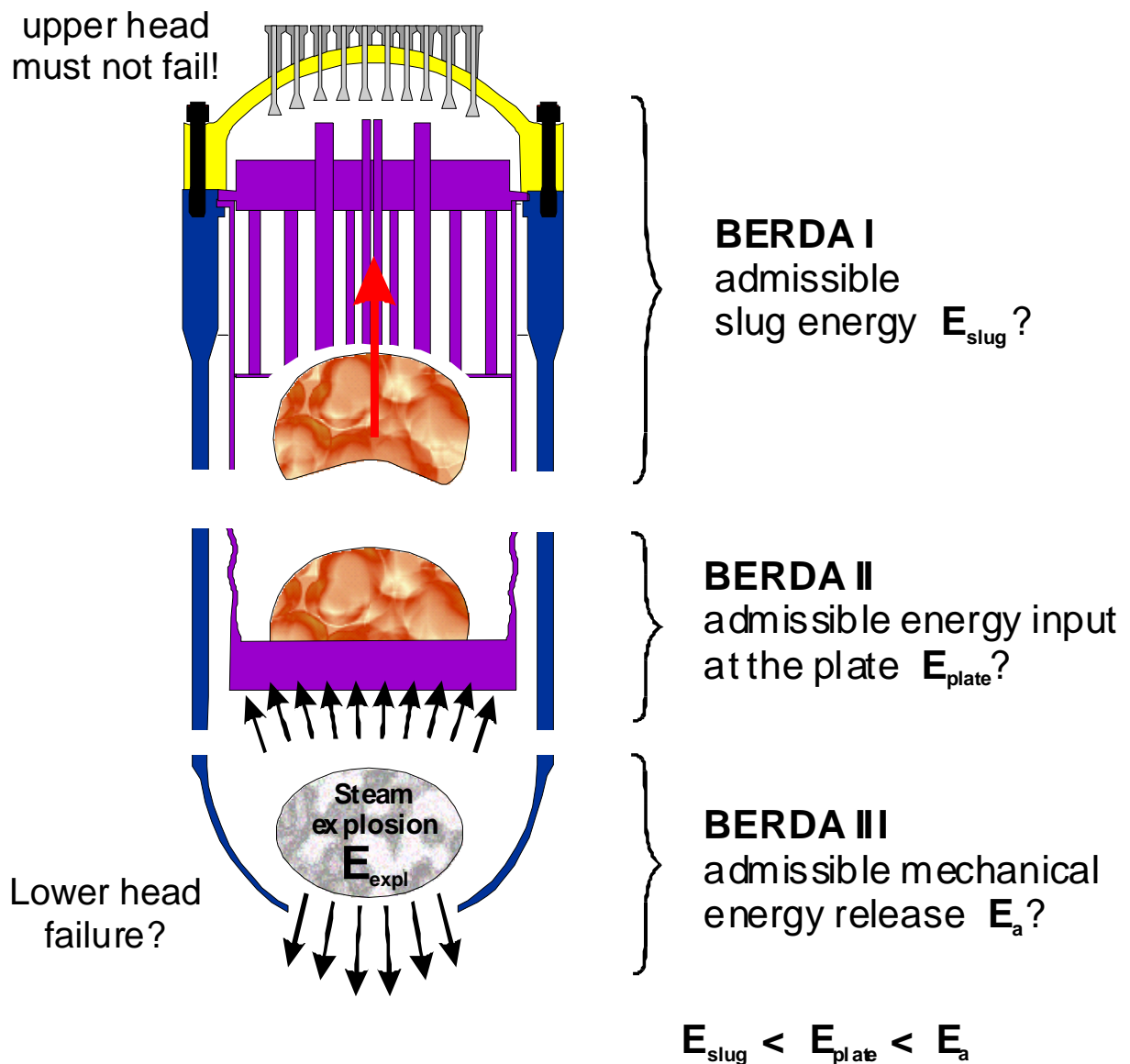### 10.3 Determination of the admissible mechanical energy release Ea; BERDA III partial program

The admissible mechanical energy release E_a is larger than E_{plate}, as energy sinks other than the vertical acceleration of the core support plate exist. For simplicity, two possible sinks shall be considered only:

The ejection of water and core melt into the downcomer. It is assumed that the ratio between this energy and the energy input into the core support plate corresponds to the ratio of the downcomer cross-section to the surface area of the core support plate. In case a, this yields $E_a = 1.3 \cdot E_{plate}$. In the cases b, c and d, this energy sink may not exist, as the downcomer may be closed by the expanded core barrel.

Large deformations or failure of the lower reactor pressure vessel calotte. Computations and previous experiments indicate that failure occurs at a pressure ranging from 600 to 900 bar [14]. With a degree of certainty, this value is reached at an energy of $E_{plate} > 2 - 3$ GJ, and possibly even at a smaller energy. In this case, E_a would roughly correspond to $2 \cdot E_{plate}$.

These effects are considered in Table 10.2.

Of course, also the values for E_a represent rough estimates only. Detailed analysis and experiments would be required for more reliable statements.

upper head
must not fail!

BERDA I
admissible
slug energy E_{slug} ?

BERDA II
admissible energy input
at the plate E_{plate} ?

Lower head
failure?

Steam
explosion
E_{expl}

BERDA III
admissible mechanical
energy release E_a ?

$$E_{slug} < E_{plate} < E_a$$

If $E_{expl} \lessgtr E_a$, then upper head integrity is confirmed

Figure 10.1   Investigation program BERDA on the behaviour of the reactor pressure
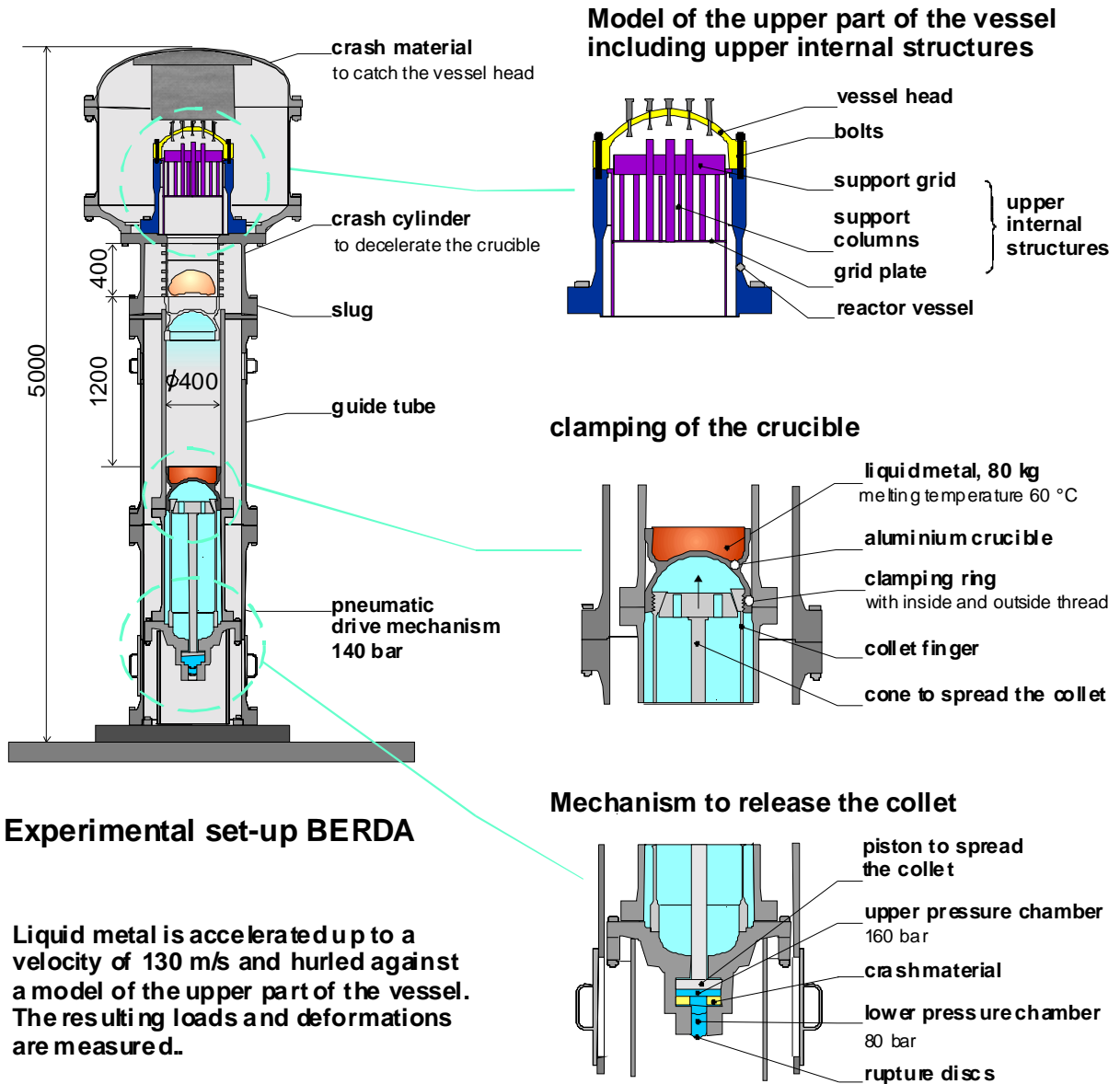vessel head during a postulated steam explosion

Model of the upper part of the vessel including upper internal structures

crash material
to catch the vessel head

crash cylinder
to decelerate the crucible

slug

guide tube

pneumatic
drive mechanism
140 bar

5000

400

1200

φ400

vessel head

bolts

support grid

support
columns

grid plate

reactor vessel

upper
internal
structures

clamping of the crucible

liquid metal, 80 kg
melting temperature 60 °C

aluminium crucible

clamping ring
with inside and outside thread

collet finger

cone to spread the collet

Experimental set-up BERDA

Liquid metal is accelerated up to a velocity of 130 m/s and hurled against a model of the upper part of the vessel. The resulting loads and deformations are measured..

Mechanism to release the collet

piston to spread
the collet

upper pressure chamber
160 bar

crash material

lower pressure chamber
80 bar

rupture discs

Figure 10.2   Model experiments BERDA I on the slug impact against the reactor pressure vessel head
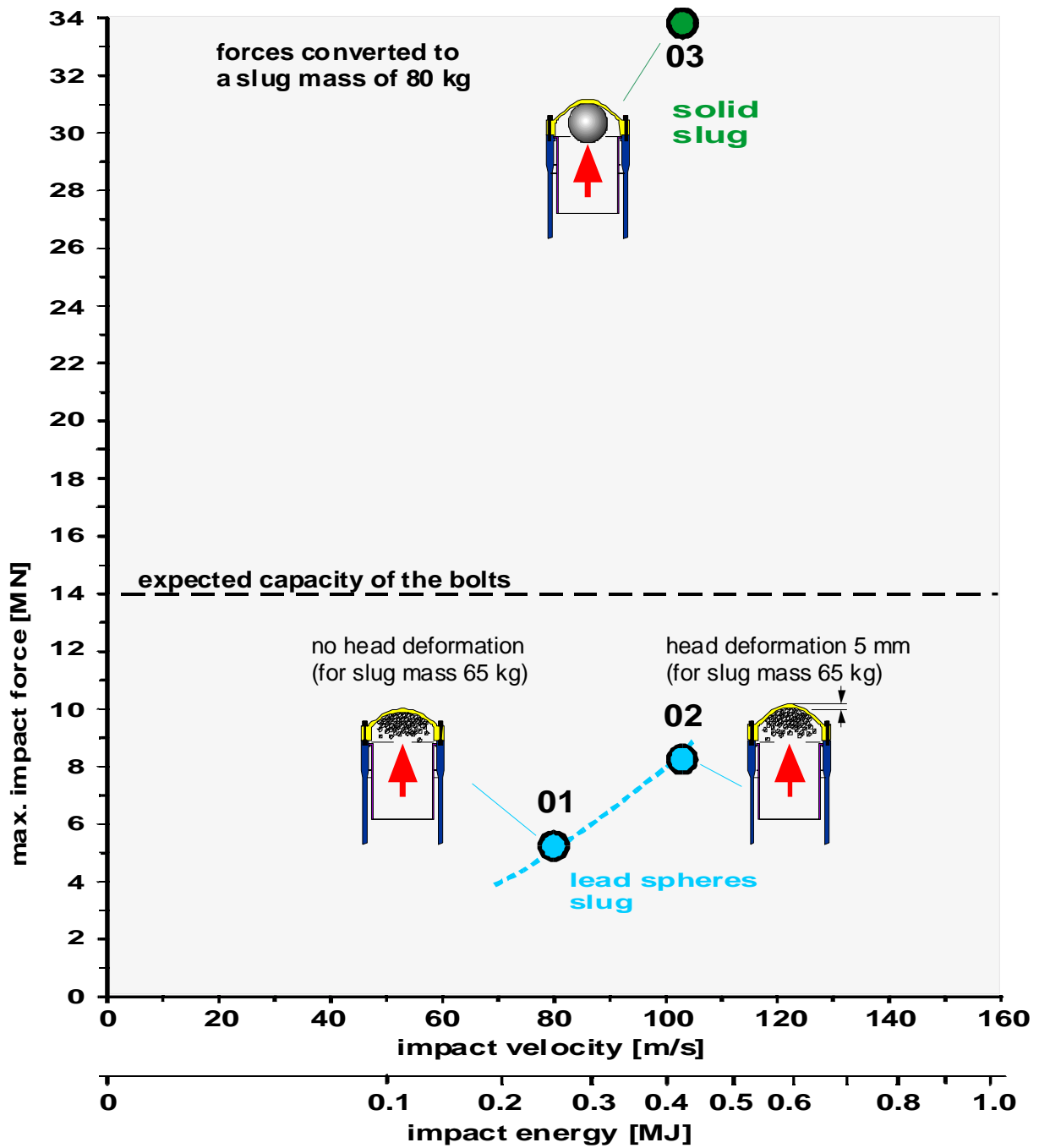
Figure 10.3 Results of model experiments BERDA I, solid body and lead spheres slug impact
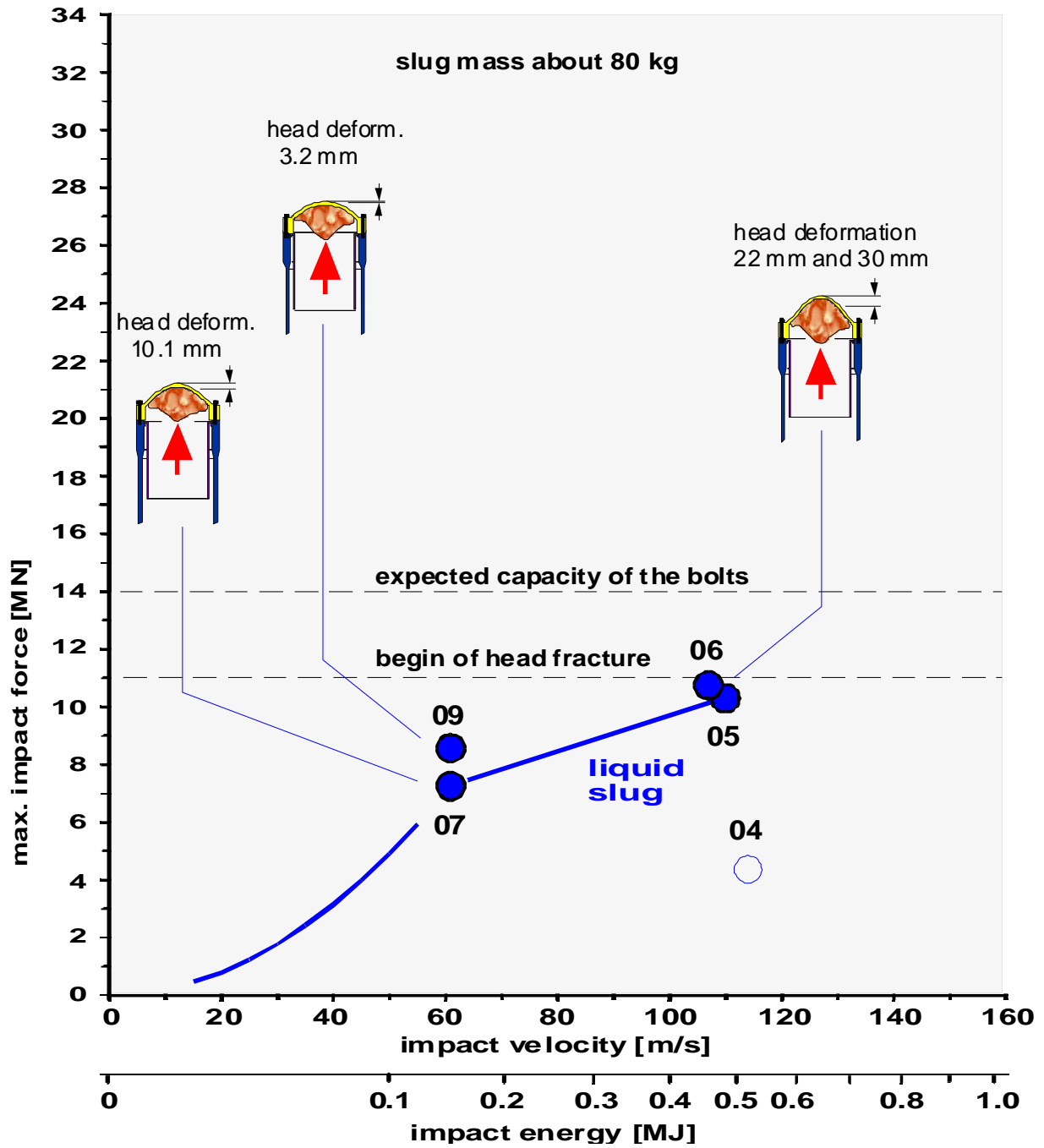
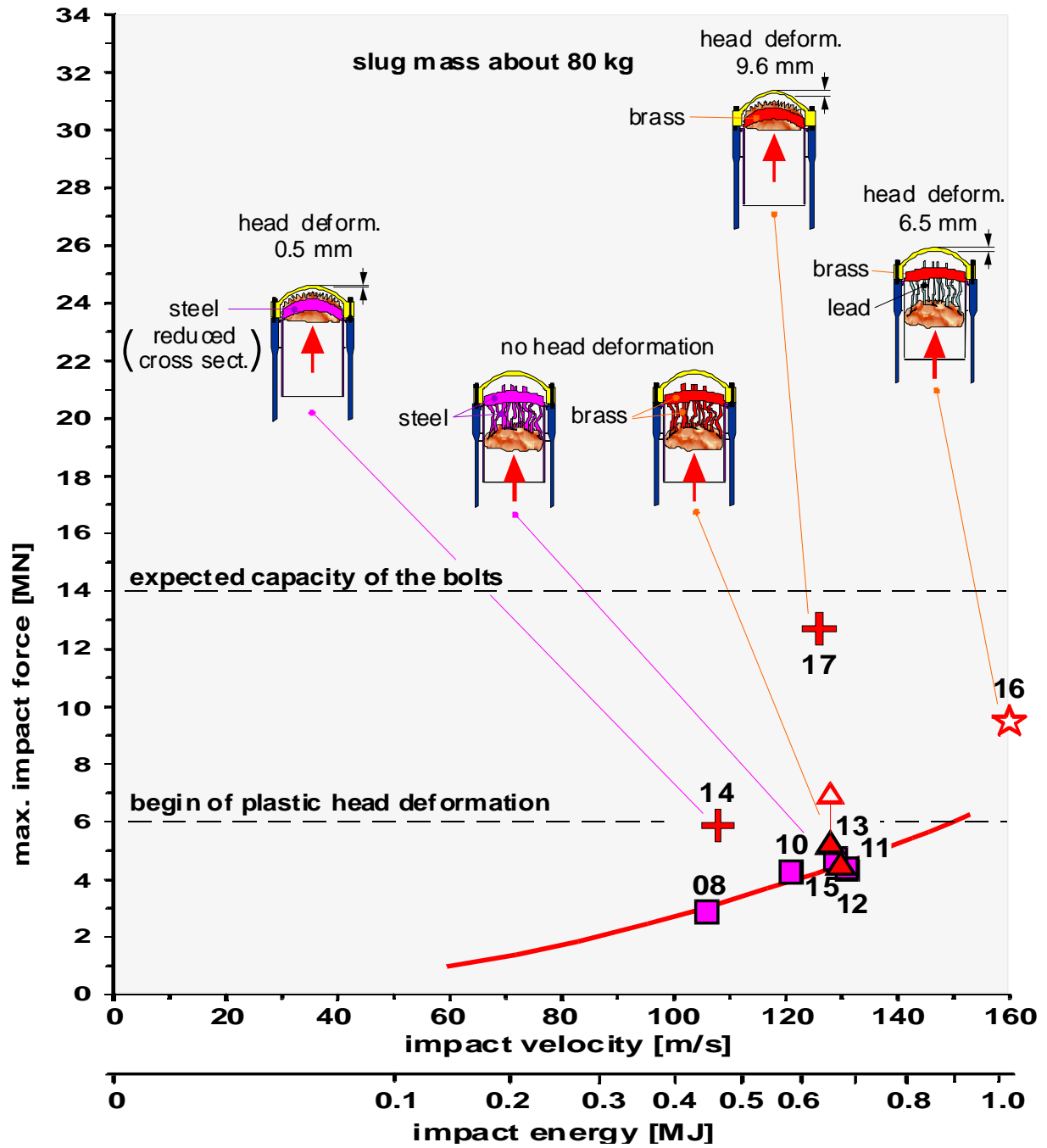Figure 10.4   Results of model experiments BERDA I, liquid slug impact without upper internal structures
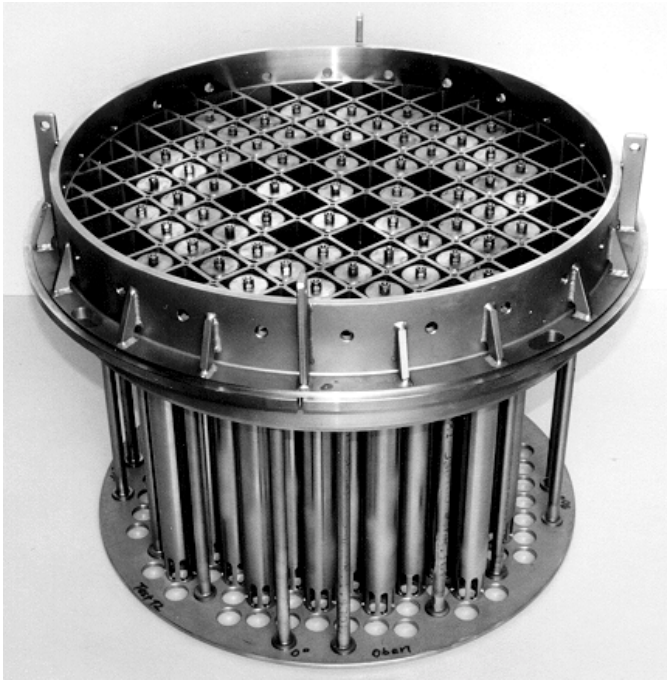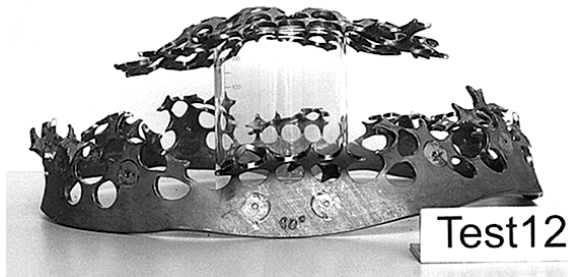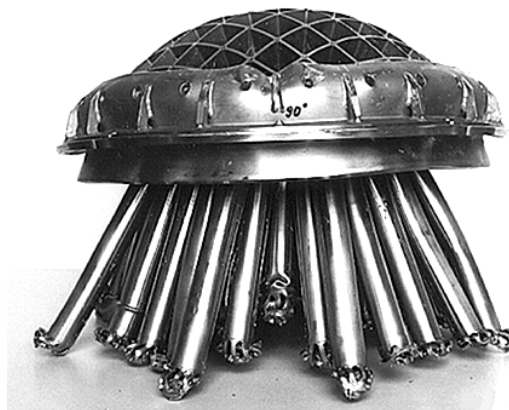
Figure 10.5   Results of model experiments BERDA I, liquid slug impact including upper internal structures

Model of the
internal structures
prior to the slug impact

Internal structures of
after the slug impact
(only a part of the
pieces is shown)

Internal structures of
after the slug impact

Figure 10.6   Various deformations and cracks of the upper internal structures made
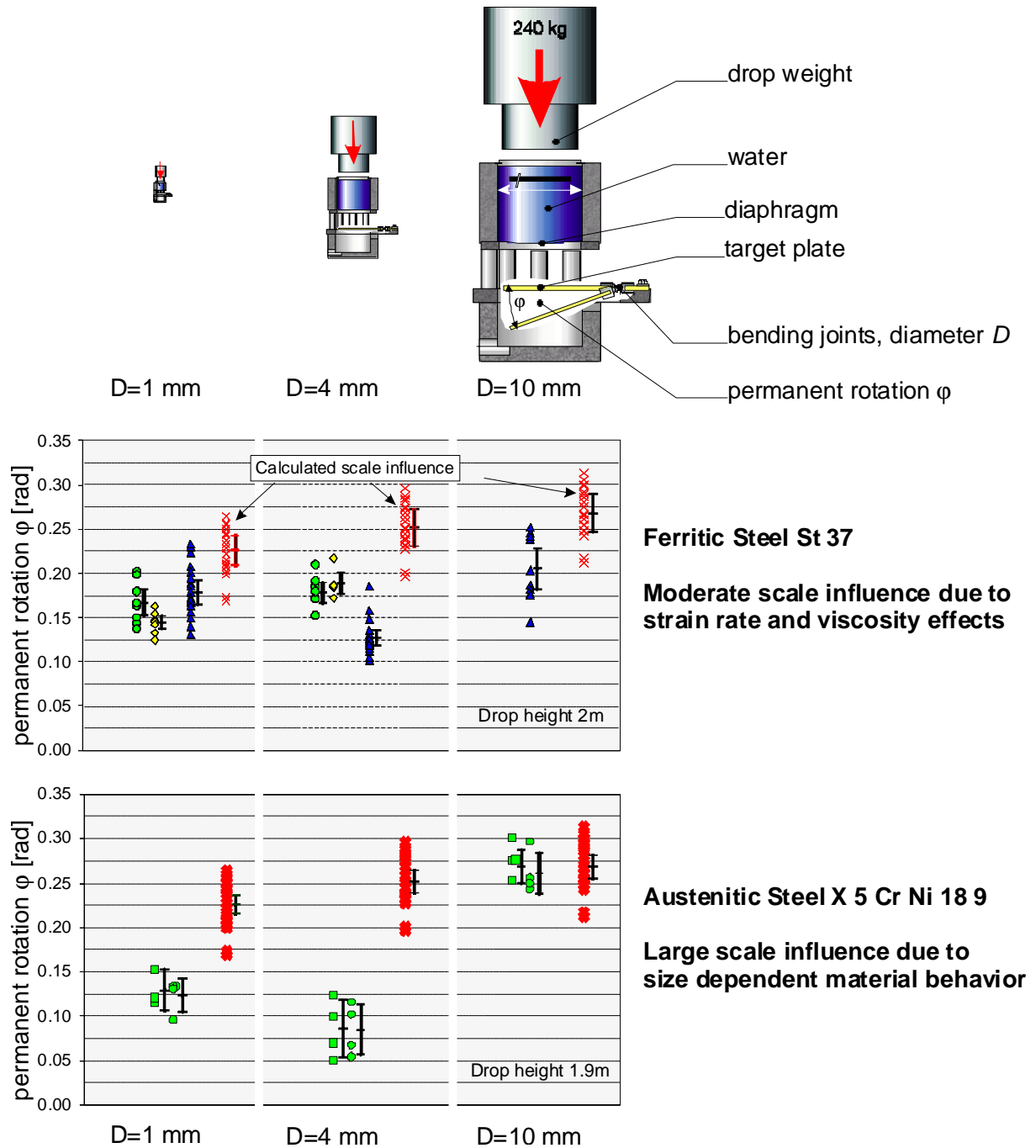of brass and steel

Figure 10.7   Similarity experiments FLIPPER, size effect for liquid impact on deformable structures
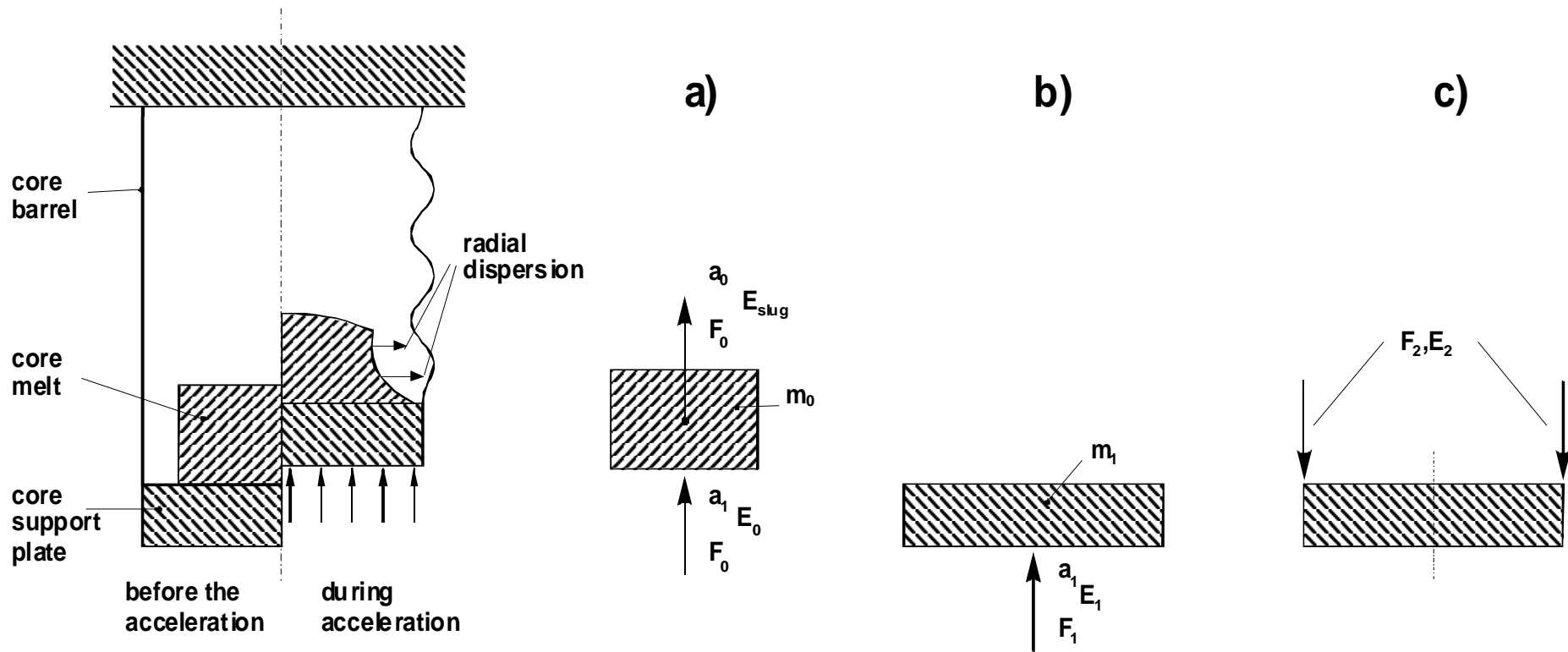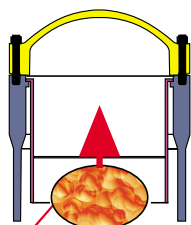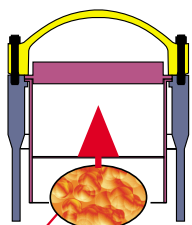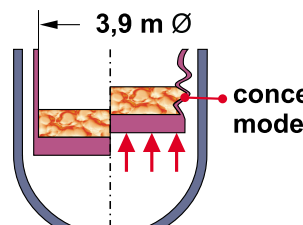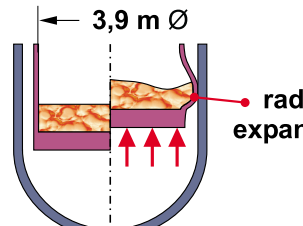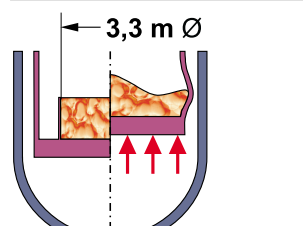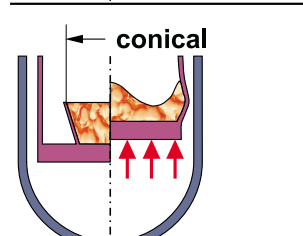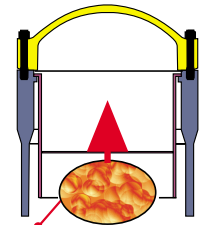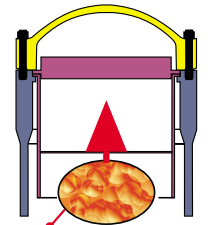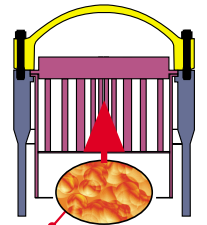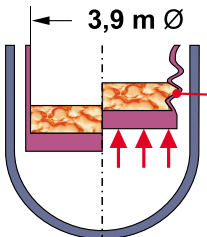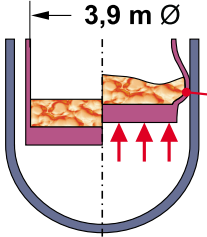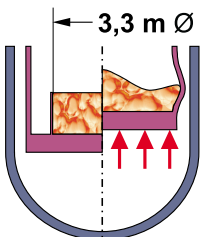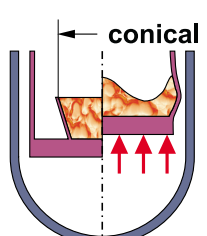
Figure 10.8   Computational model describing the acceleration of the core melt
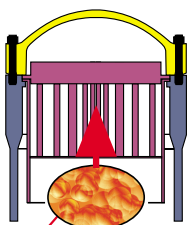
159

Table 10.1 Assessment of the admissible energy input at the support plate E_{plate}

upper line: mass of the heavy reflector __not__ considered

lower line: half of the mass of the heavy reflector added to the mass of the support plate

	A Upper int. struct. molten E_{slug} = 0,1 GJ	**B** Only upper grid available E_{slug} = 0,4 GJ	**C** Upper int. struct. available E_{slug} = 0,8 GJ
a 3,9 m Ø — concertina mode	E_{plate} = 0,15 GJ 0,20	For case B and C concertina mode not expected	
b 3,9 m Ø — radial expansion	For case A rad. expansion not expected	E_{plate} = 1,0 GJ 1,4	2,0 2,8
c 3,3 m Ø	0,4 0,6	1,6 2,4	3,2 4,8
d conical	0,5 0,8	2,2 3,5	4,4 7,0

Berda II_Table_I

161

Table 10.2   Assessment of the admissible mechanical energy release E_a

	A Upper int. struct. molten	B Only upper grid available	C Upper int. struct. available
upper line: mass of the heavy reflector not considered lower line: half of the mass of the heavy reflector added to the mass of the support plate	E_{slug} = 0,1 GJ	E_{slug} = 0,4 GJ	E_{slug} = 0,8 GJ
a 3,9 m Ø concertina mode	E_a = 0,20 GJ 0,25	For case B and C concertina mode not expected	
b 3,9 m Ø radial expansion	For case A rad. expansion not expected	E_a = 1,0 GJ 1,4	2,0 2,8
c 3,3 m Ø	0,4 0,6	1,6 2,4	> 3,2 4,8
d conical	0,5 0,8	> 2,2 3,5	> 4,4 7,0

Berda III_Table_I

162

11 Conclusions

For consequence evaluation of in-vessel fuel coolant interactions in the European Pressurised Water Reactor several items have been treated in a consistent manner.

Three core melt initiators have been found of interest to define representative initial and boundary conditions of the analyses. These were the Loss-of Offsite-Power Accident, the Surge Line Rupture Accident and the Small Break LOCA-Accident. Results of calculations for these three representative accident initiators with MAAP, MELCOR and SCDAP-RELAP5 were compared with each other and were used to derive conditions of interest to be analysed in more depth. Characteristic data of the core melt at the expected time of core melt outflow from the original core area into the lower plenum do not differ too much if different core melt initiators are considered. Similarly it can be stated that remnant water levels in the lower plenum as well as ambient pressure in the primary system at the time of core melt outflow onset are quite similar in the different calculations and for the different core melt initiators. However, larger differences in the results have been observed when temperature levels of pipes and structure components of the primary system are considered. But this information about the state of the reactor system needs better precision only when consequences of fuel coolant interactions are further analysed under the condition that the upper vessel head remains intact as well as the lower vessel head. Then it is to be analysed whether the primary system stays mostly intact and that consequences of fuel coolant interactions are limited solely to the primary system. However, that kind of analysis was not the objective of the current evaluation.

Integral code calculations do not provide sufficiently detailed information about failure modes of the enclosure of the molten pool and the direction of core material outflow. However, separate effect analyses provide information that radial outflow scenarios seem to be more likely. The axial location of crust failure most probably is close to the upper end of the molten pool at the interface between the corium pool and the overlying steel melt. But theoretical as well as experimental information is not yet sufficiently persuasive to exclude the possibility of an axial outflow scenario. Therefore three different outflow scenarios have been defined as base cases, two axial ones and one radial scenario. The two base cases of the axial outflow scenario assume the failure cross-section to be of similar size but porous in the one case and compact in the other case. The radial outflow scenario assumes a failure cross-section of similar size, in the 2-d calculations homogeneously distributed around the core barrel circumference and being distributed along a 1/8th part of the circumference in the one 3D calculation. Dependence of results on transiently increasing failure cross-sections has been evaluated as well as the dependence from different axial locations of the failure height in case of the radial outflow scenarios. The assumptions on the promptly available cross-sections for core material outflow from the original core area have been chosen in a rather conservative manner. More detailed analyses might help to reduce the level of conservatism in future analyses campaigns.

Two codes have been applied to calculate premixing conditions in the lower plenum as consequence of the different core melt outflow scenarios. These were MC3D using the TRITHYD-application and MATTINA. Both codes are intensively used for theoretical interpretation of experimental information deduced from programmes as QUEOS, FARO and PREMIX. Though progress has been made when interpreting the high pressure FARO-experiments and some of the QUEOS-experiments difficulties in interpretation of the low pressure FARO- and PREMIX-experiments are not yet resolved. Current understanding of these difficulties is that they arise from a complex superposition of an incomplete modelling

of physical processes and of consequences of numerical diffusion problems which are due to the first order difference schemes used in space and time in both codes. Alternative formulations are world wide not available. These code difficulties lead to a situation that one has to expect that the calculated displacement of the water after core material outflow onset is overestimated, that the release of the vapour from the interaction zone is not sufficiently well described and that the stronger separation of melt and water reduces thermal interaction during premixing. To compensate for this inaccuracy of currently available models an evaluation strategy of the calculated results has been chosen which defines premixed masses and energies on the basis of an unreasonably low value of the water volume fraction in a node. To prove the level of conservatism of that evaluation procedure formally is not possible. However analysing individual results carefully helps to evaluate calculated results if it is done on a case to case basis considering experimental knowledge appropriately when applicable to the considered case.

Generally the two codes show similar results. The MATTINA-code gives lower thermal premixing energies due to stronger water displacement, which is caused by strong evaporation events after intensive fragmentation of droplets. The presently used MC3D code version simulates a more moderate fragmentation behaviour leading to less evaporation and water depletion. Premixing is intensified by large melt release cross-sections, large initial droplet diameters and pressure loss along the lower plenum flow distribution plate. Other model parameters do not influence results similarly strongly. The conservatively oriented evaluation of all investigated cases leads to a maximum of thermal premixing energies of 3 GJ and an average water volume fraction of about 0.5 to 0.6 in the considered interaction zone. In the majority of the calculated cases thermal premixing energies vary between 0,5 GJ to 2,0 GJ only and the values of the respective average water volume fraction between 0.2 to 0.5. The total amount of melt in the lower plenum can be much larger than the premixed melt mass with a considerable water inventory still available. At the end of the calculations residual amounts of water are largely separated from a rather compact molten corium pool. Both codes predict removal of non negligible amounts of fragmented core material into the primary circuit when radial outflow scenarios are considered.

In the absence of a verified steam explosion model that is able to calculate reliably the pressure development and the production of mechanical energy, one way to estimate mechanical consequences of a steam explosion is to apply an energy conversion factor to the thermal energy content of the melt that is considered as participating in the steam explosion. These values are taken then from results of the premixing calculations. Review of the available information on this topic led us to the conclusion that an energy conversion factor below 15 % cannot be defended as being conservative at the moment and 15 % are not unrealistically high. So we have adopted this value as reference for the further evaluation. Besides that, we used also a value of 30 %. However, we are aware that this value is with certainty very conservative, possibly too much so. On basis of this approach one gets estimates for the maximum mechanical energy releases which amount to values of 0.45 GJ up to 0.9 GJ. If one considers results of the majority of the calculated cases as well, estimates of the mechanical energies vary between values of 0.075 GJ up to 0.6 GJ. This broad spectrum of estimates results on the one side from the broad spectrum of cases and parameters considered in premixing investigations and on the other side it reflects the fact that part of the items considered are still not very precisely known and needed careful and cautious selection of involved model parameters.

Mechanical energy releases do not convert directly to the kinetic energy of the core melt slug. Part of the released energy is consumed to accelerate the lower core support plate together

with the core melt accumulated on top of it and part is consumed deforming the lower reactor vessel head. However this consumes considerable amounts of the released mechanical energy only in case of really high mechanical energy releases. On basis of rather cautious estimates about these reduction factors we arrive at values for the load energies which amount to 0.03 GJ up to at most 0.36 GJ.

The load energies which the reactor vessel head can withstand are determined on basis of experimental results from the BERDA facility that cover a broad spectrum of conditions and applying similarity theory to convert experimental results to the reactor scale. In addition, experimental results are provided and theoretical considerations qualified to determine explosion energies which are admissible to occur without violating the upper head integrity. Results of these evaluations were presented and result in a quite complicated dependency of admissible explosion energies from the actual state of in-vessel reactor structures and temperature levels of these structures. As one representative figure it can be mentioned that a conservatively estimated value for the admissible load energy deduced from the BERDA-experiments amounts to 0.4 GJ which holds for a configuration where the upper core support plate and the respective guide tubes have been fully molten and where the upper grid is still available.

In general one can conclude from results of these investigations, that the kinetic energy of a core melt moving potentially rapidly upward as consequence of an in-vessel fuel coolant interaction might reach the load carrying capabilities of the vessel head. However, this result is only obtained when the most pessimistic assumptions are applied in every step of the analyses. In the majority of the considered pessimistic cases the kinetic energy remains below the load carrying capabilities of the reactor vessel head. In so far there is no need for additional design measures against steam explosions and alpha-mode containment failure sequences need not to be considered.

This study has been performed with not all of the required theoretical tools being available and others not being verified to the necessary extent. So, some remaining uncertainties had to be covered in a definitely conservative way and this report is not a final statement on the topic. Rather the report describes what can be concluded on the basis of the presently assured knowledge and available tools. Further improved analyses become necessary, especially concerning the following items:

- Evaluation of possible relocation paths for the core melt after failure of either molten pool enveloping crusts, the core barrel, and/or the lower core support plate

- Realistic assessment of pressure time histories and explosion energy releases that might result from steam explosions following different premixing conditions

- Realistic assessment of the kinetic energy in the upward accelerated core material

- Assessment of the lower vessel head integrity.

-

12 Appendix

12.1   Appendix A: Slug penetration by Rayleigh-Taylor (RT) instabilities

Details and references in: H. Jacobs, Analytical correlations for Rayleigh-Taylor instability growth, Nucl Tech **71** (1985) 131-144

If a circular cylindrical liquid slug is accelerated uniformly by a much less dense gas, the backward gas/liquid interface is hydrodynamically unstable. Small perturbations on it will grow exponentially (as long as they are small – so-called linear stage) and during some transition time they will develop into the so-called RT bubbles that penetrate the liquid at a constant terminal bubble velocity v_{bt} (finite amplitudes – nonlinear stage). The diameters of these bubbles are equal to the wave length of the instability. While the linear theory is appropriate for studying whether a certain situation is stable or not (stability analysis), the nonlinear behaviour governs any problem involving finite amplitudes.

There is a simple correlation for the terminal bubble velocity:

$$v_{bt} = Fr\,(b\,\lambda)^{0.5} \tag{1}$$

Here Fr is a nondimensional number, the so-called Froude number. For 3D bubbles with circular cross section it can be taken as Fr = 0.345. b denotes the acceleration and λ the wavelength. Equation one applies in case of an infinitely large density ratio.

Under the action of a constant acceleration b and assuming the terminal bubble speed to apply from the beginning, the time for penetrating a slug of height h is

$$t_p = h \,/\, [Fr\,(b\,\lambda)^{0.5}] \tag{2}$$

During this time a slug initially at rest travels a distance

$$s_p = b/2 \bullet (t_p)^2 = h^2 \,/\, (0.24\,\lambda) \tag{3}$$

This is independent of the acceleration.

Equation 1 shows that the largest possible bubble penetrates the fastest. (This is different for very small amplitudes but that detail can be neglected here.) The largest possible wave length is the diameter D of the cylinder. So the slug will be penetrated after having traveled a distance

$$s_p = h^2 \,/\, (0.24\,D) \tag{4}$$

12.2 References to section 2

[1] The RELAP5 Development Team: RELAP5/mod3 Code Manual, Vol 1 - 7 NUREG/CR-5535, INEL-95/0174, 1995.

[2] M. Allison et al.: SCDAP/RELAP5 mod3.1 Code Manual, Vol. I - IV. NUREG/CR-6150, EGG-2720, Oct. 1993.

[3] E. Coryell et. al., SCDAP/RELAP5 mod3.2 Code Manual, Vol. I-V. NUREG/CR-6150, INEL-96/0422, Nov.1997.

[4] SCDAP/RELAP5 mod 3.2, Home page: http://relap5.inel.gov/scdap/home.html

[5] MAAP:

[6] Summers et al.: MELCOR Computer Code Manuals, Vol 1 - 2 (Vers: 1.8.3), NUREG/CR-6119, SAND93-2185, March 1995.

[7] MELCOR Home page: http://www.nrc.gov/RES/MELCOR_INFO/intro.html

[8] W. Hering, Results of FZK Calculations for the projected European Pressurized Water Reactor using SCDAP/RELAP5 mod3.1, FZKA to be published in 1999.

References to section 3

[1] S. Vandroux-König, M. Valette, MC3D: Note de presentation, Centre d'etude nucleaires de Grenoble, STR/LML/93-174, August 1993

[2] M. Valette, MC3D V3.0 Directions for use, Commissariat a l'energie atomique Grenoble, STR/LTEM, STR-LTEM-96-52, September 1997

[3] G. Berthoud, M. Valette, Development of a multidimensional model for the premixing phase of a fuel coolant interaction, Nucl. Engngn. and Design 149 (1994), 409

[4] L. Meyer, G. Schumacher, QUEOS, a Simulation-Experiment of the Premixing Phase of a Steam Explosion with Hot Spheres in Water Base Case Experiments, Forschungszentrum Karlsruhe, Wissenschaftliche Berichte, FZKA 5612, 1996

[5] D. Magallon, H. Hohmann, High Pressure Corium Melt Quenching Tests in Faro, Nucl. Eng. Des. 155 (1995) 253

[6] F. Huber, A. Kaiser, M. Steinbrück, H. Will, PREMIX, Documentation of the Results of Experiments PM01 to PM06, Wissenschaftliche Berichte, FZKA 5756, Forschungs-zentrum Karlsruhe, 1996

[7] U. Imke, Application of MC3D to simple test cases and fuel coolant interaction experiments, IRS-1 Notiz 1/98, Institut für Reaktorsicherheit, Forschungszentrum Karlsruhe, 1998

[8] A. Annunziato, C. Addabbo, G. Leva, OECD/CSNI International Standard Problem No. 39 on FARO Test L-14, Reference Specification, Institute for Systems, Informatics and Safety, Joint Research Center, Ispra, Technical Note No. 1.96.64, April 1996

[9] A. Kaiser, W. Schütz, H. Will, PREMIX-13 Description and First Results, IRS-4-Notiz Nr. 1388/97, Institut für Reaktorsicherheit, Forschungszentrum Karlsruhe, 1997

[10] H. Jacobs, Analysis of large-scale melt-water mixing events, Proceedings of the CSNI Specialists Meeting on Fuel-Coolant Interactions, Santa Barbara, California, USA January 5-8, 1993, NUREG/CP-0127 (1994) pp. 14-26

[11] H. Jacobs, M. Lummer, L. Meyer, B. Stehle, K. Thurnay and L.Väth, "Multifield simulations of premixing experiments,"Proc. of 'A Multidisciplinary International Seminar on Intense Multiphase Interactions,' Santa Barbara, CA, USA, June 9-13, 1995, pp. 56-69

[12] G. Arnecke et al., Theoretische Arbeiten zur Schmelze-Kühlmittel-Wechselwirkung, in: Projekt Nukleare Sicherheitsforschung, Jahresbericht 1997, FZK Report FZKA 6126 (September 1998) pp. 168-75

[13] H. Jacobs, L. Väth and K. Thurnay, "Constitutive relations for multiphase flow modelling," Proc. OECD/CSNI Spec. Mtg. on Fuel-Coolant Interactions, Tokai-Mura, Japan, May 19-21, 1997, Report JAERI-Conf 97-011 Japan Atomic Energy Research Institute, NEA/CSNI/R(97)26 (January 1998) Part I, pp. 205-217

[14] H. Jacobs, L. Meyer, "Highly transient and intense multiphase interactions in the QUEOS premixing experiments," Proc. Intl. Sem. On Vapor Explosions and Explosive Eruptions, Sendai, Japan, May 22-25, 1997, pp. 253-262

[15] L. Meyer, G. Schumacher, H. Jacobs, K. Thurnay, "Investigation of the premixing phase of a steam explosion with hot spheres, Nuclear Technology 123 (1998) 142-155

[16] N. I. Kolev, "IVA3: A transient 3D three-phase, three-component flow analyzer," Proc. Int. Topcl Mtg on Safety of Thermal Reactors, Portland, OR, July 21-25, 1991, pp.171-180

[17] N. I. Kolev, "The code IVA3 for modelling of transient three-phase flows in complicated 3D geometry," Kerntechnik 58 (1993) 147-156

[18] C. Addabbo, A. Annunziato, and D. Magallon, "Synopsis of the results of ISP-39 on FARO test L-14," Proc. OECD/CSNI Spec. Mtg. on Fuel-Coolant Interactions, Tokai-Mura, Japan, May 19-21, 1997, Report JAERI-Conf 97-011 Japan Atomic Energy Research Institute, NEA/CSNI/R(97)26 (January 1998) Part II, pp. 493-509

[19] Annunziato, C. Addabo, A. Yerkess, R. Silverii, W. Brewka, and G. Leva, "OECD/CSNI International Standard Problem 39 on FARO Test L-14 on Fuel Coolant Interaction and Quenching, Participants Comparison Report'" Report EUR 17737 EN, Institute of Systems, Informatics and Safety, JRC Ispra

References to section 4

[1] L. Meyer, G. Schumacher, QUEOS, a Simulation-Experiment of the Premixing Phase of a Steam Explosion with Hot Spheres in Water Base Case Experiments, Forschungszentrum Karlsruhe, Wissenschaftliche Berichte, FZKA 5612, 1996

[2] F. Huber, A. Kaiser, M. Steinbrück, H. Will, PREMIX, Documentation of the Results of Experiments PM01 to PM06, Wissenschaftliche Berichte, FZKA 5756, Forschungszentrum Karlsruhe, 1996

[3] I.E. Idelchik, Handbook of Hydraulic Resistance, Springer-Verlag Berlin, 1986, page 404

Reference to section 9

[1] I. Huhtiniemi, H. Hohmann, and D. Magallon, "FCI experiments in the corium/water system," Nucl Eng Des **177** (1997) 339-349

[2] M. J. Bird, "An experimental study of scaling in core melt/water interactions," 22nd Natl Heat Transfer Conf., Niagara Falls, NY, August 1984

[3] M. Berman (Ed.), "Light Water Reactor Safety Research Program Quarterly Progress Report, January-March 1981," SNL Report NUREG/CR-2163/1of4, SAND81-1216/1of4 (July 1981)

[4] Y. Maruyama, N. Yamano, T. Kudo, A. Hodaka, and J. Sugimoto, "Accident management measures on steam explosion and debris coolability for light water reactors," CSNI Spec. Mtg on Selected Containment Severe Accident Management Strategies, Stockholm, S, June 13-15, 1994

[5] D. F. Fletcher, "Propagation investigations using the CULDESAC model," Proc. of CSNI Spec. Mtg on Fuel-Coolant Interactions, Santa Barbara, CA, January 5-8, 1993, NUREG/CP-0127, NEA/CSNI/R(93)8 (March 1994) pp.180-192

[6] D. D. Cline, L. T. Pong, D. F. Beck, and M. Berman, "An equation of state formulation for Hicks-Menzies FCI efficiencies, in: S. B Yilmaz (Ed.): Heat Transfer – Philadelphia, 1989, AiChE Symp. Series # 269, Vol 85, 1989, 48-53

[7] T. G. Theophanous, B. Najafi, and E. Rumble, "An Assessment of Steam Explosion-Induced Containment Failure, Part I: Probabilistic Aspects," Nucl Sci Eng **97** (1987) 259-281

[8] R. P. Anderson and D. R. Armstrong, "Comparison between vapor explosion models and recent experimental results," in D. Gidaspov (Ed.): Heat transfer – research and design, AiChE Symp. Series # 138, Vol. 70, 1974, 31-47

[9] M. Berman (Ed.), "Light Water Reactor Safety Research Program Semiannual Report, October 1983 - March 1984," SNL Report NUREG/CR-4459, SAND85-2500 (February 1986)

[10] D. E. Mitchel and N. A. Evans, "Steam Explosion Experiments at Intermediate Scale: FITSB Series, SNL Report NUREG/CR-3983, SAND83-1057 (February 1986)

[11] Y. M. Farawila and S. I. Abdel-Khalik, "On the Calculation of Steam Explosion Conversion Ratios from Experimental Data," Nucl Sci Eng 104 (1990) 288-295

[12] M. Corradini, D. Cho, D. Magallon, and S. Basu, "FCI Experiments and Analysis: Contribution to Basic Understanding," Proc. of OECD/CSNI Spec. Mtg on Fuel-Coolant Interactions, Tokai-Mura, J, May 19-21, 1997, JAERI-Conf 97-011 (Part II), NEA/CSNI/R(97)26 (January 1998), pp. 609-622

[13] M.-D. Oh, "Thermal-Hydraulic Modelling and Analysis for for Large-Scale Vapor Explosions," Thesis, University of Wisconsin Report UWRSR 29 (August 1985); M. D. Oh and M. Corradini, "A Propagation/Expansion Model For Large Scale Vapor Explosions," Nucl Sci Eng 95 (1987) 225-240

[14] R. Krieg, "Mechanical efficiency of the energy release during a steam explosion," Nucl Tech 117 (1997) 151-157

[15] W. H. Amarasooriya and T. G. Theofanous, "An Assessment of Steam-Explosion-Induced Containment Failure. Part III: Expansion and Energy Partition," Nucl Sci Engn 97 (1987) 296-315

[16] H. Jacobs, "Analytical correlations for Rayleigh-Taylor instability growth," Nucl Tech 71 (1985) 131-144

[17] N. I. Kolev, "Numerical modeling of in-vessel melt water interaction in large scale PWR's", Proc. of OECD/CSNI Specialist Mtg on Fuel-Coolant Interactions, Tokai, Japan, 19-21 May 1997, Report JAERI-Conf 97-011 (Part I), pp. 145-9 (January 1998)

[18] L. Meyer, G. Schumacher, H. Jacobs, and K. Thurnay, "Investigation of the premixing phase of a steam explosion with hot spheres," Nucl Tech 123 (1998) 142-55

[19] J. S. Seo and S. G. Bankoff, "Entrainment and condensation effects in the upward acceleration of a liquid column," Int. J. Multiphase Flow **15** (1989) 925-935

References to section 10

[1] R. Krieg, Missiles Caused by Severe Pressurized-Water Reactor Accidents, Nuclear Safety, 36, 299 (1995)

[2] R. Krieg, T. Malmberg, G. Messemer, T. Stach, E. Stratmanns, Slug Impact Loading on the Vessel Head during a Postulated In-Vessel Steam Explosion in Pressurized Water Reactors – Assessments and Discussion of the Investigation Strategy, Nucl. Technology, 111, 369 (1995)

[3] R. Krieg, T. Malmberg, G. Messemer, G. Hoffmann T. Stach, E. Stratmanns, Model Experiments BERDA Describing the Impact of Molten Core Material Against a PWR Vessel Head, Int. Conf. on Advanced Reactor Safety ARS'97, Orlando, USA (June 1997)

[4]   B. Dolensky, B. Göller, A. Hirt, R. Krieg, Theoretical Models Describing the Impact Loading of a PWR Vessel Head, Int. Conf. on Advanced Reactor Safety ARS'97, Orlando, USA (June 1997)

[5]   R. Krieg, B. Göller, A. Hirt, G. Hoffmann, T. Jordan, T. Malmberg, G. Messemer, T. Stach , G. Vorberg, Mechanical Behavior of the Reactor Vessel during an In-Vessel Steam Explosion, The European Pressurized Water Reactor EPR, Cologne, Germany (Oct. 1997)

[6]   R. Krieg, B. Dolensky, B. Göller, G. Hailfinger, G. Hoffmann, T. Malmberg, G. Messemer H. Benz, W. Ratajczak, Schadenspotential von Dampfexplosionen bei Kernschmelzunfällen, FZK Nachrichten, Jhrg. 29, 4/97

[7]   B. Dolensky, B. Göller, Calculations to interprete the BERDA tests 05, 06, 07 and 09 without internal structures, Forschungszentrum Karlsruhe, Interner Bericht IRS 14/98, PSF 3306

[8]   A. Hirt, Rechenmodell zum Aufprall von Kernschmelze auf die oberen Einbauten und den Deckel eines Reaktordruckbehälters, FZKA 6054, (April 1998)

[9]   T. Malmberg, Aspects of Similitude Theory in Solid Mechanics, Part I: Deformation Behavior, FZKA 5657 (Dec. 95)

[10] T. Stach, Zur Skalierung von Modellversuchen zum Aufprall flüssiger Massen auf deformierbare Strukturen, FZKA 5903 (Mai 1997)

[11] T. Stach, T. Malmberg, R. Krieg, Scaled Experiments for a Simple Deformation Structure under Liquid Slug Impact, 14th Int. Conf. on Struct. Mech. in Reactor Technology, Session P02, Lyon, France, 1997

[12] T. Jordan, G. Messemer, Slug Impact Tests against the Reactor Pressure Vessel Head Scaled Down 1:50, to be published

[13] R. Krieg, B. Göller, G. Hailfinger, Transient, Three-Dimensional Potential Flow Problems and Dynamic Response of the Surrounding Structures, Part I, Comput. Phys., 8, 2, 139 (1980)

[14] B. Dolensky, R. Krieg, The PWR Lower Head under Excessive Loading – Model Experiments and Theoretical Assessments, 13th Int. Conf. on Struct. Mech. in Reactor Technology, Division C, Porto Alegre, RS, Brasil, 1995

[15] R. Krieg, "Mechanical efficiency of the energy release during a steam explosion," Nucl Tech **117** (1997) 151-157